

Copyright is owned by the Author of the thesis. Permission is given for a copy to be downloaded by an individual for the purpose of research and private study only. The thesis may not be reproduced elsewhere without the permission of the Author.



# **Physico-chemical properties and stability of lipid droplet-stabilised emulsions**

A thesis presented in partial fulfilment of the requirements

for the degree of

**Doctor of Philosophy in Food Technology**

at Massey University, Manawatū, New Zealand

**Lirong Cheng**

**2022**





## **Abstract**

It is known that the structure of the interfacial layer impacts the stability and the function of emulsions. Hierarchical emulsions, known as droplet-stabilized emulsions (DSEs), were made from nano-sized primary oil droplets that coated with protein particles for potentially advanced functionality. In this study, the primary droplets were made of either rigid (whey protein microgel, WPM) or soft protein ( $\text{Ca}^{2+}$ -cross-linked caseinate, Ca-CAS) particles. The structure of the protein particles and primary droplets in solution and at the oil-water interface were characterised; the oil exchange process between the surface and core oil droplets were examined, using light scattering, microscopy, small angle scattering, ultra-small angle scattering techniques, etc. The emulsification capacity of the primary emulsion has been shown to be improved by using soft and flexible protein particles, resulting in small droplet sizes and smooth interfacial layers of the DSE. The droplet-stabilised interfacial layer has been shown to provide DSE a good stability against coalescence during gastric enzymatic hydrolysis, long-term storage, and heating, as well as improved functionalities in the rate of the lipolysis during simulated intestinal digestion and the rheological properties at high oil content.

Overall, this research provided new information on DSE physical-chemical properties and stability as affected by the structure of emulsifiers (protein particles and the subsequent primary droplets), digestion destabilisation, pH, storage time and temperature. The outcomes have potential for designing functional foods with improved active compound delivery and mechanical strength.

### **Acknowledgements**

During my time at the Riddet Institute, Massey University, I have had the privilege of meeting and learning from my supervisors, colleagues, and collaborators. The work described in this thesis represents the outcomes of my PhD project but does not include all the work I have been able to do and all the people I have been able to work with. Their professionalism, enthusiasm, optimism, and resilience have energised my PhD journey. I have also been fortunate to have received a lot of love from my friends and families. I could not have accomplished this journey with joy without them, and I am grateful to all of them.

First and foremost, I would like to express my deepest gratitude to my chief supervisor, Professor Aiqian Ye, and my co-supervisors, Professor Yacine Hemar and Distinguished Professor Harjinder Singh, for their continuous support, encouragement, guidance, and challenge. They built a supportive, harmonious, and flexible working environment for me to carry out my research. I am thankful for their insightful comments and immense knowledge, which guided me through difficulties and challenges. They also helped me build up my knowledge and skillsets in conducting research work independently. I am grateful for their dedication, motivation, inspiration, and patience. The knowledge and experience I have learned from them are lifelong and will continue to support and inspire me in my future career and life.

Secondly, I want to send my sincere appreciation to scientists Dr. Zhi Yang from Massey University, and Professor Elliot Paul Gilbert, Dr. Liliana de Campo, Dr. Robert Knott, and Mr. Ben Storer from Australian Nuclear Science and Technology Organization (ANSTO), and Dr. Rainer Mittelbach from Australian National University. They have guided my studies and research in small-angle scattering, given support in experimental designs and data analyses. I will never forget the time that we spent together in conducting our research, and every

## *Acknowledgements*

---

productive and enthusiastic discussion about the rationale of the experimental design and the validity of the data. The profound and creative scientific insights from Professor Elliot Paul Gilbert, Dr. Zhi Yang and Dr Liliana de Campo have always enlightened me. Without their support, I would not have been able to complete the research in Chapter 3-5. In particular, during the difficult time between year 2020-2022 due to COVID-19, Professor Elliot Paul Gilbert, Dr. Liliana de Campo, and Dr. Robert Knott offered me opportunities to run the experiment remotely that described in Chapter 4 and Chapter 5. Dr. Liliana de Campo has even gone above and beyond her duties by providing generous help with sample preparation at ANSTO for the *in-situ* kinetics study described in Chapter 5. Dr. Rainer Mittelbach has kindly provided a customised Python coding to present the vast kinetic data efficiently and reliably.

I am grateful to Dr. Pat Edwards from the Massey Nuclear Magnetic Resonance (NMR) Centre for providing experiments in pulsed diffusion NMR and for lending me deuterium oxide for my small angle scattering studies. I want to thank my colleagues Ms. Maggie Zou, Mr. Chris Hall, Ms. Michelle Tamehana, Mr. Steve Glasgow, from School of Food and Advanced Technology, Massey University for their help in lab inductions, equipment trainings, chemical orderings and provided technical and safety advice.

Last, but not least, I want to thank my dear mom Ms. Yinghua Sun (孙英华) and my husband Dr. Zhi Yang (杨志). Thank you for your eternal and unconditional love. Your love fills my mind with strength. This thesis is dedicated to you, with love.

**Table of Contents**

Abstract .....i

**Acknowledgements.....ii**

**Table of Contents .....iv**

**List of Tables ..... xiii**

**List of Figures .....xiv**

**List of Abbreviations.....xxvi**

**List of Peer-reviewed Publications .....xxvii**

**Chapter 1 Introduction..... 1**

**Chapter 2 Literature review ..... 7**

    2.1 *Emulsion formation and interfaces* ..... 7

    2.2 *Conventional emulsifiers* ..... 9

    2.3 *Particle emulsifiers*..... 11

        2.3.1 Rigid and soft protein-based particles ..... 23

        2.3.2 Solid and soft lipid-based particles ..... 26

    2.4 *Emulsion rheological properties* ..... 29

    2.5 *Emulsion interfacial rheology* ..... 34

    2.6 *Emulsion stability* ..... 36

        2.6.1 Physical destabilisation ..... 36

            2.6.1.1 Gravitational separation ..... 38

            2.6.1.2 Flocculation ..... 39

iv

## *Table of Contents*

---

2.6.1.3 Coalescence.....	41
2.6.1.4 Ostwald ripening .....	41
2.6.1.5 Oil exchange .....	42
2.6.1.6 Phase inversion .....	42
2.6.2 Chemical destabilization.....	43
2.6.3 Digestive destabilisation.....	44
2.6.3.1 Structural disintegration and aggregation .....	44
2.6.3.2 Droplet coalescence in the gastric phase.....	46
2.6.3.3 Lipid digestion in the small intestinal phase.....	46
2.7 <i>Techniques and methods to characterise emulsions</i> .....	47
2.7.1 Visual and tactile observation.....	47
2.7.2 Microscopy .....	49
2.7.2.1 Optical microscopy .....	49
2.7.2.2 Confocal laser scanning microscopy .....	50
2.7.2.3 Electron microscopy .....	51
2.7.3 Particle sizing by light scattering.....	55
2.7.3.1 Static light scattering.....	55
2.7.3.2 Dynamic light scattering .....	56
2.7.4 Small-angle scattering .....	57
2.7.4.1 Small angle X-ray scattering in emulsion studies.....	62
2.7.4.2 Small angle neutron scattering in emulsion studies .....	66
2.8 <i>Conclusion</i> .....	70



**Chapter 3 Interfacial structures of droplet-stabilized emulsions formed with whey protein microgel particles as revealed by small and ultra-small angle neutron scattering.....73**

    3.1 *Introduction*..... 74

    3.2 *Materials and methods* ..... 75

        3.2.1 *Materials* ..... 75

        3.2.2 *Preparation of WPM particles* ..... 76

        3.2.3 *Emulsion preparation*..... 77

            3.2.3.1 *PE preparation*..... 77

            3.2.3.2 *DSE preparation*..... 77

        3.2.4 *Dynamic light scattering (DLS)*..... 78

        3.2.5 *Static light scattering (SLS)*..... 78

        3.2.6 *Confocal laser scanning microscopy*. ..... 78

        3.2.7 *Transmission electron microscopy*. ..... 79

        3.2.8 *Pendant drop method for interfacial tension (IFT)* ..... 79

        3.2.9 *Small and ultra-small angle neutron scattering*. ..... 80

    3.3 *Results and discussion*..... 84

        3.3.1 *Characterisation of the WPM particles*..... 84

        3.3.2 *Characteristics of PEs stabilised by WPM particles*..... 90

        3.3.3 *Characteristics of oil-in-water emulsions stabilized by PE droplets (DSEs)* ... 93

    3.4 *Conclusions* ..... 103

3.5 Acknowledgments ..... 104

3.6 Supplementary material ..... 105

**Chapter 4 Small-angle X-ray scattering (SAXS) and small-angle neutron scattering (SANS) study on the structure of sodium caseinate in dispersions and at the oil-water interface: effect of calcium ions .....109**

4.1 Introduction..... 110

4.2 Materials and methods ..... 114

4.2.1 Materials ..... 114

4.2.2 Preparation of CAS and Ca-CAS particle dispersions ..... 114

4.2.3 Emulsion preparation..... 115

4.2.4 Particle size distribution ..... 115

4.2.5 Zeta potential measurements ..... 115

4.2.6 Interfacial tension measurements ..... 116

4.2.7 Negative staining TEM..... 116

4.2.8 Small-angle X-ray scattering ..... 117

4.2.9 Small-angle neutron scattering ..... 120

4.3 Results and discussion..... 122

4.3.1 Surface charges of CAS and Ca-CAS ..... 122

4.3.2 Structure of CAS and Ca-CAS dispersions ..... 124

4.3.3 Interfacial tension of CAS and Ca-CAS at the oil-water interface..... 130

4.3.4 Interfacial layer structure of droplets stabilised by CAS and Ca-CAS ..... 133

4.3.4.1 Transmission electron microscopy.....	133
4.3.4.2 Small-angle neutron scattering analysis.....	136
4.4 Conclusions .....	140
4.5 Acknowledgements .....	141
4.6 Supplementary material .....	142
<b>Chapter 5 Oil exchange mechanisms in droplet-stabilised emulsions as revealed by contrast variation USANS and SANS .....</b>	<b>144</b>
5.1 Introduction.....	145
5.2 Materials and methods .....	148
5.2.1 Materials .....	148
5.2.2 Preparation of calcium cross-linked caseinate particle (Ca-CAS) .....	148
5.2.3 Emulsion preparation.....	149
5.2.3.1 Primary emulsion .....	149
5.2.3.2 Droplet-stabilised emulsions.....	149
5.2.3.3 Mixed emulsions .....	150
5.2.4 Microstructure of the droplets .....	150
5.2.5 Droplet size distributions .....	150
5.2.6 Ultra- small-angle neutron scattering (USANS) and small-angle neutron scattering (SANS).....	151
5.2.7 USANS and SANS data analysis.....	152
5.3 Results and discussion.....	153
5.3.1 DSE stability towards coalescence .....	153

5.3.2 Oil exchange in DSE .....	155
5.3.3 Oil exchange in the mixed emulsion .....	159
5.3.4 Possible pathways of oil exchange between droplets .....	167
5.4 Conclusions .....	172
5.5 Acknowledgements .....	173
<b>Chapter 6 Modification of the interfacial structure of droplet-stabilised emulsions during <i>in vitro</i> dynamic gastric digestion: impact on <i>in vitro</i> intestinal lipid digestion .....</b>	<b>174</b>
6.1 Introduction .....	175
6.2 Materials and methods .....	177
6.2.1 Materials .....	177
6.2.2 Preparation of calcium caseinate (Ca-CAS) particles .....	178
6.2.3 Emulsion preparation .....	179
6.2.3.1 DSE preparation .....	179
6.2.3.2 Conventional PSE preparations .....	180
6.2.4 Dynamic <i>in vitro</i> gastric digestion .....	181
6.2.5 pH measurement .....	182
6.2.6 Measurement of oil content .....	182
6.2.7 <i>In vitro</i> intestinal digestion .....	182
6.2.8 Static light scattering .....	183
6.2.9 Confocal laser scanning microscopy (CLSM) .....	183

## *Table of Contents*

---

6.2.10 Kinetics of lipolysis .....	184
6.2.11 Statistical analysis.....	185
6.3 <i>Results and discussion</i> .....	186
6.3.1 Size and microstructure of emulsions before digestion .....	186
6.3.2 <i>In vitro</i> gastric digestion of emulsions.....	190
6.3.2.1 Chang in droplet size of emulsions during <i>in vitro</i> gastric digestion.....	190
6.3.2.2 Morphology of emulsions during gastric digestion .....	193
6.3.2.3 Oil content of the emptied digesta .....	197
6.3.3 <i>In vitro</i> small intestinal digestion of emulsions .....	200
6.3.3.1 Microstructure of emulsions during <i>in vitro</i> small intestinal digestion ..	200
6.3.3.2 Modelling of the kinetics of lipolysis .....	203
6.4 <i>Conclusions</i> .....	206
6.5 <i>Supplementary material</i> .....	207
6.6 <i>Acknowledgements</i> .....	212
<b>Chapter 7 Formation and properties of highly concentrated oil-in-water emulsions stabilised by emulsion droplets .....</b>	<b>213</b>
7.1 <i>Introduction</i> .....	214
7.2 <i>Materials and methods</i> .....	217
7.2.1 Materials .....	217
7.2.2 Preparation of calcium cross-linked caseinate particle.....	217
7.2.3 Emulsion preparations .....	218
7.2.3.1 Concentrated droplet-stabilized emulsion preparations .....	218

## *Table of Contents*

---

7.2.3.2 Concentrated CAS particle-stabilised emulsion preparation .....	218
7.2.4 Emulsion stability during storage and heat treatment.....	219
7.2.5 Particle size measurement.....	219
7.2.6 Zeta-potential measurements .....	220
7.2.7 Characterisations of rheological properties .....	220
7.2.8 Confocal laser scanning microscopy (CLSM).....	221
7.2.9 Statistical analysis.....	222
<i>7.3 Results and discussion.....</i>	<i>223</i>
7.3.1 Formation of DSE concentrated emulsions .....	223
7.3.2 Droplet size distribution of the concentrated emulsions.....	223
7.3.3 Properties and stability of the concentrated emulsions.....	226
7.3.4 Microstructure of concentrated emulsions during aging .....	228
7.3.5 Viscoelasticity of concentrated DSE emulsions during aging.....	230
7.3.6 Stability of concentrated emulsions against heating.....	237
7.3.7 Viscoelasticity of concentrated emulsions after heating .....	240
<i>7.4 Conclusions .....</i>	<i>243</i>
<i>7.5 Acknowledgements .....</i>	<i>244</i>
<b>Chapter 8 Overall conclusions, discussion and future recommendations .....</b>	<b>245</b>
<i>8.1 Overall conclusions and discussion .....</i>	<i>245</i>
<i>8.2 Recommendations for future work .....</i>	<i>250</i>
8.2.1 Protein particles .....	250

## *Table of Contents*

---

8.2.2 Oil mixing study .....	250
8.2.3 Emulsion rheology .....	250
8.2.4 Emulsion digestion .....	251
<b>Bibliography .....</b>	<b>252</b>
<b>Appendix.....</b>	<b>313</b>
<i>Appendix A: Permissions for reuse published articles.....</i>	<i>313</i>
<i>Appendix B: DRC 16 Forms.....</i>	<i>331</i>

**List of Tables**

**Table 2-1** Example of dairy-protein-based Pickering stabilizer for O/W emulsion applications  
a .....20

**Table 4-1:** Input physical parameters used to constrain Hayter-Penfold fit on SAXS scattering  
of CAS. .... 119

**Table 4-2:** Structural parameters obtained from the fit to small-angle X-ray scattering profiles  
of sodium caseinate (CAS) and Ca<sup>2+</sup>-cross-linked caseinate particles (Ca-CAS) at various  
protein concentrations. .... 128

**Table 7-1** Complex moduli  $G^*$  at 1 Hz (Pa) of PSE and DSE at pH 7.0 and 5.8 after 0 day, 30  
days aging, and heating at 80 °C for 30 min. ....232

**Table S 4-1:** Size and surface characteristics of emulsions stabilised by sodium caseinate  
particles and Ca<sup>2+</sup>-cross-linked caseinate particles (Ca-CAS)..... 142

**Table S 6-1:** Formulae of electrolyte solutions for the simulated gastric fluid (SGF) and the  
simulated intestinal fluid (SIF) .....207

**Table S 6-2:** Kinetic parameters of the emulsions during the *in vitro* intestinal digestion...208



**List of Figures**

**Figure 1-1:** Preparation of droplet-stabilized emulsions (DSE) by 2-steps emulsification. ....3

**Figure 2-1:** (a) Small spherical particle at a planar fluid-water interface for a contact angle (measured through the aqueous phase) less than  $90^\circ$  (left), equal to  $90^\circ$  (centre) and greater than  $90^\circ$  (right) [reprinted from Binks (2002), with permission by Elsevier]. (b) Corresponding probable positioning of particles at a curved fluid-water interface. For  $\theta < 90^\circ$ , solid-stabilized aqueous foams or O/W emulsions may form (left). For  $\theta > 90^\circ$ , solid-stabilised aqueous foam or W/O emulsions may form (right) [reprinted from Binks (2002), with permission by Elsevier]. (c) Desorption energy as a function of particle size, for oil-water interfacial tension of 50 mN/m or 25 mN/m, and particles with  $\theta$  of  $5^\circ$ ,  $30^\circ$ , or  $90^\circ$ . The grey dashed line represents the thermal energy at 25 °C ( $k_B T$ ) [reprinted from Berton-Carabin & Schroën (2015), with permission by Annual Reviews]..... 14

**Figure 2-2:** Cryo-SEM images of the interface morphologies of (a and b) dodecane-in-water droplet stabilized by native bovine serum albumin molecules (*n*BSA) and by galactose glycosylated BSA particles (*g*BSA) at pH 7.0 [reprinted from Xu et al. (2020b), with permission by Elsevier]; of (c and d) medium-chain triglyceride-in-water droplet stabilized by whey protein molecules and whey protein microgel particles at pH 7.0 [reprinted from Araiza-Calahorra & Sarkar (2019), with permission by Elsevier]..... 17

**Figure 2-3:** Cryo-SEM images of the interfacial morphology of (a) heptane-in-water droplet stabilized by WPMs at pH 4.8 [reprinted from Destribats et al. (2014), with permission by Royal Society of Chemistry], (b) corn oil-in-water droplet stabilized by casein particles at unknown pH [reprinted from Guo et al. (2021), with permission by Elsevier], and (c) medium-chain triglyceride-in-water droplet stabilized by casein gel particles (calcium and genipin cross-linking) at pH 6.0 [reprinted from Wang et al. (2018), with permission by Elsevier]. .....25

**Figure 2-4:** (a) SEM images of sunflower O/W emulsion stabilised by tripalmitin SLNs with 5 % WPI coating [reprinted from Pawlik et al. (2016), with permission by Royal Society of Chemistry]. (b) TEM images of n-hexadecane O/W emulsions stabilised by soft n-hexadecane primary droplets with casein micelle coating [reprinted from Ye et al. (2013b), with permission by American Chemical Society]. .....28

**Figure 2-5:** (a) Shear viscosity plotted against shear rate; soft PDMS:  $\varphi = 0.6$  (close triangle),  $\varphi = 0.7$  (close circle); hard PDMS:  $\varphi = 0.6$  (open triangle),  $\varphi = 0.7$  (open circle); silica:  $\varphi = 0.6$  (close square). (b) Elastic modulus,  $G'$  (closed symbols) and viscous modulus,  $G''$  (open symbols) plotted against shear strain at 1 Hz; soft PDMS (circle), hard PDMS (triangle) [reprinted from Saiki & Prestidge (2005), with permission by Korea Science]. .....33

**Figure 2-6:** (a) Strain sweep of poly (*n*-isopropylacrylamide)-*co*-Methacrylic acid polymers (PNIPAM-*co*-MAA) microgel layers cover heptane-water interfaces at pH 3 and (b) at pH 9 [reprinted from Brugger et al. (2010), with permission by Royal Society of Chemistry]. (c) Hydrodynamic diameter ( $D_h$ ) of PNIPAM microgel particles with different crosslinking density as function of the solution temperature, S/N 1, soft particles, and S/N 8, rigid particles, and (d) strain sweep of S/N 1 and S/N 8 microgel layers cover heptane-water interfaces [reprinted from Li et al. (2015), with permission by American Chemical Society]. .....35

**Figure 2-7:** Principal factors affecting oil-in-water emulsion stability .....37

**Figure 2-8:** (a) 0.1 % WPMs-stabilised heptane droplets observed by optical microscopy and by (b) cryogenic-scanning electron microscopy (cryo-SEM); insert is 4 % WPMs particles in water observed by optical microscopy [reprinted from Destribats et al. (2014), with permission by Royal Society of Chemistry]. (c) WPMs-coated-primary emulsion-stabilised soy oil droplet observed by confocal laser scanning microscopy (CLSM) and by (d) transmission electron microscopy (TEM); in CLSM observation, the red colour represents the oil phase stained by

Nile Red and the green colour represents the protein particles stained by Fast Green FCF [reprinted from Cheng et al. (2019), with permission by American Chemical Society]. .....54

**Figure 2-9:** The basics of small angle scattering in food colloids. (a) Scattering geometry for a SAXS or SANS measurement; (b) Neutron scattering length densities for common food-based materials; (c) Core-shell structure in solution showing the possibility of selectively contrast matching two of the phases through changing solvent H<sub>2</sub>O/D<sub>2</sub>O composition: by matching the scattering length density of the solvent to core, only the shell is visible, while matching the solvent to the shell yields information only on the core [reprinted from Gilbert (2019a), with permission by Elsevier].....59

**Figure 2-10:** (a) SAXS curves obtained from 4 % w/w WPM dispersions at selected pH values after subtraction of the solvent scattering. The curves are shifted vertically for better visibility. The fitting model consisted of a lognormal distribution of homogeneous spheres plus a power law decay of the intensity. The sample close to the isoelectric point (IEP) show correlation peak at the high  $Q$ -regime due to aggregation. (b) Enlargement of the high- $Q$  regime of the SAXS curves showing the correlation peak at  $Q = 0.67 \text{ nm}^{-1}$ . (c) Theoretical scattering curve that results from a combination of a form factor of polydisperse spheres (10% polydispersity) and a contribution from the fractal internal structure of the microgel. At low- $Q$  regime the curve is dominated by the overall size and shape of the particles. At high- $Q$  regime the contribution of the fractal internal structure becomes important, leading to a power-law decay of the scattering curve. Relatively densely packed aggregates (e.g., fractal dimension of 2) give raise to a scattering curve which is decaying steeply ( $q^{-2}$ ) than more open structures with smaller fractal dimensions ( $q^{-1}$ ) [reprinted from Schmitt et al. (2010), with permission by Royal Society of Chemistry]. .....63

**Figure 2-11:** USAXS scattering curves of GNP with perfluorooctane sonicated at (a) various acoustic pressures. A model containing 2 spheres was used to fit the sample sonicated at acoustic pressures lower than the cavitation threshold (<6.4 MPa), and a Debye model was used to fit the sample sonicated at 7.2 MPa. Scattering length densities were fixed for water ( $9.47 \times 10^{-6} \text{ \AA}^{-2}$ ), gold ( $124.69 \times 10^{-6} \text{ \AA}^{-2}$ ) and perfluorooctane ( $14.47 \times 10^{-6} \text{ \AA}^{-2}$ ). Scattering profiles of GNP with perfluorooctane sonicated at (b) 4 MPa (no cavitation) and (c) 7.2 MPa (cavitation) with increasing sonication time [reprinted from Lee et al. (2019), with permission by Elsevier]. .....65

**Figure 2-12:** SANS profiles for O/W emulsion of fish oil (red and black dot) and deuterated hexadecane (blue dot) emulsified by combination of CAS (1.05% w/w) and various PC concentrations (0.35 and 1.75 % w/w). The solid lines are calculated total scattering from PC monolayer and CAS particles with a constant background contribution, while dashed lines represent the individual scattering contribution from CAS particles (black) and PC monolayer (blue) [reprinted from Yesiltas et al. (2019), with permission by Elsevier]. .....67

**Figure 2-13:** Scattering profiles of droplet oil exchange at (a) 35 °C, (b) 45 °C, and (c) 60 °C of a 1 vol % hexadecane emulsions stabilized by 1 mM SDS sample. Increasing sample environment temperature results in a faster decrease in scattering intensities [reprinted from Lee & Pozzo (2019), with permission by American Chemical Society]. .....69

**Figure 3-1:** (A) (■), WPM-NPB particles, microgels formed without phosphate buffer; (▲), WPM-PB particles, microgels formed with 10 mM pH 5.9 phosphate buffer. (B) Droplet size distributions by MasterSizer of the PEs at 25 °C and natural pH: (■), PE-NPB stabilized by 10 wt% WPM-NPB particles; (▲), PE-PB stabilized by 10 wt% WPM-PB particles. ....85

**Figure 3-2:** Microscope images of (A) WPM-NPB, microgels formed without phosphate buffer, and (B) WPM-PB, microgels formed with 10 mM phosphate buffer during heating. (A-1) and

(B-1): optical images for the whey protein aggregates without and with phosphate buffer, respectively; scale bar is 50  $\mu\text{m}$ . (A-2) and (B-2): negative-staining TEM images for WPM-NPB and WPM-PB particles, respectively; scale bar is 200 nm. ....86

**Figure 3-3:** Combined USANS (open symbols) and SANS (solid symbols) data for WPM-NPB particles (blue) and WPM-PB particles (red). The WPM concentration is 0.2 wt%. Solid lines represent fits using the Guinier–Porod model. ....89

**Figure 3-4:** Confocal images: (A-1), PE-NPB stabilized with WPM-NPB particles; (B-1), PE-PB stabilized with WPM-PB particles. Negative-staining TEM images: (A-2), PE-NPB; (B-2), PE-PB. ....91

**Figure 3-5:** Droplet size distributions of two series of DSEs coated with (A) PE-NPB and (B) PE-PB in a concentration range from 10 to 60 wt%. ....95

**Figure 3-6:** (A and B) Confocal images, and (C and D) associated high magnification confocal images, of DSEs and individual DSE droplets, stabilized with (A and C) PE-NPB and (B and D) PE-PB at concentrations of 10, 30, and 60 wt%. Red colour represents the oil and green colour represents the protein. Scale bar is 20  $\mu\text{m}$ . ....97

**Figure 3-7:** TEM images of DSEs stabilized with PE droplets: (A-1), DSE droplets stabilized by 60 wt% PE-NPB droplets (DSE-NPB 60); (B-1), DSE droplets stabilized by 60 wt% PE-PB droplets (DSE-PB 60). The curve between the interfacial layer and the aqueous phase is drawn as a guide for the eye. (A-2) and (B-2) are TEM images for the interfaces of DSE-NPB 60 and DSE-PB 60, respectively. ....98

**Figure 3-8:** Combined USANS (open symbols) and SANS (solid symbols) profiles for 0.2 wt% emulsion dispersions of: (A), PE-NPB (blue) and PE-NPB following SDS treatment (black); (B), DSE-NPB 10 (orange), DSE-NPB 30 (green), and DSE-NPB 60 (purple) without SDS

treatment, and with SDS treatment (black); the power law fitting for the DSE samples listed is shown in the inset to (B). ..... 102

**Figure 4-1:** Zeta potentials of sodium caseinate (CAS, black squares) and Ca<sup>2+</sup>-cross-linked sodium caseinate particle (Ca-CAS, red circles) dispersions at protein concentrations of 0.5, 1.5 and 3.0% w/v and neutral pH (6.9 ± 0.1) and 20 °C. Error bars represent the standard deviation from triplicates. .... 123

**Figure 4-2:** Small-angle X-ray scattering profiles of (A) sodium caseinate and (B) Ca<sup>2+</sup>-cross-linked sodium caseinate particles at protein concentrations of 0.5, 1.5 and 3.0% w/v. The solid black lines are the unified fits to the scattering data. The scattering curves were shifted vertically for clarity. The insets are visualisations of the associated protein dispersions..... 129

**Figure 4-3:** Interfacial tensions of toluene–water (blue), toluene–3% w/v sodium caseinate (CAS, black) and toluene–3% w/v Ca<sup>2+</sup>-cross-linked caseinate particles (Ca-CAS, red) at neutral pH (6.9 ± 0.1) and 20 °C. Error bars represent the standard deviation from triplicates. .... 132

**Figure 4-4:** Negative staining transmission electron microscopy images (20.5kx magnification) of (A) 0.03 % w/v sodium caseinate (CAS), (B) 0.03 % w/v Ca<sup>2+</sup>-cross-linked caseinate (Ca-CAS) particles, (C) interface of 10 % v/v toluene emulsion droplet stabilised by 3 % w/v CAS and (D) interface of 10 % v/v toluene emulsion droplet stabilised by 3 % w/v Ca-CAS. Scale bars are 500 nm. .... 135

**Figure 4-5:** Small-angle neutron scattering profiles of (A) the deuterated toluene emulsion stabilised by sodium caseinate and (B) the deuterated toluene emulsion stabilised by Ca<sup>2+</sup>-cross-linked sodium caseinate particles. SANS measurements were performed in 12%, 40% (highlighting the scattering of oil droplets by matching out the scattering of the proteins) and 89% (highlighting the scattering of the protein shell by matching out the scattering of the oil

droplets) deuterium oxide (D<sub>2</sub>O). The scattering curves shown in A and B (on the absolute scale) have been shifted vertically for clarity in C and D, respectively. The solid black lines are the unified fits to the scattering data. .... 139

**Figure 5-1:** Droplet size distributions of freshly prepared droplet-stabilised emulsions (DSE) in 12% (—■—), 40% (—●—), 60% (—▲—), and 89% D<sub>2</sub>O (—▼—) and the DSE in 89 % D<sub>2</sub>O (—◆—) after 72 hours..... 154

**Figure 5-2:** Scattering curves of the DSE measured by (a) USANS and (b) SANS in the solvent containing 12 % (—●—), 40 % (—■—), 89 % (—▲—), and 60 % (—▼) D<sub>2</sub>O. (c) The intensity of DSE at selective  $Q$  as the function of D<sub>2</sub>O concentration; the solid red line represents the linear fit of the intensity value obtained at the fixed  $Q$  and various D<sub>2</sub>O concentration, the arrow guides the calculated contrast matching point (62.5 % D<sub>2</sub>O) of the DSE. (d) USANS kinetic scattering curves of DSE in 89 % D<sub>2</sub>O from 3 – to 2301 min after addition of the  $d$ -toluene into the aqueous phase, and the solid red line represents the power-law fit; inset is the optical microscopy image of the fresh DSE in 89 % D<sub>2</sub>O. .... 158

**Figure 5-3:** (a) Droplet size distribution of the Ca-CAS-stabilised soy-oil emulsion (—■—) and of the Ca-CAS-stabilised  $d$ -toluene emulsion at 3 min (—●—), 240 min (—▲—) and 360 min (—▼—) after preparation. (b) USANS scattering curves of the Ca-CAS-stabilised soy-oil emulsion (diamond symbols) and Ca-CAS-stabilised  $d$ -toluene emulsion (circle symbols) during time from 3 to 392 min after addition of the  $d$ -toluene into the aqueous phase; the solid red line indicates the power-law fit..... 161

**Figure 5-4:** (a) Intensity at  $Q = 9 \times 10^{-5} \text{ \AA}^{-1}$  of pure  $d$ -toluene emulsion (—●—), pure soy-oil emulsion (—▲—) at 3 min after preparation, and intensity decay curve of the mixed soy-oil/ $d$ -toluene emulsion (—■—) as function of time at  $Q = 9 \times 10^{-5} \text{ \AA}^{-1}$  by USANS single-point method. (b) USANS kinetics scattering curves of the mixed soy-oil/ $d$ -toluene emulsion (—●—)

for 15 – 493 min after mixing two emulsions. (c) the intensity decay curve of the mixed soy-oil/*d*-toluene emulsion (—■—) as function of time at  $Q = 9 \times 10^{-5} \text{ \AA}^{-1}$ ; the solid red lines indicate the power-law fit. (d) The droplet size distribution of mixed soy-oil/*d*-toluene emulsion for 1 – 300 min after mixing two emulsions. (e-g) Optical microscopy images of the mixed soy-oil/*d*-toluene emulsion for 3, 15 and 120 min after mixing two emulsions, scale marks the diameter of the selective *d*-toluene droplet, and the red square indicates the presence of soy-oil droplets..... 166

**Figure 5-5:** Theoretical calculated corresponding D<sub>2</sub>O volume concentration (%) used for contrast matching of DSE is plotted as a function of varying the volume concentration *d*-toluene (%) in DSE. The maximum volume concentration *d*-toluene (%) in DSE is the volume of *d*-toluene added into the emulsion prior to homogenisation. The horizontal red line indicates the experimentally determined contrast matching point of DSE after homogenisation, and the vertical blue line indicates the calculated volume concentration *d*-toluene (%) in DSE after homogenisation..... 171

**Figure 6-1:** (A) The representative particle size distribution of Ca<sup>2+</sup> cross-linked caseinate particles (protein particles, ★) were measured by static light scattering and droplet size distributions of different emulsions before gastric digestion: the protein particle-stabilised small-sized emulsion (Small emulsion, ■), protein particle-stabilised large-sized emulsion (Large emulsion, ▼), small droplet-stabilised emulsion (DSE, ●) and the protein-stabilised emulsion containing small- and large-sized emulsion (PSE, ▲). The solid symbols represent the emulsion in the absence of sodium dodecyl sulphate (SDS), and the open symbols represent the emulsion in the presence of SDS. Confocal images of (B) 40×-magnification and (C) high-magnification of the DSE (upper row) and the PSE (bottom row); red colour represents the oils and green colour represents the proteins. The scale bar is 20 μm. .... 188



**Figure 6-2:** Droplet size ( $d_{4,3}$ ) of (A) the gastric digesta and (B) the gastric chyme of the droplet-stabilised emulsion (DSE, ●) and the protein-stabilised emulsion (PSE, ▲). The solid symbols represent the samples in the absence of sodium dodecyl sulphate (SDS) and the open symbols represent the samples in the presence of SDS. Error bars represent standard deviations from triplicates. .... 192

**Figure 6-3:** Confocal images of the gastric digesta and the gastric chyme of the droplet-stabilised emulsion (DSE) and the protein-stabilised emulsion (PSE) after 5–240 min of gastric digestion. Red colour represents the oils and green colour represents the proteins. The scale bar is 20  $\mu\text{m}$ . .... 196

**Figure 6-4:** Oil contents of the droplet-stabilised emulsion (DSE) and the protein-stabilised emulsion (PSE) before digestion (0 min) and of the gastric digesta at different digestion times (20–240 min). Error bars represent standard deviations from triplicates. .... 199

**Figure 6-5:** (A) Droplet size distributions of the droplet-stabilised emulsion (DSE, —) and the protein-stabilised emulsion (PSE, ---) during *in vitro* small intestinal digestion. (B) Confocal images of the DSE (left-hand column) and the PSE (right-hand column) during *in vitro* small intestinal digestion. Red colour represents the oils and green colour represents the proteins. The scale bar is 20  $\mu\text{m}$ . .... 202

**Figure 6-6:** Free fatty acid release profiles of the droplet-stabilised emulsion (DSE, solid black line) and the protein-stabilised emulsion (PSE, solid grey line) during *in vitro* small intestinal digestion. The solid lines represent the experimental data determined by pH-stat titration and the dashed lines represent the model data that were superimposed on the experimental data. Error bars represent the standard deviations from triplicate. .... 205

**Figure 7-1:** (a) The zeta-potential of Ca-CAS dispersions and Ca-CAS-stabilized nano-sized primary emulsions at pH 7.0 and 5.8; (b) particles size distributions of Ca-CAS dispersions and

Ca-CAS-stabilized nano-sized primary emulsions at pH 7.0 and 5.8; (c) droplet size distributions of Ca-CAS particle stabilized-emulsion (PSE) at pH 7.0 and 5.8 in the absence and presence of SDS; (d) droplet size distributions of droplet stabilized-emulsion (DSE) at pH 7.0 and 5.8 in the absence and presence of SDS.....225

**Figure 7-2:** Appearance of concentrated emulsion with 70% of oil volume fraction in the sealed inverted glass vials for (-1) 0 day and (-2) 30 days. Emulsion stabilized by (a) Ca-CAS at pH 7.0, (b) Ca-CAS at pH 5.8, (c) primary emulsion at pH 7.0, and (d) primary emulsion at pH 5.8. (e) The average droplet size ( $d_{4,3}$ ) of PSE and DSE at pH 7.0 and 5.8 as a function of a storage time for 0, 7, 14 and 30 days. (f) The average droplet size ( $d_{4,3}$ ) of PSE and DSE at pH 7.0 and 5.8 as a function of a storage time for 0, 7, 14 and 30 days in the presence of SDS.227

**Figure 7-3:** 63× Magnification confocal images of concentrated emulsion with 70 % of oil volume fraction that stabilized by (a) Ca-CAS at pH 7.0, (b) Ca-CAS at pH 5.8, (c) primary emulsion droplets at pH 7.0, and (d) primary emulsion droplets at pH 5.8 for (-1) 0, (-2) 10 and (-3) 30 days aging. Red colour represents the oil phase stained by Nile red and green colour represents the protein stained by fast green. Scale bar is 20  $\mu\text{m}$ . Insets are associated zoom-in images with scale bar of 10  $\mu\text{m}$ . .....229

**Figure 7-4:**  $G'$  (solid symbols) and  $G''$  (open symbols) as (a) a function of frequency and (b) as a function of the strain for concentrated emulsion PSE (stabilized by Ca-CAS) and DSE (stabilised by primary emulsion) at pH 5.8 and pH 7.0 at (1) 0 day and (2) 30 days aging. (c) Complex modulus  $G^*$  (1Hz) and (d) breaking stress of PSE and DSE at pH 7.0 and 5.8 as the function of aging time. ....236

**Figure 7-5:** Appearance (left panel) of 70 % concentrated emulsions stabilized by (a) Ca-CAS at pH 7.0, (b) Ca-CAS at pH 5.8, (c) primary emulsion at pH 7.0, and (d) primary emulsion at pH 5.8 in the inverted seal glass vials after heating in oven at 80 °C for 30 min. The average

droplet size ( $d_{4,3}$ ) of PSE and DSE at pH 7.0 and 5.8 before and after heating (e) with the absence of SDS and (f) with the presence of SDS. 63× Magnification confocal images of concentrated emulsion that stabilized by (G) Ca-CAS at pH 7.0, (h) Ca-CAS at pH 5.8, (i) primary emulsion droplets at pH 7.0, and (j) primary emulsion droplets at pH 5.8 after heating. Scale bar is 20  $\mu\text{m}$ . Insets are associated zoom-in images with scale bar of 10  $\mu\text{m}$ . .....239

**Figure 7-6:** (a) The frequency dependence, (c) strain amplitude behaviour, and (e) viscosity of  $G'$  (solid symbols) and  $G''$  (open symbols) for concentrated emulsion stabilized by Ca-CAS and primary emulsion at pH 5.8 and pH 7.0 after heating at 80 °C for 30 min. (b) The complex moduli  $G^*$  (1Hz), (d) breaking stress and (f) intermediate shear rate ( $1 \text{ s}^{-1}$ ) viscosity for PSE and DSE at pH 7.0 and 5.8 as the function of temperature at 25 and 80 °C.....242

**Figure S 3-1:** Sodium dodecyl sulfate polyacrylamide gel electrophoresis patterns of nonaggregated whey proteins in the supernatant after the centrifugation of WPM-NPB particles. Heated whey protein aggregate dispersions were washed with Milli-Q water five times (from left to right).  $\beta$ -Lactoglobulin (BLG) and  $\alpha$ -lactalbumin (ALA) bands are indicated. ....105

**Figure S 3-2:** (A) Dynamic interfacial tension (IFT) and (B) interfacial tension decay rate ( $\text{IFT}/\text{IFT}_0 = \text{interfacial tension}/\text{interfacial tension at time zero}$ ) as a function of time. ( $\text{---}\blacktriangle\text{---}$ ), soya oil and Milli-Q water; ( $\text{---}\blacksquare\text{---}$ ), 10 wt% WPM-NPB particle dispersion; ( $\text{---}\square\text{---}$ ), 10 wt% WPM-PB particle dispersion; ( $\text{---}\bullet\text{---}$ ), PE-NPB; ( $\text{---}\circ\text{---}$ ), PE-PB. The first 250 s decay of interfacial tension is indicated by the vertical dotted line..... 106

**Figure S 3-3:** Average size  $D_{32}$  (solid symbols) and  $D_{43}$  (open symbols) of DSEs stabilized with PE-NPB (black) and PE-PB (red) as a function of the concentration of the PE at 10, 30, and 60 wt%. .... 107

**Figure S 3-4:** Intensity at fixed  $q$  value plotted as a function of the concentration of PE in the aqueous phase. The blue, red, and black symbols represent the intensities at  $q$  values of  $2.4 \times 10^{-4}$ ,  $1.0 \times 10^{-4}$ , and  $5.5 \times 10^{-5} \text{ \AA}^{-1}$ , respectively. The linear regression fits are represented as dotted lines in corresponding color..... 108

**Figure S 4-1:** Particle size intensity distribution of  $\text{Ca}^{2+}$ -cross-linked caseinate (Ca-CAS) particle dispersions at protein concentrations of 0.5 (black), 1.5 (red) and 3.0% w/v (blue) at neutral pH ( $7.0 \pm 0.1$ ) and  $20 \text{ }^\circ\text{C}$  from ZetaSizer dynamic light scattering intensity measurements..... 143

**Figure S 6-1:** Illustration of the set-up for the human gastric simulator.....209

**Figure S 6-2:** Changes in pH during gastric digestion of the droplet-stabilised emulsion (DSE, ●) and the protein-stabilised emulsion (PSE, ▲). Error bars represent standard deviations from triplicates.....210

**Figure S 6-3:** Average droplet size ( $d_{4,3}$ ) of the droplet-stabilised emulsion (DSE, ●) and the protein-stabilised emulsion (PSE, ▲) during *in vitro* small intestinal digestion. Error bars represent standard deviations from triplicates. ....211

**List of Abbreviations**

BSA	Bovine serum albumin
CAS	Sodium caseinate
Ca-CAS, CaCas	Ca <sup>2+</sup> -cross-linked sodium caseinate particles
CM	Micellar casein
CLSM	Confocal laser scanning microscopy
Cryo	Cryogenic
CV	Contrast variation
DLS	Dynamic light scattering
D <sub>2</sub> O	Deuterium oxide
DSC	Differential scanning calorimetry
DSE	Droplet-stabilised emulsion
FFA	Free fatty acid
GI	Gastro-intestinal
GNP	Gold nanoparticles
HGS	Human gastric simulator
HLB	Hydrophilic-lipophilic balance
IFT, $\gamma$	Interfacial tension
IEP	Isoelectric point
LVR	Linear viscoelastic region
LMWE	Low-molecular-weight emulsifier
MPC	Milk protein concentrate
O/W	Oil-in-water
PB	Phosphate buffer
PC	Phosphatidylcholine
PDI	Polydispersity index
PDMS	Polydimethylsiloxane
PE	Primary emulsion
PNIPAM-co-MAA	poly ( <i>n</i> -isopropylacrylamide)- <i>co</i> -methacrylic acid polymers
PSE	Protein-stabilised emulsion
WPI	Whey protein isolate
WPM	Whey protein microgel particle
W/O	Water-in-oil
SAS	Small-angle scattering
SANS	Small-angle neutron scattering
SAXS	Small-angle X-ray scattering
SLD	Scattering length density
SEM	Scanning electron microscopy
SLN	Solid lipid nanoparticle
SDS	Sodium dodecyl sulphate
SLS	Static light scattering
SGF	Simulated gastric fluid
SIF	Simulated intestinal fluid
USAXS	Ultra-small-angle X-ray scattering
USANS	Ultra-small-angle neutron scattering
TEM	Transmission electron microscopy
<i>d</i> -toluene	Deuterated toluene

**List of Peer-reviewed Publications**

Cheng, L., Ye, A., Hemar, Y., Gilbert, E. P., de Campo, L., Whitten, A. E., & Singh, H. (2019). Interfacial structures of droplet-stabilized emulsions formed with whey protein microgel particles as revealed by small- and ultra-small-angle neutron scattering. *Langmuir*, 35(37), 12017–12027. <https://doi.org/10.1021/acs.langmuir.9b01966>

Cheng, L., Ye, A., Hemar, Y., & Singh, H. (2022). Modification of the interfacial structure of droplet-stabilised emulsions during in vitro dynamic gastric digestion: Impact on in vitro intestinal lipid digestion. *Journal of Colloid and Interface Science*, 608, 1286–1296. <https://doi.org/10.1016/j.jcis.2021.10.075>

Cheng, L., Ye, A., Yang, Z., Gilbert, E. P., Knott, R., de Campo, L., Storer, B., Hemar, Y., & Singh, H. (2022). Small-angle X-ray scattering (SAXS) and small-angle neutron scattering (SANS) study on the structure of sodium caseinate in dispersions and at the oil-water interface: Effect of calcium ions. *Food Structure*, 32(April), 100276. <https://doi.org/10.1016/j.foostr.2022.100276>

## **Chapter 1 Introduction**

Emulsions are typically a mixture of two immiscible liquid phases (e.g., oil and water), where one liquid phase is dispersed in the other as droplets of few nm to few  $\mu\text{m}$  size (Lu & Weitz, 2013). Emulsions are widely used in a range of applications, from petroleum, cosmetics, pharmaceuticals to foods (Raya et al., 2020; Tan & McClements, 2021; Yukuyama et al., 2016). During droplet formation, a large amount of interfacial area and interfacial free energy is generated as the droplet size decreases. To kinetically stabilize emulsion and prevent phase separation, emulsifiers (e.g., surfactants, proteins) are needed. Emulsifiers typically have amphiphilic properties, can rapidly adsorb to the interfaces between oil and water phases, reduce the interfacial tension, and form an interfacial layer on the droplet surface.

The interfacial layer formed by proteins is typically several nanometres thick and can be regarded as a separate pseudo-phase of the emulsion, protecting the droplets from aggregation and coalescence through steric and/or electrostatic repulsions. Hence, the physicochemical properties and stability of emulsions are largely related to the composition and structure of the interfacial layer. A considerable amount of research has been done to understand these phenomena to rationalize the design of functional interfaces and to improve the performance of emulsions. Examples of recent advances in interfacial design for food emulsions include the development of multi-layered interfaces (Dickinson, 2011; Guzey & McClements, 2006), the chemical modification of adsorbing proteins (Delahaije et al., 2013), as well as particle-stabilized interfaces (Dinsmore et al., 2002) to increase emulsion functionality. For the latter one, stabilising the interface with particles is an established approach commonly known as Pickering stabilisation.

A variety of particle emulsifiers have been developed, such as rigid and soft protein-based particles (e.g., whey protein microgels vs. casein particles) (Davidov-Pardo et al., 2015; Destribats et al., 2014; Li et al., 2013b; Li & Ngai, 2013; Lv et al., 2020; Shi et al., 2020; Su et al., 2018; Xu et al., 2020b; Yan et al., 2020; Zhang et al., 2021b), as well as solid and soft lipid-based particles (e.g., fat crystals, tripalmitin, *n*-hexadecane) (Gupta & Rousseau, 2012; Liu & Tang, 2014; Pawlik et al., 2016; Sakellari et al., 2021; Ye et al., 2013b). It is known from previous studies that the soft gel particles show better emulsification performance than rigid particles (Richtering, 2012) and that the interfacial layer stabilised by soft protein particles or soft lipid particles (or known as primary droplet) (Guo et al., 2021; Wang et al., 2018; Ye et al., 2013b) is fully covered and denser than that by solid protein particles or solid lipid particles (Araiza-Calahorra & Sarkar, 2019; Destribats et al., 2014; Liu & Tang, 2014; Pawlik et al., 2016; Sakellari et al., 2021). The primary droplet with casein micelle layer has been demonstrated to form a network structure at the interface (Ye et al., 2013b). Based on the hypothesis that soft droplets can deform and relax mechanical stresses better than solid particles, it is believed that soft primary droplets can bring new interfacial properties and potential functional advantages. However, to date, very few studies have been conducted on soft lipid particles (protein coated oil droplets). The mechanism of droplet-stabilised emulsion formation and their physicochemical properties in response to environmental conditions has not been fully understood. Therefore, there is still much to learn about designing new soft lipid particles used for interfacial modifications and potential functions.

The overall aim of this study is therefore to provide in-depth characterisation of the properties of droplet-stabilised emulsion including the bulk emulsion's characteristics (e.g., viscoelasticity), droplet characteristics (e.g., size and composition), and interfacial characteristics (e.g., composition, charge, thickness, and structure), as well as oil molecules



diffusion between droplets. Different protein structures are used to rationalise the design of new soft lipid particles, i.e., when protein microgel coated primary droplets in **Chapter 3** and casein particle coated primary droplets in **Chapter 4** to **Chapter 7** to obtain different interfacial structures in the resultant droplet-stabilised emulsion. The general process for preparing the droplet-stabilized emulsions is a 2-steps emulsification as shown in **Figure 1-1**, in which the primary droplet is produced by a high-pressure homogeniser and the final droplet-stabilised emulsion is prepared by a high-speed rotor-station mixer/ultra-turax.

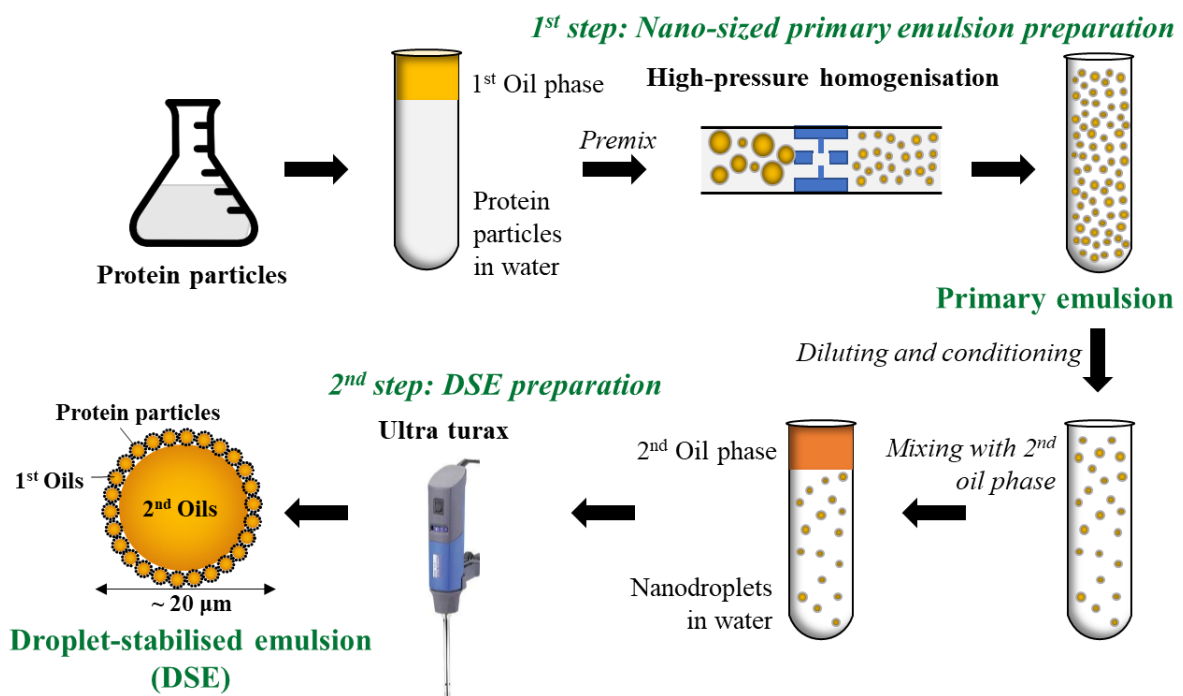


**Figure 1-1:** Preparation of droplet-stabilized emulsions (DSE) by 2-steps emulsification.

The use of emulsion-based delivery systems for functional foods has also been developed in food applications, as emulsions are ideal carriers for a variety of micronutrients and provide controlled delivery during consumption and digestion (Tan & McClements, 2021). Oil-in-water emulsions stabilised by soft droplets gave rise a novel interfacial layer structure and could potentially co-deliver two or more active substances in one vehicle (Hettiarachchi et al., 2009; Sakellari et al., 2021). For utilising the hierarchical emulsion as delivery vehicles and control the release rate and site of the bioactive compounds, it is important to understand the mass transport between the adsorbed primary droplet and the core droplet.

Droplet coalescence and Ostwald ripening are two well established mechanisms accounting for oil transfer between two droplets which involving droplet size increment over time. The oil molecules are generally considered to be isolated from adjacent droplets by thick surfactant or particle interfacial films as droplet coalescence and Ostwald ripening strongly hindered. However, a third mechanism of contact ripening (oil molecules transfer across the interface) has been reported in emulsion stabilised with sufficient surfactant loading when there are no coalescence and Ostwald ripening (Roger et al., 2015). Factors, such as the oil phase solubility in the aqueous phase (McClements & Dungan, 1993; Webster & Cates, 1998), collision and direct contact between droplets (Lee & Pozzo, 2019; Malassagne-Bulgarelli & McGrath, 2009; Roger et al., 2015) are reported to affect the oil exchange kinetics. By studying oil exchange in emulsions stabilised by primary droplets coated by protein particles, in **Chapter 5**, the understanding of the contact ripening mechanism will be extended to protein particle interfacial films. Previously, the oil exchange between droplets were studied using differential scanning calorimetry (DSC) to monitor the changes in crystallisation temperature (McClements et al., 1992; McClements & Dungan, 1993). More recently, contrast-variation small-angle neutron scattering (CV-SANS) has been employed to determine the rate of oil exchange between

insoluble oil droplets (Lee & Pozzo, 2019; Roger et al., 2015). The unique advantage of CV-SANS utilized as a molecular-transportation characterization techniques arises from the difference in neutron scattering length densities (SLDs) between hydrogenated and deuterated oil molecules (Gilbert, 2019; Lopez-Rubio & Gilbert, 2009). This allows researchers to directly observe oil composition changes in the droplet in situ without extensive sample preparations or additional molecular labelling. Therefore, advanced techniques of contrast-variation ultra-small angle scattering (CV-USANS) and CV-SANS, along with microscopy and particle sizing techniques are used to measure oil composition in **Chapter 5**. In addition, the structure of particles and interfacial layer in **Chapter 3** to **Chapter 5** were also quantified using USANS/SANS, as well as using small-angle X-ray scattering (SAXS).

During the digestion process, conventional simple emulsions stabilised with proteins are subjected to the destabilisation due to mechanical shear, acidification, enzymatic hydrolysis, and bile salt replacement of emulsifiers, resulting structure changes in disintegration, aggregation, coalescence, and droplet shrinkage. The structures (aggregation or coalescence) induced during gastric digestion destabilisation are affected by the protein structures and compositions at the interface, which in turn affect the rate of free-fatty acid release in the small intestinal digestion (Wang et al., 2019). Thus, by modifying the interfacial layer composition of emulsions from simply protein layer to droplet layer, it is possible to alter the emulsion droplet aggregation and coalescence behaviour in response to the acidification and enzymatic digestion, thereby affecting the rate of lipid digestion. However, information on the structural changes of droplet-stabilised emulsions during digestion is missing, and there is a need to fill this gap by studying the droplet stability and lipolysis kinetics of droplet-stabilised emulsion using *in vitro* dynamic gastric digestion model and *in vitro* static digestion (**Chapter 6**).

Concentrated emulsions, as a model system for semi-solid foods, have drawn increasing interests in investigating the relationship between the droplet characteristics and their rheological properties. Factors affecting the emulsion rheology and stability have been widely discussed in the literature. Typically, the volume fraction of the disperse phase, the droplet size distribution, the viscosity of both the dispersed and the continuous phases are usually applied to modify the bulk viscoelasticity of the emulsions. Nevertheless, the ratio between the interfacial layer thickness to the droplet diameter has been suggested to play an important role in influencing the effective volume fraction of dispersed phase and the bulk viscoelasticity of the emulsion (Mason, 1999; Pal, 1996; Tadros, 1994). In the case where the interfacial layer consists of primary droplets, the thickness of the interfacial layer is expected to be significant, and the effective volume fraction of the dispersed phase is expected to increase. Furthermore, the possible deformation of the primary droplets and the interaction between the adsorbed primary droplets may affect the reconstruction of the spatial structure of the emulsion under shear. It is therefore worthwhile to fill this gap by investigating the rheological properties of emulsions stabilised with soft primary droplets (**Chapter 7**).

---

## Chapter 2 Literature review

This chapter provides a review of emulsions formation, conventional emulsifiers, rigid and soft protein-based particle emulsifiers, solid and liquid lipid-based particle emulsifiers, emulsion rheology, mechanisms of emulsion instability, as well as techniques and methods used in the studies of emulsion structure, including microscopy, light scattering, and advanced small-angle scattering (SAS) techniques.

### 2.1 Emulsion formation and interfaces

An emulsion is a colloidal dispersion that consists of two immiscible phases such as water and oil. One phase exists as discrete droplets referred to as the dispersed phase, while the other phase that constitutes the surrounding liquid is called the continuous phase. Emulsion formation is a highly dynamic process that converts two separate immiscible liquid to a dispersion containing small droplets. In food emulsions, the droplet size generally ranges between 0.1 to 100  $\mu\text{m}$  (McClements, 2015b). The breakdown of the oil phase is usually carried out using high-energy methods, for example, ultra-turraxing (Rotor-stator mixing, sonication, and high-pressure valve homogenizers). As the oil phase breaks down into small droplets, the total interfacial area in the system increases, and this interfacial area is related to the oil volume fraction and droplet size. The specific surface area,  $A_{spec}$  ( $\text{m}^2/\text{g}$  oil), of the dispersed phase is generally large as several  $\text{m}^2/\text{g}$  oil, which can be simply calculated from the droplet radius,  $R$  ( $\mu\text{m}$ ), and the dispersed phase density,  $\rho$  ( $\text{g/mL}$ ), using **equation (2-1)** (Gallet et al., 2009):

$$A_{spec} = \frac{3}{R\rho} \quad (2-1)$$

With the increased contact between the oil and water phase, the formed emulsions are thermodynamically unstable because the overall free energy in the system increases as shown in **equation (2-2)** (Walstra et al., 2005):

$$\Delta G = \gamma \Delta A \quad (2-2)$$

where  $\gamma$  (N/m) is the interfacial tension between the two immiscible phases and  $\Delta A$  (m<sup>2</sup>) is the change in the surface area in the system.

As shown in the **equation (2-2)**, the high free energy is unfavourable, due to  $\gamma$  (N/m), between oil and water, because water molecules can form strong hydrogen bonds with other water molecules, but not with oil molecules. Thus emulsion tend to reduce the surface area,  $\Delta A$  (m<sup>2</sup>), between the two immiscible liquids by separating into a thermodynamic stable system made of an oil and water layers (Dalgleish, 1997; McClements, 2015a).

To create a kinetically metastable emulsion that remains stable for a reasonable time (e.g., from a few days to several years) to provide the desired product quality during the shelf life, the addition of emulsifiers prior to homogenization is needed. Emulsifiers are surface-active molecules that adsorb onto the surface of the newly formed droplets during homogenization and form a protective layer preventing the droplets from coming close enough together to coalesce (Boyd et al., 1972; Dalgleish, 1997). Most emulsifiers are amphiphilic molecules having polar and nonpolar regions distributed on the same molecule. The amphiphilic molecules can adopt an orientation where the hydrophobic part adsorbs to the oil phase, while the hydrophilic part stays in water (Walstra et al., 2005; Zhai et al., 2011). The decrease in the contact between the oil and water molecules at the interface, reduces the interfacial tension. When the interfacial tension is lowered, the droplet break-up during homogenization is more favourable and smaller droplets are formed.

Depending on the hydrophilic-lipophilic balance (HLB) of the emulsifier in use, emulsion can be water-in-oil (W/O) or oil-in-water (O/W) systems (Aveyard et al., 1986; Boyd et al., 1972). Emulsifiers with high HLB values are more hydrophilic and therefore more conducive to stabilizing O/W emulsions, while emulsifiers with low HLB values are more conducive to forming W/O emulsions. As most of the emulsifiers available for food applications are water-soluble, O/W emulsion products are more abundant in food than W/O emulsions. Examples of food O/W emulsions include milk, infant formula, soups, salad dressings, ice cream, chocolate ganache, cream, and mayonnaise, which vary in oil content between 3-80 %. A typical example of W/O emulsion is margarine that usually contains high oil content of 80%. The various oil fractions of the emulsion contribute to a wide range of rheological properties of the product, which in turn affects its functional properties and practical applications (e.g., processability, stability, mouthfeel, and biological response) (Akbari & Nour, 2018; Camacho et al., 2015; Liu et al., 2019; Tadros, 2013b; van Aken et al., 2011; Zembyla et al., 2020; Zhu et al., 2019).

### **2.2 Conventional emulsifiers**

Conventional emulsifiers used to stabilise food emulsions commonly fall into two main categories: low-molecular-weight emulsifiers (LMWEs) and amphiphilic biopolymers. LMWEs are small molecules (also known as surfactants) which can be natural or synthetic and they have molecular weights ranging from approximately 250 g/mol to approximately 1200 g/mol (Kralova & Sjöblom, 2009; McClements & Gumus, 2016). Examples of synthetic food-grade LMWEs are Tweens, Spans, and DATE, while LMWEs of natural origin (e.g., animal, plant, or microbial based) include saponins, glycolipids, and phospholipids (often available as lecithins). LMWEs typically have a hydrophilic head, which can be non-ionic but polar (e.g., Tween 20) or fully charged (e.g., lecithin), and a hydrophobic tail with at least one acyl chain. LMWEs are known to be particularly effective at reducing interfacial tension and are highly

mobile at the interface, so they can rapidly coverage the newly created oil-water interface during the emulsification process (Kralova & Sjöblom, 2009). Given their high interfacial activity, LMWEs are commonly used for small droplet or even nanoemulsion (< 100 nm) formation (Amagliani et al., 2022; Dammak et al., 2020).

Most amphiphilic biopolymers used as food emulsifiers are proteins. Considerable studies on the interfacial behaviour of proteins in food emulsions are related to milk proteins (whey proteins and caseins) (Demetriades et al., 1997a, 1997b; Hu et al., 2003; Schröder et al., 2017) or to individual protein molecules (e.g.,  $\alpha$ -lactalbumin,  $\beta$ -lactoglobulin,  $\alpha_s$ -casein and  $\beta$ -casein) (Dickinson et al., 1988b, 1989; Zhai et al., 2011). Upon adsorption to the oil-water interface, the conformational change of many proteins occurs, which creates a two-dimensional network of protein aggregates in the interfacial layer that has sufficient mechanical strength to resist deformation and coalescence of the droplets (Beverung et al., 1999; Dickinson, 2003; McClements et al., 1993b; Monahan et al., 1996; Norde, 1986). Upon adsorption at the interface, soft and flexible  $\beta$ -casein experiences a rapid conformational change, whereas compact  $\beta$ -lactoglobulin may undergo a conformational rearrangement after adsorption over a longer time (Damodaran, 2006; Dickinson, 1992b; Wilde et al., 2004). The physical properties of protein-based interfacial layers in emulsions, such as thickness, viscoelasticity, and mechanical resistance, are influenced by the structure and flexibility of the proteins. For example, flexible and disordered proteins (such as caseins) form thicker but less dense interfacial layers at the oil-water interface, while rigid and globular proteins (such as  $\beta$ -lactoglobulin) form dense interfacial layers (Dickinson, 1992b).

The characteristics of interfaces stabilised by LMWEs and by proteins have been reported and compared in previous studies (Bos & Vliet, 2001; Tcholakova et al., 2008; Wilde et al., 2004). The interfacial layer stabilised by LMWEs has been described as more close-packed,



and fluid than proteins, whereas proteins tend to form immobile, viscoelastic interfacial films (Dickinson, 1992b; Grigoriev & Miller, 2009; Wilde et al., 2004). The interface thickness is typically few nanometres for both types of emulsifiers (Dickinson, 2009; Singh, 2011), and the surface load is generally  $\sim 1\text{--}2\text{ mg/m}^2$  for LWMEs and  $2\text{--}3\text{ mg/m}^2$  for proteins (Bos & Vliet, 2001). In real food emulsions, a mixture of LWMEs (Tween 20 or soy lecithin) and biopolymers (whey protein isolate,  $\beta$ -lactoglobulin, sodium caseinate, or  $\beta$ -casein) is usually used to form a finer emulsion. However, there is a competitive adsorption between proteins and LWMEs, and the LWMEs interfere with the viscoelastic protein-adsorbed layer, resulting in an emulsion with reduced stability (Mackie et al., 1996; MacKie et al., 1993; Mao et al., 2009; Xue & Zhong, 2014). For example, emulsions stabilized by milk proteins tend to coalesce under turbulent shearing in the presence of Tweens, because the presence of surfactant increases the mobility of the interfacial layer and sensitivity to disruption (Dickinson et al., 1993; Nambam & Philip, 2012). However, high hydrostatic pressure-induced flocculation in concentrated whey protein-stabilised emulsion can be reduced by the addition of Tween 20 (Dickinson & James, 1999). The principle of competitive adsorption between LWME and biopolymers combined with processing conditions can be used as a mean to manipulate the microstructure of milk proteins stabilized emulsions.

### 2.3 Particle emulsifiers

Emulsions stabilised by particles and not conventional emulsifier molecules have been referred to as Pickering emulsions since the pioneering work of Ramsden (1904) (Ramsden, 1904) and Pickering (1907) (Pickering, 1907). The similarities and differences between particles and conventional emulsifiers in emulsion stabilisation have been discussed intensively in the literature (Binks, 2002; Binks & Rodrigues, 2007; Dickinson, 2009; Tcholakova et al., 2008). Regardless of the type of emulsifying agent, once the emulsion is made, the one major

factor determining its coalescence stability is the steric barriers between the droplet surfaces. When the concentration of the emulsifying agent is low and electrostatic interactions are largely suppressed, the initially formed droplets tend to coalesce rapidly, until their surfaces are sufficiently protected by a stabilizing layer of particles or molecules. This is usually accompanied by some bridging flocculation due to sharing of adsorbed particles or macromolecules amongst neighbouring droplets. At a high concentration of emulsifying agent, the inter-droplet repulsive interactions and the thickness of the stabilizing layer are sufficient to provide a stable emulsion (Dickinson, 2009).

One of the major advantages of Pickering emulsion over conventional emulsion is the long-term stability. For Pickering emulsion, three factors in generally govern the particles that reside at the interface forming a steric barrier that efficiently prevents the interfacial layer rupture: (1) particle size must be considerably small compared to the droplet size (Binks & Lumsdon, 1999); (2) particles should weakly flocculate to achieve efficient interfacial coverage (Aveyard et al., 2003); (3) particles used must partially be wetted by both emulsion phases (Finkle et al., 1923). The position of a particle at the oil-water interface depends on its relative affinity for both phases, which can be characterized by the contact angle (noted  $\theta$ , °), as shown in **Figure 2-1a** (Binks, 2002). Particles will bend the interface toward their lower affinity phase, i.e., particles preferentially wetted by water are suitable for forming O/W emulsion, while particles preferentially wetted by oil are suitable for forming W/O emulsions (**Figure 2-1b**). The free energy of spontaneous desorption of particles (noted  $\Delta G_D$ , J) has been proposed to be related to  $\theta$ , the interfacial tension (noted  $\gamma$ , N/m) as well as the particle radius (noted  $R$ , m) as shown in (2-3) (Aveyard et al., 2003; Berton-Carabin & Schroën, 2015; Binks, 2002; Chevalier & Bolzinger, 2013; Leal-Calderon & Schmitt, 2008):

$$\Delta G_D = \pi\gamma r^2(1 - |\cos \theta|)^2 \quad (2-3)$$

This means that, if  $\theta$  is not too close to  $0^\circ$  (or  $180^\circ$ ), the predicted value of  $\Delta G_D$  for a particle of colloidal size is large compared with the thermal energy ( $k_B T$ , J) as depicted in **Figure 2-1c**; hence the particle is effective for permanent adsorption, giving the emulsion outstanding long-term stability.

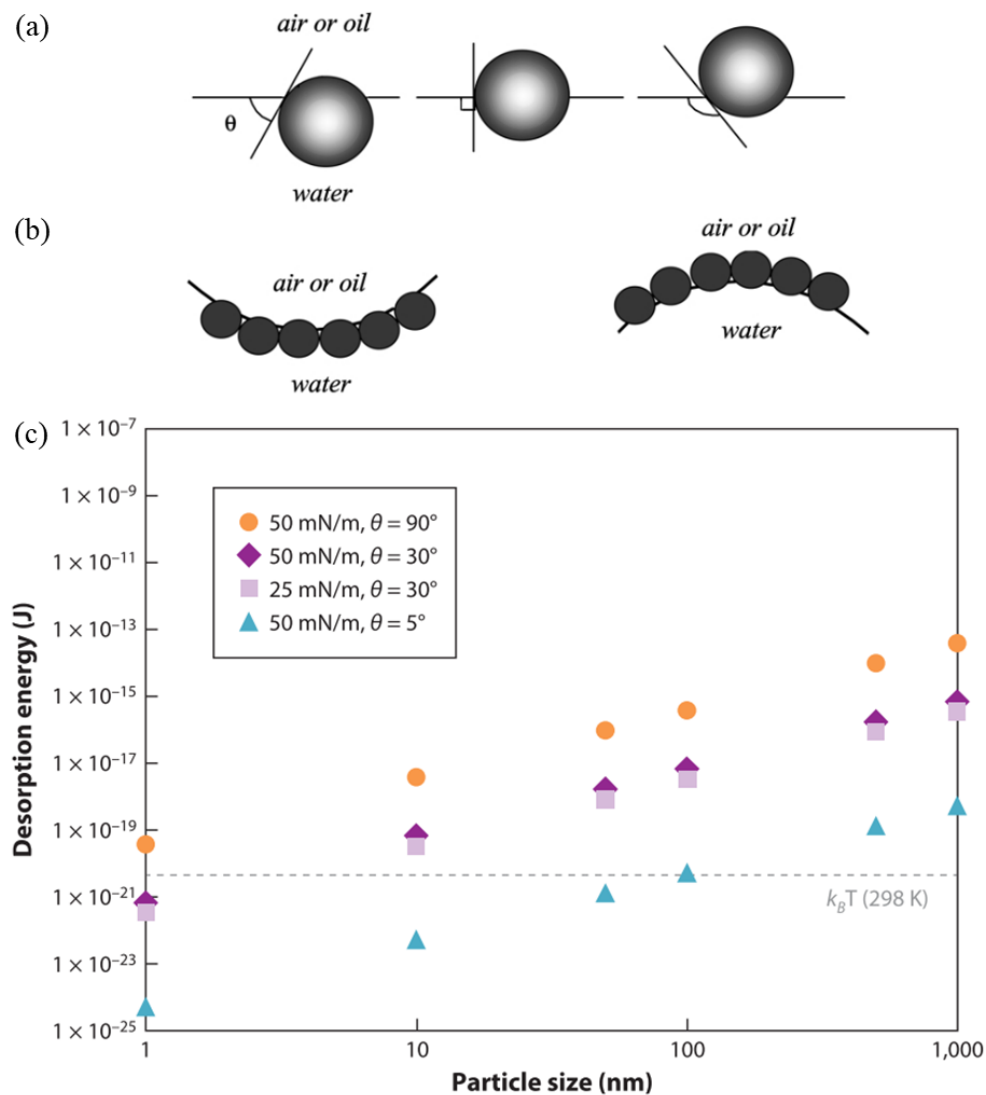


**Figure 2-1:** (a) Small spherical particle at a planar fluid-water interface for a contact angle (measured through the aqueous phase) less than  $90^\circ$  (left), equal to  $90^\circ$  (centre) and greater than  $90^\circ$  (right) [reprinted from Binks (2002), with permission by Elsevier]. (b) Corresponding probable positioning of particles at a curved fluid-water interface. For  $\theta < 90^\circ$ , solid-stabilized aqueous foams or O/W emulsions may form (left). For  $\theta > 90^\circ$ , solid-stabilised aqueous foam or W/O emulsions may form (right) [reprinted from Binks (2002), with permission by Elsevier]. (c) Desorption energy as a function of particle size, for oil-water interfacial tension of 50 mN/m or 25 mN/m, and particles with  $\theta$  of  $5^\circ$ ,  $30^\circ$ , or  $90^\circ$ . The grey dashed line represents the thermal energy at  $25^\circ\text{C}$  ( $k_B T$ , J) [reprinted from Berton-Carabin & Schroën (2015), with permission by Annual Reviews].

Assuming a monolayer of molecules or particles adsorbed at the interface, the thickness of the adsorbed layer is much greater for particles compared to that of conventional emulsifiers, given that the thickness of the interfacial layer is of a similar order of magnitude to the particles size. Accordingly, the surface load ( $\text{mg}/\text{m}^2$ ) for particle stabilised emulsion is also much larger as compared to the typical values for emulsion stabilised by conventional emulsifiers. Many studies have already demonstrated that the thick interfacial layer and high surface load of particle adsorption can improve the stability of emulsions against aging or heating compared to emulsions stabilised by molecules (Araiza-Calahorra & Sarkar, 2019; Destribats et al., 2014; Xu et al., 2019). For examples, the cryogenic scanning electron microscopy (cryo-SEM) observations of droplets stabilized by particles that formed with galactose glycosylated bovine serum albumin (gBSAs), showed that the surface was composed of rough particles (**Figure 2-2b**), while that for the droplet surface stabilised by native BSA molecules (*n*BSAs) was smooth and featureless (**Figure 2-2a**) (Xu et al., 2020). The smooth surface for droplets stabilised by *n*BSAs is in good agreement with the fact that *n*BSAs experienced a dramatic structural unfolding and flattening upon adsorbing at the interface. As a result, a thin and homogeneous interfacial protein layer was formed. In contrast, gBSAs with strong structural integrity no distinct structural changes and deformation occurred when adsorbed at the interface, and the rigid gBSAs form a much thicker and rougher layer at the interface. Thus, the robust steric stabilisation of gBSAs thus greatly prevented droplets from the coalescence over 90 days of storage or when heated at 100 °C for 15min.

Similar features of the droplet interface stabilised by molecules of whey protein isolate (WPI) and whey protein microgel particles (WPMs) have been reported using cryo-SEM observations (Araiza-Calahorra & Sarkar, 2019). The WPMs-stabilised interface (**Figure 2-2d**) features a discrete configuration with either individual particles or small aggregates forming a network

surrounding the bare interface, while the WPI-stabilised interfaces (**Figure 2-2c**) did not show any visible particle features as expected owing the small molecular size and structural deformation. In addition, the interfacial shear viscosity (mN. s/m) of the WPM emulsion is almost an order of magnitude higher than that with WPI-stabilisation after 24 h storage. The high interfacial shear viscosity values obtained for WPMs is indicative of strengthening of the interfacial films due to the presence of adsorbed particles.

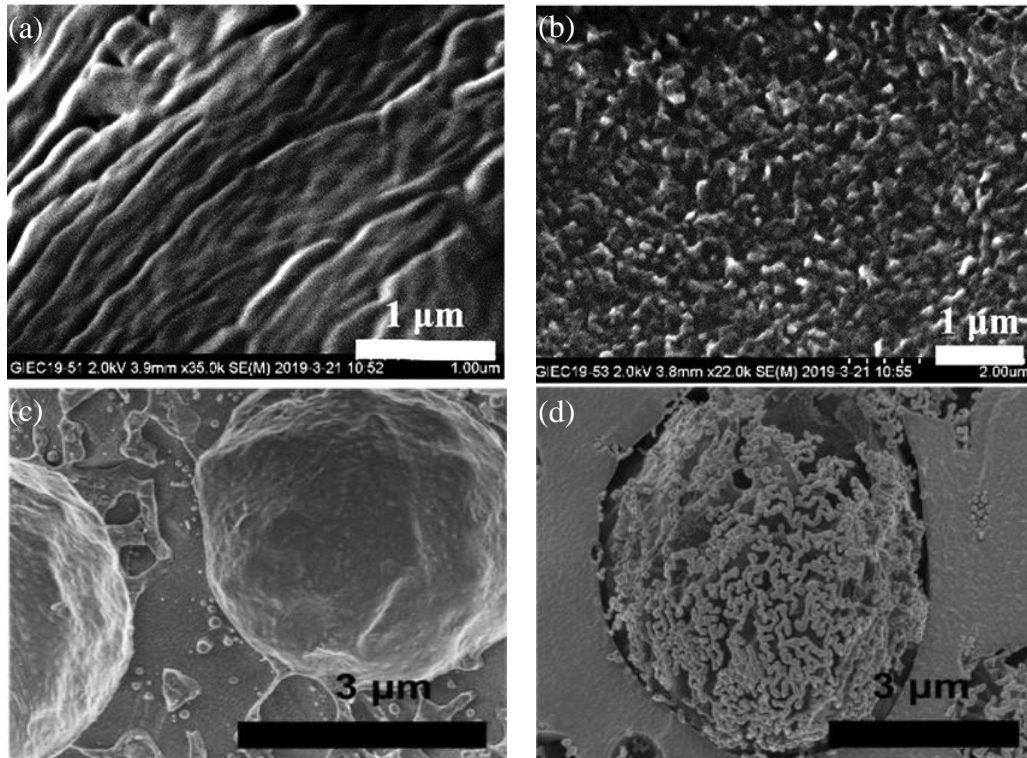


**Figure 2-2:** Cryo-SEM images of the interface morphologies of (a and b) dodecane-in-water droplet stabilized by native bovine serum albumin molecules (*n*BSA) and by galactose glycosylated BSA particles (*g*BSA) at pH 7.0 [reprinted from Xu et al. (2020b), with permission by Elsevier]; of (c and d) medium-chain triglyceride-in-water droplet stabilized by whey protein molecules and whey protein microgel particles at pH 7.0 [reprinted from Araiza-Calahorra & Sarkar (2019), with permission by Elsevier].

One noteworthy point is that solid particle stabilization typically leads to large emulsion sizes and a tendency toward gravitational creaming (Yang et al., 2017). The size of the emulsified droplet is mainly determined by the interfacial tension under controlled hydrodynamic conditions of emulsification. The relevant value of the tension here is the dynamic value of slowly adsorbing particles rather than the equilibrium value of rapidly adsorbing small molecules (Araiza-Calahorra & Sarkar, 2019; Tcholakova et al., 2008). The slow adsorption of particles is given by their large size and the high (de)adsorption energy of particles. The high desorption energy of particle **equation (2-3)** implies that the adsorption of particle is non-spontaneous and requires overcoming an energy barrier, in contrast to conventional emulsifiers that can diffuse to the interface and adsorb spontaneously (Kaz et al., 2012). This is possible if the kinetic energy of a particle approaching an interface is of the same order of magnitude as the energy barrier of adsorption (Salari et al., 2014). Despite the slow adsorption, the discrete and porous interfacial coverage by rigid particles also contribute to a relative higher interfacial tension due to more unfavourable interaction between oil and water molecules.

Hence, it is appealing to develop Pickering stabilizers with several attractive features to enhance interfacial coverage and effectively decrease the interfacial tension, leading to small particle size, large specific area, fast diffusion and adsorption, good dispersion and deformable upon adsorption. Furthermore, to accommodate the need for long-shelf life foods and functional active compounds/drug delivery, particles of organic and biocompatible origin are more of interest rather than inorganic or synthesized particles (Corstens et al., 2017a; Du et al., 2022; Jiao et al., 2018; Santos et al., 2021; Tan et al., 2014).

To date, most of the studies on food-grade Pickering emulsifiers were conducted on plant-based ingredients, including polysaccharides with surface modifications such as celluloses and



modified starches (Guida et al., 2021; Wang et al., 2020; Xu et al., 2020; Zhu, 2019), alcohol-soluble plant proteins such as zein and gliadin and water-soluble plant proteins such as soy protein (Sarkar & Dickinson, 2020). The research on water-soluble proteins derived from milk is rather limited. Several studies has been conducted on milk globular proteins, such as lactoferrin (Wei et al., 2020) , bovine serum albumin (Dickinson, 1994b; Li et al., 2013b; Xu et al., 2020b), and whey protein (Araiza-Calahorra & Sarkar, 2019; Destribats et al., 2014; Lv et al., 2020; Zhao et al., 2021b); several studies have fabricated protein particles from casein or sodium caseinate by pH-precipitation and cross-linking (Shi et al., 2020; Yan et al., 2020; Zhang et al., 2021). The type of fabricated protein particles depends mainly on molecular properties of the protein and the manufacturing conditions used. Although there is also a growing interest in exploring various shape of protein-based Pickering emulsifier that go beyond spheres, the development of the spherical protein particles appears still as the mainstream, given their high specific surface area available for emulsification (Zhang et al., 2021).

In the last decade, small lipid particles coated with proteins or LWMEs have also been investigated for the potential use as Pickering emulsifiers (Lim et al., 2020; Pawlik et al., 2016; Sakellari et al., 2021; Schröder et al., 2018). A non-exhaustive list of particles fabricated from milk proteins for use in O/W Pickering emulsions is presented in **Table 2-1**, with examples of globular protein, random coils casein, as well as protein coated solid/soft lipid particles.

**Table 2-1** Example of dairy-protein-based Pickering stabilizer for O/W emulsion applications <sup>a</sup>

Type of protein	Type of particle	Particle preparation procedure	Particle diameter and zeta-potential	Aqueous phase conditions	Type of lipid, volume fraction, and emulsification	Droplet radius ( $\mu\text{m}$ )	Reference
Bovine Serum albumin (BSA)	BSA glycated with galactose (gBSA)	Maillard glycation at pH 7.0, 60 °C for 6 – 48 hours	6.5 nm -21 to -28 mV	0.1 – 1.0 % w/w gBSA in water. pH 7.0	20 to 93 % Dodecane, shearing at 5000 rpm for 1 min	30 – 60	Xu et al., 2020b
Whey protein isolates (WPI)	Whey protein microgel particles (WPMs)	Heating at pH 5.9, 85 °C for 1 hours and sonicating for 20 min	235 nm at pH 6.5 +40 to -50 mv	0.1 – 0.6 % w/w WPMs in water, pH 2.0 - 8.0, 0 / 150 mM NaCl	50 % Miglyol 812N, ultra-turraxing, 13500 rpm for 1 min	85 – 200	Destribats et al., 2014
	WPMs	Heating at pH 7.0, 90 °C for 30 min with 20 mM phosphate buffer (PB) and homogenizing at 250/50 bars for 2 cycles	250–300 nm -36.5 mV	1.0 % w/w WPMs in water, 20 mM PB, pH 7.0	20 % w/w Sunflower oil, High pressure homogenising at 250/50 bars rpm for 2 cycles	42.9	Sarkar et al., 2016a
	WPMs	Heating at pH 5.8, 85 °C for 15 min with 160 mg/L Na <sup>+</sup> ; and homogenizing at 5000 psi for 3 cycles	209 – 360 nm +31 to -36 mV	0.5 – 10 % w/w WPMs in water, pH 3.0 - 7.0	20 - 90 % w/w Grape seed oil, ultra-turraxing at 10000 rpm for 3 min	20 – 200	Su et al., 2018
	WPI gel particles	High hydrostatic pressure induced WPI gel particles, pH 7.0, 600 MPa for 30 min; and homogenizing at 100 MPa for 3 cycles	~0.1 – 2 $\mu\text{m}$ +28 to -45 mV	0.1 – 3.0 % w/w WPI gel particles in water, pH 2.0 – 8.0, 0 – 200 mM NaCl	20 – 70 % Canola oil, ultra-turraxing at 12000 rpm for 3 min	40 – 160	Lv et al., 2020

Table 2-1 Continued

Type of protein	Type of particle	Particle preparation procedure	Particle diameter and zeta-potential	Aqueous phase conditions	Type of lipid, volume fraction, and emulsification	Droplet radius ( $\mu\text{m}$ )	Reference
Sodium caseinate (CAS)	CAS gel particles by genipin cross-linking	Ultracentrifuged CAS dispersions with or without $\text{CaCl}_2$ ; Mixing with genipin alcohol solution and incubating at pH 7.1, 50 °C for 24 hours; precipitating the casein at pH 4 and removing calcium ions ( $\text{Ca}^{2+}$ ) by centrifugal washing; redispersing the casein pellet at pH 8.0 with sonication	~18 or 114 nm -47 to -60 mV	3 % w/w casein dispersed in water with 0.33 % w/v alcohol, pH 6.0	20 % v/v Medium-chain triglyceride, ultra-turraxing at 6500 rpm for 2 min followed by 9500 rpm for 1 min	~2 – 13	Wang et al., 2018
Casein	Casein nanogels	Glutaraldehyde induced casein crosslinking at pH 8, 50 °C for 24 hours	~125 – 325 nm +13 to -33 mV	0.25 – 2.5 % w/w casein nanogels dispersed in water, pH 2 – 11, 0 – 1.0 M NaCl	80 % w/w Olive oil, handshaking	50 – 170	Chen & Zhang, 2019
	Casein flocs	Adjusting casein solution to pH 11 and then pH 5, followed by ultrasonication	~25 $\mu\text{m}$ at pH 5 N.A.	3 % Casein flocs dispersed in water, pH 5	80 % w/w Edible oil, ultra-turraxing at 8000 rpm for 3 min	3.9 – 7.1	Bi et al., 2020
	Casein particles	Adjusting casein solution to pH 11 and then pH 10, 8, 6, 3, 2	pH 6 – 10: ~300 nm, -22 to -31 mV  pH 2 – 3: ~5 $\mu\text{m}$ , +22 to +5 mV	3 % w/v Casein particles dispersed in water, pH 2 – 10	80 % w/w Corn oil, ultra-turraxing at 8000 rpm for 3 min	~10 – 50	Guo et al., 2021

Table 2-1 Continued

Type of protein	Type of particle	Particle preparation procedure	Particle diameter and zeta-potential	Aqueous phase conditions	Type of lipid, volume fraction, and emulsification	Droplet radius ( $\mu\text{m}$ )	Reference
WPI	Tripalmitin solid lipid nanoparticles (SLNs) coated with WPI	Emulsifying 5 % w/w tripalmitin by 5 % w/w WPI at 75 °C with sonication for 3 min.	Bimodal of 150 and 700 nm  N.A.	Droplet dispersion of 5 % w/w tripalmitin coated with 5 % w/w WPI	20 % w/w Sunflower oil, Shearing at 10000 rpm for 2 min in the ice bath	~10	Pawlik et al., 2016; Sakellari et al., 2021
CAS	Tripalmitin SLNs coated with CAS	Emulsifying 5 % w/w tripalmitin by 1 % w/w CAS at pH 7.0 with at 80 °C, 800 bars for 5 cycles; removing excess CAS and aggregated droplets before use	~ 170 nm  -37 mV	1 % w/w Droplet dispersion, 10 mM PB pH 7.0	10 % w/w Sunflower oil, homogenizing at 4 °C, 400 bars for 5 cycles	~1	Schröder et al., 2018
Micellar caseins (CMs)	n-Hexadecane droplets coated with CMs	Emulsifying 20% w/w n-hexadecane by 4% w/v CM at 10 mM PB (pH 7.0) with microfluidizer at 300 MPa	150 nm	2 – 16 % w/w droplet dispersion, 10 mM PB, pH 7.0	20 % w/w n-Hexadecane, ultra-turraxing at 1000 rpm for 2 min	~ 2 - 24	Ye et al., 2013b
Whey protein concentrate	Phytosterol particles coated with whey protein	Emulsifying 1.2 % w/v Phytosterol in ethanol by 0.05 % w/v whey protein concentrate solution with 10 nm PB (pH 7.0) at 8000 rpm for 2 min and evaporating ethanol	Aggregated	0.1 - 3 % w/v phytosterol dispersion, 10 mM PB, pH 7.0	20 – 60 % w/v Soybean oil, ultra-turraxing at 135000 rpm for 3 min	~50-230	Liu & Tang, 2014
Bovine milk phospholipids and whey proteins	Milk fat nanodroplets Coated with phospholipid – whey proteins	Homogenizing milk fat globule membrane rich ingredient (69 – 76% whey protein, 12 – 22% fat, 6 – 8% PL) with high-pressure homogeniser at 400 – 800 bars for 3 cycles	200 nm	2 % w/w homogenised MFGM-rich dispersion	20 – 40 % w/w Soybean oil, high-pressure homogenising at 50 – 400 bars for 1 cycle	~1.3 – 6.9	Weng et al., 2021

<sup>a</sup> Three series of examples are shown consecutively, corresponding to applications of globular proteins, random coil caseins, and lipid particles/droplets coated with dairy proteins

### 2.3.1 Rigid and soft protein-based particles

In food science, given their relatively easy preparation, the development of spherical protein nanoparticles is mainstream for Pickering emulsion stabilisation (Davidov-Pardo et al., 2015; Destribats et al., 2014; Li et al., 2013b; Li & Ngai, 2013; Lv et al., 2020; Su et al., 2018; Xu et al., 2020b). Although milk proteins such as whey proteins or caseins are major food emulsifiers, most of protein particles for Pickering emulsion are prepared from relatively hydrophobic plant proteins such as zein or soy protein (Gao et al. 2013, 2014; Liu & Tang 2013, 2014a) via ultrasonication, solvent-induced precipitation or heat-induced aggregation. Only few studies have focused on fabricating the Pickering emulsifier from water-soluble dairy proteins (**Table 2-1**). An example of such protein particles for Pickering emulsion stabilisation is WPMs made from thermal-induced whey protein aggregation (Destribats et al., 2014). WPMs can efficiently decrease the O/W interfacial tension from 20.5 mN/m to 12.5 mN/m and successfully protect droplets from coalescence for up to 8 months after preparation. Over the following years, such thermal-induced WPMs have been applied to form Pickering emulsion in several studies (Sarkar et al., 2016a, 2017; Su et al., 2018). Until recently, a WPI gel particle prepared by different methodology that in robust high hydrostatic pressure-induced whey protein gel has been reported for Pickering emulsion stabilisation (Lv et al., 2020). Although different methods have been used to prepare whey protein particles, the resulting particles exhibited similar interfacial behaviours at different pH conditions. The intensive covalent cross-linking (disulphide bonding, S-S) and hydrophobic interactions between whey proteins induced by heating or high hydrostatic pressure result in rigid whey protein particles with limited penetration and deformation at the interfaces upon adsorption. The formed Pickering emulsions have large sizes (~ 50 – 200  $\mu\text{m}$ ) and undergo a rapid creaming within 1-2 hours.

Subsequently, some studies have shifted the focus to using caseins rather than whey proteins to synthesize protein particles, which were inspired by existing natural colloidal particles - the casein micelles (Chen & Zhang, 2019; Dickinson, 2010b) or soft gel particles made from slightly cross-linked polymers (Deshmukh et al., 2015; Wang et al., 2018). To date, casein particles preparation has been carried out using three general procedures: (1) non-covalently crosslinking of sub-micelles by calcium ions ( $\text{Ca}^{2+}$ ) (Chen & Zhang, 2019; Dickinson et al., 2001; Sosa-Herrera et al., 2012), (2) covalently crosslinking casein molecules by chemicals such as genipin (Wang et al., 2018) or glutaraldehyde (Chen & Zhang, 2019), and (3) hydrophobic aggregation near the isoelectric point of casein (Bi et al., 2020; Guo et al., 2021). The particle size of the fabricated casein particles was similar to that of WPMs of about 200 nm, however, the droplet size of the formed Pickering emulsion stabilized by casein particles was about  $10\ \mu\text{m}$  (Bi et al., 2020; Chen & Zhang, 2019; Guo et al., 2021), significantly smaller than the droplet size of the emulsion stabilized by whey protein particles of about  $50 - 200\ \mu\text{m}$  (Destribats et al., 2014; Lv et al., 2020; Su et al., 2018). The main advantages of the soft casein particles compared to rigid whey protein particles are that (1) the surface of the casein particles has a large number of dangling polymer chains that can anchor to the oil-water interfaces like a bio-polymer emulsifier (casein micelles), (2) the high flexibility and deformability of soft gel particles allow them to spread and cover the interface better after adsorption (Bi et al., 2020; Guo et al., 2021; Wang et al., 2018). As shown in **Figure 2-3**, the interface of O/W droplets that is stabilised by relatively rigid whey protein microgel particles has a porous structure (**Figure 2-3a**) (Araiza-Calahorra & Sarkar, 2019; Destribats et al., 2014), whereas the interface stabilised by flexible and deformable casein particles is fully covered (**Figure 2-3b-c**) (Guo et al., 2021; Wang et al., 2018). Therefore, the soft gel particles show better emulsification performance than rigid particles (Richtering, 2012).

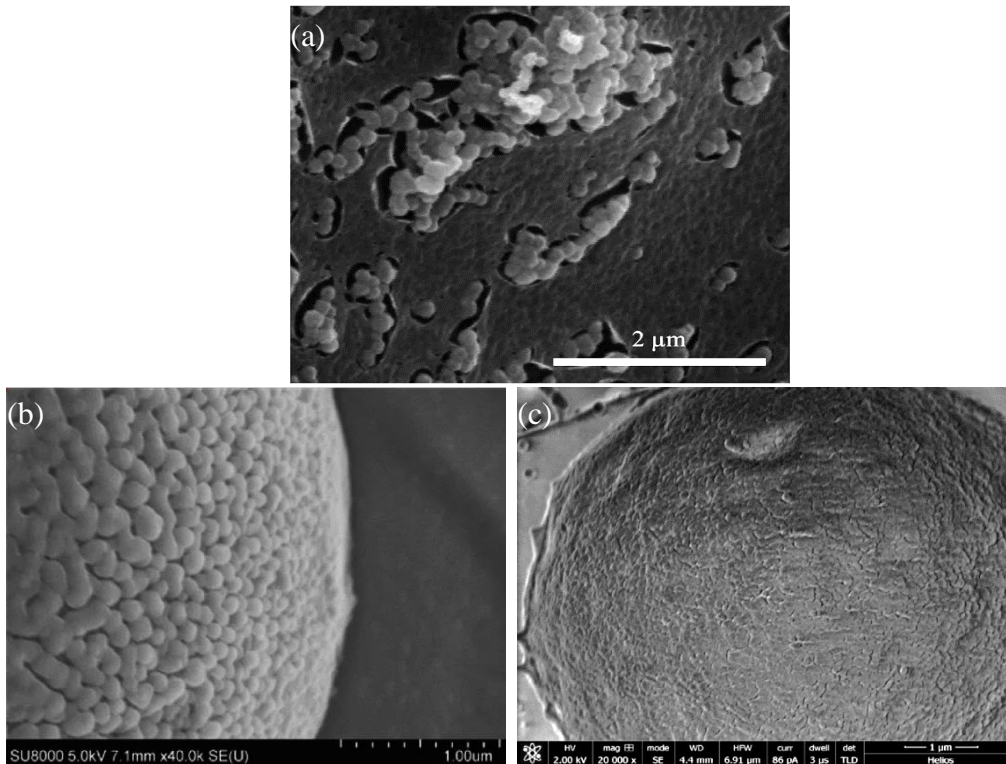


**Figure 2-3:** Cryo-SEM images of the interfacial morphology of (a) heptane-in-water droplet stabilized by WPMs at pH 4.8 [reprinted from Destribats et al. (2014), with permission by Royal Society of Chemistry], (b) corn oil-in-water droplet stabilized by casein particles at unknown pH [reprinted from Guo et al. (2021), with permission by Elsevier], and (c) medium-chain triglyceride-in-water droplet stabilized by casein gel particles (calcium and genipin cross-linking) at pH 6.0 [reprinted from Wang et al. (2018), with permission by Elsevier].

### 2.3.2 Solid and soft lipid-based particles

In early studies of lipid-based particles for Pickering emulsions, the particles are mainly fat-crystals, which have been widely recognized as efficient stabilizers for W/O emulsions such as edible spreads (Frasch-Melnik et al., 2010; Rousseau, 2000, 2013). The inherent relatively high hydrophobicity of such particles makes them able to position at oil-water interfaces with an angle higher than  $90^\circ$ , hence favouring the stabilization of water droplets in a lipid-based matrix (Paunov et al., 2007).

Several studies have investigated the potential of particles made from a combination of lipids and emulsifiers as Pickering stabilizers (Gupta & Rousseau, 2012; Liu & Tang, 2014; Pawlik et al., 2016; Sakellari et al., 2021; Ye et al., 2013b). Lipid particles coated with surfactants are usually favoured to form W/O Pickering emulsions (Pawlik et al., 2016). Conversely, lipid particles coated with milk proteins are able to act as Pickering emulsifiers and form O/W type emulsions due to the fact that proteins can form thick protein interfacial layers and particles exhibit more hydrophilic properties (**Table 2-1**) (Liu & Tang, 2014; Pawlik et al., 2016; Sakellari et al., 2021; Ye et al., 2013b). The preparation of lipid particles is similar to the routine emulsion homogenization, where lipids are emulsified with proteins by a high-pressure homogenization process and solid lipids with high melting points (e.g., tripalmitin) are processed at high temperature. The structure of the resulting particles varies from un-solubilized aggregates in water (Liu & Tang, 2014), to solid lipid nanoparticles (SLNs) (Pawlik et al., 2016; Sakellari et al., 2021), or even as conventional emulsions that are soft and deformable (Ye et al., 2013b). The latter soft droplets were prepared from casein-micelle-stabilised hexadecane droplet and used to form emulsion-stabilised emulsion. Owing to the difference in deformability between SLNs and soft lipid droplets, these lipid particles produce different interfacial structures upon adsorption. The interfacial configuration of SLN



stabilization and of soft lipid droplets stabilization were observed using SEM and transmission electron microscopy (TEM) as shown in **Figure 2-4**. The interface of O/W droplets that stabilised by SLNs showed a discrete and porous configuration (**Figure 2-4a**) (Pawlik et al., 2016), whereas the interface by soft and deformable emulsion are fully covered (**Figure 2-4b**) (Ye et al., 2013b). Considerable flattening and networking of the initially spherical soft lipid droplets on the surface of the larger hexadecane droplets was also observed, which may even be enhanced by interparticle bonds (Ye et al., 2013b). The interfacial layer of soft, deformable, and networking droplets is an exciting example of building emulsion-based systems with new interfacial design. It will be interesting to extend the study of this new emulsion-stabilised emulsion to its functions, such as stability, lipid delivery and emulsion viscoelasticity.

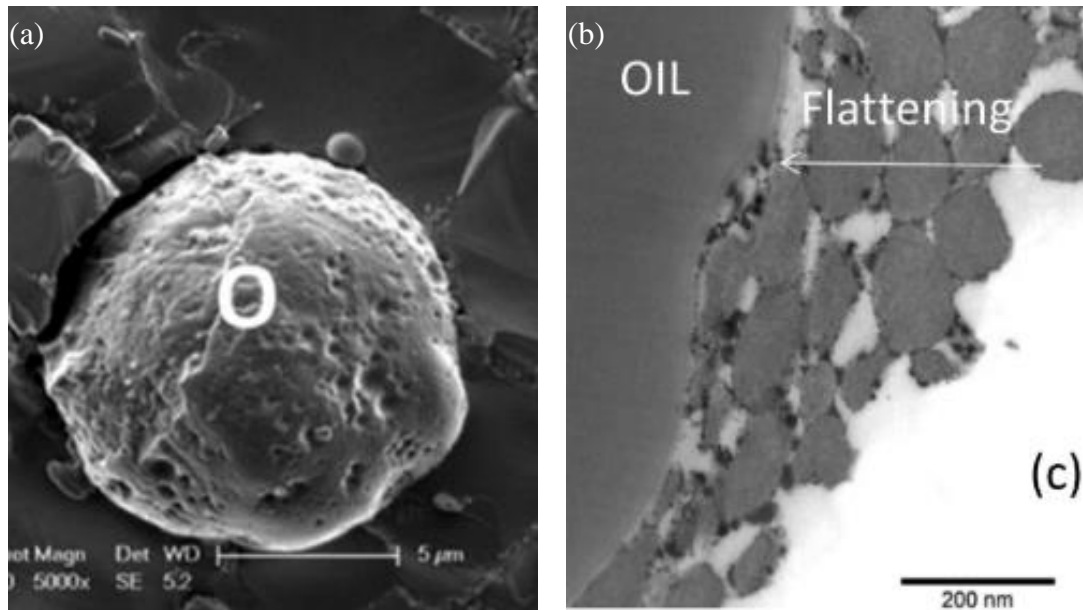


**Figure 2-4:** (a) SEM images of sunflower O/W emulsion stabilised by tripalmitin SLNs with 5 % WPI coating [reprinted from Pawlik et al. (2016), with permission by Royal Society of Chemistry]. (b) TEM images of *n*-hexadecane O/W emulsions stabilised by soft *n*-hexadecane primary droplets with casein micelle coating [reprinted from Ye et al. (2013b), with permission by American Chemical Society].

### 2.4 Emulsion rheological properties

Emulsions formulated from a variety of compositions, processing conditions, and environmental conditions exhibit a wide range of rheological properties from diluted fluid, to viscous liquid, to viscoelastic semi-solid, which in turn impacts emulsion functional properties and applications (e.g., processability, texture, mouthfeel, and biological response) (Akbari & Nour, 2018; Camacho et al., 2015; Liu et al., 2019; Tadros, 2013b; van Aken et al., 2011; Zembyla et al., 2020; Zhu et al., 2019). The rheological properties of emulsions are a direct display of the various interactions that occur in the system. Thus, after emulsion preparation, the rheological properties of the emulsions are constantly changing during storage in response to the structural changes and instability of the droplets. For example, the viscosity or elastic modulus of an emulsion becomes greater as a result of flocculation and aggregation of droplets but decreases as a result of coalescence of droplets (Chanamai & McClements, 2000; Chuang et al., 2020; Dickinson et al., 1988a; Dickinson & Ritzoulis, 2000; Dimitrova & Leal-Calderon, 2004; Hu et al., 2016; Pal, 1996; Robins et al., 2002). Knowledge of factors affecting the emulsion rheology and stability is necessary for successfully developing high-quality emulsion-based products with desirable rheological properties.

The factors that affect the rheology of emulsions have been intensively reviewed in the literature (Derkach, 2009; Félix et al., 2020; Kim & Mason, 2017; Pal, 2011; Tadros, 1994, 2004; Zhu et al., 2019). In summary, these factors are the volume fraction of the disperse phase ( $\phi$ ), the droplet size distribution, the viscosity of both the dispersed and the continuous phases, and the rheological property of the interfacial film.

Typically, dispersed phase volume fraction ( $\phi$ ) is the most important factor governing the rheological properties of emulsions (Lacasse et al., 1996; Mason, 1999; Mason et al., 1995). At relatively low  $\phi$  ( $< 0.1$ ), the main force driving droplet motion is Brownian forces and the

interactions between the emulsion droplets are relatively weak because they are so far apart from each other (Pal, 2011). When the ability of one droplet to disrupt the flow pattern of the continuous phase does not affect the flow pattern experienced by another droplet, the apparent viscosity of the low  $\varphi$  emulsions is therefore dominated by the rheological properties of the continuous phase. As the droplet concentration increases, the apparent viscosity of emulsion is influenced by increasing hydrodynamic interactions and droplet–droplet collisions. When the  $\varphi$  is sufficient high, the droplets are packed very closely together and become trapped by surrounding droplets, emulsions could have some elastic properties displaying a yield transition and complex rheology. Typically, they appear to flow at high shear rates but solidify at low shear rates, exhibiting a self-supporting texture (Li et al., 2020). Owing to the unique gel-like rheological properties, special texture and long-term stability against phase separation, concentrated emulsions have attracted increasing attention from both academic research and industry (Li et al., 2018; Patel & Dewettinck, 2016).

In the case of concentrated emulsions, droplet size distribution is particularly important as it affects the emulsion rheology in terms of effective volume fraction ( $\varphi_{eff}$ ) and the maximum volume packing ( $\varphi_{max}$ ). For the same  $\varphi$ , small droplets can have a much larger effective volume fraction ( $\varphi_{eff}$ ) than larger droplets because the ratio between the thickness of the adsorbed layer ( $h$ ) and the droplet diameter ( $D$ ) is increasing as expressed in **equation (2-4)** (Mason, 1999; Pal, 1996; Tadros, 1994)

$$\varphi_{eff} \approx \varphi \left[ 1 + \frac{2h}{D} \right]^3 \quad (2-4)$$

Moreover, the average distance between droplets decreases as the droplet size decreases, which means that droplet-droplet interactions become more important (Pal, 1996). Theoretically, for the rigid spherical particles with a narrow polydispersity of 0.1, the  $\varphi_{max}$  is

0.74 for hexagonal packing (Mason, 1999; Scott & Kilgour, 1969). However, a  $\phi_{max}$  can be greater than 0.74 when the droplet polydispersity is high. In the polydisperse emulsion, the space is filled more efficiently by small droplets (Lubachevsky & Stillinger, 1990; Scott & Kilgour, 1969; Tadros, 1994). Therefore, the viscosity of the polydisperse system is usually lower than that of the monodisperse system at the same  $\phi$  (Farr & Groot, 2009; Foudazi et al., 2012, 2015). As a result, the viscosity of an emulsion may increase as the droplet size decreases and decrease with an increase in polydispersity.

Many studies have indicated that rheological properties of concentrated emulsions can be manipulated prior to emulsification by emulsion compositions and conditions (e.g., emulsifier concentration, pH, ionic strength, additives, etc.) to obtain different droplet size distribution as well as the continuous phase viscosity (Berli, 2007; Chuang et al., 2020; Desmond & Weeks, 2014; Foudazi et al., 2012; Geremias-Andrade et al., 2017; Hemar & Horne, 2000; Lacasse et al., 1996; Mason et al., 1996; Pal, 1996; Princen & Kiss, 1986; Zhang et al., 2021a; Zhu et al., 2019). With this knowledge, a low  $\phi$  of emulsion could be designed to have the same rheological properties of the high  $\phi$  through decreasing the droplet size, introducing droplet aggregations, or adding thickeners.

It is worth noting that the deformability of emulsion droplets (Saiki & Prestidge, 2005) and of the emulsifier at the interfaces (Brugger et al., 2010; Li et al., 2015) also affect the rheology of emulsion. However, the relationship between the emulsifier deformability and the bulk rheology is not clear (Tadros, 1994).

Saiki & Prestidge (2005) have investigated that shear thinning and elastic properties of deformability controllable polydimethylsiloxane (PDMS) emulsions stabilised with sodium dodecyl sulphate (SDS) (Saiki & Prestidge, 2005). They found that at  $\phi = 0.6$  the hard droplets

behave as hard sphere and is more shear thinning, while soft droplet is less shear thinning at low  $\phi$  due to high level of structural flexibility of the emulsion against shear (**Figure 2-5a**). However, at high  $\phi = 0.7$ , the soft emulsion exhibited extra shear thinning that is comparable with the hard emulsion, presumed due to lateral distortion of droplet structures (**Figure 2-5a**). In contrast, at  $\phi = 0.7$  the hard emulsion showed a relatively high elasticity than soft emulsion against dynamic oscillation deformation (**Figure 2-5b**). Combining the steady shear and dynamic oscillation studies, they concluded that the viscoelasticity of droplets provides the great magnitude of elasticity for the hard emulsion, while formation of planar films between droplets is the origin of the elasticity of soft emulsion.

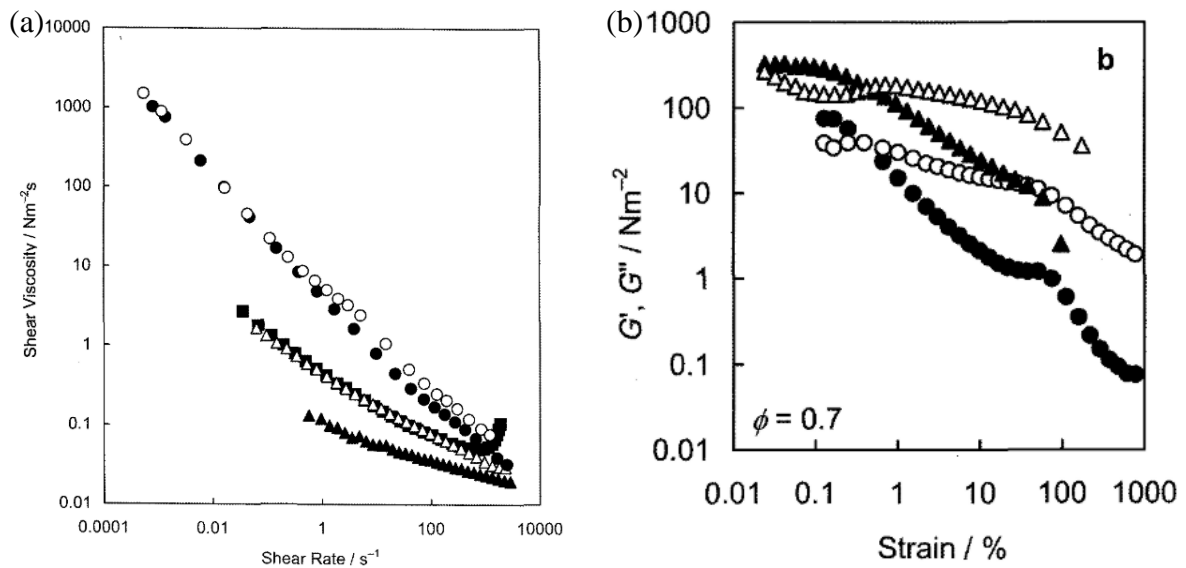


**Figure 2-5:** (a) Shear viscosity plotted against shear rate; soft PDMS:  $\phi = 0.6$  (close triangle),  $\phi = 0.7$  (close circle); hard PDMS:  $\phi = 0.6$  (open triangle),  $\phi = 0.7$  (open circle); silica:  $\phi = 0.6$  (close square). (b) Elastic modulus,  $G'$  (closed symbols) and viscous modulus,  $G''$  (open symbols) plotted against shear strain at 1 Hz; soft PDMS (circle), hard PDMS (triangle) [reprinted from Saiki & Prestidge (2005), with permission by Korea Science].

### 2.5 Emulsion interfacial rheology

The influence of the deformability of emulsifiers on rheology properties have been mainly studied using interfacial rheology and related to emulsion formation and stability against interfacial rupture. Brugger et al. (2010) investigated the interfacial rheological properties of microgel-covered oil–water interfaces by means of the pendent drop technique as well as by shear deformation with double-wall ring geometry (Brugger & Richtering, 2008). They observed at high pH where the particles are charged, the interface exhibited a soft gel-like structure that gave rise to an elastic response to mechanical deformation (**Figure 2-6b**). In contrast, at low pH where the charge on the particles is lower, the particle layer was compact and brittle (**Figure 2-6a**). Li et al. (2015) investigated the interfacial shear rheology of microgels prepared with different cross-linking densities (**Figure 2-6c**) (Li et al., 2015). They also observed that the interface formed by soft particles (S/N 1) exhibit a greater shear elasticity and yield point compared with the interface formed by rigid particles (S/N 8) (**Figure 2-6d**). Both studies propose that the viscoelastic properties of the microgel covered interfaces were positively correlated with the stability of the emulsion. It is clear that the stimulus-responsive nature of these microgel particles leads to a rich behavioural and morphological transition with interesting effects on interfacial rheology.

However, these studies were carried out in the context of non-food systems with a highlight on interfacial rheological properties. The relationship between the bulk and interfacial rheology is missing. Since food systems are often soft solids it is important to consider both the bulk and interfacial rheology. It would be interesting to extend this approach to model emulsions consisting of food-grade ingredients and to correlate the particle-emulsifier deformability to the bulk rheology of emulsions.



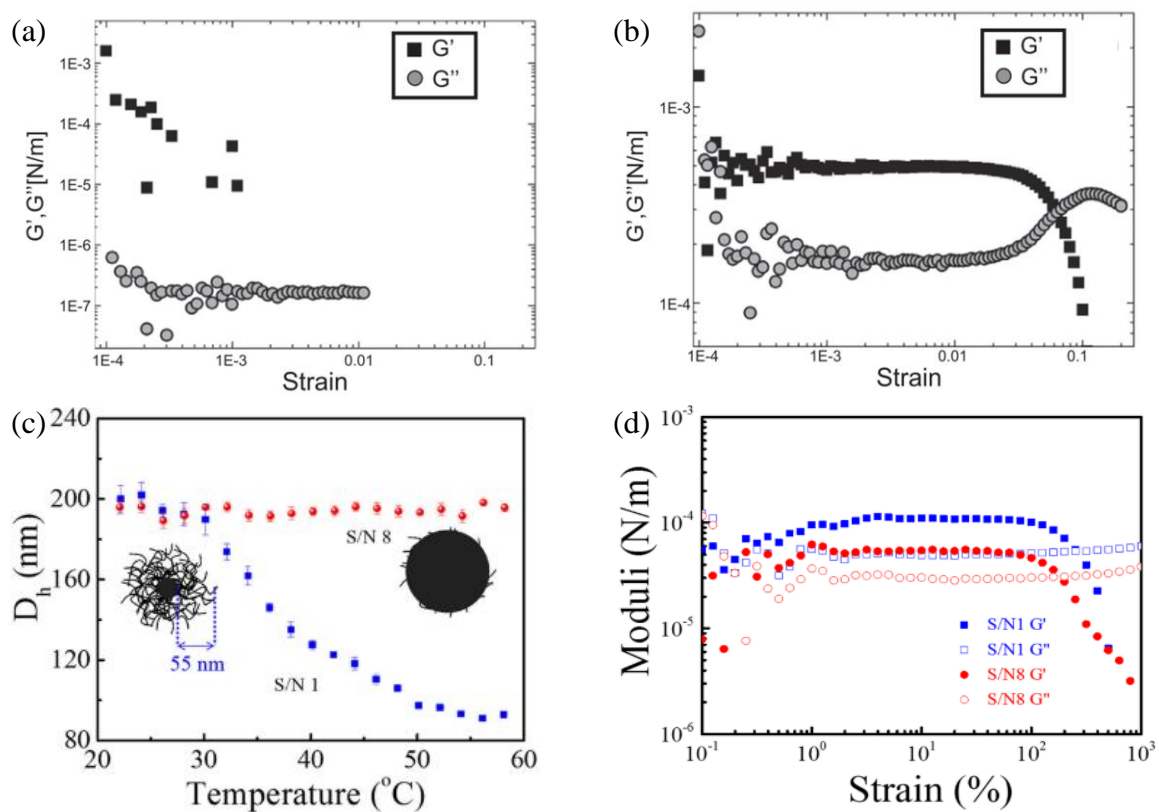


**Figure 2-6:** (a) Strain sweep of poly (*n*-isopropylacrylamide)-*co*-methacrylic acid polymers (PNIPAM-*co*-MAA) microgel layers cover heptane-water interfaces at pH 3 and (b) at pH 9 [reprinted from Brugger et al. (2010), with permission by Royal Society of Chemistry]. (c) Hydrodynamic diameter ( $D_h$ ) of PNIPAM microgel particles with different crosslinking density as function of the solution temperature, S/N 1, soft particles, and S/N 8, rigid particles, and (d) strain sweep of S/N 1 and S/N 8 microgel layers cover heptane-water interfaces [reprinted from Li et al. (2015), with permission by American Chemical Society].

### 2.6 Emulsion stability

Emulsions can be destabilised by different mechanisms, most of which are undesirable. The effects of three types of destabilisations are described below.

#### 2.6.1 Physical destabilisation

A good physical stability commonly implies that there is no discernible change in the size distribution or the spatial arrangement of droplets over the experimental time-scale, e.g., from a few days to several months (Dickinson, 1994a). Due to the thermodynamic instability, almost all emulsions will coalesce resulting in phase separation with time. The long-term stability of emulsion can be achieved by electrostatic and steric stabilization (repulsion forces) of emulsifying agents that form an adsorbed layer at the surface of the droplets. Beside the nature of the interfacial adsorbed layer, the droplet size, and the nature of continuous phase can also affect the emulsion stability as depicted in **Figure 2-7**. In practices, loss of stability may involve several physical and chemical changes, which take place simultaneously or consecutively depending on the circumstances. The most important physical mechanisms of instability are creaming, flocculation, coalescence, Ostwald ripening and phase inversion. All these mechanisms act individually and can also influence one another (McClements, 2009). These destabilizations are related, although sometimes indirectly, to the properties of the O/W interface. In flocculation, adsorbed emulsifiers may cause electrostatic attraction and/or bridging between droplets, depending on the environmental conditions and emulsifier structures (e.g., pH, ionic strength, emulsifier concentration and interfacial structure). In the case of coalescence, there is drainage of the continuous phase followed by the creation of a hole in the interfacial layers between the droplets, which can be seen as dilatational deformation (Murray et al., 2011). The mobility of the adsorbed molecules and the viscoelasticity of the interfacial layer can thus affect the coalescence process (Dickinson et al., 1993; Nambam &

Philip, 2012). Gravitational separation can be facilitated by flocculation or coalescence, which is affected by interfacial mobility and results in an increase of the effective droplet size. In nanoemulsions (sizes less than 100-200 nm), the volume fraction of the interfacial composition is no longer negligible due to the large surface to volume ratio and can significantly influence the droplet density (Mason et al., 2006). In surfactant-stabilised emulsion, Ostwald ripening can be accelerated because the surfactant is reversibly adsorbed and can form micelles in the continuous phase; these surfactant micelles are able to act as carries of oil between droplets and increase the rate of ripening, whereas in the case of particle stabilisation there is no such process (Ashby & Binks, 2000; Weiss et al., 1999, 2000). However, in the case of particle stabilisation, droplets can be ripened through a mechanism of diffusion or exchange of oil molecules, which is driven by the solubility of the molecules in the continuous phase (Ashby & Binks, 2000). Details of these several types of mechanisms are described below.

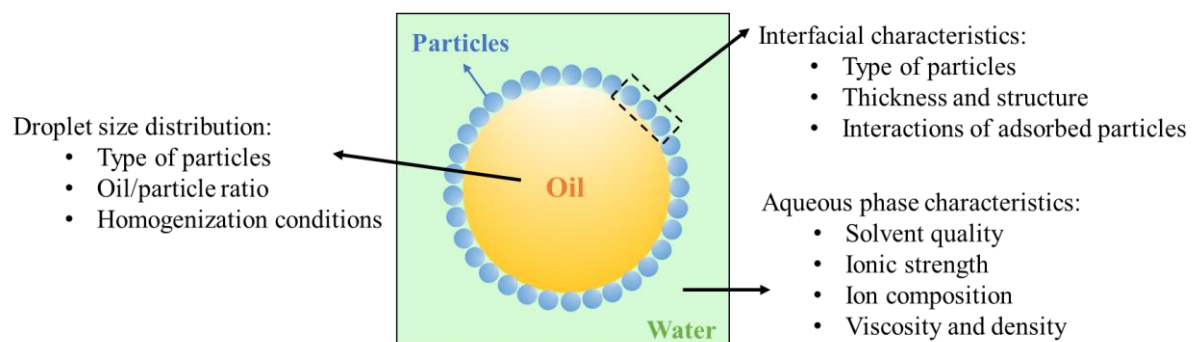


**Figure 2-7:** Principal factors affecting oil-in-water emulsion stability

### 2.6.1.1 Gravitational separation

Gravitational separation in forms of creaming or sedimentation are the consequence of the different density between the dispersed droplets and surrounding aqueous phases. If the droplets have a lower density than the surrounding aqueous phase, they tend to move upward, which is referred to as creaming. If they have a higher density than the surrounding liquid they tend to move downward, which is referred to as sedimentation (McClements, 2015b). The droplet migration produces a vertical concentration gradient of droplets. In the case of O/W emulsion, the rate at which an emulsion droplet creams in an ideal liquid are determined by the balance between the gravitational and frictional forces. This can be described by the ‘Stokes’ law as shown in **equation (2-5)**:

$$v_{stokes} = \frac{2g_a R^2 (\rho_1 - \rho_2)}{9\eta_1} \quad (2-5)$$

where the  $v_{stokes}$  is the velocity of creaming,  $R$  is the emulsion droplet radius,  $\rho_1$  and  $\rho_2$  are the densities of continuous and dispersed phases, respectively,  $\eta_1$  is for the viscosity of the continuous phase and  $g_a$  is the acceleration of gravity.

The speed of gravitational separation in food emulsions is influenced by many factors such as Brownian motion, interactions between droplets (droplet flocculation) and/or interactions between droplets and continuous phase components (McClements, 2015b). In practice, the gravitational separation can be reduced by reducing droplet size ( $< 0.7 \mu\text{m}$ ), minimizing the density difference, decreasing the degree of droplet flocculation, increasing the continuous phase viscosity.

**2.6.1.2 Flocculation**

Droplet flocculation is the process whereby two or more droplets associate with each other without coalescence occurring (Tadros, 2013a). This phenomenon involves aggregation of two or more emulsion droplets to form a floc, but the droplets maintain their individual integrity; in other words, the dispersed phase material of the droplets involved in the floc does not merge, and the phenomenon may be reversible. The mechanism of flocculation can be attributed to droplet-droplet interactions. A model to describe droplet flocculation in colloidal dispersions containing monodisperse spherical particles (Evans & Wennerström, 1999) was proposed:

$$dn_t/dt = -\frac{1}{2} FE \quad (2-6)$$

where  $n_t$  is the total number of particles per unit volume,  $t$  is the time,  $dn_t/dt$  is the flocculation rate,  $F$  is the collision frequency, and  $E$  is the collision efficiency. This equation indicates that the flocculation rate depends on two factors: (1) the frequency of collisions between droplets and (2) the fraction of collisions that leads to aggregation. The collision frequency (i.e., the total number of droplets encountered per time per unit volume of emulsion), is dependent on the Brownian motion and gravitational separation. If every encounter between droplets leads to aggregation, the emulsion will be very unstable. To prevent aggregation of droplets, it is necessary to have a sufficiently high-energy barrier to stop them coming too close. The collision efficiency can be explained by the height of energy barrier, which is determined by the nature of interfacial film and droplet-droplet interactions (i.e. van der Waals interactions, electrostatic interactions, steric interactions, hydrophobic interactions, bridging interactions, depletion interactions, hydrodynamic interactions and covalent interactions)(McClements, 2015b).

In general, the presence of sufficient emulsifiers to completely saturate the droplet surface can provide strong and long-range repulsions and prevent flocculation (e.g., bridging, or hydrophobic interactions) (McClements, 2015b). However, an excess of non-adsorbing colloidal emulsifiers present in the continuous phase of an emulsion leads to an increase in the attractive forces between the droplets, which is referred to as depletion flocculation, due to an osmotic effect associated with the exclusion of the colloidal emulsifiers from a narrow region around each droplet (Jenkins & Snowden, 1996). There is an optimum size of colloidal emulsifiers required to promote depletion flocculation, which depends on a balance between (1) the number of emulsifiers per unit volume (which increases with decreasing size) and (2) the volume of the depletion zone (which decreases with decreasing size) (Asakura & Oosawa, 1954; Radford & Dickinson, 2004). The flocculation rate initially increases as the concentration of nonadsorbing colloidal emulsifiers is increased because of the enhanced attraction between the droplets, that is, a higher collision efficiency. However, once the concentration of colloidal emulsifiers exceeds a certain concentration, the flocculation rate often decreases because the viscosity of the continuous phase increases so much that the movement of the droplets is severely retarded, that is, a lower collision frequency (Bai et al., 2021; McClements, 2000, 2015b; Radford & Dickinson, 2004). It should be noted that when an emulsion exhibiting depletion flocculation is diluted for particle size measurements (e.g., light scattering), the floc usually breaks down because the concentration of nonadsorbing colloids emulsifiers is then greatly reduced, i.e., the depletion flocculation is usually weak and reversible. Such a phenomenon can lead researchers to believe that the emulsion is stable when in fact it is flocculating in its normal state.

### 2.6.1.3 Coalescence

Coalescence is a process whereby two or more droplets merge to form a single large droplet at very close contact. An emulsion moving toward thermodynamically unstable state is the principal mechanism of the coalescence because the emulsion system tries to decrease the contact area of two immiscible phases. Danov et al., (1993) proposed a mechanism of coalescence including four steps: (1) close approach of non-deformed droplets; (2) formation and expansion of plane-parallel film; (3) thinning of the film at almost constant radius; (4) rupture of the film and fusion of the droplets into a larger droplet. When repulsive forces between droplets are strong (e.g., at large enough electrostatic repulsion), the droplets deformation is unlikely, and the droplets behave as non-deformable charged spheres. Therefore, in general, emulsions are stable to coalescence because the droplets are covered by sufficient emulsifier (Dickinson et al., 1988a). However, insufficient emulsifier, film stretching, and film tearing can accelerate the rate of coalescence (van Aken et al., 2003).

### 2.6.1.4 Ostwald ripening

Ostwald ripening also leads to increased droplet size, although through different mechanisms and driving forces compared to coalescence. In polydisperse emulsions, small droplets have a larger internal Laplace pressure than do large droplets, which promotes diffusive transfer of the dispersed phase molecules from smaller to larger droplets (Leal-Calderon, 2012). Another driving force for Ostwald ripening originates from differences in oil solubility and chemical potential at the oil–water interface. Smaller droplets lead to higher oil solubilities, which results in a net diffusion of oil molecules toward larger emulsion droplets. As a result, the size distribution changes over time with larger droplets growing at the expense of smaller ones.

### 2.6.1.5 Oil exchange

Oil molecules exchanges between droplets in emulsion system is crucial for designing emulsion-based drug delivery vehicles (Hettiarachchi et al., 2009), modifying emulsion properties (Dan, 2016), or utilizing emulsion droplets as Pickering emulsifier (Ye et al., 2013b). Of all possible mass transport mechanisms, emulsion coalescence and Ostwald ripening are probably among the best understood. However, several studies have shown that poorly soluble oil molecules can also exchanges between stabilized droplets, even without Ostwald ripening or coalescence, resulting in an equilibrium oil exchange without a net size change (Malassagne-Bulgarelli & McGrath, 2009; Roger et al., 2015; Weiss et al., 2000) . Two mechanisms have been suggested that (1) surfactant solubilisation effect that surfactant micelles can be excellent molecular carriers by helping solubilize insoluble oils in their hydrophobic core and accelerating transport across the continuous phase (Weiss et al., 2000). (2) the direct emulsion contact where reversible collisions cause direct oil permeation through thin liquid films between the droplets as they collide due to Brownian motion (Roger et al., 2015). Nonetheless, in emulsion prepared using a variety oil including non-polar alkanes and polar alcohols, oil exchanges can also occur without a net size change when the chemical potentials (concentrations) of various oils compensate the capillary pressure (Laplace pressure) (Ashby & Binks, 2000).

### 2.6.1.6 Phase inversion

A phase-inversion, the process by which an original dispersed phase turn into a continuous phase and vice versa, can occur in emulsion (McClements, 2015b). Vigorous phase inversion usually occurs when the dispersed phase fraction increases to a very high level and is characterised by a sudden drop in the viscosity of the emulsion, which often happens during



the preparation of high internal phase emulsions (Zeng et al., 2017). Transitional phase inversion is generally triggered by some change in the emulsion's environmental conditions (e.g., temperature, ionic strength) and is generally associated with a modification in the geometry of emulsifiers, and hence of the spontaneous curvature of the interface.

### 2.6.2 Chemical destabilization

Food emulsions are prone to chemical destabilization during processing (e.g., sonication) and storage (e.g., UV radiation), mostly through oxidative reactions that degrade polyunsaturated lipids (e.g., lipid oxidation) or labile micronutrients (e.g., vitamins, pigments)(Berton-Carabin & Schroën, 2019; Camargo-Perea et al., 2020; McClements & Decker, 2018; Zhou et al., 2021). In sonication, the formation and collapse of air bubbles leads to the cleavage of water molecules and the formation of free radicals (Rao et al., 2016). Being one of strong oxidants,  $\cdot\text{OH}$  can oxidize any substance they encounter in emulsions, or they can react with each other to form  $\text{H}_2\text{O}_2$ . The amino acids such as tryptophan, histidine and cysteine can be easily oxidized by the  $\cdot\text{OH}$  (Quansah et al., 2013; Su & Cavaco-Paulo, 2021). The free radicals and  $\text{H}_2\text{O}_2$  also attack polyunsaturated fatty acids of lipids (Chemat et al., 2004; Yu et al., 2018). The natural emulsifiers and the oil phase might be oxidized when they are exposed to free radicals. In emulsions prepared by homogenisation, protein oxidation rarely occurs, but lipid oxidation may begin at the surface of the oil droplet where the labile lipid substrate encounters aqueous pro-oxidants (e.g., reactive oxygen species and metal ions).

Because of the health benefits of polyunsaturated lipids, increasing their amounts in food has become a priority, and thus counteracting lipid oxidation a major challenge. Recently, it has been suggested that propagation of the reaction may involve the transfer of reactive species and/or intermediate reaction products from the core of an oxidised oil droplet, through the interface and then through the continuous phase to neighbouring oil droplets (Laguerre et al.,

2017). Barrier effects of the oil-water interface are hence desirable to prevent the initiation and propagation of the reaction. In that respect, the composition and structure of the oil-water interface are thought to control, at least partly, the rate and extent of lipid oxidation (Berton-Carabin et al., 2014; Okubanjo et al., 2021; Singh & Indra, 2020; Yang et al., 2019a).

### 2.6.3 Digestive destabilisation

The ultimate step in food emulsion's lifespan is delivering nutrients, that is, its fate in the gastrointestinal tract, which has become an important field of research and an integral part of food emulsion formulation. When it comes to emulsion design, the composition and structure of emulsion-based systems have often been claimed to modulate their digestibility and thus control their digestive fate. Promoting the digestion and bioavailability of lipophilic bioactive compounds or delaying lipolysis via the emulsion structural design has been an active research area (Acevedo-Fani & Singh, 2022; Berton-Carabin & Schroën, 2019; Golding & Wooster, 2010; Mao & Miao, 2015; Sarkar et al., 2019; Singh & Ye, 2013; Ye, 2021). Substantial digestion studies on emulsions have been conducted using *in vivo* animal models and *in vitro* static and dynamic digestion models (Bohn et al., 2018; Brodkorb et al., 2019; Cheng et al., 2022a; Maldonado-Valderrama, 2019; McClements & Li, 2010a; Wang et al., 2019). However, the point of the present section is not to provide a comprehensive overview of the emulsion digestion process, but the possible physical and chemical changes during digestion.

#### 2.6.3.1 Structural disintegration and aggregation

Emulsions exist as liquid or semi-solid foods for consumer consumption. For semi-solid emulsions, such as aggregated emulsions or emulsion gels, the first destabilisation of the emulsion occurs in the oral cavity due to chewing, followed by further disruption in the stomach and the small intestine due to peristalsis and emptying, as well as dilution by saliva

and gastro-intestinal (GI) digestive fluids. Different from the semi-solid emulsion, the structure of liquid emulsions is unlikely be altered by chewing during the oral phase due to the short residence time. In the gastric phase, droplet-droplet aggregation induced by gastric acidification may occur in protein-stabilised emulsions. In gastric digestion, the pH of the gastric mixture decreases gradually by the secreted acids. When the pH is close to the isoelectric point of the proteins, the electrostatic repulsion between protein-stabilised droplets is minimised and droplet-droplet aggregation occur. Meanwhile, the extent of droplet aggregation varies with the protein structures and compositions at the O/W interface. For example, in the emulsions stabilised with whey proteins after heating, the droplet are aggregated but less coalescence during gastric digestion as compared to whey protein-stabilised emulsion without heating (Ye et al., 2020). For emulsion stabilised with various type of milk proteins showed different extent of droplet flocculation: milk protein concentrate (MPC)-stabilised emulsion > calcium-depleted-MPC-stabilised emulsion > sodium caseinate-stabilised emulsion (Wang et al., 2019). However, all types of the droplet aggregation via the adsorbed protein, from initial emulsion preparation or gastric acidification, can eventually be broken down by pepsin hydrolysis during the gastric phase (Kenmogne-Domguia et al., 2012). When the droplets flocs are emptied into the small intestine, bile salts diffuse to the droplet surface, and replace the adsorbed protein, thus the droplet flocs are disrupted (Bellesi et al., 2014; Sarkar et al., 2016b). Together, droplets will finally be released from the aggregated or gel matrix, which increases the surfaces exposure to lipolysis in the GI tract. As a result, a faster lipid digestion will be observed in emulsions with small droplet size distribution after gastric digestion (Bellesi et al., 2014; Kenmogne-Domguia et al., 2012; Sarkar et al., 2016b; Wang et al., 2019; Ye et al., 2020).

### 2.6.3.2 Droplet coalescence in the gastric phase

Droplet coalescence in the GI tract is mainly caused by the increase of interfacial mobility due to the loss of intact protein through proteolysis action. In the absence of a protein layer acting as a mechanical barrier, it is possible for droplets to coalesce. The resulting small peptides generally have less electrostatic repulsion and less steric barrier than intact proteins (van Aken, 2003; Caessens et al., 1999; Li et al., 2013a; Sarkar et al., 2009). Therefore, coalescence of the droplets occurs in the emulsions when their adsorbed proteins are hydrolysed into small peptides.

### 2.6.3.3 Lipid digestion in the small intestinal phase

In the human GI tract, lipid digestion starts in the stomach but mainly takes place in the small intestine, where the digestion products are also absorbed (Golding & Wooster, 2010). Food lipids are mainly triacylglycerols, which are digested by lipases that hydrolyse the ester bonds at the sn-1 and sn-3 positions of the glycerol backbone. Lipases act at the oil-water interface, where the water-soluble lipase and the lipid substrate meet (Wilde & Chu, 2011). To ensure optimal lipolysis in the small intestine, bile salts and to a lesser extent phospholipids remove digestion products from the interface by solubilising them in mixed micelles in the bulk aqueous phase to prevent inhibition by lipolysis products (Golding & Wooster, 2010). This facilitates further lipid digestion by driving the reaction equilibrium towards continued lipolysis. The formation of mixed micelles, together with phospholipid vesicles, completes the lipid digestion/absorption cycle by facilitating absorption across the intestinal lumen. Eventually, the emulsion droplets will shrink as the emulsified lipid in the interior of the

droplets convert to free fatty acids and mixed micelles during digestion (Sarkar et al., 2019; Wilde & Chu, 2011).

### 2.7 Techniques and methods to characterise emulsions

Emulsions formulated from a variety of ingredients and processing conditions display a wide range of physical and chemical characteristics that give food emulsions essential functions in which stability, texture, taste, appearance, and biological response can be tailored to meet the target requirements of any given product. For example, droplets of different emulsions have different droplet and interfacial characteristics, including their size, charge, concentration, interaction, and rheological behaviour. For this reason, experimental and analytical methods are necessary to provide information on these characteristics. It is important to be cautious when describing emulsion behaviour based on any single analytical method, as each has limitations; evidence needs to be obtained through comparable or complementary measurements to draw meaningful conclusions. In this section, common methods used to assess emulsion structures related to appearance, morphology, and size are summarized and compared. Advanced techniques of (ultra-) small angle X-ray/neutron scattering for quantifying interfacial layer structure and oil molecule diffusion in emulsions are subsequently discussed.

#### 2.7.1 Visual and tactile observation

Emulsion appearance is affected by the emulsion properties and stability, which can be observed directly by the naked eye. Visual observation is probably the cheapest and fastest method to assess the emulsion instability at the macroscopic scale, and tactile assessment is its viscosity.

For the diluted (volume fraction of dispersed phase  $\varphi < 0.1$ ) and semi-diluted emulsion ( $0.3 < \varphi < 0.64$ ), the emulsion is a liquid-like dispersion that flows easily upon inverting the

container up-side-down (Pal, 2011). The emulsion can turn into a viscous-like fluid with increasing  $\varphi$ , and flows slowly in the inversed container and stick on the wall of the container, which is attributed to droplet-droplet interactions at the higher  $\varphi$ . At low  $\varphi$  where the emulsion can flow, gravitational separation can lead to creaming or sedimentation in still emulsions, if the droplets are large. In this sense, the phenomena of creaming or sedimentation can be qualitatively assessed by observing the presence of creaming or sedimentation layer with a naked eye, or quantitatively measuring the thickness of the layers (as a ratio on the total emulsion height) to define the extent of gravitational separation. In emulsions with large initial droplet size ( $> 1 \mu\text{m}$ ), such as Pickering emulsions, rapid gravitational creaming (within minutes or hours) can be observed, where the emulsion undergoes further droplet flocculation or coalescence. However, the droplet flocculation or coalescence occurring in such emulsions is difficult to discern by simple visualisation. The creaming of emulsions with nanoscale droplet size caused by mechanisms such as flocculation, coalescence, and Ostwald ripening is usually slow and is only observed when the extent of instability is considerable and droplet growth exceeds the micron size. Thus, the initial stage of nanoemulsions instability cannot be captured by visual observation.

The appearance of concentrated emulsions ( $\varphi > 0.64$ ) is usually seen in its high viscosity, in some case to the point of soft-gel characteristics, which is due to the jamming of the droplets, conferring a stability against the movement of droplets driven by gravity. Thus, gravitational separation in concentrated emulsion is extremely slow and hard to observe, until a great extent of instability resulting in an oil layer and in some cases phase inversion. Therefore, identifying further the causes of emulsion instability, e.g., initial droplet size, flocculation, coalescence, Ostwald ripening, and oil exchange need to be precisely measured with the aid of analytical instruments.

### 2.7.2 Microscopy

Many of the structural components in emulsions are smaller than the low limit ( $100\ \mu\text{m}$ ) of visual observation. For example, droplet morphology, droplet-droplet distance, and interfacial layer organisation, needs microscopy for fine observation. A number of microscopic techniques are now available to characterise the structures of the emulsions including the droplets interfaces. The methods include optical microscopy, confocal laser scanning microscopy (CLSM), SEM and TEM (Dudkiewicz et al., 2011; Klang et al., 2012; Mertz, 2019; Murphy & Davidson, 2012; Sriamornsak et al., 2008). These techniques are capable of providing information about complex structures in the form of images that are relatively easy to visualise. Each microscopic technique works on different physicochemical principles and can be used to examine different levels and types of structural organization (Dudkiewicz et al., 2011; Klang et al., 2012). To study the emulsion's microstructure, all types of microscopic observations share common shortcomings: (1) sample preparation alters the original structure; (2) sample preparation and analysis are usually time consuming; and (3) a large sampling size is required to obtain reliable quantitative data. For this reason, it is important that investigators select the appropriate microscope instrument for their samples and follow appropriate sample preparation procedures.

Nevertheless, any type of microscope that is to be used to examine the structure of small objects must have three qualities: resolution (the ability to distinguish between two objects in proximity), magnification (the number of times the image is larger than the object being examined), and contrast (the extent of difference between the object and the background) (Aguilera et al. 1999).

#### 2.7.2.1 Optical microscopy

Optical microscopy can provide valuable information about the particle size distribution of emulsions as well as distinguishing between flocculation and coalescence, which is often difficult using particle sizing techniques that are based on light scattering. The major advantage of optical microscopy over other microscopic techniques is simple sample preparation involving spreading an emulsion across a slide. However, in practice, conventional optical microscopy is not suitable for emulsions made of droplets below about 1  $\mu\text{m}$ . The Brownian motion of small particles could cause images to appear blurred. For example, the WPMs with a diameter of 200 nm are invisible in water (**Figure 2-8a insert**) and at the heptane droplet interfaces by optical microscopy (**Figure 2-8a**) (Destribats et al., 2014). Another drawback of optical microscopy, that even using the conventional bright field, it is difficult to reliably distinguish different components in food emulsions because the natural contrast of food components has close refractive indices.

### 2.7.2.2 Confocal laser scanning microscopy

Compared to conventional light microscopy, CLSM can provide better resolution, allow selective observation of the location of specific components, and generate three-dimensional structural images without physical sectioning of the specimen. CLSM techniques are often combined with fluorescent dyes to observe the microstructure of multiple components in emulsions. This is made possible by the fact that fluorescent dyes can selectively bind to specific components such as proteins, lipids, or carbohydrates; for example, by using Fast Green FCF staining and irradiating with a He-Ne laser, adsorbed protein particle layer at the oil droplet interface could be selectively observed at wavelengths around 619 nm (**Figure 2-8c**). Scanning of the laser beam in a specific X-Y plane within the sample allows the acquisition of a two-dimensional image. Through a combination of consecutive X-Y planes at different vertical depths (Z-plane), a three-dimensional image of the emulsion can be created. Moreover,



the new generation of the Airyscan confocal super-resolution microscope is able to improve the resolution two-fold and signal-to-noise ratio eight-fold relative to conventional confocal microscopes (Wu & Hammer, 2022). As the Airyscan confocal super-resolution microscope can push the probed size down to 100 nm, it has been popular in cell biology and protein morphological studies, and considered as an alternative to electron microscopy (Deroubaix et al., 2020; Hennig & Manstein, 2021; Romero et al., 2020).

### 2.7.2.3 Electron microscopy

Electron microscopy is commonly used to observe structures ( $< 1 \mu\text{m}$ ) that are too small to observe using optical microscopy and CLSM, which is attributed to electron beams having much smaller wavelengths than light beams. TEM and SEM are two microscopies that are commonly used to examine the structure of emulsions. In practice, the smallest size of the structure that can be resolved is about 1 nm. Hence, it can be used to provide information about protein aggregates, nanoemulsion droplets, surfactant micelles, and interfacial layers (Dudkiewicz et al., 2011; Klang et al., 2012).

TEM is commonly used to provide information of a two-dimensional cross-section of the structure. For example, a cross-sectional image of soy oil droplet interface, observed by TEM, shows that it is stabilised by droplets coated with WPMs, the dimensions of the droplets and WPMs being approximately 500 and 200 nm, respectively (**Figure 2-8d**) (Cheng et al., 2019). In TEM, the electron beam is focused and directed through the samples by a series of magnetic lenses. Part of the electron beam is either absorbed or scattered by the object, while the rest is transmitted. The transmitted electron beam is magnified by a magnetic lens and then projected onto a screen to create an image of the specimen. Electrons are highly attenuated by most materials and therefore samples must be sectioned to extremely thin ( $\sim 50 - 100 \text{ nm}$ ) layers.

To enhance the electron density contrast between components, selectively staining the sample with various heavy metal salts, such as lead, tungsten, or uranium, is applied. These metal salts may bind to the component itself (positive staining) or to the surrounding material (negative staining). The need to use very thin dehydrated samples that often require staining means that sample preparation is considerably more time-consuming and cumbersome than for other forms of microscopy and may lead to appreciable image artefacts.

A more three-dimensional structure, i.e., the surface topography of samples, can usually be observed by SEM. Rather than measuring the electrons passing directly through the sample, the measurement relies on the secondary electrons produced when the sample is bombarded by the electron beam. Sample preparation for SEM is much easier than for TEM and does not require an ultra-thin sample. However, attempt to directly observe hydrated samples using any electron microscopy techniques, either SEM or TEM, would result in an instantaneous vaporization of water due to the high vacuum. Therefore, the sample used in conventional SEM needs also to be dehydrated by freeze-drying, which may alter the structure of the sample, such as causing shrinkage and aggregation between particles. Recent advances in electron microscopy techniques allow the observation of liquid containing samples under a frozen state by cryogenic preparation (Echlin, 1992). In the cryo-microscopy technique, the sample is frozen and is maintained within the microscope at low temperature. This enables the sample to remain hydrated under high vacuum. The freezing step permits the preservation of the original structure, and the technique is relatively fast and requires few preparation steps. For example, with the cryo-SEM techniques, the droplet interface maintain its shape without vigorous shrinking allowing the observation of thin film between the WPMs aggregates at the heptane-in-water interfaces (**Figure 2-8b**) (Destribats et al., 2014).

Despite the advancement in microscopic instrumentation, the optical microscope is still by far the most used instrument in many laboratories because it is easily accessible and can be used without extra sample preparation such as staining, drying, and sectioning. Therefore, it is frequently used to obtain information on the shapes and size of droplets of the emulsion in the initial formulation stage, and even to monitor the droplet size evolution. However, because optical microscopes do not provide enough information for identifying the emulsion composition, confocal microscope is usually used, in combination, to provide more useful information on the distribution and structure of the compositional materials (e.g., emulsifiers and oils). To further examine the topological structure of specimens, TEM and SEM are also used to supplement confocal and optical microscopy observations.

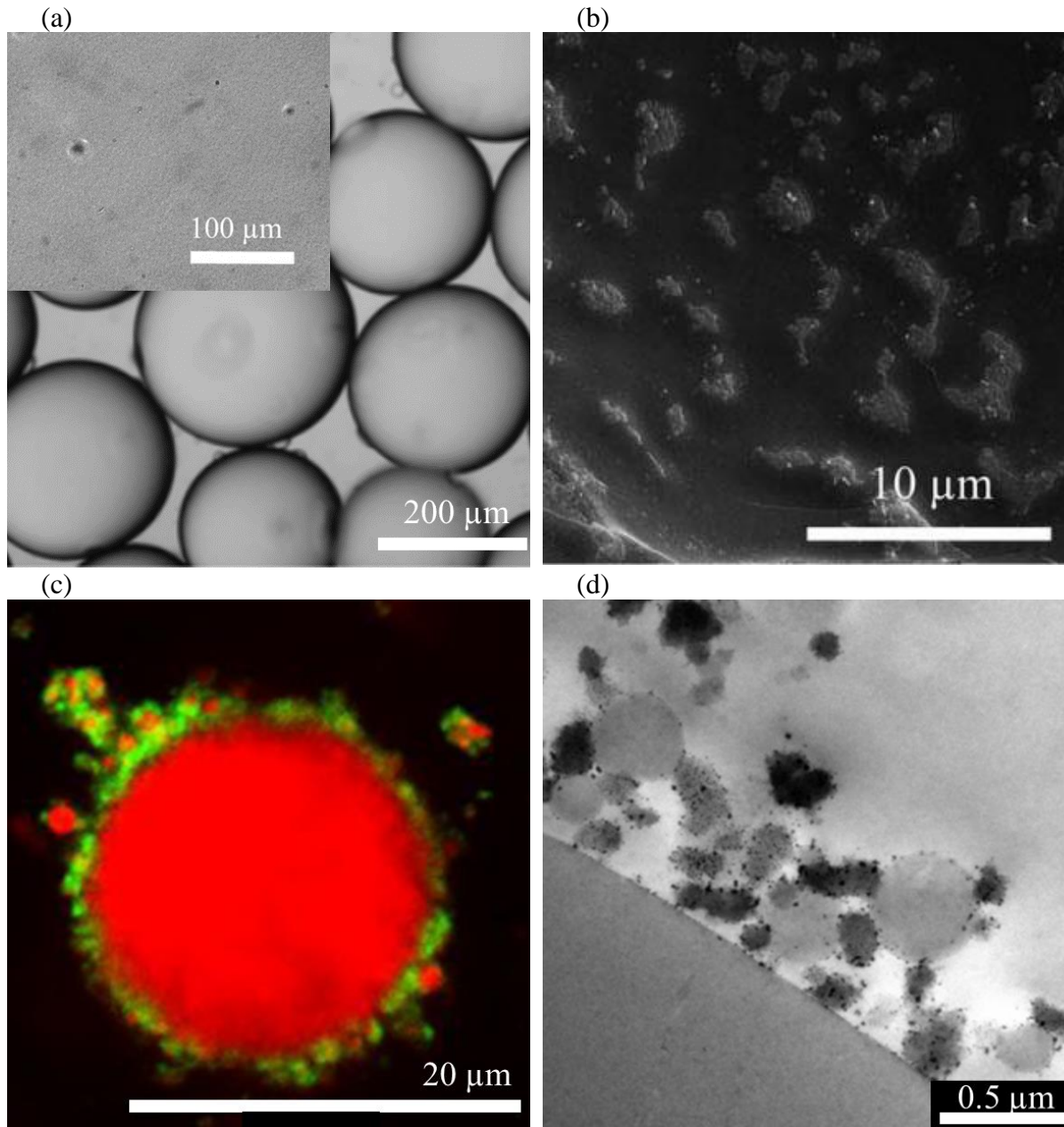


**Figure 2-8:** (a) 0.1 % WPMs-stabilised heptane droplets observed by optical microscopy and by (b) cryogenic-scanning electron microscopy (cryo-SEM); insert is 4 % WPMs particles in water observed by optical microscopy [reprinted from Destribats et al. (2014), with permission by Royal Society of Chemistry]. (c) WPMs-coated-primary emulsion-stabilised soy oil droplet observed by confocal laser scanning microscopy (CLSM) and by (d) transmission electron microscopy (TEM); in CLSM observation, the red colour represents the oil phase stained by Nile Red and the green colour represents the protein particles stained by Fast Green FCF [reprinted from Cheng et al. (2019), with permission by American Chemical Society].

### 2.7.3 Particle sizing by light scattering

Most current particle sizing analyses are based on static light scattering (SLS) that is measuring the angular dependence of the scattered light or are based on dynamic light scattering (DLS) that measuring the intensity fluctuations in the scattered light. The advantages of determining particle size by scattering techniques over microscopic observation are (1) the scattering pattern recorded by the detectors is analysed automatically by software yielding particle size distributions, (2) they provide an average size of all droplets within minutes, whereas particle size determination by microscopic observation is subjective due to the limitations of the sample size and the bias of the observer. Monitoring particle size distribution of an emulsion with time is essential for predicting its long-term stability to creaming, flocculation, coalescence, and Ostwald ripening. The time-dependent evolution of the particle size distribution can be used to monitor the kinetics of these destabilization processes.

#### 2.7.3.1 Static light scattering

Particle sizing using SLS is based on the principle that a monochromatic beam of light generated by a laser (e.g., He-Ne,  $\lambda = 632.8$  nm) passed through the emulsions, where it is scattered by the emulsion droplets. The intensity of the scattered light is measured as a function of scattering angle using an array of photosensitive detectors located around the sample. The scattering angle is inversely related to the particle size, and the calculation of particle size distribution requires the input of the refractive index of both the scatter and surrounding liquid at the wavelength of the laser used. Many of commercial static light scattering instruments are now fully automated, easy to use, and provide full particle size distribution of an emulsion within seconds, i.e., the MasterSizer 2000/3000 measures the particle size distribution from 0.02 to 2000  $\mu\text{m}$  in diameter.

However, it should be noted that light scattering methods are suitable for measuring diluted emulsions but not suitable for in situ analysis of food emulsions that are optically opaque or solid-like (e.g., salad dressings, mayonnaise, butter, margarine, and ice-cream) because of problems associated multiple-scattering. In practice, SLS instruments are usually equipped with a water tank and stirring pump for dispersing the sample. This is designed for diluting the emulsion to a relatively low concentration of droplets (~ 0.1 %, translucent appearance) before the measurement, and preventing the multiple scattering effect that causes the underestimation of the droplet size. Thus, the dilution and stirring in SLS instrument disrupt the reversible droplet-droplet interactions and may alter the continuous phase of the emulsion. When SLS is used to determine the individual droplet size of an irreversibly aggregated emulsion, a surfactant (such as SDS) is usually added to disaggregate the oil droplets.

### 2.7.3.2 Dynamic light scattering

DLS, also known as photon correlation spectroscopy, are based on measurements of the translational diffusion coefficient of droplets determined by analysing the interaction between a laser beam and a particle (Dalglish & Hallett, 1995). It does this by illuminating the object with a laser and analysing the intensity fluctuations in the scattered light. It faces the similar problem of multiple scattering to SLS and requires a low dispersion concentration of emulsion that is a translucent Newtonian fluid. DLS are particularly useful for measuring the size of particles that are smaller than 5  $\mu\text{m}$ , for example, nano-scale emulsion droplets, protein aggregates, surfactant micelles, and other nanoparticles. Commercial instruments, such as the ZetaSizer, based on this principle are typically capable of analysing particles with diameters between 0.003 and 5  $\mu\text{m}$ . As well as determining particle sizes, dynamic light scattering techniques can also be used to monitor the flocculation of particles in suspensions because aggregation causes them to move more slowly (Dalglish & Hallett, 1995). It can also be used

to determine the thickness of adsorbed layers of emulsifier on spherical particles (Fang & Dalglish, 1993; Hemar et al., 2021; Stetefeld et al., 2016). The radius of the spherical particles is measured in the absence of the emulsifier (providing they are stable to aggregation) and then in the presence of the emulsifier. The difference in radius is equal to the thickness of the adsorbed layer, although this value may also include the presence of any solvent molecules associated with the emulsifier. Alternatively, the change in particle radius can be monitored when a substance is added that causes the interfacial layer to be degraded and/or displaced, which also provides some measure of the dimensions of the interfacial layer (provided the particles remain stable to aggregation after the layer is removed).

### 2.7.4 Small-angle scattering

Small-angle scattering (SAS) techniques are widely used to probe the structure and interaction of materials at the Angstrom to micron length scale (Feigin & Svergun, 1987; Gilbert, 2019; Jeffries et al., 2021). SAS applications in colloids, complex fluids, and emulsions have benefited from the continued developments in instrument and sample environments capable of *in-situ* quantification of the structures of colloids or materials in response to changes in external conditions, such as SAS coupled with a rheometer to study structures under shear or flow (Rheo-SAS) (Burdette-Trofimov et al., 2020; Eberle & Porcar, 2012), with ultrasonication to study emulsion formation (Lee et al., 2019; Lee & Pozzo, 2019), and with high-pressure cell to investigate protein denaturation (Yang et al., 2016). SAS techniques are based on measurement of the angular-dependent intensity,  $I(Q)$ , of scattered X-rays (SAXS) or neutrons (SANS) versus the magnitude of the wave vector,  $Q$ ; with  $Q$  is given by

$$Q = \frac{4\pi \sin\theta}{\lambda} \quad (2-7)$$

where  $2\theta$  is the scattering angle of the incident beam and  $\lambda$  is the wavelength of the incident beam as shown in **Figure 2-9a**. To reach lower  $Q$  and access information on larger length scales, ultra-small-angle scattering (USAS) instruments are used to provide sufficient angular resolution since the probing length scale,  $d$ , in the scatter is inversely relate to the  $Q$  as

$$d = \frac{2\pi}{Q} \quad (2-8)$$

The resulting scattering intensity pattern,  $I(Q)$ , thereby, is a summed convolution of scattering of all length scale scatters illuminated in an incident beam as the function of  $Q$ , and can be expressed as

$$I(Q) = \Delta\rho^2 V_P \phi_P F(Q) S(Q) \quad (2-9)$$

where  $\Delta\rho$  is the contrast between the scattering particle and the surrounding solvent,  $V_P$  is the volume of scattering particle,  $\phi_P$  is the dimensionless particle volume fraction,  $F(Q)$  is the form factor, and  $S(Q)$  is the structure factor that accounts for the correlation between the colloidal particles.



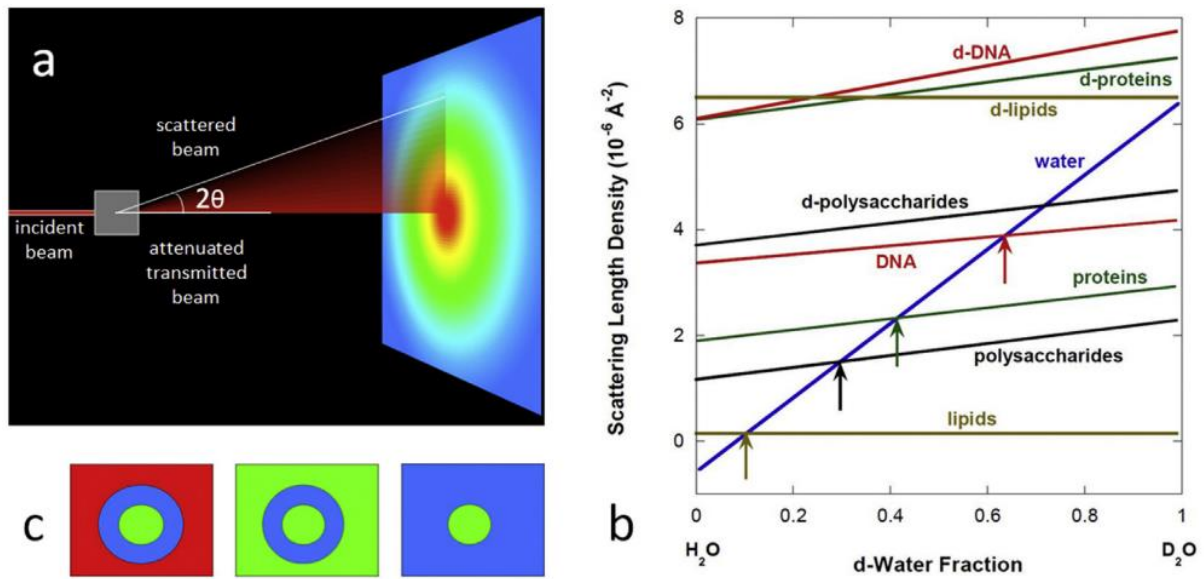


**Figure 2-9:** The basics of small angle scattering in food colloids. (a) Scattering geometry for a SAXS or SANS measurement; (b) Neutron scattering length densities for common food-based materials; (c) Core-shell structure in solution showing the possibility of selectively contrast matching two of the phases through changing solvent H<sub>2</sub>O/D<sub>2</sub>O composition: by matching the scattering length density of the solvent to core, only the shell is visible, while matching the solvent to the shell yields information only on the core [reprinted from Gilbert (2019a), with permission by Elsevier].

For SAS to function, there must be a contrast between the species of interest and its surrounding. The scattering contrast,  $\Delta\rho$ , is equal to  $\Delta\rho = \rho_p - \rho_s$ , where  $\rho_p$  and  $\rho_s$  are the SLDs of the species of interest and solution or surrounding matrix, respectively. The SLD,  $\rho$ , of a molecule with  $i$  atoms can be calculated from.

$$\delta N_A \sum b_i / M \quad (2-10)$$

where  $\delta$  is the bulk physical density of the molecule ( $\text{gcm}^{-3}$ ),  $N_A$  is Avogadro's number,  $b_i$  is the X-ray or neutron, as appropriate, scattering length of the  $i^{\text{th}}$  atom in the molecule and  $M$  is the molecular weight.

Thus, the SLD of the molecules and contrast between them can be calculated from knowledge of the physical density and the chemical formula of the molecules. Contrast is radiation source dependent, the X-ray scattering length is determined by the number of electrons, whereas the neutron scattering length is determined by the structure of the atomic nucleus. Contrast in SANS can be manipulated through 'contrast variation' which relies on the different neutron SLD of hydrogen and deuterium. As the SLD for  $\text{H}_2\text{O}$  is negative and for deuterium oxide ( $\text{D}_2\text{O}$ ) is positive, components may be strategically contrast matched using mixtures of  $\text{D}_2\text{O}$  and  $\text{H}_2\text{O}$  so that they effectively become transparent to neutrons as illustrated in **Figure 2-9b**; this greatly simplifies the scattering contributions in multicomponent systems as is shown in **Figure 2-9c** for a model core-shell particle with regions of different SLDs. Contrast variation may also be achieved through intrinsic differences in chemical composition and physical density or via strategic selective deuteration (Lee & Pozzo, 2019).

There is no doubt that measuring the structure of sample as close as possible to its "native" state, i.e., under the set environmental conditions, is desirable but also challenging. In this sense, SANS possesses particularly attractive attributes for food colloids as a non-invasive technique

over SAXS, because neutrons fluxes per unit area of the beam are significantly lower than X-ray. This implies that SANS measurement requires a larger sample exposure size (or say beam size) and longer exposure time. In addition, neutrons interact primarily with the nuclei of the elements, thus penetrating deeply into the sample without producing secondary ionising radiation. Compared to the radiation damage caused by X-rays, neutron scattering generally causes less damage to the structure of the sample. However, the high fluxes rate of synchrotron radiation source X-rays allow the unique experimental design for very rapid time-resolved studies and high-throughput screening of low-concentration and limited-volume samples (Lee et al., 2019).

The absence of special sample preparation, such as staining and sectioning, undoubtedly creates fewer possible sample artefacts giving small angle scattering techniques more advantages over microscopy for quantitative analysis of structures. However, unlike microscopy techniques which provide direct visualisation of images, SAS produces non-visual information, providing structural information in 'reciprocal space'. This means that the scattering data must be inverted to real space or fitted with a reciprocal space model through mathematical functions and constrained by existing known parameters of the system. Information obtained from complementary techniques, e.g., microscopy and light scattering, is therefore essential. In practices, conducting SANS measurements with multiple contrasts serves to reduce the number of possible models. Mathematical form factors have been developed and applied to many scattering symmetries. These form factors can be combined with a range of structure factors to describe interparticle interactions and separation, the latter giving rise to correlation peaks. Occasionally, complicated models are not strictly required, and some structural parameters can be extracted from data in a straightforward manner, for example, Guinier or Porod analysis and in systems exhibiting fractal behaviours.

### 2.7.4.1 Small angle X-ray scattering in emulsion studies

SAXS technique is a powerful tool for characterising the overall structures of colloids in Pickering emulsions, such as the internal structure of potential Pickering emulsifier, as whey protein microgel particles (Schmitt et al., 2010), and for *in-situ* monitoring on of the formation of Pickering emulsion stabilised with amphiphilic gold nanoparticles (Lee et al., 2019). In these colloidal systems, the scattering contrast arises between the scatters (particles or whole droplets) and their surrounding aqueous phase. For example, the structure of WPMs was investigated by SAXS at a range of pH conditions from pH 2.0 to 8.0 (Schmitt et al., 2010). As shown in **Figure 2-10a**, the scattering profiles are primarily expected to reflect the overall size and shape of the WPMs at low  $Q$  regime (left end on X-axis). At high  $Q$  regime, the internal structure of the WPMs is primarily observed. A closer observation at scattering intensity the high  $Q$  regime showed that WPMs at all pH values exhibited a correlation peak at  $Q = 0.67 \text{ nm}^{-1}$  (**Figure 2-10b**). This correlation peak corresponds to a real-space distance of 9.2 nm, which could be related to the internal organization of the denatured whey protein monomers within the microgel. At pH values close to the isoelectric point (IEP), the correlation peaks are more pronounced due to the higher average number of close neighbours compared to the case of the highly charged building blocks at pH away from IEP. As the internal structure is proposed to be fractal, a power-law decay of the scattering curve should be observed (**Figure 2-10a**). The slope or fractal dimension is directly related to the compactness of the aggregate, where densely packed structures give rise to a scattering intensity which is decaying more steeply than more open structures with a smaller fractal dimension as illustrated in **Figure 2-10c**. The limiting case of a fractal dimension of 1 corresponds to a situation where the strands are stretched and are locally becoming cylindrical (Burchard, 1999; Schaefer, 1989; Zemb & Lindner, 2002).

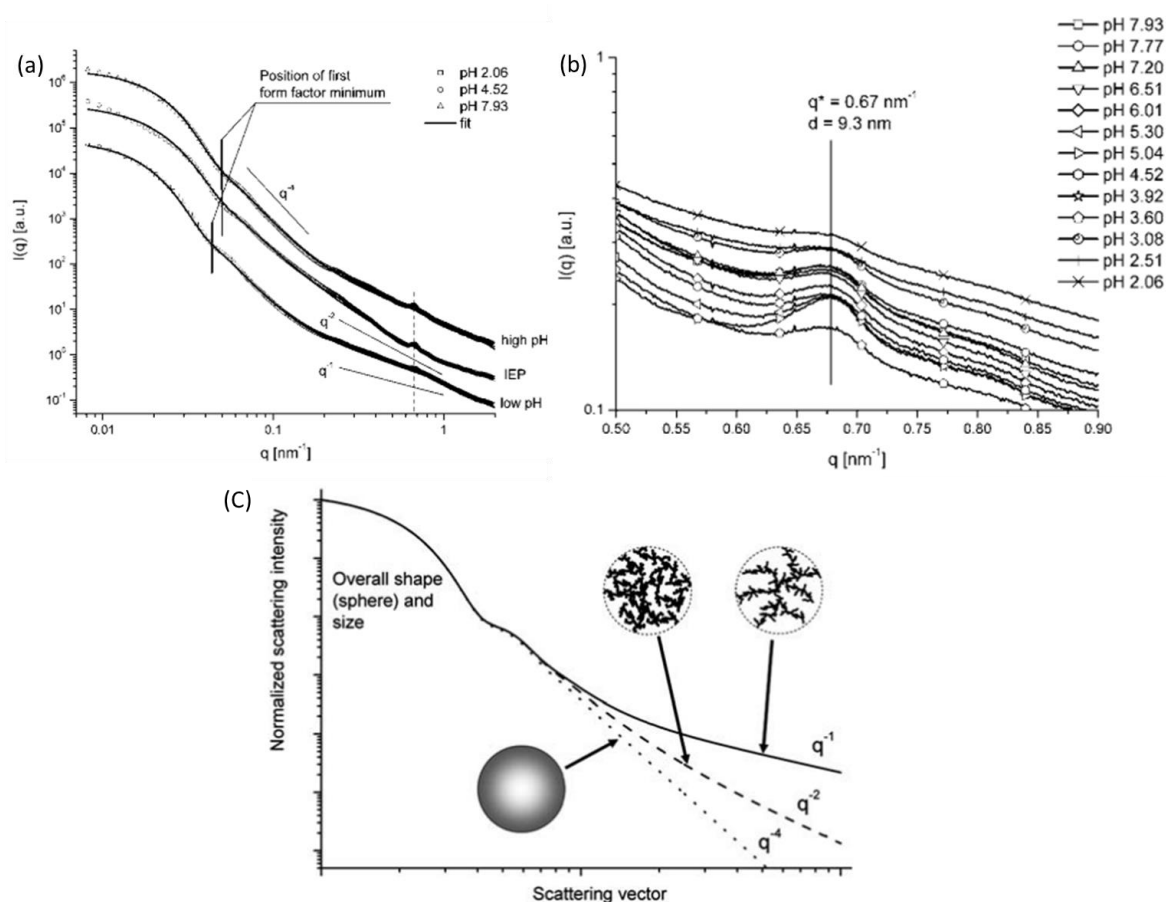


**Figure 2-10:** (a) SAXS curves obtained from 4 % w/w WPM dispersions at selected pH values after subtraction of the solvent scattering. The curves are shifted vertically for better visibility. The fitting model consisted of a lognormal distribution of homogeneous spheres plus a power law decay of the intensity. The sample close to the isoelectric point (IEP) show correlation peak at the high  $Q$ -regime due to aggregation. (b) Enlargement of the high- $Q$  regime of the SAXS curves showing the correlation peak at  $Q = 0.67 \text{ nm}^{-1}$ . (c) Theoretical scattering curve that results from a combination of a form factor of polydisperse spheres (10% polydispersity) and a contribution from the fractal internal structure of the microgel. At low- $Q$  regime the curve is dominated by the overall size and shape of the particles. At high- $Q$  regime the contribution of the fractal internal structure becomes important, leading to a power-law decay of the scattering curve. Relatively densely packed aggregates (e.g., fractal dimension of 2) give rise to a scattering curve which is decaying steeply ( $q^{-2}$ ) than more open structures with smaller fractal dimensions ( $q^{-1}$ ) [reprinted from Schmitt et al. (2010), with permission by Royal Society of Chemistry].

SAXS has advantages over other techniques in terms of examining emulsion formation in-situ (Larson-Smith & Pozzo, 2012; Lee et al., 2019). Lee et al., (2019) has conducted the USAXS experiment at a custom designed acoustic sample environment to quantitatively examine structural changes of perfluorooctane during the application of acoustic forces (**Figure 2-11**). The gold nanoparticles (GNP) and the coarse surfactant-free perfluorooctane were co-dispersed at a volume ratio of 1:50. The dispersions of oil droplets and GNP were then sonicated using a focused ultrasound sample environment at various acoustic conditions. **Figure 2-11** shows the structural changes quantified using ultra- small-angle X-ray scattering (USAXS) during sonication at various acoustic pressures (**Figure 2-11a**) as well as at different sonication time when the acoustic power is fixed (**Figure 2-11b-c**). With increasing acoustic pressure, two major changes in the scattering curves can be observed: one is in the low- $Q$  regime that is typically associated with a change in the droplet size distribution, and the other is in the medium- $Q$ , which is the characteristic features for Pickering emulsion formation, i.e. presence of a broad correlation peak arising from in-plane correlations of particles located at the oil droplet interface (Larson-Smith & Pozzo, 2012).

As suggested by Larson-Smith & Pozzo (2012), the interparticle distance can be estimated by the position of the correlation peak using  $D = 4\pi/\sqrt{3Q_{peak}}$ . As the scattering profiles at different acoustics pressure shown in **Figure 2-11a**, only samples sonicated at 7.2 MPa showed this characteristic inflection. Lee et al., (2019) have defined that cavitation events were crucial for Pickering emulsion formation and its threshold is above 6.4 MPa. Thus, the sub-threshold sample did not show any characteristic features of Pickering emulsion regardless of sonication time but only the changes on the perfluorooctane emulsion (surfactant free) size distribution (**Figure 2-11b**). However, the sample sonicated at 7.2 MPa showed an immediate change in the scattering profile (**Figure 2-11c**).

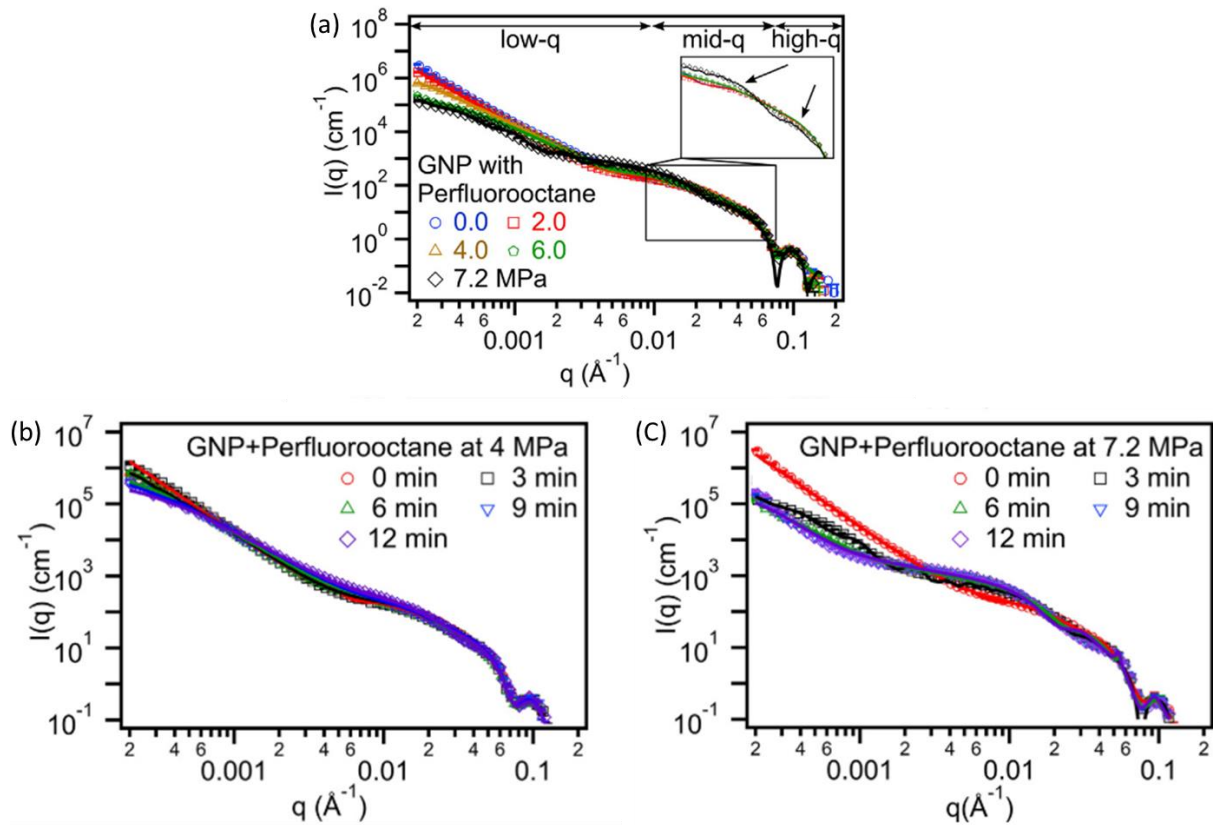


**Figure 2-11:** USAXS scattering curves of GNP with perfluorooctane sonicated at (a) various acoustic pressures. A model containing 2 spheres was used to fit the sample sonicated at acoustic pressures lower than the cavitation threshold (<6.4 MPa), and a Debye model was used to fit the sample sonicated at 7.2 MPa. Scattering length densities were fixed for water ( $9.47 \times 10^{-6} \text{ \AA}^{-2}$ ), gold ( $124.69 \times 10^{-6} \text{ \AA}^{-2}$ ) and perfluorooctane ( $14.47 \times 10^{-6} \text{ \AA}^{-2}$ ). Scattering profiles of GNP with perfluorooctane sonicated at (b) 4 MPa (no cavitation) and (c) 7.2 MPa (cavitation) with increasing sonication time [reprinted from Lee et al. (2019), with permission by Elsevier].

### 2.7.4.2 Small angle neutron scattering in emulsion studies

SANS has two major advantages over SAXS: (1) the different isotopes have different SLDs, which are particularly valuable in organic molecules, i.e., the SLDs of H is  $-0.374 \times 10^{-12}$  cm and of D is  $0.6674 \times 10^{-12}$  cm; (2) the small adsorption cross-section of cold-thermal neutron makes them a penetrating probe that causes relatively little radiation-induced damage. SANS can, therefore, be used as non-invasively tool to probe buried interfaces, with the added benefit of contrast variation, allowing the use of isotopes to highlight specific components of the system.

Yesiltas et al. (2019) has investigated the interfacial structure of 70 % O/W emulsion stabilized with combinations of CAS and phosphatidylcholine (PC) by SANS (Yesiltas et al., 2019) . The contrast-variation is implemented by varying the oil phase with fish oil and deuterated hexadecane. **Figure 2-12** showed the SANS curves of fish oil (red dot and black dot curves) are dominated by  $q^{-4}$  slope which arises from overall globular droplets including the contributions from all components. The scattering curve with deuterated hexadecane (blue dot curve) follows  $q^{-2}$  slope, which means that the scattering of hexadecane is matched out by the solvent D<sub>2</sub>O, and the scattering comes from a thin film where a lamella structure of the interfacial layer as  $q^{-2}$  slope extends to middle- $Q$ . This allows to calculate the interface thickness as  $T \approx 3.2$  nm by  $q \propto 1/T$ , which corresponds to the monolayer of PC. The researchers proposed that the interface is dominated by a well-defined PC monolayer while CAS particles remain loosely bound and are influenced by their proximity, forming so-called patchy arrays on the PC layer.



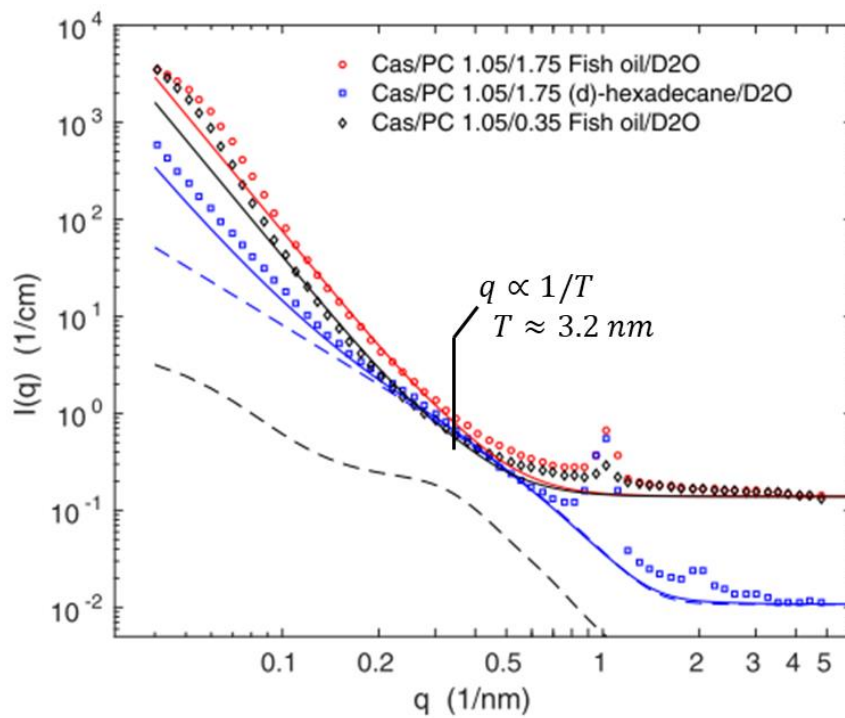


**Figure 2-12:** SANS profiles for O/W emulsion of fish oil (red and black dot) and deuterated hexadecane (blue dot) emulsified by combination of CAS (1.05% w/w) and various PC concentrations (0.35 and 1.75 % w/w). The solid lines are calculated total scattering from PC monolayer and CAS particles with a constant background contribution, while dashed lines represent the individual scattering contribution from CAS particles (black) and PC monolayer (blue) [reprinted from Yesiltas et al. (2019), with permission by Elsevier].

The main advantage of contrast variation-SANS as a molecular-transport characterization tool originates from differences in SLDs between hydrogenated and deuterated versions of identical molecules. This allows researchers to directly examine exchange kinetics using nearly identical molecular isotopes without the need for any additional labelling. Lee & Pozzo (2019) have investigated the kinetics of oil exchange between (*d*-)hexadecane droplets in emulsions with and without the presence of SDS as shown in **Figure 2-13**. The emulsions without the presence of surfactant had hydrodynamic diameter of 907 nm with a polydispersity index (PDI) of 0.3, while emulsions emulsified by SDS had a mean diameter of 98 nm with a PDI of 0.2 as determined by DLS. Examples of the obtained SANS profiles and its modelled fits are shown in **Figure 2-13**. As can be seen in the figures, all the samples showed a decrease in scattering intensities over time, indicating that oil molecules were able to exchange between droplets regardless of whether SDS were present or not. Interestingly, the decrease in scattering intensity was extremely slow for samples without SDS. Still, ultimately the emulsion systems would reach a fully mixed state where minimal scattering intensities were recorded in the mixed control samples. When surfactants were present, the recorded scattering intensities decreased at a significantly faster rate. However, the exchange rate was not significantly accelerated when surfactant micelles were present. This suggests that micellar-mediated transport mechanisms do not play the dominant role in these systems. Primary mechanisms for oil exchange in insoluble anionic surfactant-stabilized emulsion systems are hypothesized to be through direct emulsion contact, reversible coalescence, and/or direct oil permeation through thin liquid films.

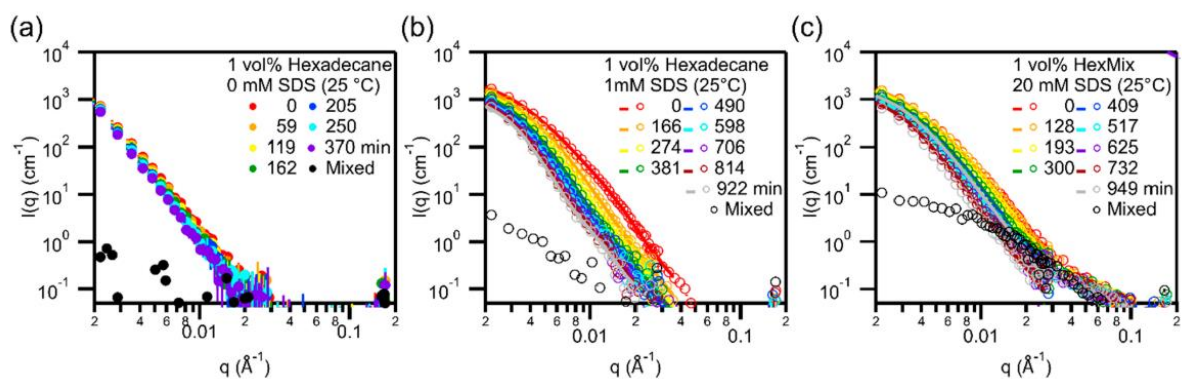


**Figure 2-13:** Scattering profiles of droplet oil exchange at (a) 35 °C, (b) 45 °C, and (c) 60 °C of a 1 vol % hexadecane emulsions stabilized by 1 mM SDS sample. Increasing sample environment temperature results in a faster decrease in scattering intensities [reprinted from Lee & Pozzo (2019), with permission by American Chemical Society].

### 2.8 Conclusion

During the last decade, various types of particles have been developed and studies for their applications in emulsion-based system. Substantial attention has already been given to the suitability of protein-based particles derived from milk proteins (Araiza-Calahorra & Sarkar, 2019; Destribats et al., 2014; Dickinson, 1994b; Li et al., 2013b; Lv et al., 2020; Shi et al., 2020; Wei et al., 2020; Xu et al., 2020b; Yan et al., 2020; Zhang et al., 2021b; Zhao et al., 2021b) and lipid-based particles coated with milk proteins to stabilise oil-in-water emulsions (Lim et al., 2020; Pawlik et al., 2016; Sakellari et al., 2021; Schröder et al., 2018; Ye et al., 2013b). Benefits in terms of physical stability have already been shown for different types of particles, which can be related to the fundamentally different mechanism of stabilisation as compared to conventional emulsifiers. Interfacial coverage and emulsion rheology have been shown to be influenced by particle structures, where soft particles can lead to a full and dense interfacial coverage as they can undergo substantial flattening at the oil-water interface (Destribats et al., 2014; Pawlik et al., 2016; Wang et al., 2018; Ye et al., 2013b). Additional benefits of using lipid particles over protein particles to stabilise emulsion have been shown to be the co-delivery of active compounds (Sakellari et al., 2021).

However, there are several potential mechanisms that must be understood prior to the functional applications of droplet-stabilised emulsions, including the formation, physicochemical properties, and stabilities (e.g., coalescence and oil-exchange between droplets) of droplet stabilised emulsions. In emulsion characterisation, small-angle neutron/X-ray scattering techniques are powerful tools, not only for probing particle/droplet structures at high resolution (Angstrom length scale), but also for examining droplet compositions using different scattering length densities of materials. The high sample penetration and resolution, as well as the absence of special sample preparation, undoubtedly can create fewer possible

sample artefacts, giving small angle scattering techniques more advantages over light scattering and microscopy and for quantitative analyses.

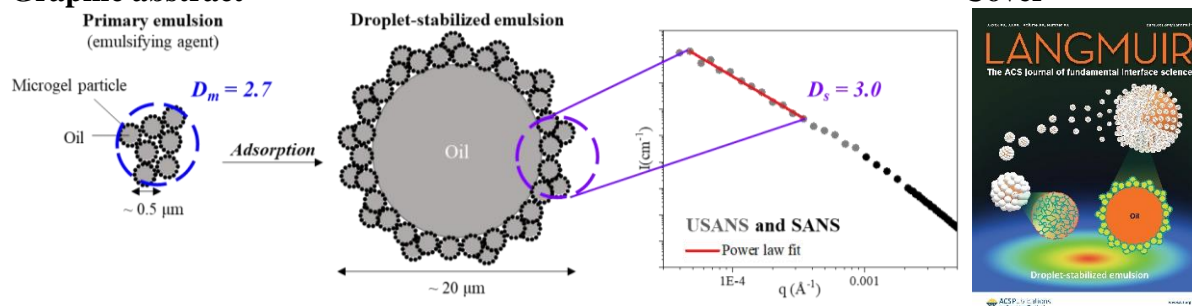
Herewith, the objectives of this project are:

1. Producing colloidal particles using milk proteins for making nano-sized primary droplets, and the production of droplet-stabilised emulsions. It is hypothesised that by varying the interfacial layer structure of the primary droplet, the subsequent adsorption behaviour of the primary droplet would be altered.
2. Characterising the adsorption of the primary emulsion at the interface of droplet-stabilized emulsion as affected by environmental conditions (i.e., concentration of primary droplet, ionic strength, and pH). It is hypothesised that adsorption of the primary droplets at the interface is enhanced by removing the adsorption competition from the co-existing free proteins and by decreasing the pH and droplet-droplet repulsion.
3. Investigating the mechanical properties and long-term stability of droplet-stabilised emulsions at a high dispersed droplet volume fraction of 70 % as affected by the adsorption of the primary emulsions and the environmental conditions. The primary emulsion droplet layer is assumed to be pH and temperature responsive. It is hypothesised that mechanical properties of concentrated droplet-stabilised emulsions are enhanced by a thicker primary droplet layer induced by lowering pH and by heating.
4. Investigating the behaviour of these DSE emulsions during *in vitro* dynamic gastric and intestinal digestion. The hypothesis is that the thick interface made of the nano-sized primary droplets slows down the enzymatic digestion of the core oil droplets.

5. Developing a methodology to characterise oil diffusion between the adsorbed primary droplets and the core droplet. It is hypothesised that inter-droplet oil exchange occurs in the emulsion due to the narrow contact between the primary and core droplets.

## Chapter 3 Interfacial structures of droplet-stabilized emulsions formed with whey protein microgel particles as revealed by small and ultra-small angle neutron scattering

### Graphic abstract



### Abstract

Droplet-stabilized emulsions (DSEs) were made from oil droplets coated with whey protein microgel (WPM) particles. The WPM particles with  $z$ -average hydrodynamic diameters of  $270.9 \pm 4.7$  and  $293.8 \pm 6.7$  nm were obtained by heating whey proteins with 10 mM phosphate buffer pH 5.9 (-PB) and no buffer (-NPB), respectively. The primary emulsions coated by WPM-NPB and WPM-PB particles had mass fractal dimensions of  $\sim 2.75$ , as determined by small and ultra-small angle neutron scattering (SANS and USANS). The size of the subsequently formed DSEs ( $D_{32} \approx 7 - 23 \mu\text{m}$ ), which were stabilized by the primary emulsion droplets, made with either WPM-NPB (termed DSE-NPB) or WPM-PB (termed DSE-PB) was dependent on the concentration of the primary emulsion (10 – 60 wt%) in the aqueous phase. At the DSE-NPB interface, the adsorbed primary emulsion droplets formed a fractal network with a surface fractal dimension of about 3, indicating a rough interfacial layer. Combined

SANS and USANS allowed a comprehensive understanding of the multi-length scale structures from WPM particles to DSEs.

### 3.1 Introduction

Proteins are important natural emulsifiers for the manufacture of edible oil-in-water emulsions, because of their amphiphilic characteristics and high surface activity. They adsorb on to oil–water interfaces through hydrophobic interactions and stabilize the emulsion with a combination of electrostatic and steric mechanisms (McClements, 2015b). To provide long term stability, colloidal protein particles can be used to produce Pickering emulsions (Binks, 2002; Destribats et al., 2014). One such type of colloidal particle is the whey protein microgel (WPM) with a diameter of ~ 150 nm, which is stable under different pH conditions, and can be obtained at pH 5.9 by heat treatment and homogenization (Schmitt et al., 2010). Pickering emulsions formed with these nano-sized WPM particles have been reported to be stable towards coalescence for up to 8 months of storage at pH 7 and 150 mM NaCl (Destribats et al., 2014). With changes in pH, the WPM particles assemble into different structures at the interface: at pH values near the isoelectric point of the WPM, the particles form a continuous two-dimensional network; at pH values far from the isoelectric point, they assemble as sparse individual aggregates, resulting in a differently structured interfacial layer (Destribats et al., 2014).

A novel type of protein-based particle, comprising a soft core of oil coated with casein micelles, has also been used as an emulsion stabilizer; it has the advantages of long term stability and lipophilic compound delivery (Ye et al., 2013b). These primary emulsion (PE) droplets were able to emulsify a newly formed oil–water interface, inducing a hierarchical oil-in-water emulsion that is referred to here as a droplet-stabilized emulsion (DSE). In the DSE system, Ye et al. (2013) reported that the PE droplet deformed significantly at the interface of



the DSE droplet. This deformation was probably driven by a tendency to maximize the interaction of the casein aggregates (adsorbed at the PE droplet surface) with the oil–water interface through the bridging of the protein between the interface of the PE droplet and the DSE droplet.

In the present study, we explore the effect of PE droplets coated with different WPM particles on the formation of a DSE and quantitatively describe the interfacial layer of the DSE. Different types of WPM particle dispersions were obtained by heating a whey protein solution in the absence and in the presence of 10 mM phosphate buffer pH 5.9. The adsorption and interfacial properties of both the WPM particles, and the subsequently produced PE droplets, were characterized. The arrangement of the PE droplets at the interface of the DSE were probed using small and ultra-small angle neutron scattering (SANS and USANS), transmission electron microscopy (TEM), and confocal laser scanning microscopy (CLSM). SANS and USANS were chosen because these are powerful non-invasive techniques for characterizing complex structures in various fields, e.g., biology (Heller & Littrell, 2009), environment science (Jarvie & King, 2007), and food science (Gilbert, 2019; Lopez-Rubio & Gilbert, 2009). They complement microscopy analyses well, providing bulk quantitative structure information of the whole sample (Lopez-Rubio & Gilbert, 2009). The influences of the structure of the WPM particles and the concentration of the PE on the interfacial structure of the DSEs are discussed.

### **3.2 Materials and methods**

#### **3.2.1 Materials**

Whey protein isolate (WPI) powder manufactured by ion exchange and proprietary ultra-filtration was obtained from Fonterra Co-operative Group Limited, Auckland, New Zealand. WPI powder contained 93.0 wt% protein, 4.8 wt% moisture, 1.0 wt% fat, 0.3 wt% lactose, 0.54

wt% sodium and 0.08 wt% calcium. Soya oil was purchased from Davis Trading Company, Palmerston North, New Zealand. All other chemicals used were of analytical grade and were obtained from either BDH Chemicals (BDH Ltd, Poole, UK) or Sigma-Aldrich (St. Louis, MO).

### 3.2.2 Preparation of WPM particles

The method for producing heat-induced WPM particles was adapted from Schmitt et al. (2010) with some modifications. The protein concentration was set to 4 wt% to obtain the optimum aggregation conversion yield of WPI. WPI powders were dissolved in ultrapure Milli-Q water (18.2 M $\Omega$ ·cm) or in Milli-Q water containing 10 mM phosphate buffer pH 5.9. The protein dispersions were stirred at room temperature for 1 h, followed by overnight storage at 4 °C to ensure complete hydration. The pH of the protein dispersions was adjusted to 5.90  $\pm$  0.01 using 2 M HCl or 2 M NaOH prior to heating.

The protein dispersions were heated at 85.0  $\pm$  1.0 °C in a water bath for 45 min under magnetic stirring at 500 rpm, with the heating time commencing from when the temperature of the dispersions reached 85.0 °C; the heated dispersions were subsequently cooled in a circulating cold-water bath at 18  $\pm$  1.0 °C. To remove the unwanted nonaggregated whey proteins and phosphate buffer, heated samples were washed by adding Milli-Q water and centrifuging at 20 °C and 20,000  $\times$  g for 15 min, and the supernatant was removed; this process was repeated five times. The nonaggregated whey proteins in the supernatant were checked with sodium dodecyl sulphate (SDS) polyacrylamide gel electrophoresis using a Bio-Rad mini-gel slab electrophoresis unit (Bio-Rad Laboratories, Richmond, CA) as described by Ye (2010). A negligible amount of whey proteins remained in the supernatant even after five washing steps (**Supplementary material, Figure S 3-1**). The centrifuged pellets were redispersed in Milli-Q water to a final protein concentration of 10 wt%.

To obtain a homogeneous WPM particle size, the WPM dispersions were homogenized using a micro-fluidizer (M-110EH; Microfluidics Corporation, Newton, MA) with three passes at a pressure of 138 MPa. In this article, the WPM particles made from the WPI dispersed in 10 mM phosphate buffer pH 5.9 are named WPM-PB particles and those made without phosphate buffer are named WPM-NPB particles. The extent of aggregation of whey protein and the structure of two WPM particles were expected to be different because the additional ionic strength from phosphate buffer promoted protein aggregation via charge screening and is unfavourable towards the thiol-disulphide bond exchanges (de la Fuente et al., 2002).

### **3.2.3 Emulsion preparation**

#### **3.2.3.1 PE preparation**

WPM particle dispersions with 10 wt% protein concentration were used for PE preparation. The pH of the WPM particle dispersions was adjusted to  $7.00 \pm 0.01$  using 2 M HCl or 2 M NaOH. Soya oil was mixed with the WPM particle dispersions to give an oil concentration of 10 wt% in the final emulsion, and a protein concentration of 9 wt%. The mixtures were warmed in a water bath to 55 °C and were pre-homogenized by a rotor–stator Ultra-Turrax (D500; LabServ, Germany) at 10,000 rpm for 2 min, followed by two-stage homogenization (Homolab 2; FBF Italtia, Italy) at pressures of 25 MPa (first stage)/5 MPa (second stage) with three passes. Sodium azide was added at a concentration of 0.02 wt% for sample preservation.

#### **3.2.3.2 DSE preparation**

The PEs were diluted in Milli-Q water to concentrations of 10, 30, and 60 wt% for DSE preparation (corresponding to oil concentrations of 1, 3, and 6 wt%, and protein concentrations of 0.9, 2.7, and 5.4 wt%, respectively). These DSE samples are denoted as DSE-NPB X or DSE-PB X, where X is 10, 30, or 60 as appropriate. Soya oil (10 wt%) was mixed with the

diluted PE dispersions to final total oil concentrations of 11, 13, and 16 wt%. The mixtures were warmed in a water bath to 55 °C and were pre-homogenized by magnetic stirring at 1,000 rpm for 5 min, followed by homogenization using a rotor–stator Ultra-Turrax (D-130; LabServ, Mexico) at 30,000 rpm for 2 min. Sodium azide was added at a final concentration of 0.02 wt% as a preservative.

### 3.2.4 Dynamic light scattering (DLS)

DLS (ZetaSizer Nano ZS, Malvern Instruments Ltd, Worcestershire, UK) was used to determine the intensity-based *z*-average hydrodynamic diameter of the WPM particles. The ZetaSizer was equipped with a laser emitting at 633 nm at a power of 4 mW. The detector position was located at 173°, giving a backscattering configuration. The attenuation was automatically adjusted depending on the turbidity of the sample. The refractive index of water was set to 1.33. Measurements were performed at 25 °C and were repeated three times for each sample.

### 3.2.5 Static light scattering (SLS)

SLS (MasterSizer Hydro 2000, Malvern Instruments Ltd, Worcestershire, UK) was used to determine the average diameters of the emulsion droplets. The refractive indexes of the aqueous phase and the droplet-dispersed phase were set to 1.33 and 1.47, respectively. Measurements were performed at room temperature and were repeated three times for each sample. Average droplet sizes were reported as the Sauter mean diameter ( $D_{32}$ ), or the volume mean diameter ( $D_{43}$ ).

### 3.2.6 Confocal laser scanning microscopy.

A confocal microscope (Leica, Heidelberg, Germany) equipped with a 63× oil immersion objective lens was used to characterize the microstructure of the emulsion droplets. Nile Red

and Fast Green dyes were dissolved in acetone (1 mg/mL) and Milli-Q water (10 mg/mL), respectively. For oil staining, 20  $\mu$ L of Nile Red in 500  $\mu$ L of emulsion was used; for protein staining, 20  $\mu$ L of Fast Green was used. A 5 wt% agarose solution was mixed with the emulsion at a 1:1 (w/w) ratio for sample fixing. Nile Red was excited by an argon laser at 488 nm and the emitted fluorescence between 494 and 605 nm was measured. Fast Green was excited by a helium–neon laser at 633 nm and the emission between 638 and 750 nm was measured. To enhance the image quality, sequential scanning was used. Images were captured with LAS AF software (version 2.7.3.9723) at room temperature. They were analysed using ImageJ software (ImageJ, National Institutes of Health, Bethesda, MD).

### **3.2.7 Transmission electron microscopy.**

Sample preparation followed the method reported by Ye et al.(2013) Samples were placed into an embedding capsule and were cured at 60 °C for 48 h. The embedded samples were then sectioned to a thickness of 90 nm using a Reichert Ultra-cut microtome. These sections were mounted on 3 mm copper grids and were stained with lead citrate before observation using a Philips transmission electron microscope (NL-5600 MD; Philips, Eindhoven, The Netherlands) at an acceleration voltage of 60 kV.

### **3.2.8 Pendant drop method for interfacial tension (IFT)**

A contact angle and surface tensiometer (KSV Instruments Ltd, Helsinki, Finland) was used to examine the time evolution of the IFT of the WPM particles and the PE droplets using the pendant drop method. The tensiometer was operated in a volume-controlled regime, via continuous measurement of the drop area and volume, approximated by a Laplacian profile. During measurement, the WPM particle dispersion, or the PE, was the drop phase hanging from the syringe tip, against the surrounding pure soya oil. The volume of the drop was about

40  $\mu\text{L}$ . The shape of the drop was determined from the balance of forces, which includes the IFT of the liquid. The IFT at the liquid interface can be related to the drop shape through:

$$\gamma = \frac{\Delta\rho \times g \times R_0^2}{\beta} \quad (3-1)$$

where  $\gamma$  is the interfacial tension,  $\Delta\rho$  is the difference in density between the fluids at the interface,  $g$  is the gravitational constant,  $R_0$  is the radius of the drop curvature at the apex, and  $\beta$  is the shape factor. The shape factor can be defined through the Young–Laplace equation.(Neeson et al., 2014)

### **3.2.9 Small and ultra-small angle neutron scattering.**

SANS and USANS experiments were performed on the BILBY(Sokolova et al., 2016, 2019) and KOOKABURRA(Rehm et al., 2013; Rehm & de Campo, 2016) instruments, respectively, at the OPAL reactor at ANSTO, Sydney, Australia. SANS (BILBY) was used to probe the structures and interfaces of the particles in the bulk on a length scale ranging between approximately 6 and 600 nm. USANS (KOOKABURRA) extended the range of the experimentally measurable length scale accessible by BILBY, by between one and two orders of magnitude, into the micrometre scale with a maximum at about 16  $\mu\text{m}$ .

BILBY was configured in a time-of-flight configuration using a neutron wavelength range of  $\lambda = 2\text{--}20 \text{ \AA}$  ( $\Delta\lambda/\lambda = 9.6\text{--}15.0\%$ ). The rear detector was positioned at 15.0 m from the sample, and the other detectors were positioned at 3.5 m (horizontal curtains) and 2.5 m (vertical curtains), giving access to a  $q$  range of  $\sim 0.001\text{--}0.4 \text{ \AA}^{-1}$ , corresponding to a probed periodic length scale from about 1.6 nm up to 628 nm, where  $q$  is the magnitude of the scattering vector  $= (4\pi/\lambda) \sin \theta$ ,  $\lambda$  is the wavelength ( $\text{\AA}$ ), and  $2\theta$  is the scattering angle. KOOKABURRA was set up in the long wavelength configuration (4.74  $\text{\AA}$ ), giving access to a  $q$  range of  $\sim 4.0 \times 10^{-5}\text{--}0.01 \text{ \AA}^{-1}$ , corresponding to a periodic length scale from about 62.8 nm up to 16  $\mu\text{m}$ .

Samples of 10 wt% protein for WPM particle dispersions or of 10 wt% oil for emulsions (PEs and DSEs) were diluted by a factor of 50 (v/v) in D<sub>2</sub>O to avoid multiple scattering. This gave an aqueous phase with 98.1 wt% D<sub>2</sub>O for the WPM particle dispersions and 98.4 wt% D<sub>2</sub>O for the emulsions. Two of these emulsions – pure PE-NPB and DSE-NPB 60 (i.e., stabilized with 60 wt% PE-NPB) – were also diluted by a factor of 50 (v/v) in a 5 wt% SDS solution in D<sub>2</sub>O to reveal the structure of individual emulsion droplets, because SDS breaks hydrophobic interactions and displaces protein molecules from the oil–water interface. (Mackie et al., 2000; Taneja et al., 2015) For the BILBY measurements, samples were loaded into Hellma QS-120 cells with a 1 mm path length, using a 12.5 mm beam size; for the KOOKABURRA measurements, samples were enclosed in larger cells of 40 mm diameter and 1 mm path length, and where the beam size was defined by a 29 mm diameter gadolinium aperture. Both the USANS data and the SANS data were reduced. The USANS data were desmeared and combined with the SANS data to give a full  $q$  range from  $4.0 \times 10^{-5}$  to  $0.4 \text{ \AA}^{-1}$ . It is worth noting that the data beyond  $0.04 \text{ \AA}^{-1}$  from BILBY were affected by strong incoherent scattering of the hydrogenous material and did not contain structural information. (Schaefer et al., 2003) Hence, the  $q$  range ( $4.0 \times 10^{-5}$ ,  $0.02 \text{ \AA}^{-1}$ ) was considered for data analyses in the present work. The data were analyzed with IGOR Pro 8.02 ([www.wavemetrics.com](http://www.wavemetrics.com)).

A Guinier–Porod model, which was used to fit the USANS/SANS data, describes the radius of gyration and the power law behavior of a scattering system. The scattered intensity is given by:

$$I(q) = G \exp\left(\frac{-q^2 R_g^2}{3}\right) \text{ for } q \leq q_1, \text{ and}$$
$$I(q) = \frac{D}{q^\alpha} \text{ for } q \geq q_1 \quad (3-2)$$

where  $q$  is the scattering vector,  $I(q)$  is the scattered intensity,  $R_g$  is the radius of gyration,  $\alpha$  is the Porod exponent, and  $G$  and  $D$  are the Guinier and Porod scale factors, respectively. The Guinier form is used for  $q \leq q_1$  and the Porod form is used for  $q \geq q_1$ . The neutron scattering data are fitted using the Guinier–Porod treatment proposed by Hammouda, (Mehalebi et al., 2008) as opposed to the unified model proposed by Beaucage (Beaucage, 1995). The latter approach ensures mathematical continuity of values of the Guinier and Porod terms and their slopes at a value  $q_1$ , which are constrained by:

$$q_1 = \frac{1}{R_g} \left( \frac{3\alpha}{2} \right)^{1/2}, \text{ and}$$

$$D = G \exp \left( \frac{-q^2 R_g^2}{3} \right) q_1^\alpha = G \exp \left( -\frac{\alpha}{2} \right) \left( \frac{3\alpha}{2} \right)^{\alpha/2} \frac{1}{R_g^\alpha} \quad (3-3)$$

It should be noted that the value of  $q_1$  is not set, but is calculated using **equation (3-3)**.

If the Porod slope lies in the range  $-3 > \alpha > -4$ , the scattering can be related to the surface fractal dimension  $D_s$ , where  $\alpha = D_s - 6$ ; an object with  $D_s = 2$  would indicate a smooth surface whereas an object with  $D_s$  varying between 2 and 3 would indicate a rough surface (Schaefer, 1989; Schaefer et al., 2003; Yang et al., 2019b). If the Porod slope lies in the range  $-1 > \alpha > -3$ , the scattering can be related to the mass fractal dimension  $D_m$ , where  $\alpha = -D_m$ . An increasing mass fractal dimension ( $1 < D_m < 3$ ) can be related to an increasing network compactness of the aggregate (Hammouda, 2016; Schmitt et al., 2010).

In the present work, there were two different Porod slopes: one at high  $q$  in the case of the WPM particle dispersion; one at low  $q$  for the PE flocs and the DSE droplets. In the latter case, there was a lack of size information for the PE flocs and the DSE droplets, because the data did not extend to very low  $q$  (Yang et al., 2019b; Zank et al., 2006).





### 3.3 Results and discussion

For ease of reading, the main abbreviations used for the different systems in this study are repeated. WPM-PB and WPM-NPB are the whey protein microgels (WPMs) formed in the presence of phosphate buffer (PB) and in the absence of phosphate buffer (NPB). The primary emulsions (PEs) made with WPM-PB and WPM-NPB are named PE-PB and PE-NPB, respectively. The droplet-stabilized emulsions (DSEs) stabilized by PE-PB and PE-NPB are named DSE-PB and DSE-NPB, respectively.

#### 3.3.1 Characterisation of the WPM particles

The particle size distributions of the WPM particles in Milli-Q water determined by DLS were found to be monomodal with a size range from 100 to 800 nm, as shown in **Figure 3-1A**. The *z*-average hydrodynamic diameters ( $D_h$ ) were  $270.9 \pm 4.7$  and  $293.8 \pm 6.7$  nm with relatively narrow polydispersity indexes of 0.06 and 0.11 for the WPM-NPB and WPM-PB particles, respectively. The optical microscopy images [**Figure 3-2(A-1)** and **(B-1)**] showed that the parent whey proteins formed small aggregates after heat treatment without phosphate buffer, whereas they formed coarse aggregates after heat treatment with phosphate buffer. The TEM images [**Figure 3-2(A-2)** and **(B-2)**] show that, after size reduction of aggregates by microfluidizer, both the WPM-NPB particles and the WPM-PB particles were approximately spherical with diameters of about 200 nm, which was consistent with the DLS measurements and in good agreement with previous studies (Destribats et al., 2014; Sarkar et al., 2016a; Schmitt et al., 2010). In addition, the backgrounds of the TEM images [**Figure 3-2 (A-2)** and **2(B-2)**] showed that the WPM-PB particle dispersion contained small protein aggregate fragments (black dots), in the range of a few nanometres, coexisting with the WPM-PB particles; in contrast, the WPM-NPB particle dispersion had a negligible amount of protein aggregate fragments.

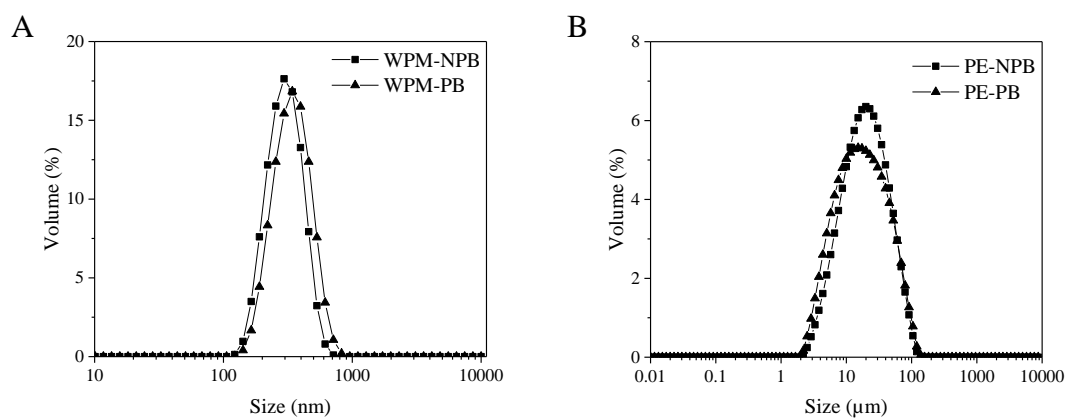


**Figure 3-1:** (A) (■), WPM-NPB particles, microgels formed without phosphate buffer; (▲), WPM-PB particles, microgels formed with 10 mM pH 5.9 phosphate buffer. (B) Droplet size distributions by MasterSizer of the PEs at 25 °C and natural pH: (■), PE-NPB stabilized by 10 wt% WPM-NPB particles; (▲), PE-PB stabilized by 10 wt% WPM-PB particles.

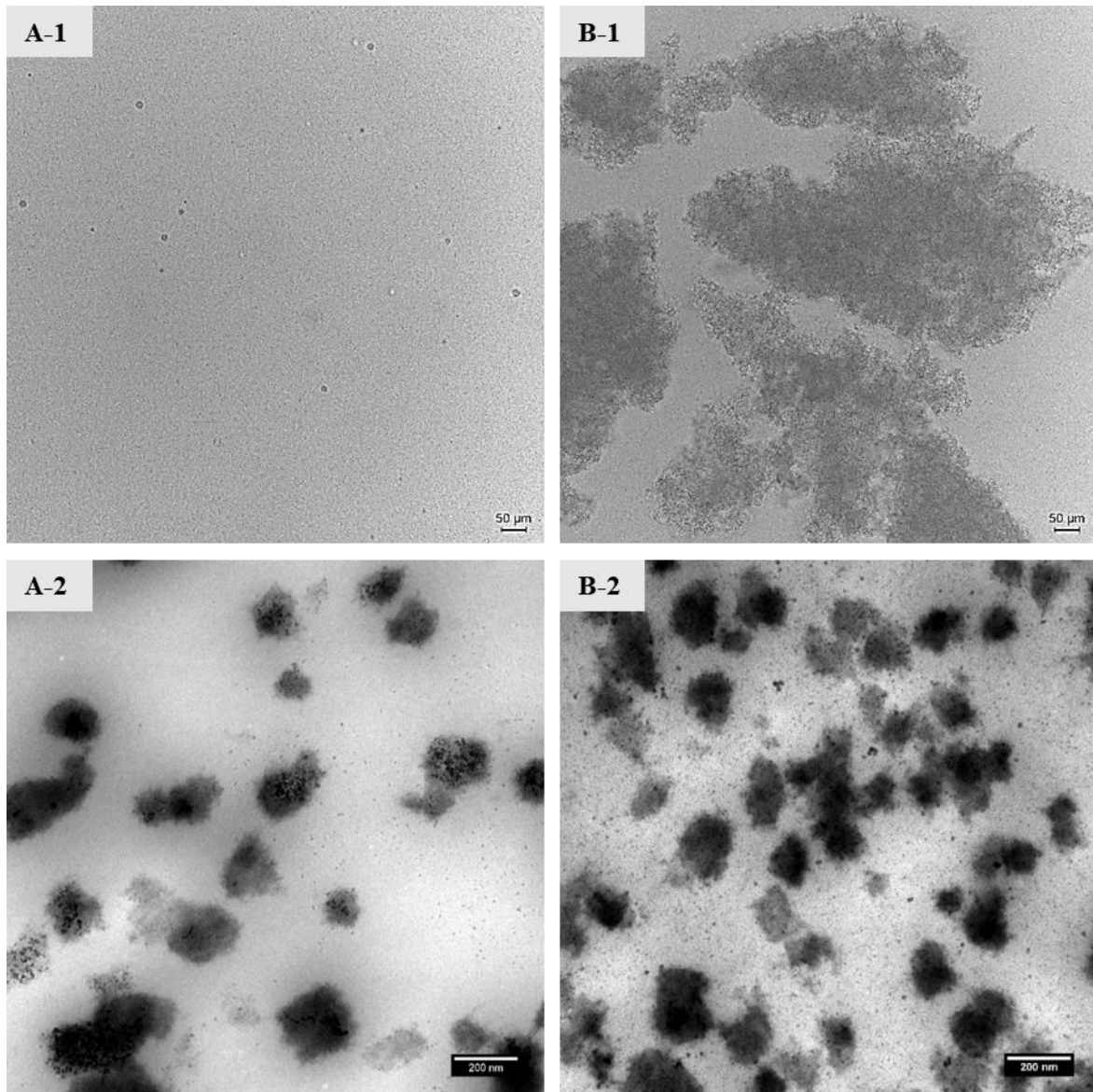


**Figure 3-2:** Microscope images of (A) WPM-NPB, microgels formed without phosphate buffer, and (B) WPM-PB, microgels formed with 10 mM phosphate buffer during heating. (A-1) and (B-1): optical images for the whey protein aggregates without and with phosphate buffer, respectively; scale bar is 50  $\mu\text{m}$ . (A-2) and (B-2): negative-staining TEM images for WPM-NPB and WPM-PB particles, respectively; scale bar is 200 nm.

It has been shown that, at pH 5.9, heat treatment at 85 °C promotes the conversion of whey proteins into covalently cross-linked aggregates through disulphide bonds (Schmitt et al., 2010). The subsequent formation of WPMs has been attributed to secondary non-covalent interactions of primary disulphide-linked aggregates (Brugger et al., 2008; de la Fuente et al., 2002; Hoffmann et al., 1996; Schmitt et al., 2010). The extensive aggregation in the WPM-PB particles, where the proteins were dispersed in phosphate buffer, was the consequence of the charge screening by the presence of ions in the buffer, in which the electrostatic repulsion decreased, thereby accelerating aggregation through noncovalent interactions (Ako et al., 2010; Kharlamova et al., 2016; Salis et al., 2011; Wijayanti et al., 2014). The size reduction of the whey protein aggregates, as a result of the micro-fluidization, led to the formation of WPM particles as well as to small protein aggregate fragments.

To further characterize the microstructures of the WPM particles, Guinier–Porod fitting was applied to the USANS and SANS data (**Figure 3-3**). The scattering intensity exhibited a plateau at low  $q$ , followed by steep decays at higher  $q$  for both particles. The slopes at high  $q$  yield the surface fractal dimension ( $D_s$ ) of the WPM particles, representing their surface roughness. The plateaus were limited in the low  $q$  range by a curvature at transition points of  $q_a = 0.0023 \text{ \AA}^{-1}$  for the WPM-NPB particles and of  $q_b = 0.0014 \text{ \AA}^{-1}$  for the WPM-PB particles. The best fit in the range  $4.0 \times 10^{-5} < q/\text{\AA}^{-1} < 0.02$  yielded  $R_g$  values of  $132.9 \pm 0.7$  and  $153.0 \pm 1.0$  nm and  $D_s$  values of  $2.07 \pm 0.01$  and  $2.40 \pm 0.01$  for the WPM-NPB particles and the WPM-PB particles, respectively. These results suggest that the WPM-NPB particles had a smaller size and a smoother surface, whereas the WPM-PB particles had a larger size and a rougher surface. Assuming spherical particles of uniform scattering density, and using  $R_g = (3/5)(D_p/2)$ , (Witten et al., 2004) the associated particle diameters corresponded to 327.1 and 395.0 nm, respectively. Even though the not strictly spherical shape of the WPM particles may have affected the

accuracy of the diameter calculation, the calculated diameters ( $D_h$ ) from the  $R_g$  equation were in reasonable agreement with the  $D_h$  values, measured by DLS, of 270.9 and 293.8 nm for WPM-NPB and WPM-PB, respectively.

The rough surface for the WPM-PB particles may have been the combined result of the size-reduction process and the relatively loose internal structure of the particles. As well as causing extensive aggregation, the phosphate buffer probably slowed down the thiol–disulphide exchange because it would have had the effect of maintaining the pH constant at around 5.9 upon heating (de la Fuente et al., 2002). From our observation in the present study, the final pH values were recorded as 6.18 for sample without buffer and 5.92 for the one with buffer, respectively. The differences in the size, surface roughness, and the extent of coexisting fragments for the two WPM particle dispersions may have influenced their adsorption behaviours at the oil–water interface of the PE.

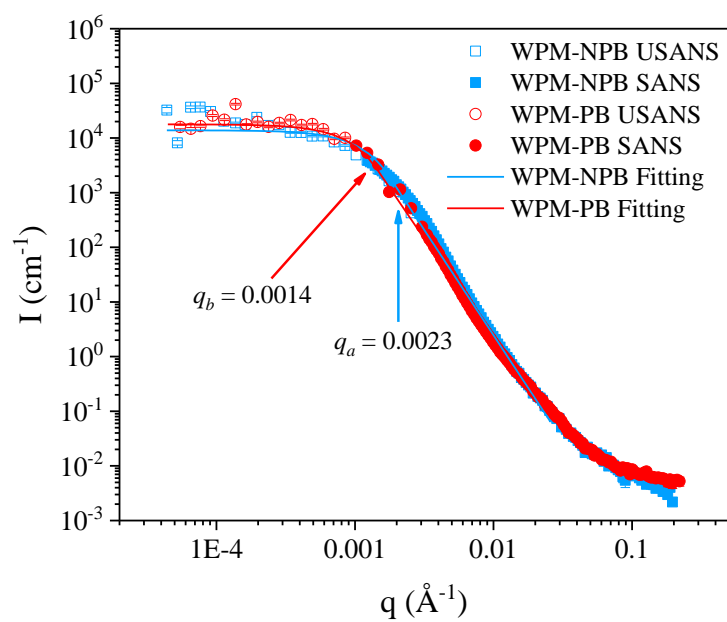


**Figure 3-3:** Combined USANS (open symbols) and SANS (solid symbols) data for WPM-NPB particles (blue) and WPM-PB particles (red). The WPM concentration is 0.2 wt%. Solid lines represent fits using the Guinier–Porod model.

### 3.3.2 Characteristics of PEs stabilised by WPM particles

Prior to emulsification, all heated whey protein aggregates were washed with Milli-Q water to remove phosphate buffer and to achieve the same low ionic strength in the emulsions. The CLSM images [Figure 3-4(A-1) and 4(B-1)] demonstrated that droplet flocculation occurred in both PE-NPB and PE-PB. The size distributions of the PE-NPB and PE-PB flocs were comparable, as measured by the MasterSizer (Figure 3-1B), ranging from 2.5 to 158.5  $\mu\text{m}$ . The average Sauter mean droplet diameters ( $D_{32}$ ) were 14.7 and 12.5  $\mu\text{m}$  for the PE-NPB and PE-PB flocs, respectively.



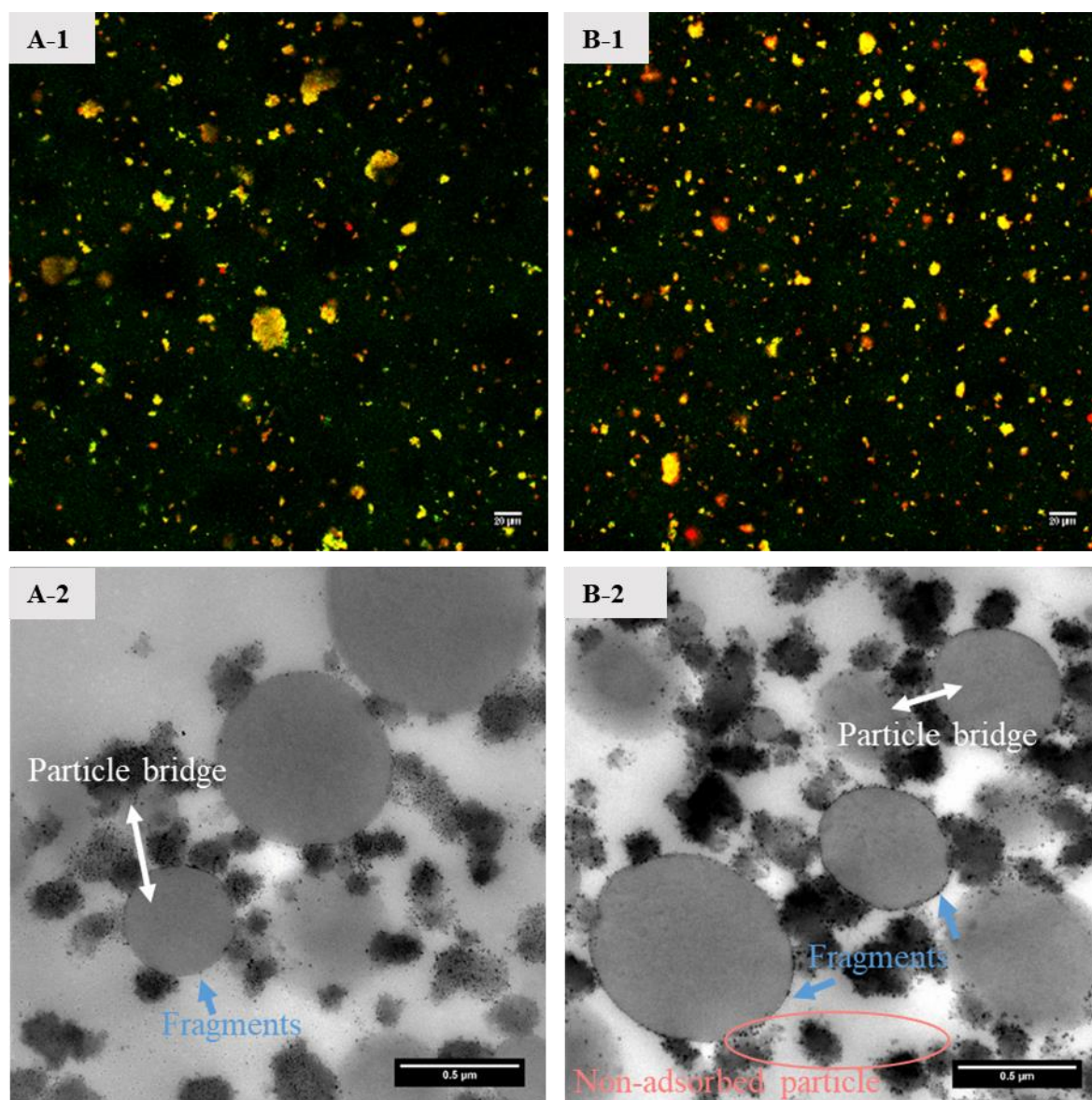


**Figure 3-4:** Confocal images: (A-1), PE-NPB stabilized with WPM-NPB particles; (B-1), PE-PB stabilized with WPM-PB particles. Negative-staining TEM images: (A-2), PE-NPB; (B-2), PE-PB.

The TEM images [Figure 3-4(A-2) and 4(B-2)] showed that, between neighbouring droplets in both PE-NPB and PE-PB, two different interfaces were bridged by the WPM particles, which caused the droplet flocculation. The adsorbed WPM particles formed a monolayer at the interfaces and remained globular in shape. At neutral pH, Destribats et al. (2014) also reported that emulsion droplets stabilized by WPM particles tended to flocculate. In addition to the mechanism of particle bridging, they proposed that the flocculation could result from the attractive force between the particle films formed between the emulsion droplets, as observed by optical microscopy; this has also been discussed by Gautier et al. (2007). Flocculation induced by particle–particle interactions is commonly encountered in large emulsion droplets, because the attractive forces at close droplet separations are dominant (Destribats et al., 2014; Dickinson, 2010a; Gautier et al., 2007; McClements, 2004). However, as the PE droplets in the present study were much smaller than the emulsion droplets ( $D_{32}$  about 80  $\mu\text{m}$ ) reported by Destribats et al. (2014) it is likely that, in the present system, particle bridging was the major mechanism.

Aggregate fragments (small black dots indicated by the blue arrows) were adsorbed at the interface of the droplets [Figure 3-4(A-2) and 4(B-2)], filling the gaps between the WPM particles. These aggregate fragments were more obvious at the interface of the PE-PB droplets and showed as a thin black layer around the droplets on the TEM image. In addition, some non-adsorbed WPM particles (indicated by the red ellipse) remained in the aqueous phase of PE-PB, possibly as a consequence of competition for adsorption with the aggregate fragments.

The interfacial properties of the PE droplets and the WPM particles were examined using the pendant drop method. The initial IFT value for the PE-NPB droplets was  $18.9 \pm 0.2$  mN/m, which was lower than the oil–water IFT of  $23.1 \pm 0.1$  mN/m; for comparison, the initial IFT values were  $16.7 \pm 0.4$  mN/m for the PE-PB droplets, and  $13.5 \pm 0.1$  and  $13.3 \pm 0.1$  mN/m for

the WPM-NPB and WPM-PB particles, respectively (**Supplementary material, Figure S 3-2A**). The lower IFT of the PE-PB droplets than of the PE-NPB droplets was probably due to the excess WPM-PB particles in the aqueous phase. These results indicate the importance of the amount of WPM particles available for decreasing the interfacial tension.

The decay rate, i.e., the IFT value relative to the IFT value at time zero (IFT/IFT<sub>0</sub>) as a function of time, showed that the oil–water interfacial tension decreased at a similar rate for all samples in the first 250 s (**Supplementary material, Figure S 3-2B**). Between 250 and 7000 s, the decay rates for the PE droplets were slower than those for the WPM particles, but there was no significant difference between the two PE droplets or between the two WPM particles. These results suggest that, during homogenization, both WPM particles and PE droplets effectively adsorbed onto the oil–water interfaces, although they were different in size and composition. These particle-coated droplets can be considered to be effective colloidal emulsifiers. The colloidal properties of the PE droplets may contribute to forming an interfacial structure that is different from that formed by the WPM particles.

### 3.3.3 Characteristics of oil-in-water emulsions stabilized by PE droplets (DSEs)

The droplet size distributions for both DSE-NPB and DSE-PB were bimodal (**Figure 3-5**). The droplet size distribution for DSE-NPB 10 with a  $D_{32}$  of 22.7  $\mu\text{m}$  (**Figure 3-5A**) showed a prominent droplet population in the size range 7–100  $\mu\text{m}$  and a minor droplet population in the size range 2–7  $\mu\text{m}$ . Increasing the concentration of the DSE-NPB to 60 wt% resulted in the prominent droplet peak shifting towards the small size range and the minor droplet peak increasing. The minor droplet peak probably corresponded to a mixture of small DSE-NPB droplets and excess PE-NPB droplets in aqueous solution. This was supported by the observation that the droplet size of this peak was similar to the apparent size of the small DSE-NPB droplets and PE-NPB droplets observed in the CLSM and TEM images (**Figure 3-6** and

**Figure 3-7**). The CLSM images (**Figure 3-6**) showed that the proportion of small DSE droplets increased with increasing PE concentration. As the concentration of PE droplets in the systems was increased, smaller droplets were produced in the DSE, probably because of the greater surface coverage (**Supplementary material, Figure S 3-3**).

The droplet size distribution for DSE-PB (**Figure 3-5B**) was similar to that for DSE-NPB, i.e., the population of larger particles was reduced with an increase in the PE concentration. Additionally, the relative proportion of small droplets (size 2–7  $\mu\text{m}$ ) in all DSE-PB samples was greater than that in the DSE-NPB samples, indicating that a larger amount of small DSE-PB droplets formed with the stabilization of the PE-PB dispersion. This result indicates that the excess WPM particles had also participated in emulsifying a newly formed oil–water interface, which is supported by the results of the lower IFT of PE-PB (**Supplementary material, Figure S 3-2A**).

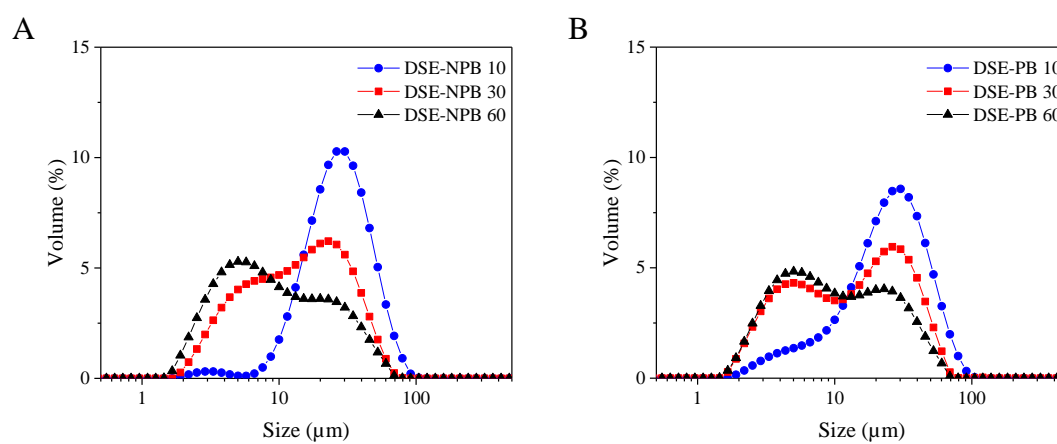


**Figure 3-5:** Droplet size distributions of two series of DSEs coated with (A) PE-NPB and (B) PE-PB in a concentration range from 10 to 60 wt%.

The interfaces of the DSEs were examined using CLSM and TEM. The interfacial layers of the DSE-NPB droplets were almost fully covered with small droplets at 10 wt% PE-NPB concentration, as shown in **Figure 3-6**. The thickness of the interfacial layer appeared to increase with increasing PE-NPB concentration. The TEM images show that the PE-NPB droplets (**Figure 3-7**) formed a cluster-like network at the DSE interfaces, contributing to a thick multilayer, rather than monolayer coverage, and that the interfaces of the DSE-PB 60 droplets (**Figure 3-7B**) consisted of PE-PB droplets and WPM-PB particles. A higher amount of the PE-PB droplets, than of the PE-NPB droplets, remained in the aqueous phase of the DSE. These results suggest that the coexisting WPM-PB particles in the PE-PB dispersion had competed with the PE-PB droplets for adsorption and may have further interfered with the PE-PB droplet network at the interface. An interfacial layer network, instead of a homogeneous layer, is commonly encountered on the surface of droplets stabilized by aggregated colloidal particles (Arditty et al., 2005; Gautier et al., 2007). It has been suggested that an interfacial layer formed by this particle network might confer additional stabilization to the emulsion (Binks, 2002; Ye et al., 2013b). It should be noted that the PE droplets and the WPM particles retained their spherical morphologies at the interfaces, whereas casein-micelle-coated PE droplets deformed at the interface, as reported by Ye et al. (2013).

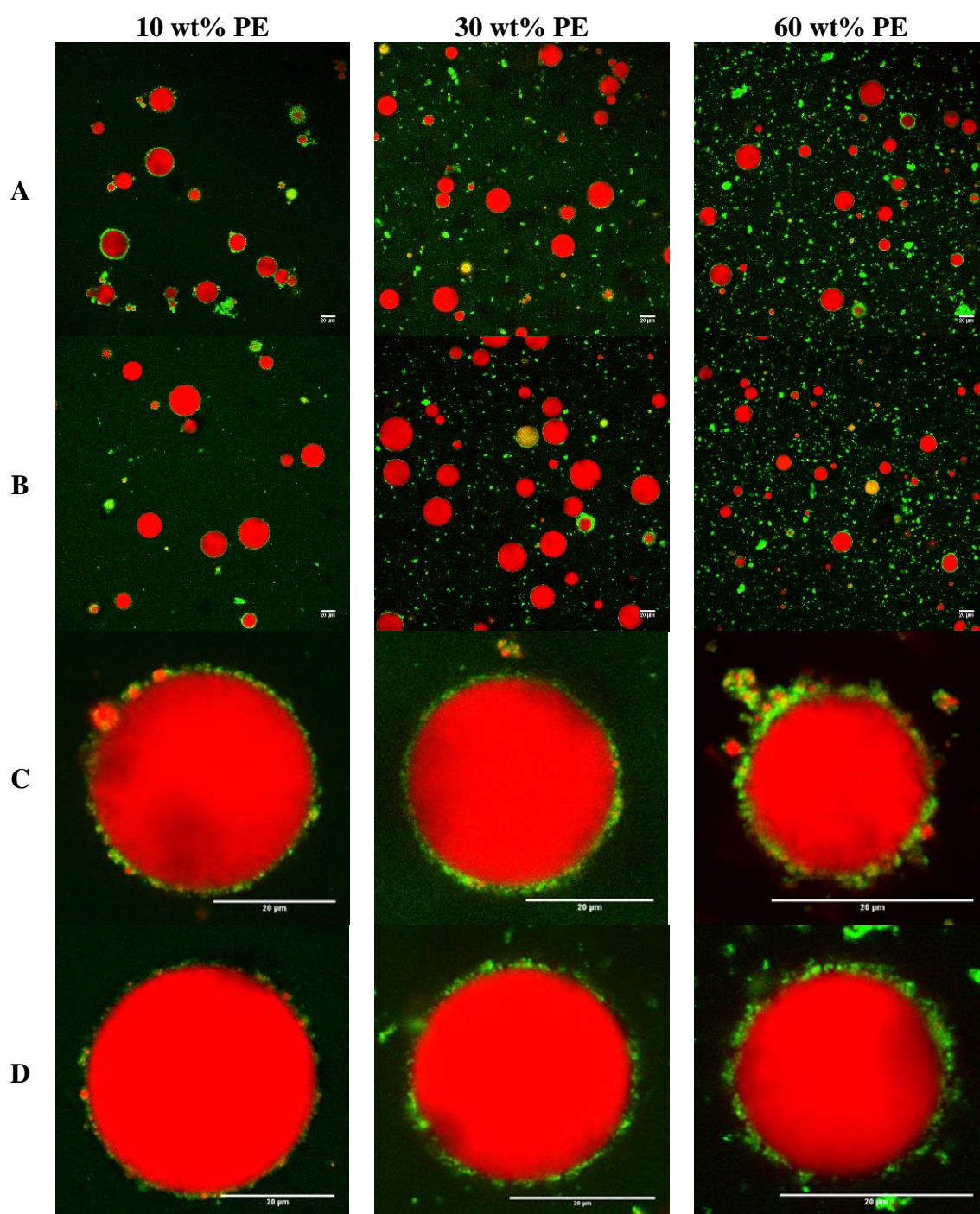


**Figure 3-6:** (A and B) Confocal images, and (C and D) associated high magnification confocal images, of DSEs and individual DSE droplets, stabilized with (A and C) PE-NPB and (B and D) PE-PB at concentrations of 10, 30, and 60 wt%. Red colour represents the oil and green colour represents the protein. Scale bar is 20  $\mu\text{m}$ .

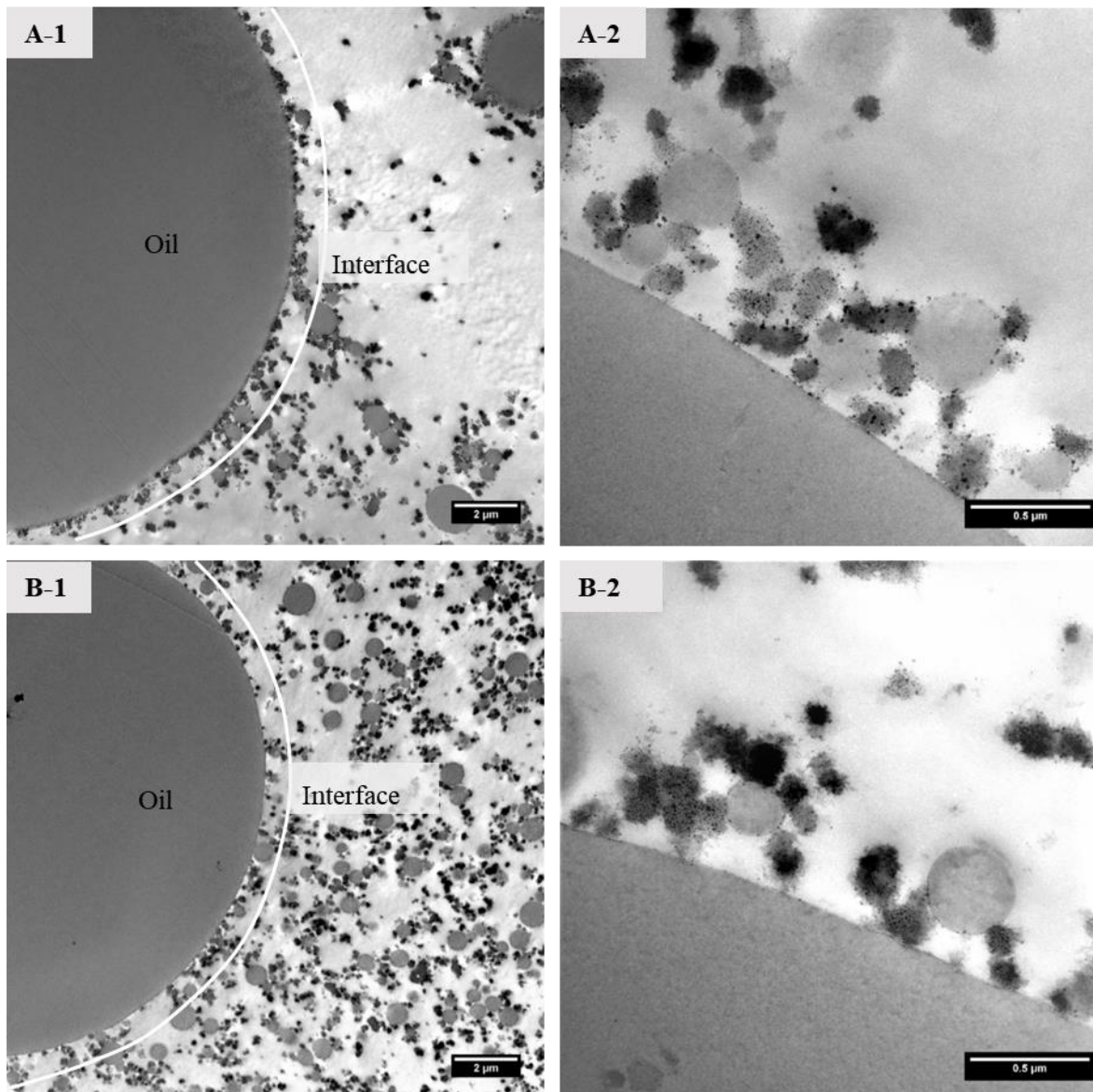


**Figure 3-7:** TEM images of DSEs stabilized with PE droplets: (A-1), DSE droplets stabilized by 60 wt% PE-NPB droplets (DSE-NPB 60); (B-1), DSE droplets stabilized by 60 wt% PE-PB droplets (DSE-PB 60). The curve between the interfacial layer and the aqueous phase is drawn as a guide for the eye. (A-2) and (B-2) are TEM images for the interfaces of DSE-NPB 60 and DSE-PB 60, respectively.



The multilayer interfacial structures of the DSEs were further characterized using SANS/USANS. One concern with using SANS/USANS to analyse the interfacial structure of DSE-NPB is the contribution from the presence of the PE-NPB flocs in the aqueous phase. As the size distribution of DSE-NPB overlaps with that of the PE-NPB flocs within the range 7–100  $\mu\text{m}$ , as shown by light scattering (**Figure 3-1B** and **Figure 3-5**), the aqueous PE-NPB flocs may also scatter within the same low  $q$  range as DSE-NPB. As SDS is able to dissociate the flocs into individual droplets, the scattering curves in the low  $q$  range of PE-NPB and DSE-NPB with and without SDS treatment were compared.

**Figure 3-8(A)** and **(B)** show the scattering curves for PE-NPB and DSE-NPB containing 10, 30, and 60 wt% PE-NPB. There was a steep increase in intensity with decreasing low  $q$ , indicating that the droplet size was much greater than was accessible with USANS. Upon the addition of SDS, the scattering intensity at low  $q$  ( $4.0 \times 10^{-5}$ ,  $3.4 \times 10^{-4} \text{ \AA}^{-1}$ ) was reduced for PE-NPB (**Figure 3-8A**). This indicates that the PE-NPB flocs were dissociated by SDS to yield smaller sized droplets. The mid- $q$  ( $0.00024 < q/\text{\AA}^{-1} < 0.006$ ) of the USANS scattering pattern of PE-NPB treated with SDS, when fitted with a Guinier–Porod model, yielded an  $R_g$  of  $0.40 \pm 0.08 \mu\text{m}$ , which was comparable with the size observed with the TEM images (**Figure 3-4** and **Figure 3-7**). At low  $q$ , the Guinier region did not fully flatten, as would be expected for monodisperse spherical PE particles; instead, two more weak shoulders appeared at low  $q = 0.00028$  and  $0.00008 \text{ \AA}^{-1}$ . The  $R_g$  values from these low  $q$  shoulders were estimated to be  $0.82 \pm 0.16$  and  $2.22 \pm 0.44 \mu\text{m}$ . This suggests that there were some large droplets in the PE-NPB samples. In the absence of SDS, fitting with a simple power law model  $I(q) \sim q^\alpha$  in the  $q$  range  $0.00004 < q/\text{\AA}^{-1} < 0.002$  yielded a slope of  $2.76 \pm 0.05$ , which could be associated with a fractal structure of the flocs of the PE-NPB droplets. A slope of  $2.75 \pm 0.05$  was obtained for the PE-NPB flocs (data not shown), which indicated a similar network density to that of the PE-NPB

flocs. This similarity in network density for the PE-PB and PE-NPB flocs may have been due to the similar sizes of the WPM-PB and WPM-NPB particles used to stabilize them. Furthermore, within the flocs, the distance between neighbouring interfaces was probably comparable with the size of the WPM particles.

At the same low  $q$  ( $4.0 \times 10^{-5}$ ,  $3.4 \times 10^{-4} \text{ \AA}^{-1}$ ), the scattering curve showed only a slight reduction of the slope for DSE-NPB 60 with the addition of SDS (**Figure 3-8B**). In comparison with the SDS PE-NPB curve (**Figure 3-8A**), this result indicates that the fractal structure of DSE-NPB 60 was not markedly affected by the PE flocs present in the DSE-NPB aqueous phase. The steep slope at low  $q$  (USANS) of large droplet water-in-oil emulsions has been discussed by Zank et al. (2006) who suggested that it arises from droplet interface scattering from a complex multilayer decorated by aggregated surfactant. This slope in the DSE-NPB samples can probably provide information on the fractal dimension and the roughness of its interfaces, which are stabilized by the PE droplets. Within a  $q$  range of  $3.9 \times 10^{-5} < q/ \text{ \AA}^{-1} < 3.4 \times 10^{-4}$ , a simple power-law fit,  $I(q) \sim q^\alpha$ , yielded an exponent of 3 for DSE-NPB 10, 30, and 60. This results was consistent with the fractal structure of natural aquatic colloids analysed by SANS, where the power law exponent was 3 within a  $q$  range of  $\sim 23 < q/ \text{ \AA}^{-1} < 14$  (Jarvie & King, 2007). This exponent represents the extreme value for a very rough interface. We could not draw further conclusions because of the limited  $q$  range over of USANS which the assessment could be made; however, the value agreed with the TEM observations [**Figure 3-7 (A-2)**], which show that the interface of DSE-NPB 60 was decorated by a network of PE droplets.

In addition, the USANS curves of all DSE-NPB samples featured a small shoulder at  $q \sim 0.001 \text{ \AA}^{-1}$ . The scattering intensity of these shoulders decreased with a decreasing amount of PE-NPB. The scattering intensity at selected  $q$  values of  $2.4 \times 10^{-4}$  and  $5.5 \times 10^{-5} \text{ \AA}^{-1}$  was

plotted as a function of the concentration of PE to examine their relationships (**Supplementary material, Figure S 3-4**). At  $q = 2.4 \times 10^{-4} \text{ \AA}^{-1}$ , equivalent to a periodic length scale of  $\sim 2.6 \mu\text{m}$ , the intensity was linearly proportional ( $R^2 = 0.9885$ ) to the PE concentration in the aqueous phase. This result confirms that the increase in the USANS scattering intensity was affected by the excess amount of PE flocs present in the aqueous phase. At the lower  $q$  of  $5.5 \times 10^{-5} \text{ \AA}^{-1}$ , probing a periodic length scale of  $\sim 11.5 \mu\text{m}$ , the scattering intensity was no longer linearly proportional to the PE concentration in the aqueous phase ( $R^2 = 0.7689$ ). The deviation from a linear relationship is in agreement with a strong scattering contribution from the DSE-NPB droplet interface. In fact, the CLSM results showed that the interfacial structure of DSE-NPB depended on the PE-NPB content (**Figure 3-6, high magnification**).

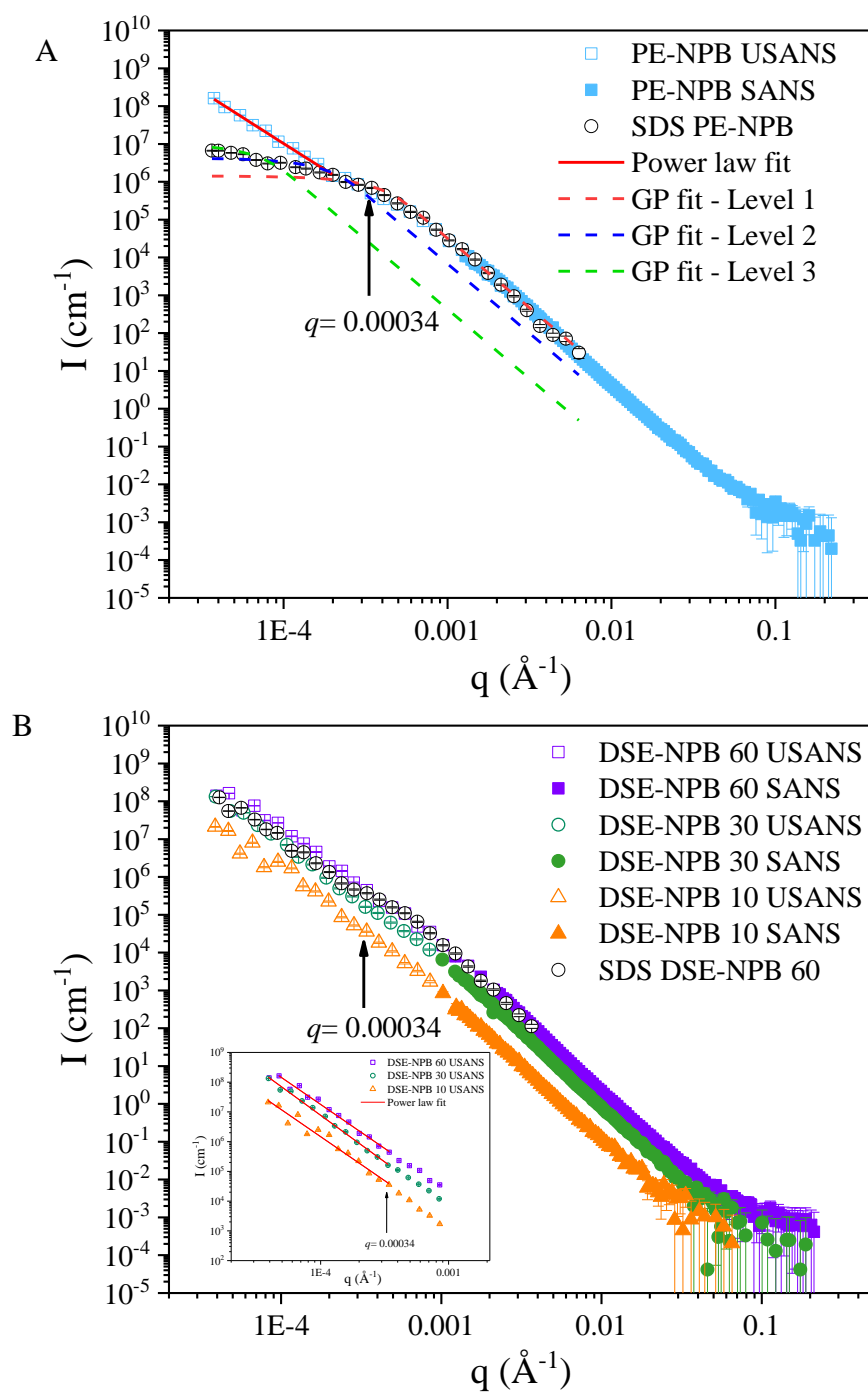


**Figure 3-8:** Combined USANS (open symbols) and SANS (solid symbols) profiles for 0.2 wt% emulsion dispersions of: (A), PE-NPB (blue) and PE-NPB following SDS treatment (black); (B), DSE-NPB 10 (orange), DSE-NPB 30 (green), and DSE-NPB 60 (purple) without SDS treatment, and with SDS treatment (black); the power law fitting for the DSE samples listed is shown in the inset to (B).

### 3.4 Conclusions

This work demonstrated the formation of an oil-in-water emulsion in which the emulsifying agent comprises small PE droplets coated by WPM particles. The fractal network at the oil-water interface, formed by the PE droplets, was directly observed using TEM, and was probed by SANS and USANS measurements; the fractal networking interface depended on the structure and the concentration of the WPM particles. The optimal conditions for the formation of WPM particles, to be used for the production of these emulsion systems, is heat treatment at pH 5.9 in the absence of buffer. At neutral pH and low ionic strength (no buffer), SANS and USANS indicated that a PE with a fractal dimension of 2.75 was obtained. The DSE (no buffer) with a fractal dimension of 3 was probably due to the formation of a multilayer structure by the adsorbed PE droplets at the interface. The surface structure was consistent with an extremely rough interface. This study provides important knowledge on the structure of DSEs and will assist in the development of novel emulsion-based formulations for various food applications.

### **3.5 Acknowledgments**

This work was funded by the Riddet Institute, a national Centre of Research Excellence, funded by the New Zealand Tertiary Education Commission. We acknowledge the travel grants and the support of ANSTO, Australia, for access to the small angle neutron scattering (BILBY) and ultra-small angle neutron scattering (KOOKABURRA) facilities under proposal P6070. We thank Dr. Zhi Yang of Oak Ridge National Laboratory, Oak Ridge, TN, USA, for supplying the first version of the model fitting procedure. We also thank Dr. Matthew Savoian, Jordan Taylor, and Niki Minards from the Manawatu Microscopy and Imaging Centre at Massey University for their technical support.

### 3.6 Supplementary material

SDS polyacrylamide gel electrophoresis patterns of nonaggregated whey proteins in the supernatant, dynamic interfacial tension patterns of whey protein microgel particles and primary emulsions, average size  $D_{32}$  and  $D_{43}$  of droplet-stabilized emulsions, neutron scattering intensity of droplet-stabilized emulsions at fixed  $q$  value plotted as a function of the concentration of primary in the aqueous phase.

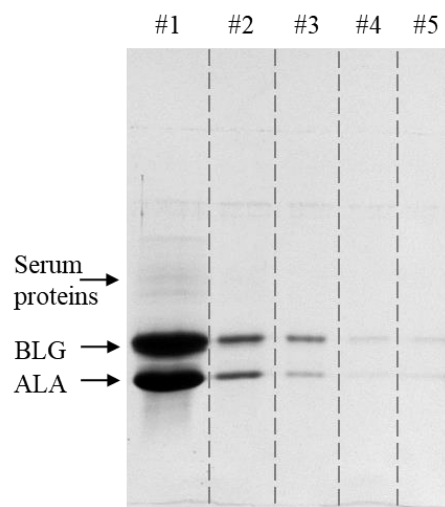


**Figure S 3-1:** Sodium dodecyl sulfate polyacrylamide gel electrophoresis patterns of nonaggregated whey proteins in the supernatant after the centrifugation of WPM-NPB particles. Heated whey protein aggregate dispersions were washed with Milli-Q water five times (from left to right).  $\beta$ -Lactoglobulin (BLG) and  $\alpha$ -lactalbumin (ALA) bands are indicated.

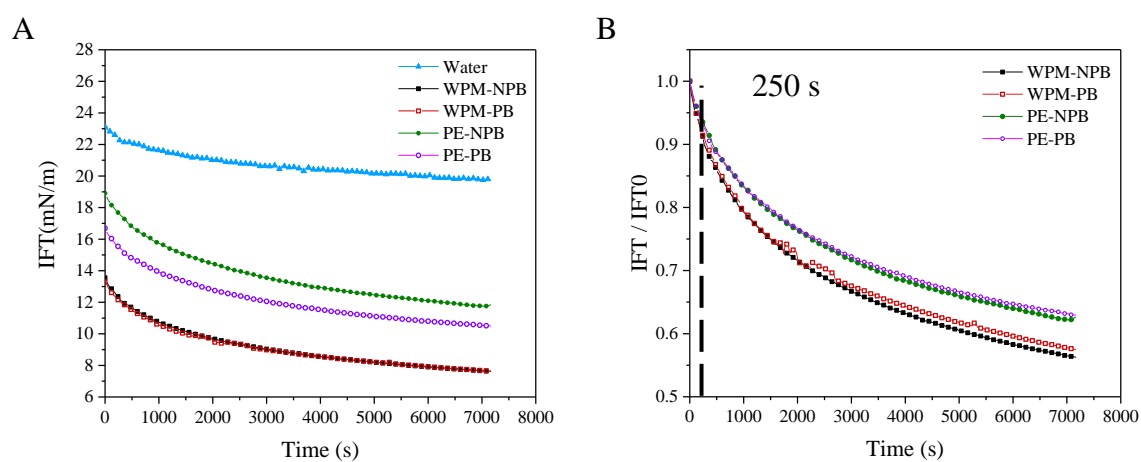


**Figure S 3-2:** (A) Dynamic interfacial tension (IFT) and (B) interfacial tension decay rate ( $IFT/IFT_0 = \text{interfacial tension}/\text{interfacial tension at time zero}$ ) as a function of time. ( $\text{---}\blacktriangle\text{---}$ ), soya oil and Milli-Q water; ( $\text{---}\blacksquare\text{---}$ ), 10 wt% WPM-NPB particle dispersion; ( $\text{---}\square\text{---}$ ), 10 wt% WPM-PB particle dispersion; ( $\text{---}\bullet\text{---}$ ), PE-NPB; ( $\text{---}\circ\text{---}$ ), PE-PB. The first 250 s decay of interfacial tension is indicated by the vertical dotted line.



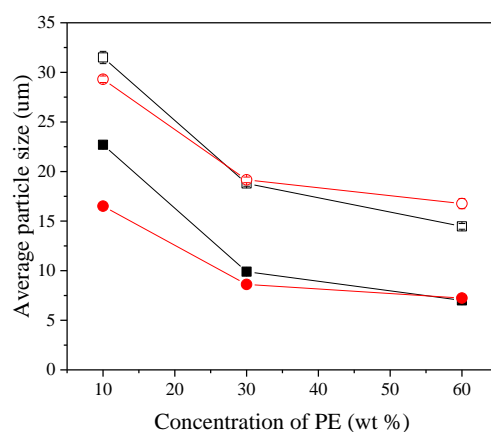


**Figure S 3-3:** Average size  $D_{32}$  (solid symbols) and  $D_{43}$  (open symbols) of DSEs stabilized with PE-NPB (black) and PE-PB (red) as a function of the concentration of the PE at 10, 30, and 60 wt%.

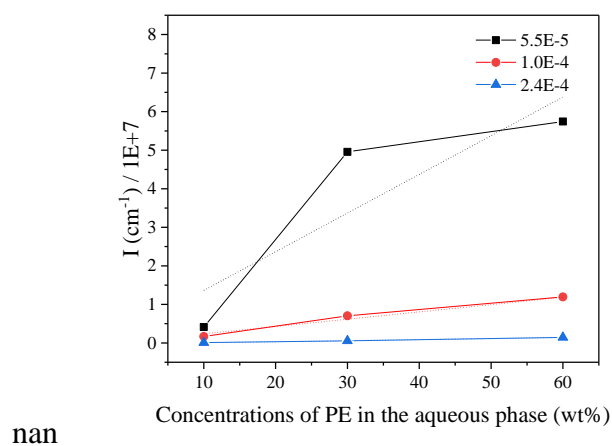
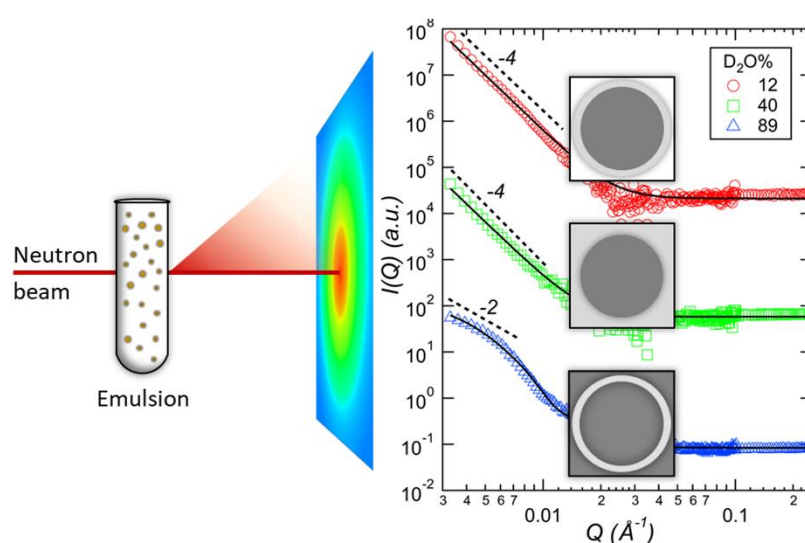


**Figure S 3-4:** Intensity at fixed  $q$  value plotted as a function of the concentration of PE in the aqueous phase. The blue, red, and black symbols represent the intensities at  $q$  values of  $2.4 \times 10^{-4}$ ,  $1.0 \times 10^{-4}$ , and  $5.5 \times 10^{-5} \text{ \AA}^{-1}$ , respectively. The linear regression fits are represented as dotted lines in corresponding color.

## Chapter 4 Small-angle X-ray scattering (SAXS) and small-angle neutron scattering (SANS) study on the structure of sodium caseinate in dispersions and at the oil-water interface: effect of calcium ions

### Graphic abstract



### Abstract

The structure of sodium caseinate particles, as affected by the presence of calcium ions ( $Ca^{2+}$ ), in aqueous solution and in oil (toluene)-in-water emulsions, was investigated by small-angle X-ray and neutron scattering (SAXS and SANS). SAXS analyses indicated that the sodium caseinate dispersed in water as small particles with electrostatic interactions, which has a radius of gyration ( $R_g$ ) of  $\sim 5$  nm and an effective radius ( $R_{eff}$ ) of  $\sim 10$  nm with an assuming spherical shape. In the presence of  $Ca^{2+}$ , the caseinate particles aggregated as large particles with a hydrodynamic diameter  $> 100$  nm as determined by dynamic light scattering. The networks within the large particles were self-assembled from the small  $Ca^{2+}$ -cross-linked

particles ( $R_g \sim 6.5\text{--}8.0$  nm), as probed by SAXS. The fractal-like dimension increased from 2.5 to 3.4 with increasing protein and  $\text{CaCl}_2$  concentrations, suggesting a denser structure. The integrity of the caseinate particles at the oil-water interface was enhanced by  $\text{Ca}^{2+}$  cross-linking, as observed by transmission electron microscopy. The oil–water interface stabilised by  $\text{Ca}^{2+}$ -cross-linked caseinate particles was  $\sim 30$  nm thick, six times thicker than that stabilised by sodium caseinate ( $\sim 5$  nm) as analysed by SANS with contrast variation technique. Quantifying the structure of sodium caseinate in an aqueous solution and at the oil-water interface provides valuable insights for designing new casein-based functional materials.

### 4.1 Introduction

Sodium caseinate (CAS) is widely used in food emulsions because of its excellent surface activity; it can impart low interfacial tension during emulsification. CAS consists of a mixture of caseins ( $\alpha_{S1}$ -,  $\alpha_{S2}$ -,  $\beta$ - and  $\kappa$ -caseins, with a weight ratio of approximately of 4:1:4:1) and is prepared by precipitating the caseins from milk at the isoelectric point. In an aqueous solution at neutral pH, CAS molecules tend to associate to form small submicelles through hydrophobic interaction or electrostatic attraction (Leonard & Harold M, 1982). Previous studies by several research groups (Chu et al., 1995; HadjSadok et al., 2008; Hemar et al., 2021; Kumosinski et al., 1988; Lucey et al., 2000; Nash et al., 2002; Smialowska et al., 2017; Sosa-Herrera et al., 2012) showed that the CAS size [hydrodynamic radius or radius of gyration ( $R_g$ )] varied from 3 to 100 nm with mono-, bi- and tri-modal distributions that were measured using static and dynamic light scattering (SLS and DLS) or small-angle X-ray scattering (SAXS). The discrepancies in the results can be attributed mainly to differences in the production methods (e.g., commercial ingredients and laboratory-freeze-dried and pilot-plant-spray-dried samples), protein concentration, ionic strength and purification steps (filtration and ultracentrifugation) used for preparing the CAS dispersions. However, the method used to present the data obtained

by DLS could also have affected the size of CAS, as reported in the literature. Hemar et al. (2021) and Smialowska et al. (2017) pointed out that the particle size distribution of CAS dispersion by intensity from DLS was trimodal, with peaks at 5–10, 10–60 and 60–700 nm. In contrast, the particle size distribution of CAS showed only monomodal distribution between 4 – 6 nm by volume distribution (Smialowska et al., 2017) or between 5 – 20 nm by number distribution (Hemar et al., 2021) from DLS. These results suggest that small-sized particles predominate in CAS, and that large-sized particles represent only a small fraction of the total material. Represented by their scattered intensity in DLS measurements, these large particles could give a misleading view of the size distribution of CAS because, based on Rayleigh scattering theory, the scattered intensity is proportional to the dimension to the power of 6 or, equivalently, to the square of the particle volume (Barnett, 1942; Stetefeld et al., 2016). However, the sizes of CAS, as determined by SAXS and reported by the two research groups, were similar (about 6 nm).

The thickness of the adsorbed protein layer of CAS at solid surfaces or oil–water droplet interfaces has previously been determined using DLS (Dalglish, 1993; Fang & Dalglish, 1993; Hemar et al., 2021; Wooster & Augustin, 2006). The thickness of the adsorbed CAS layer at the interface of latex particles, determined as the increase in the diameter of latex particles after adding CAS, was measured as 11 nm and was independent of the casein concentration (0.01–0.1 wt%) (Hemar et al., 2021). In the quantification of the adsorbed protein layer at an oil–water interface, the DLS measurements need to be combined with enzymatic hydrolysis. The thickness of the adsorbed layer is then measured as the decrease in the diameter of the emulsion droplets after proteolysis (Dalglish et al., 1995; Fang & Dalglish, 1993; Wooster & Augustin, 2006). For emulsions stabilised by laboratory-prepared CAS, the change in droplet diameter varied between 10 and 20 nm depending on the casein concentration (0.2–

2.0% w/v); this difference corresponded to twice the thickness of the adsorbed layer of protein (5–10 nm) (Fang & Dalgleish, 1993). For emulsion droplets stabilised by commercial CAS, the adsorbed layer was about 11 nm thick and was independent of the casein concentration (0.5–2.0 wt%) (Dalgleish et al., 1995). However, researchers noted that with the proteolysis method, there are some residual peptides on the interface after proteolysis and have not been included in the reported thickness of the adsorbed layer, which could lead to some underestimation (Dalgleish, 1993; Wooster & Augustin, 2006).

In terms of improving the stability and functionality of emulsions, a thick interfacial layer is desirable. A thick layer can act as a mechanical barrier to protect the droplets from coalescence during long-term storage and to prevent lipid oxidation and delay lipid digestion (Berton-Carabin et al., 2013; Corstens et al., 2017b; Gudipati et al., 2010; Xu et al., 2014). In addition, for the use of nano-sized emulsion droplets as an emulsion stabiliser, a thick interfacial layer is essential to enable the nano-sized droplets to adsorb onto the surface of a second oil droplet, where the nano-sized droplets coated by protein particles (Cheng et al., 2019, 2022a; Ye et al., 2013b). When CAS is used as an emulsifier, it has been suggested that the amount of the casein adsorbed at the oil–water interface is affected by the state of casein aggregation before emulsification (Mulvihill & Murphy, 1991; Srinivasan et al., 1996; Ye & Singh, 2001). To meet the requirement of a high surface protein loading of the emulsion droplets, one approach is to include calcium ions ( $\text{Ca}^{2+}$ ) in the CAS dispersion before emulsification. It is well recognised that  $\alpha_{\text{S1}}$ - and  $\alpha_{\text{S2}}$ -caseins are rich in phosphoserine and are sensitive to  $\text{Ca}^{2+}$ . The addition of  $\text{Ca}^{2+}$  to CAS could lead to the formation of caseinate aggregates, because the binding of  $\text{Ca}^{2+}$  to the phosphoserines of the caseins can reduce the electrostatic repulsions between the protein molecules (Dalgleish & Parker, 1980; Parker & Dalgleish, 1981; Smialowska et al., 2017; Swaisgood, 2003). Ye and Singh (2001) reported

that the surface protein concentration of an emulsion stabilised by 3.0% commercial CAS increased from 1.6 to 6.3 mg/m<sup>2</sup> by increasing the calcium chloride (CaCl<sub>2</sub>) concentration in the protein solution from 0 to 20 mM before emulsification. However, there is a lack of information on the structures of the Ca<sup>2+</sup>-cross-linked sodium caseinate (Ca-CAS) particles and the interfacial layers that are stabilised by the Ca-CAS particles. In particular, quantification of the thickness of the Ca-CAS layer at the oil-water interfaces is important for studies focusing on the droplet-droplet interactions (Mougel et al., 2006).

In the present study, the adsorption of CAS and Ca-CAS at the oil-water interface was studied using small-angle neutron scattering (SANS) combined with contrast variation. SANS is a non-invasive method for probing the interfacial structure of emulsions because of the high-penetrating and non-destructive nature of neutrons and the absence of special sample preparation (Jestin et al., 2007; Reynolds et al., 2000; Verruto & Kilpatrick, 2008; Yesiltas et al., 2019). The use of solvent contrast variation exploits the neutron scattering length density (SLD) differences between different phases, providing the ability to selectively highlight the scattering from the emulsion, the oil droplets or the interfacial protein layer. In the present study, the SLD difference between the oil phase and interfacial protein layer was enhanced by using deuterated toluene as the oil phase of the model emulsion. It benefits the quantification of the details of the interfacial protein layer on the nanometre scale. In addition to SANS, SAXS was employed to probe the structure of CAS with and without Ca<sup>2+</sup>. By combining these methods with transmission electron microscopy (TEM), DLS and interfacial tension ( $\gamma$ ) measurements, this study allowed us to understand better the interfacial structure of emulsions stabilised by CAS and Ca-CAS particles.

### 4.2 Materials and methods

#### 4.2.1 Materials

CAS (Alanate 180: 92.7 wt% protein, 4.3 wt% moisture, 0.7 wt% fat and 0.2 wt% carbohydrates) was purchased from Fonterra Co-operative Group Ltd (Auckland, New Zealand). As reported by the manufacturer, 100 g of CAS powder contains 1300 mg of sodium, 30 mg of calcium and 22 mg of chloride. Deuterated toluene (*d*-toluene) was purchased from Sigma Aldrich (St. Louis, MO, USA). Milli-Q water (Millipore Corp., Bedford, MA, USA) and deuterium oxide (D<sub>2</sub>O) (Sigma Aldrich) were used to prepare emulsion samples for the SANS studies. All chemicals used were of analytical grade and were purchased from Sigma Chemical Co. (St. Louis, MO, USA) or BDH Chemicals (BDH Ltd, Poole, England) unless otherwise specified.

#### 4.2.2 Preparation of CAS and Ca-CAS particle dispersions

A stock CAS dispersion of 3.1% w/v protein concentration was prepared by dissolving CAS powder in ultrapure Milli-Q water (resistivity = 18.2 MΩ.cm) at 50 °C and stirring for 2 h, followed by overnight storage at room temperature to ensure complete hydration. The pH of this CAS dispersion was  $6.90 \pm 0.2$ . The Ca-CAS dispersion was prepared by adding an appropriate amount of stock CaCl<sub>2</sub> solution (1 M filtered through a 0.22 μm filter) dropwise into the stock CAS dispersion under gentle stirring for 30 min, followed by adjusting the pH to  $6.90 \pm 0.2$  using 2 M NaOH or 2 M HCl and equilibrating at room temperature overnight, as the aggregation of casein requires at least 5 h to reach equilibrium (Pitkowski et al., 2009). The Ca-CAS dispersion contained 3.0% w/v protein and 20 mM CaCl<sub>2</sub>, which were close to the concentrations of protein and colloidal calcium found in milk (Cheng et al., 2022a; Smialowska et al., 2017; Ye & Singh, 2001). The CAS and Ca-CAS dispersions were then diluted with



Milli-Q water to different protein concentrations (0.5, 1.5 and 3.0% w/v). Sodium azide was added at a final concentration of 0.04% w/v as a preservative.

### 4.2.3 Emulsion preparation

CAS- and Ca-CAS-stabilised emulsions were prepared by firstly mixing *d*-toluene (10% v/v) with the protein dispersions with 3.0% protein concentration at pH  $6.90 \pm 0.2$ . A total volume of 5 mL of the mixture was then homogenised with an Ultra-Turrax T10 (IKA<sup>®</sup>-Werke GmbH & Co. KG, Staufen, Germany) at 24,000 rev/min for 1 min.

### 4.2.4 Particle size distribution

The *z*-average hydrodynamic diameters of CAS and Ca-CAS were measured by DLS at 20 °C using a ZetaSizer Ultra (Malvern Instruments Ltd, Malvern, UK). The instrument used a backscattering configuration with detection at a scattering angle of 173° using an avalanche photodiode and a helium–neon laser at  $\lambda = 633$  nm; refractive indices of 1.50 and 1.33 were used for protein and water, respectively.

The droplet sizes of the CAS- and Ca-CAS-stabilised emulsions were determined by SLS using a Malvern MasterSizer 2000 (Malvern Instruments Ltd, Malvern, UK). The refractive index of toluene was 1.49 and that of water (the dispersing medium) was 1.33. The absorbance value of the emulsion droplets was 0.001. Droplet size measurements are reported as the De Broukere mean ( $d_{4,3}$ ). Mean particle diameters were calculated as the average of duplicate measurements.

### 4.2.5 Zeta potential measurements

The zeta potentials of CAS and Ca-CAS particles, and their associated emulsions, were determined by DLS at 20 °C using a ZetaSizer Ultra (Malvern Instruments Ltd, Malvern, UK). The dispersions of CAS and Ca-CAS were measured without dilution, whereas the emulsions

stabilised by CAS and Ca-CAS were diluted 100 times with Milli-Q water before measurement to avoid multiple scattering effects. The pH of the diluted emulsions was adjusted to 6.9 using 0.1 M NaOH or 0.1 M HCl.

### 4.2.6 Interfacial tension measurements

The interfacial tension ( $\gamma$ ) of the protein dispersions and emulsions was measured by the pendant drop method at room temperature using a surface tensiometer (Biolin 239 Scientific Instruments, Sweden). The tensiometer was operated in a volume-controlled regime, via continuous measurement of the drop area and volume, approximated by a Laplacian profile. During measurement, the drop phase (5  $\mu$ L) was composed of protein dispersions or emulsions hanging from the syringe tip inside *d*-toluene. The shape of the drop was determined from the balance of forces, which include  $\gamma$ . The  $\gamma$  at the drop–toluene interface can be related to the drop shape through:

$$\gamma = \frac{\Delta\rho \times g \times R_0^2}{\beta} \quad (4-1)$$

where  $\Delta\rho$  is the difference in the density between the fluids,  $g$  is the gravitational constant,  $R_0$  is the radius of the drop curvature at the apex and  $\beta$  is the shape factor. The shape factor is determined by the Young–Laplace equation (Neeson et al., 2014).

### 4.2.7 Negative staining TEM

The morphology and the microstructure of the protein dispersions and emulsions were observed using TEM with the negative staining method. The protein dispersions containing 3% w/v protein and their associated emulsions were both diluted 100-fold using Milli-Q water. A copper TEM grid coated with Formvar was placed on a drop of diluted sample solution for 5 min and then transferred on to a drop of 2% uranyl acetate for 5 min. The grid was washed on a drop of Milli-Q water for 5 min. The excess liquid was then drained off from the copper grid

using filter paper. The negatively stained grid was examined with a Philips electron microscope (NL-5600 MD, Philips, Eindhoven, The Netherlands) at an acceleration voltage of 60 kV.

### 4.2.8 Small-angle X-ray scattering

Protein dispersions of CAS and Ca-CAS with different protein concentrations (0.5, 1.5 and 3.0% w/v) were studied using SAXS. They were transferred into 2 mm ID quartz capillary tubes that were subsequently sealed with wax to prevent evaporation during measurement. SAXS measurements were performed on a Bruker NanoSTAR SAXS instrument (Bruker, Germany) in a  $Q$ -range from 0.01 to 0.35  $\text{\AA}^{-1}$ . All measurements were performed at room temperature ( $\sim 20$  °C) and the data were reduced and subtracted using water as a background. The scattering intensity from a colloidal system,  $I(Q)$ , can be expressed as a function of the wave vector,  $Q$ , using:

$$I(Q) = \Delta\rho^2 V_p \phi_p F(Q) S(Q) \quad (4-2)$$

where  $\Delta\rho$  is the contrast between the scattering particle and the surrounding solvent,  $V_p$  is the volume of scattering particle,  $\phi_p$  is the dimensionless particle volume fraction,  $F(Q)$  is the form factor, and  $S(Q)$  is the structure factor that accounts for the correlation between the colloidal particles.

Modelling of SAXS data of CAS dispersions was performed using Modelling II tool of Irena SAS macros (Ilavsky & Jemian, 2009) embedded in Igor Pro software (v8.04, Wavemetrics, USA). A two-level structural model was used. In the first level for the low- $Q$  region [ $0.01 < Q$  ( $\text{\AA}^{-1}) < 0.08$ ], the CAS particle was modelled with a form factor  $F(Q)$  of spheres (aspect ratio = 1) (Pedersen, 1997) and was assumed to follow a log-normal distribution, given by:

$$N(r) = \frac{1}{\sqrt{2\pi}\sigma} \exp \left\{ -\frac{1}{2} \left[ \frac{\ln \left( \frac{r}{r_{median}} \right)}{\sigma} \right]^2 \right\} \quad (4-3)$$

where  $r$  is the radius,  $r_{median}$  is the median radius and  $\sigma$  is the standard deviation of the size distribution.  $\sigma$  was fixed to 0.3 throughout the fitting (Smialowska et al., 2017). The X-ray contrast value was fixed at  $0.74 \times 10^{20} \text{ cm}^{-4}$  (Smialowska et al., 2017) which was calculated as the square of the difference between casein micelle of  $10.26 \times 10^{10} \text{ cm}^{-2}$  (Bouchoux et al., 2010) and H<sub>2</sub>O of  $9.4 \times 10^{10} \text{ cm}^{-2}$  (Ingham et al., 2016).

As SAXS profiles of CAS dispersions showed a correlation peak around  $\sim Q = 0.25 \text{ \AA}^{-1}$  for all three concentrations, a structure factor  $S(Q)$  of Hayter-Penfold Mean Spherical Approximation (MSA) was also applied (Hansen & Hayter, 1982; Hayter & Penfold, 1981). When conducting the fitting of the structure factor, the input parameters (**Table 4-1**) were fixed throughout the fitting to obtain the effective radius ( $R_{eff}$ ) and electric surface charge on the macroion ( $Z$ ).

**Table 4-1:** Input physical parameters used to constrain Hayter-Penfold fit on SAXS scattering of CAS.

CAS (% w/v)	0.5	1.5	3
Molarity (M) <sup>a</sup>	0.002 (0.001)	0.005 (0.001)	0.010 (0.003)
Particle volume fraction <sup>b</sup>	0.020 (0.002)	0.060 (0.001)	0.120 (0.001)
Dielectric constant of the solvent <sup>c</sup>	71.08	71.08	71.08
Temperature (K) <sup>d</sup>	293.15	293.15	293.15

<sup>a</sup>The molarity of monovalent salt in CAS dispersions was estimated based on the NaCl content in the CAS powder (2.1 Materials).

<sup>b</sup>The volume fraction of CAS was calculated from their mass fraction (w/v) by an approximated voluminosity (v/w) of 4 (Doudiès et al., 2019; Nöbel et al., 2012; Stothart & Cebula, 1982).

<sup>c</sup>The dielectric constant of the solvent was set as the default value of 71.08 for H<sub>2</sub>O.

<sup>d</sup>The measurement temperature was 20 °C or 293.15 K.

Numbers in parentheses represent the uncertainty from model fitting.

In the second structural level (high- $Q$  region [ $0.08 < Q$  ( $\text{\AA}^{-1}$ )  $< 0.21$ ]), the unified fit function of Irena SAXS macro (Ilavsky & Jemian, 2009) was used to fit the structures of small protein inhomogeneities within the CAS (Smialowska et al., 2017). The unified fit equation is expressed as (Beaucage, 1995, 1996):

$$I(Q) = \sum_{i=1}^n \left[ G_i \exp\left(\frac{-Q^2 R_{gi}^2}{3}\right) + B_i \exp\left(\frac{-Q^2 R_{g(i+1)}^2}{3}\right) \right] \quad (4-4)$$

where  $n$  is the number of structural levels,  $G$  is the Guinier scale factor,  $Q$  is the scattering wave vector,  $R_g$  is the radius of gyration and  $B$  represents the scale factor for power-law scattering.

The best fits in the entire  $Q$  range [ $0.01 < Q$  ( $\text{\AA}^{-1}$ )  $< 0.21$ ] were achieved by allowing the scalar, mean size,  $R_{eff}$ , and charge in the Hayter-Penfold fit level, as well as the Guinier and power-law exponent scalar ( $G$ ,  $B$ ),  $R_g$  and power-law exponent in unified fit level to flow.

As SAXS data of Ca-CAS showed an aggregation scattering feature in low- $Q$  [ $0.01 < Q$  ( $\text{\AA}^{-1}$ )  $< 0.02$ ], the scattering data in the entire  $Q$  range [ $0.01 < Q$  ( $\text{\AA}^{-1}$ )  $< 0.21$ ] were analysed using a unified fit function (equation 4) of Irena SAS macro (Ilavsky & Jemian, 2009) embedded in Igor Pro (v8.04, Wavemetrics, USA). Using this approach, the particle size ( $R_g$ ) and the power-law exponent ( $P$ ) of each structural level can be obtained.

#### **4.2.9 Small-angle neutron scattering**

SANS measurements on the emulsions stabilised by CAS and Ca-CAS were conducted on the QUOKKA instrument at the Australian Nuclear Science and Technology Organization, Sydney, Australia, at a  $Q$  range from 0.003 to 0.4  $\text{\AA}^{-1}$  (Gilbert et al., 2006; Wood et al., 2018). A set of solvent contrast variation measurements were conducted to characterise the interfacial structure of the emulsions using  $d$ -toluene (toluene- $d_8$ :  $C_6D_5CD_3$ ) as the oil phase; it has a

neutron SLD corresponding to ~ 89% D<sub>2</sub>O/11% H<sub>2</sub>O. Emulsions prepared using three different solvents, namely, water containing 0% D<sub>2</sub>O (matching none), 40% D<sub>2</sub>O (contrast matching the proteins – CAS and Ca-CAS) and 89% D<sub>2</sub>O (contrast matching the deuterated oil), were studied.

To prevent emulsion creaming, a multi-position tumbler was used during the collection of the SANS data. The scattering backgrounds for each contrast were prepared by ultracentrifugation of the corresponding emulsions at 63,000 g at 4 °C for 60 min followed by 0.1 μm syringe filtration. All the SANS data were collected at room temperature (~ 20 °C). They were reduced according to standard procedures (Kline, 2006) using the Igor Pro software (Wavemetrics, USA) with respective solvent background subtraction.

### **4.3 Results and discussion**

#### **4.3.1 Surface charges of CAS and Ca-CAS**

At 20 °C and pH 6.9, the zeta potential values of CAS and Ca-CAS at all protein concentrations were negative in a range between -11.01 and -37.47 mV (**Figure 4-1**). For a given protein concentration, the absolute zeta potential value was greater for the CAS particles than for the Ca-CAS particles. For example, at a protein concentration of 3.0% w/v, the absolute zeta potential values for CAS and Ca-CAS were 25.1 and 11.0 mV, respectively. This can be attributed to the presence of  $\text{Ca}^{2+}$  in Ca-CAS which shields the surface negative charge of the protein (Sosa-Herrera et al., 2012). The absolute zeta potential values for the CAS and Ca-CAS dispersions were found to decrease linearly with increasing protein concentration, with slopes of 5.7 and 3.9 for CAS and Ca-CAS, respectively. The assumed linear relationship between the absolute zeta potential value and the protein concentration was a consequence of the increase in ionic strength from the minerals with an increase in the protein concentration.



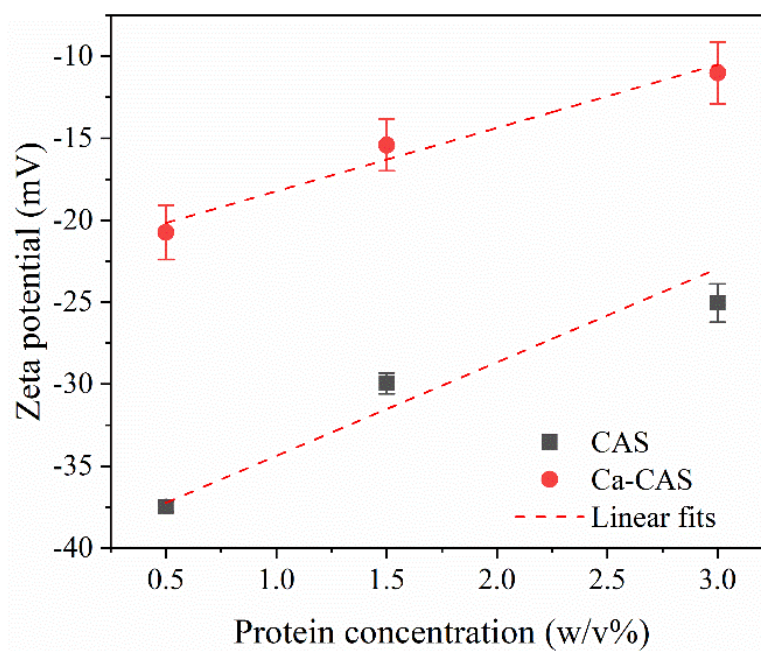


**Figure 4-1:** Zeta potentials of sodium caseinate (CAS, black squares) and  $\text{Ca}^{2+}$ -cross-linked sodium caseinate particle (Ca-CAS, red circles) dispersions at protein concentrations of 0.5, 1.5 and 3.0% w/v and neutral pH ( $6.9 \pm 0.1$ ) and 20 °C. Error bars represent the standard deviation from triplicates.

### 4.3.2 Structure of CAS and Ca-CAS dispersions

The CAS dispersions, as shown in the inset of **Figure 4-2A**, were transparent at low protein concentration and translucent at high protein concentration. In the presence of  $\text{CaCl}_2$ , the protein dispersions became opaque, indicating that the CAS had formed aggregates by calcium cross-linking (**Figure 4-2B, inset**). The structures of CAS and Ca-CAS in water at protein concentrations between 0.5 and 3.0% w/v were probed by SAXS (**Figure 4-2**). The SAXS profiles were shifted vertically along the  $y$ -axis for clarity; it can be observed that CAS and Ca-CAS showed different scattering patterns.

For CAS, a scattering maximum peak ( $Q_{max}$ ) was observed at around  $0.025 \text{ \AA}^{-1}$ , and the peak became more prominent and shifted to a higher  $Q$  when the concentration of CAS increased from 0.5 to 3.0% w/v (**Figure 2A**). This is consistent with observations from previous SAXS studies on the influence of protein concentrations from 1 to 8% w/v for CAS (Yesiltas et al., 2019) and from 0.2 to 5% w/v for bovine serum albumin (BSA) (Zhang et al., 2007). The peak position shifts to higher  $Q$  suggesting a decrease in the correlation distance with increasing protein concentration (Pitkowski et al., 2008; Yesiltas et al., 2019; Zhang et al., 2007). The average packing distance ( $D$ ) between the CAS particles could be estimated using  $D = 2\pi/Q_{max}$  (Pitkowski et al., 2008), resulting in distances of  $\sim 33.0 \pm 2.0$ ,  $26.0 \pm 2.0$ , and  $25.0 \pm 1.0$  nm for CAS at 0.5, 1.5 and 3.0 % w/v, respectively. Pitkowski et al. (2008) reported that the distance between CAS particles is  $\sim 20$  nm for 12% w/v CAS, consistent with closer packing between CAS particles at higher concentration. Yesiltas et al., (2019) proposed that the decrease in the packing distance is due to the loss of the water molecules between CAS particles at higher protein concentrations rather than a decrease in CAS size. They assumed that the CAS particles are uncharged and applied the core-shell fitting to obtain the hard sphere radius. The obtained hard sphere radius of CAS increased from 8.9 to 10.2 nm as the protein

concentration increased from 1 to 3 %, and then the radius was well maintained at 10.2 nm at protein concentrations above 3%.

However, our zeta-potential results (**Figure 4-1**) suggested that there were electrostatic repulsions between CAS particles. It has been suggested that for charged particles, at low ionic strengths ( $I < 0.3$  M), the repulsive interactions dominate in small interparticle separations and the  $S(Q)$  of Hayter-Penfold MSA should be considered for the fit (Hayter & Penfold, 1981; Qiu et al., 2006; Zhang et al., 2007).

Using  $S(Q)$  of Hayter-Penfold MSA to fit the low- $Q$  region [ $0.01 < Q$  ( $\text{\AA}^{-1}$ )  $< 0.08$ ], the radius of gyration ( $R_g$ ) of CAS increased from 4.9 to 5.9 nm with protein concentration from 0.5 to 3.0 % w/v, while the effective radius ( $R_{eff}$ ) of CAS was obtained to be  $\sim 9.1$  nm, which was not significantly affected by protein concentration (**Table 4-2**). The  $R_g$  of CAS was in line with the results of previous studies on CAS in aqueous systems using SAXS and SANS methods (Hemar et al., 2021; Pitkowski et al., 2008; Yesiltas et al., 2019). Assuming that the CAS was made of spherical particles, the hydrodynamic diameter ( $D_h$ ) could be calculated using  $D_h = 2 \times (5 \times R_g^2/3)^{0.5}$  (Witten et al., 2004), giving a  $D_h$  of  $\sim 13$  -15 nm with increasing protein concentration, which is also consistent with the size in previous studies by DLS (HadjSadok et al., 2008; Panouill e et al., 2005). The larger value of  $R_{eff}$  than that of  $R_g$  is due to the existence of double electric layers (Hayter & Penfold, 1981). The difference between  $R_{eff}$  and  $R_g$  can be regarded as the thickness of the diffuse double electric layer ( $h$ ) (Qiu et al., 2006; Zhang et al., 2007). It is known that the thickness of the diffuse double electrical layer and the absolute zeta potential are affected by the ionic strength, which decrease with increasing ionic strength due to shielding effects of counterions on the surface charge (Ram rez-Garc a et al., 2018). As expected, the  $h$  values decreased from 4.1 nm to 3.3 nm at higher protein concentrations (**Table 4-2**), which was consistent with the trend of decreasing

absolute zeta potential with increasing protein concentrations (Figure 1). The decrease in  $h$  and absolute zeta-potential indicated a shrinkage of the electrical double layer and a decrease in repulsive interactions. Meanwhile, the surface charge ( $Z$ ) of CAS obtained from Hayter-Penfold fit increased from 21 to 36 e at higher protein concentrations. These results were similar to a previous SAXS study of BSA. Using the Hayter-Penfold model, Zhang et al., (2007) found that the peak of structure factor shifted to higher  $Q$ , the  $h$  decreased and absolute  $Z$  increased with increasing protein and NaCl concentrations. It could be due to that the repulsive interactions between protein particles decreased because counterions increased in the bulk solution and more ions bound to protein surface. In another study of BSA, Salis et al., (2011) found that the absolute  $Z$  increased and absolute zeta-potential decreased with increasing NaCl concentrations at fixed pH as revealed by potentiometric titrations and zeta potential measurements.

At the high- $Q$  region [ $0.08 < Q (\text{\AA}^{-1}) < 0.21$ ], the  $R_g$  value obtained from the unified fit was 2.5 -2.8 nm for CAS of 0.5 – 3.0 % (w/v). In the previous studies, the structures with a  $R_g$  of ~ 2-3 nm in the high- $Q$  region are attributed to small protein inhomogeneities where caseins interact with each other through non-covalent forces (e.g., Van der Waals forces) (de Kruif et al., 2002; Smialowska et al., 2017).

In the presence of  $\text{Ca}^{2+}$ , the Guinier plateau at around  $\sim 0.03 \text{\AA}^{-1}$  of the CAS particles disappeared (**Figure 4-2B**). The scattering intensity increased significantly in the low- $Q$  region ( $Q < 0.03 \text{\AA}^{-1}$ ) for the Ca-CAS particles at all protein concentrations (**Figure 4-2B**). This suggests that caseins aggregate through  $\text{Ca}^{2+}$  binding, forming particles of large size. Although the overall size of these large aggregates is not accessible due to the limit of the lowest  $Q$  achievable in the present SAXS measurement, it can be achieved by DLS measurements. The hydrodynamic diameters of the Ca-CAS particles were  $103.7 \pm 5.0$ ,  $108.7 \pm 5.0$  and  $132.6 \pm$

5.0 nm for protein concentrations of 0.5, 1.5 and 3.0% w/v (**Supplementary material, Figure S 4-1**). The measured sizes in the present study were similar to those from previous DLS studies at similar concentration ratios between calcium and protein (Smialowska et al., 2017; Sosa-Herrera et al., 2012). Smialowska et al. (2017) found that a 3.3% CAS dispersion with 22 mM CaCl<sub>2</sub> resulted in Ca-CAS particle size of 130 nm and a monomodal distribution. Sosa-Herrera et al. (2012) reported a hydrodynamic diameter of Ca-CAS particles of ~ 150 nm for 1% CAS with 5 mM CaCl<sub>2</sub>. The internal structures of the large Ca-CAS particles were modelled using Unified fitting and the data are given in **Table 4-2**. For all the Ca-CAS samples, the scattering in the low- $Q$  region [ $0.01 < Q$  (Å<sup>-1</sup>) < 0.02] followed a power-law decay with an exponent in the range 2.5–3.4 (**Table 4-2**), indicating that the large-sized Ca-CAS particles (104–133 nm) possessed either mass or surface fractal-like structures. The associated networks of these large-sized aggregates comprised small-sized Ca-CAS particles ( $R_g \sim 6.5$ –8.0 nm); this agrees with a previous SAXS study on a similar system (Smialowska et al., 2017). The larger value of the power-law exponent identified at the higher concentration suggested that the small Ca-CAS particles were more densely clustered (Martin & Schaefer, 1984).

For both CAS and Ca-CAS, a power-law exponent of 2.2–2.8 (**Table 4-2**) was identified in the high- $Q$  region [ $0.08 < Q$  (Å<sup>-1</sup>) < 0.21] (**Figure 4-2**). This may imply that the conformation of caseins varies from a randomly flexible chain to a weak network formed through diffusion-limited aggregation with mass fractal-like structure of < 3.0 (Martin & Schaefer, 1984). However, there are some uncertainties around the high- $Q$  power-law exponent because of its sensitivity to the background subtraction and because it is obtained from only a limited  $Q$  range [ $0.08 < Q$  (Å<sup>-1</sup>) < 0.21]. Therefore, this exponent should be interpreted with caution to avoid ambiguous conclusions.

**Table 4-2:** Structural parameters obtained from the fit to small-angle X-ray scattering profiles of sodium caseinate (CAS) and Ca<sup>2+</sup>-cross-linked caseinate particles (Ca-CAS) at various protein concentrations.

Protein concentration (% w/v)	0.5	1.5	3.0
CAS dispersions			
0.01 < $Q$ (Å <sup>-1</sup> ) < 0.08			
$R_g$ (nm)	4.9 (0.1)	5.4 (0.1)	5.9 (0.1)
$R_{eff}$ (nm)	9.1 (0.2)	9.1 (0.1)	9.2 (0.1)
$h$ (nm)	4.1	3.7	3.3
$Z$ (e)	21 (3)	27 (1)	36 (1)
0.08 < $Q$ (Å <sup>-1</sup> ) < 0.21			
$R_g$ (nm)	2.5 (0.1)	2.6 (0.1)	2.8 (0.1)
Powe-law exponent	2.8 (0.1)	2.7 (0.1)	2.6 (0.1)
Ca-CAS dispersions			
0.01 < $Q$ (Å <sup>-1</sup> ) < 0.02			
Power-law exponent	2.5 (0.1)	3.1 (0.2)	3.4 (0.1)
0.02 < $Q$ (Å <sup>-1</sup> ) < 0.21			
$R_g$ (nm)	6.5 (0.5)	7.6 (0.5)	8.0 (0.5)
Power-law exponent	2.5 (0.1)	2.3 (0.1)	2.2 (0.1)

Numbers in parentheses represent the uncertainty from model fitting.

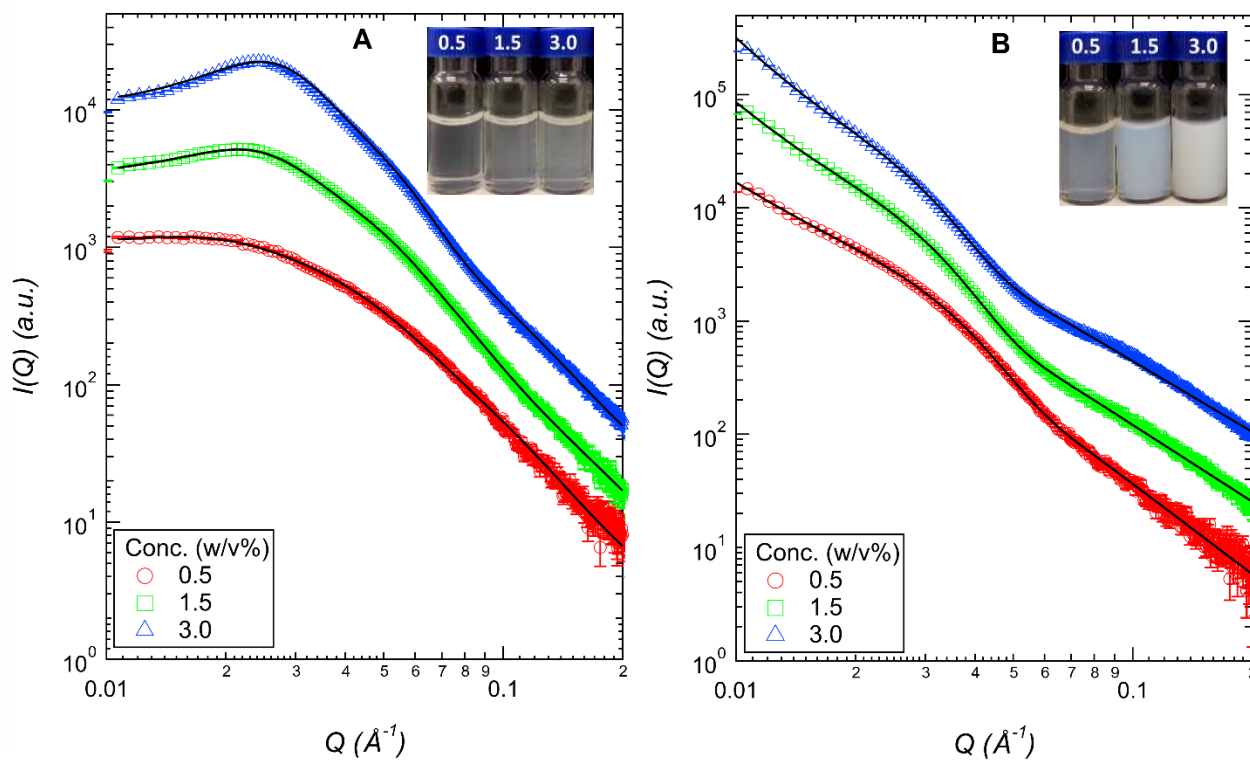


**Figure 4-2:** Small-angle X-ray scattering profiles of (A) sodium caseinate and (B)  $\text{Ca}^{2+}$ -cross-linked sodium caseinate particles at protein concentrations of 0.5, 1.5 and 3.0% w/v. The solid black lines are the unified fits to the scattering data. The scattering curves were shifted vertically for clarity. The insets are visualisations of the associated protein dispersions.

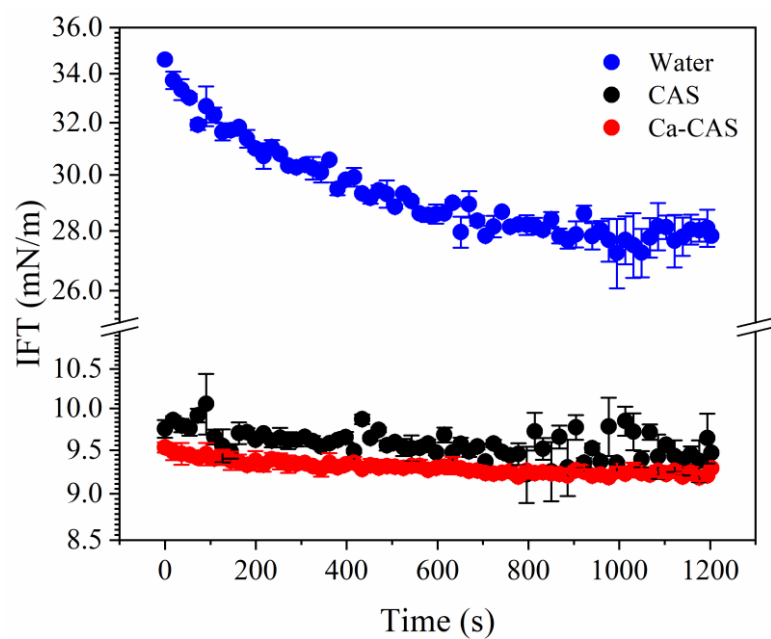
**4.3.3 Interfacial tension of CAS and Ca-CAS at the oil-water interface**

Figure 3 shows the interfacial tensions ( $\gamma$ ) of CAS and Ca-CAS at the oil (toluene)–water interface as measured using the pendant drop method for a protein concentration of 3% w/v. The decay curves show that the  $\gamma$  values for both CAS and Ca-CAS decreased rapidly at the oil-water interface and then reached equilibrium with time. When the  $\gamma$  values between 600 and 1200 s were averaged, the equilibrated  $\gamma$  values were  $9.54 \pm 0.14$  and  $9.24 \pm 0.03$  mN/m for the CAS and Ca-CAS dispersions, respectively. The equilibrium  $\gamma$  values of CAS and Ca-CAS at the toluene-water interface are similar to their equilibrium  $\gamma$  values at the sunflower oil-water interface ( $\sim 9.69 - 11.62$  mN/m) as reported in the literature (Sosa-Herrera et al., 2008), suggesting that casein adsorption at the toluene-water and sunflower-water interfaces is comparable. Consequently, toluene is used here as a model dispersed phase to study the adsorption behaviour of casein at the oil-water interface while enabling contrast variation SANS measurements to be performed. The slightly lower  $\gamma$  value at the oil–Ca-CAS interface may be related to structural changes in the caseins induced by  $\text{Ca}^{2+}$  binding that increase the protein load per unit of interfacial area for Ca-CAS (Ye & Singh, 2001).

In addition, it was observed that the measured interfacial tension of Ca-CAS was more stable than that of CAS (**Figure 4-3**). The fluctuating  $\gamma$  value for CAS can be attributed to individual casein exchange between the interface and the water phase. Previous studies at oil–water interfaces stabilised by caseins suggest that the adsorbed individual caseins at the interface have high mobility and flexibility under the conditions of low ionic strength and neutral pH, experiencing a rapid and reversible exchange between the interface and the aqueous phase (Dickinson, 1992a; Dickinson et al., 1988b). When caseins are cross-linked by  $\text{Ca}^{2+}$ , intermolecular linkages between the caseins decrease their flexibility compared with individual caseins, resulting in slower and less extensive protein exchange between the interface and the



aqueous phase (Hunt & Dalgleish, 1994). This suggests that the more stable  $\gamma$  value at the interface between Ca-CAS and oil was due to the anchored Ca-CAS aggregates at the interface.



**Figure 4-3:** Interfacial tensions of toluene–water (blue), toluene–3% w/v sodium caseinate (CAS, black) and toluene–3% w/v  $\text{Ca}^{2+}$ -cross-linked caseinate particles (Ca-CAS, red) at neutral pH ( $6.9 \pm 0.1$ ) and 20 °C. Error bars represent the standard deviation from triplicates.

### 4.3.4 Interfacial layer structure of droplets stabilised by CAS and Ca-CAS

#### 4.3.4.1 Transmission electron microscopy

Negative staining TEM characterisation was used to observe the morphologies of CAS and Ca-CAS before (Figure 4A and 4B) and after (Figure 4C and 4D) adsorption on to the interface of emulsion droplets. For the emulsion preparation, CAS and Ca-CAS with a protein concentration of 3% w/v were used to emulsify the 10 % v/v toluene. To avoid particle overlapping on the TEM grid, the protein solutions and the emulsions formed with 3% w/v protein were diluted 100-fold during sample preparation.

**Figure 4-4A** shows caseins present in different structural forms in the CAS dispersion, including particulates, fibrous shapes in a size range of a few nanometres and irregular aggregates of several hundred nanometres. These morphologies were similar to those observed in a previous study using TEM (Farrer & Lips, 1999). **Figure 4-4B** shows that, in the presence of  $\text{Ca}^{2+}$ , the caseins assembled into spherical particles of ~ 50 nm in size. Aggregates of Ca-CAS were observed and showed a nested network.

To eliminate the effect of the ratio between the droplet surface area and the protein concentration (Fang & Dalgleish, 1993; Wooster & Augustin, 2006), emulsions stabilised by different particles (CAS and Ca-CAS) were controlled in terms of droplet size and specific surface area, as shown in the **Supplementary material, Table S 4-1**. **Figure 4-4C** and **4D** show that the interfaces of the emulsion droplets were almost completely covered by CAS or Ca-CAS. The structure of CAS at the droplet interface was in the shape of irregular fibrils and formed a thin layer with a small amount of CAS aggregates. The lack of spherical particles suggested that structural rearrangement of CAS occurred upon adsorption at the droplet interface. This structural rearrangement could have been driven by hydrophobic forces that

maximised the contact area between the hydrophobic part of the caseins and the oil surface. At the emulsion droplet interface, Ca-CAS retained its regular spherical structure and size (approximately 50 nm) and was uniformly distributed over the droplet surface. Hunt & Dalgleish (1994) suggested that, when caseins are cross-linked by  $\text{Ca}^{2+}$ , the intermolecular linkages between them increase and their flexibility decreases compared with the individual caseins. This supports observations in the present study that Ca-CAS had an enhanced particle structural integrity compared with CAS after adsorption at the emulsion droplet surface.

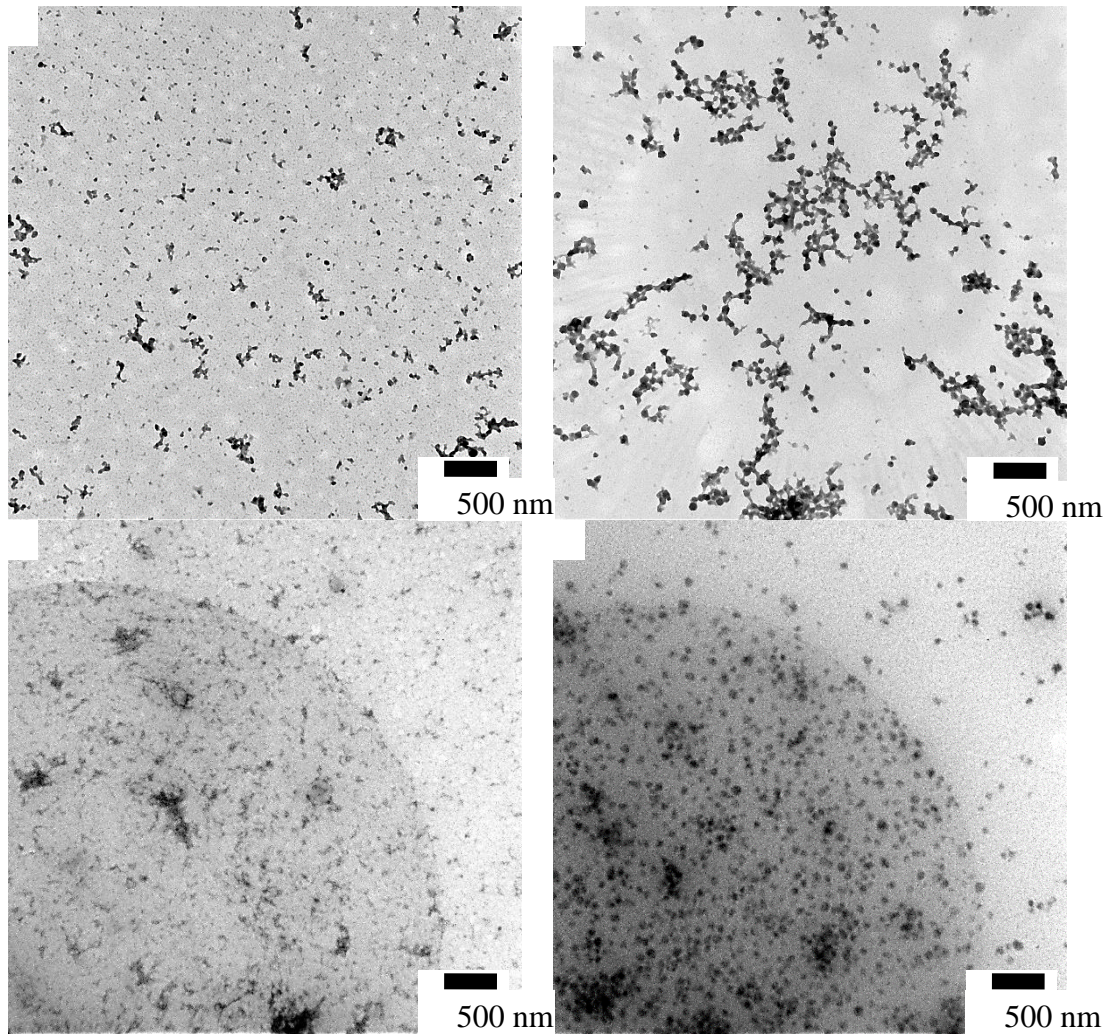


**Figure 4-4:** Negative staining transmission electron microscopy images (20.5kx magnification) of (A) 0.03 % w/v sodium caseinate (CAS), (B) 0.03 % w/v  $\text{Ca}^{2+}$ -cross-linked caseinate (Ca-CAS) particles, (C) interface of 10 % v/v toluene emulsion droplet stabilised by 3 % w/v CAS and (D) interface of 10 % v/v toluene emulsion droplet stabilised by 3 % w/v Ca-CAS. Scale bars are 500 nm.

#### 4.3.4.2 Small-angle neutron scattering analysis

The interfacial structures of the emulsions were probed by CV-SANS, as shown in **Figure 4-5**. At 12% D<sub>2</sub>O, the entire oil droplet and the adsorbed protein layer contributed to the scattering. The scattering patterns and the intensities of the emulsions stabilised by CAS and Ca-CAS were similar (**Figure 4-5A and B**), which can be attributed to their similar oil droplet sizes (**Supplementary material, Table S 4-1**). The 40 and 89% D<sub>2</sub>O solvents were used to contrast match the scattering intensity from the adsorbed protein layers and the oil droplets (*d*-toluene) respectively, thus highlighting the oil droplet only or the protein layer only. It can be observed that the variation of contrast matching solvents caused different changes in the scattering intensities of the different emulsions. For the emulsion stabilised by CAS, the intensity at the lowest  $Q$  of  $0.0033 \text{ \AA}^{-1}$  decreased from  $170 \text{ cm}^{-1}$  to  $86 \text{ cm}^{-1}$  when the amount of D<sub>2</sub>O was varied from 12 to 40%. However, there was a much more significant decrease in intensity from  $170 \text{ cm}^{-1}$  to  $36 \text{ cm}^{-1}$  in the emulsion stabilised by Ca-CAS. This suggested that the contribution of the adsorbed protein to the total emulsion scattering was much more prominent in the emulsion stabilised by Ca-CAS than in the emulsion stabilised by CAS. Indeed, in 89% D<sub>2</sub>O, in which only the adsorbed protein layer could be observed, the scattering intensity of the emulsion stabilised by Ca-CAS was much greater than that of the emulsion stabilised by CAS. This was expected as Ca-CAS has a much greater size than CAS, thereby forming a thicker interfacial layer once adsorbed at the oil droplet interface. The thickness of interfacial layers formed by CAS and Ca-CAS was determined by fitting the SANS data at 89% D<sub>2</sub>O using the models discussed below.

To better examine the scattering pattern changes under different contrast matching conditions, the scattering curves for the emulsions stabilised by CAS and Ca-CAS are shifted vertically in **Figure 4-5C and 5D**. For both emulsion samples suspended in 40% D<sub>2</sub>O, the

scattering in the low- $Q$  region ( $Q < 0.01 \text{ \AA}^{-1}$ ) followed a power-law decay with an exponent of  $-4$ , which indicated Porod scattering from the smooth surface of the oil droplet. In the 89%  $\text{D}_2\text{O}$  solvent, the scattering data changed to a  $Q^{-2}$  dependence in the low- $Q$  region, indicative of the scattering characteristics of a thin film (Martin & Schaefer, 1984). In this case, as the SLD value of the aqueous phase (89%  $\text{D}_2\text{O}$ ) is very close to that of the  $d$ -toluene phase, only the scattering from the adsorbed protein layer was observed. Similar scattering patterns were also observed in fish oil-in-water emulsions stabilised with combinations of CAS and phosphatidylcholine (Yesiltas et al., 2019), as well as in water-in-hydrocarbon emulsions stabilised by asphaltene (Alvarez et al., 2009; Jestin et al., 2007). The interfacial layer thickness can be determined from the  $Q$  ( $Q \sim 1/T$ , where  $T$  is the interface thickness) value at which the scattering deviates from  $Q^{-2}$  behaviour (Yesiltas et al., 2019). The average thicknesses of the interfacial layers for the emulsions that were stabilised by CAS and Ca-CAS were calculated to be  $\sim 5$  and  $\sim 30$  nm, respectively (**Figure 4-5C** and **5D**). The interfacial layer thickness values for CAS and Ca-CAS were smaller than their corresponding  $D_h$  in solution:  $\sim 15$  nm for CAS and  $\sim 133$  nm for Ca-CAS. This result suggests that the structures of CAS and Ca-CAS particles are flexible and can adjust their conformation to cover the interface, leading to efficient film formation. The deformation and the spreading of flexible molecules/particles, such as  $\beta$ -casein and casein micelles, on emulsion interfaces have been reported in previous studies (Robson & Dalgleish, 1987; Ye et al., 2013b). The interfacial layer thickness of 5 nm obtained in the CAS-stabilised emulsion was similar to that in a previous study using DLS combined with enzymatic hydrolysis, which reported a value of  $\sim 5$ – $10$  nm (Fang & Dalgleish, 1993). The thicker interfacial layer determined in the emulsions stabilised by Ca-CAS was also expected, as several individual caseins are cross-linked by  $\text{Ca}^{2+}$ . This agrees well with the TEM observations (**Figure 4-4**), where a more prominent Ca-CAS aggregation was observed at the surface of the oil droplets. It is also worth noting that, compared with TEM, SANS can probe

a significantly greater number of emulsion droplets given the neutron beam size used and the emulsion concentration, resulting in a more statistically robust result (Gilbert, 2019; Yang et al., 2020). Moreover, we should emphasise that the interface thickness determined by SANS is an averaged result from a large number of oil droplet interfaces. This is critical as the interfacial coverage is not homogeneous in both CAS- and CAS-stabilised emulsions and some large aggregates are locally anchored on the surface of the oil droplets.



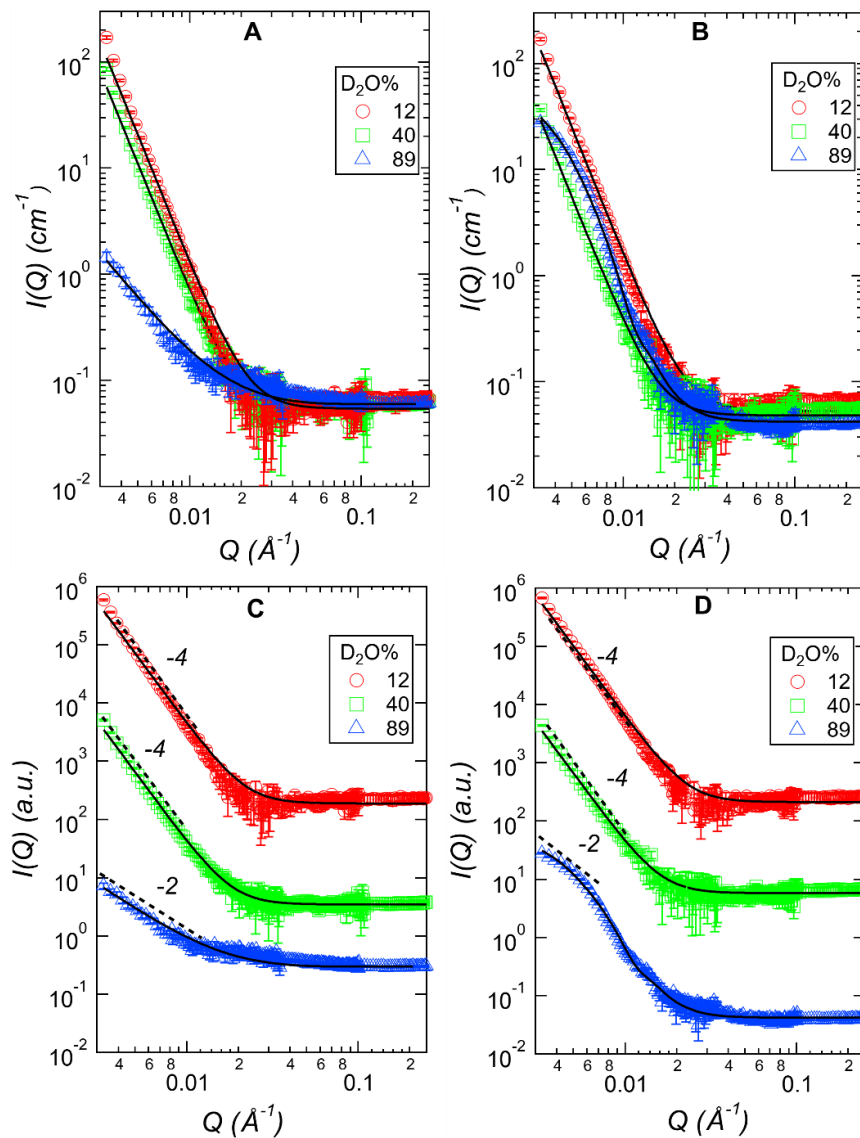


**Figure 4-5:** Small-angle neutron scattering profiles of (A) the deuterated toluene emulsion stabilised by sodium caseinate and (B) the deuterated toluene emulsion stabilised by  $\text{Ca}^{2+}$ -cross-linked sodium caseinate particles. SANS measurements were performed in 12%, 40% (highlighting the scattering of oil droplets by matching out the scattering of the proteins) and 89% (highlighting the scattering of the protein shell by matching out the scattering of the oil droplets) deuterium oxide ( $\text{D}_2\text{O}$ ). The scattering curves shown in A and B (on the absolute scale) have been shifted vertically for clarity in C and D, respectively. The solid black lines are the unified fits to the scattering data.

### 4.4 Conclusions

This study probed the effect of protein concentration and  $\text{CaCl}_2$  addition on the structure of CAS in an aqueous solution and at the oil-water interface. As the protein concentration increases from 0.05 to 3.0% w/v, CAS disperses in water as small particles with a radius of gyration ranging from  $\sim 4.9$  to  $\sim 5.9$  nm. However, the surface charges, the effective radius, the thickness of electric double layer as well as the packing distance of CAS particles decrease with an increase in protein concentrations because the counterion concentrations in the bulk phase increase. In the presence of  $\text{Ca}^{2+}$ , the caseinate particles form large aggregates with a hydrodynamic diameter  $> 100$  nm. At higher concentrations of both protein and  $\text{Ca}^{2+}$ , the network consisting of small caseinate particles inside the large aggregates is more densely packed. Moreover, the presence of  $\text{Ca}^{2+}$  enhances the integrity of Ca-CAS particles at the oil-water interface, resulting in a thick interfacial layer and providing a low and stable oil-water interfacial tension. The average thickness of the interface stabilised by Ca-CAS particles is  $\sim 30$  nm, i.e., approximately six times thicker than that stabilised by CAS ( $\sim 5$  nm). Herein we provided a simple approach to fabricate the protein particles using the source of casein protein and calcium, which can be easily applied in a wide range of applications. The thick interfacial layer of Ca-CAS would be expected to have enhanced impact on the emulsion physico-chemical properties, in particular for nano-sized emulsion. The Ca-CAS-stabilised interfacial layer may provide improved performance in some applications, such as concentrated emulsion and emulsion gels. In future, it would be interesting to determine the stability and rheological properties of Ca-CAS-stabilised emulsion at different conditions, as well as their potential as functional ingredients in food products, which would further expand their applications.

### 4.5 Acknowledgements

This work was funded by the Riddet Institute, a National Centre of Research Excellence (CoRE), funded by the New Zealand Tertiary Education Commission. We acknowledge the grants and the support of the Australian Nuclear Science and Technology Organization, Australia, for access to the small-angle X-ray scattering (Bruker) and small-angle neutron scattering (QUOKKA) facilities under proposal P8623. We also thank the Manawatu Microscopy and Imaging Centre at Massey University for technical support.

### CRediT authorship contribution statement

**Lirong Cheng:** Conceptualisation, Methodology, Validation, Formal analysis, Investigation, Data curation, Visualisation, Writing – original draft. **Aiqian Ye:** Conceptualisation, Supervision, Resources, Funding acquisition, Project administration, Writing – review & editing. **Zhi Yang:** Conceptualisation, Formal analysis, Writing – review & editing. **Elliot Paul Gilbert:** Investigation, Formal analysis, Project administration, Writing – review & editing. **Robert Knott:** Investigation, Formal analysis, Project administration, Writing – review & editing. **Liliana de Campo:** Investigation, Formal analysis, Project administration, Writing – review & editing. **Ben Storer:** Investigation, Writing – review & editing. **Yacine Hemar:** Conceptualisation, Supervision, Project administration, Writing – review & editing. **Harjnder Singh:** Supervision, Funding acquisition, Writing – review & editing

### Declaration of Competing Interest

The authors declare that they have no known competing financial interests or personal relationships that could have appeared to influence the work reported in this paper.

#### 4.6 Supplementary material

**Table S 4-1:** Size and surface characteristics of emulsions stabilised by sodium caseinate particles and Ca<sup>2+</sup>-cross-linked caseinate particles (Ca-CAS).

Parameters	CAS emulsion	Ca-CAS particle emulsion
Surface mean diameter, $d_{3,2}$ ( $\mu\text{m}$ )	0.39 (0.03)	0.39 (0.01)
Volume mean diameter, $d_{4,3}$ ( $\mu\text{m}$ )	9.60 (0.81)	9.85 (0.75)
Specific surface area ( $\text{m}^2/\text{g}$ )	15.40 (0.23)	15.30 (0.21)

CAS, native sodium caseinate; Ca-CAS particle, Ca<sup>2+</sup>-cross-linked sodium caseinate particle.

Numbers in parentheses represent the standard deviation from triplicates.

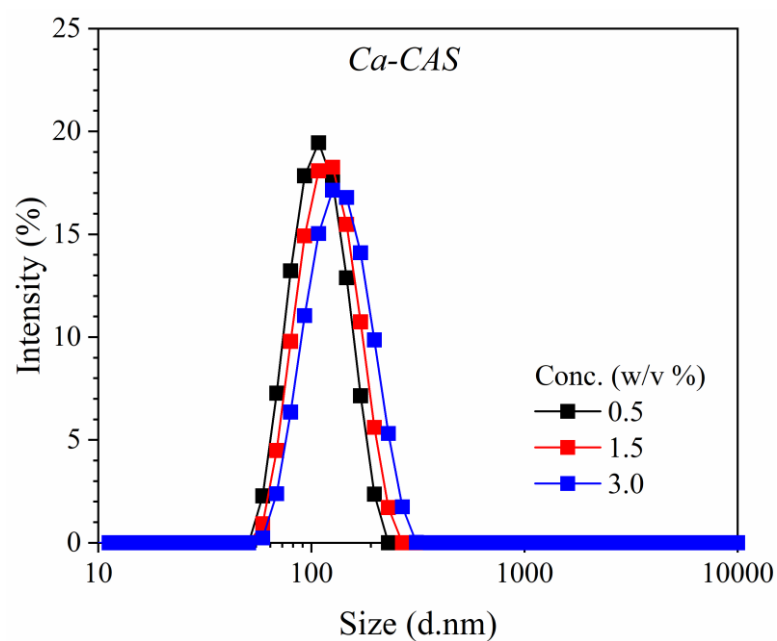
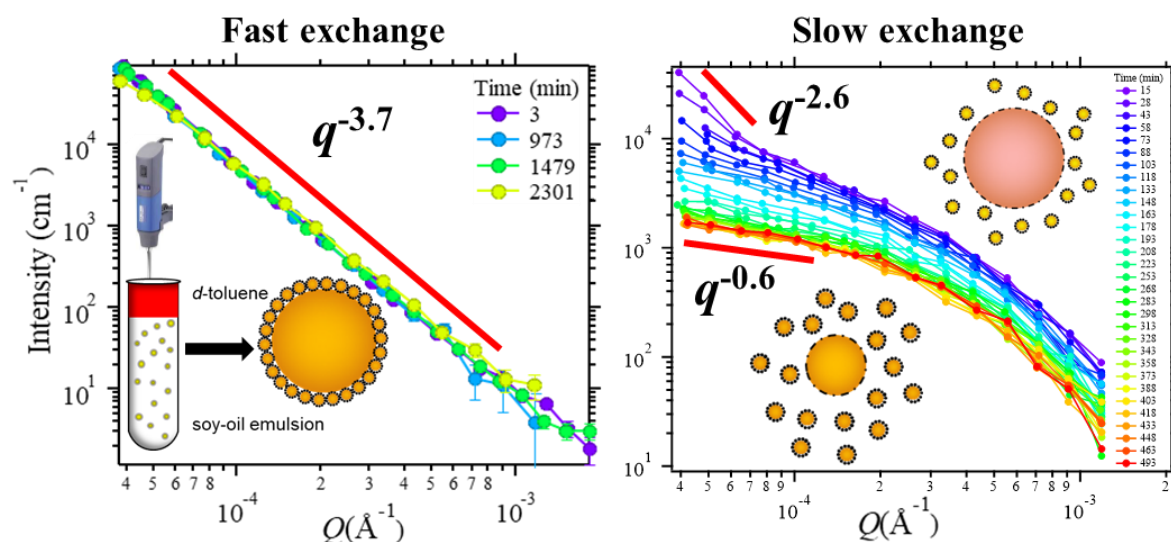


**Figure S 4-1:** Particle size intensity distribution of  $\text{Ca}^{2+}$ -cross-linked caseinate (Ca-CAS) particle dispersions at protein concentrations of 0.5 (black), 1.5 (red) and 3.0% w/v (blue) at neutral pH ( $7.0 \pm 0.1$ ) and 20 °C from ZetaSizer dynamic light scattering intensity measurements.

## Chapter 5 Oil exchange mechanisms in droplet-stabilised emulsions as revealed by contrast variation USANS and SANS

### Graphic Abstract



### Abstract

Oil-in-water emulsions that are stabilised by primary droplets (droplet-stabilised emulsion, DSE) have attracted research interests due to their high stability and potential for co-delivery of two or more active substances in one vehicle. In this study, mass transport of the different oils between the primary droplet and the stabilised core droplet is investigated using SANS and USANS. Nano-sized soya-oil-droplets covered by a protein layer made of calcium cross-linked casein particles (Ca-CAS) were used to stabilise deuterated toluene (*d*-toluene) droplets. These two oils were chosen as their scattering length densities are different. Time-resolved contrast-variation ultra-small-angle neutron scattering (CV-USANS) was used to measure the structure and composition of droplets over time, complemented by static light scattering and optical microscopy. The primary droplet layer was found to be stable to against the coalescence with

the core droplet over time, resulting a similar surface fractal dimension value of 3.7 for a rough interfacial layer of DSE. However, a rapid full mixing between soya-oil and *d*-toluene was found in DSE which yielded even distribution of mixed oil at all length scale in DSE as probed by CV-USANS and CV-SANS. The oil exchange process was slowed down by eliminating the direct adsorption of the soya-oil droplets at the *d*-toluene droplet surface. The emulsion containing dispersed soya-oil droplets and *d*-toluene droplets showed the oil exchange following an exponential decay and it took 320 min to reach an equilibration. The faster diffusion rate of *d*-toluene compared to that of soya-oil led to a shrinkage of *d*-toluene droplets and the growth of soya-oil droplets, resulting in a narrower droplet size distribution over time as supported by static light scattering and optical microscopy measurements. Knowledge of structural stability and oil exchange in the hierarchical or polydisperse emulsions will assist in the rational design of their use as co-delivery vehicles and other potential applications.

### 5.1 Introduction

Oil-in-water emulsions stabilised by primary droplets offer a potential to co-deliver two or more active substances in one vehicle (Hettiarachchi et al., 2009; Sakellari et al., 2021). For utilising the hierarchical emulsions as delivery vehicles and control the release rate and site of the bioactive compounds, it is important to understand the mass transport between the oil droplets. In emulsion systems, there are several mechanisms responsible for mass transport between oil droplets, including droplet coalescences, Ostwald ripening and oil molecule exchanges (Lee & Pozzo, 2019; Malassagne-Bulgarelli & McGrath, 2009). The first two destabilisation mechanisms can cause two oil droplets to merge into one large droplet, which can be monitored by droplet size changes with time. Droplet coalescence can occur due to colloidal interactions and interfacial film rupture. Ostwald ripening also leads to an increase in droplet size, but this is due to the different Laplace pressures between the polydisperse droplets

and to the solubility of the oil molecules in the aqueous phase. Under Ostwald ripening, the size of the large droplet will increase at the expense of the smaller ones. Due to their different effects on droplet size and distribution evolutions, coalescence and Ostwald ripening can be easily identified. Ostwald ripening leads to narrow size distributions and a gradual decrease in the droplet growth rate. In contrast under coalescence the oil droplets polydispersity increases the coarsening rate is accelerated (Bibette et al., 1992; Schmitt et al., 2004)

The third mechanism – oil exchange was proposed in previous studies and is attributed to the transport of the oil molecules between the droplets without affecting their size with time (McClements et al., 1992, 1993a; McClements & Dungan, 1993). The oil-exchange between hexadecane droplets and octane droplets stabilised by a non-ionic surfactant (polyoxyethylene sorbiton monolaurate) was studied using differential scanning calorimetry (DSC) to monitor the changes in crystallisation temperature (McClements et al., 1992; McClements & Dungan, 1993). These studies suggested that the oil exchange process only occurred at surfactant concentrations above the critical micelle concentration; the surfactant micelles accelerated the solubilisation of the insoluble oil molecules and transport of oil between droplets, through the aqueous phase. More recently, contrast-variation small-angle neutron scattering (CV-SANS) was used to determine the rate of oil exchange between oil droplets (Lee & Pozzo, 2019; Roger et al., 2015). CV-SANS relies on the difference in neutron scattering length densities (SLDs) of the hydrogenated and the deuterated oil molecules (Gilbert, 2019; Lopez-Rubio & Gilbert, 2009). This allow to direct monitoring of oil compositional changes in the droplets *in situ* without extensive sample preparations or the need for molecular labelling.

However, previous CV-SANS studies of oil exchange between hexadecane ( $C_{16}H_{34}/C_{16}D_{34}$ ) droplets have contradicted the results of DSC measurement, with significant oil exchange observed at concentrations of the surfactants (e.g., sodium dodecyl sulphate, and



polyoxyethylene alkyl ether) well below the critical micellar concentration (Lee & Pozzo, 2019; Roger et al., 2015). These two studies suggested that the underlying mechanism of the oil exchange is due to direct droplet contacts or oil permeation through thin liquid films. The oil exchange kinetics could be controlled by the surfactant layer structure, temperature, aqueous solubility of oil phases, and the probability of collisions (e.g., the concentration of droplets and long-range repulsions).

In addition, Roger et al. (2015) reported that the oil exchange rate decreased by orders of magnitude with increasing the hydrophobic chain length or the hydrophilic chain length. In contrast, Lee & Pozzo (2019) observed that the oil exchange rate of emulsions stabilised by a short hydrophobic alkyl tails (hexyl sulphate sodium salt, SHS, C6) surfactant was much slower than for those stabilised by a surfactant with identical hydrophilic head but longer hydrophobic alkyl tails (tetradecyl sulphate sodium salt, STS, C14). The STS (C14) stabilised emulsion had a smaller droplet size (85 nm in diameter) than the SHS (C6) stabilised emulsion (261 nm in diameter). Lee & Pozzo (2019), hence, suggested that the droplet size became the governing factor in oil exchange rate rather than the type of the surfactant, in which the smaller droplet had a higher collision probability and total interfacial area. Previous studies by both Lee & Pozzo (2019) and Roger et al. (2015) had highlighted the importance of the frequency of oil droplet collisions in oil exchange rates. This leads to the interest in understanding oil exchange in oil droplets stabilised emulsion (Cheng et al., 2019, 2022a) where primary droplets are homogenised with the second oil phase to form larger secondary oil droplets. In addition, previous studies of the oil exchange process had been carried out on surfactant-stabilised emulsions and their droplets are distant from each other (Lee & Pozzo, 2019; Roger et al., 2015). The oil exchange mechanism of those emulsions may not be directly applicable to droplet-stabilised emulsions with a protein particle layer separating two oil droplets in contact.

In this work, emulsions containing hydrogenated soya-oil of about 600 nm in diameter were prepared by using calcium cross-linked casein particles (Ca-CAS) as emulsifiers. Large droplet size emulsions containing deuterated toluene (*d*-toluene) of about 20  $\mu\text{m}$  in diameter were prepared by Ca-CAS-coated-emulsion stabilisation or by Ca-CAS stabilisation only. The oil exchange process between the droplet (hydrogenated oil) and the large droplet (deuterated oil) was studied in the system of droplet-stabilised emulsion (DSE) where droplet is adsorbed at the large droplet surface, or in a system where primary droplets and large size droplets are simply mixed. Time-resolved contrast-variation ultra-small-angle neutron scattering (CV-USANS) was used to monitor the oil exchange process and identify oil-exchange mechanisms. To extend the probing length from microscale to nanoscale, CV-SANS was also used in the present study.

## 5.2 Materials and methods

### 5.2.1 Materials

Sodium caseinate (Alanate 180: 92.7 % w/w protein, 4.3 % w/w moisture, 0.7 % w/w fat and 0.2 % w/w carbohydrate) was purchased from Fonterra Co-operative Group Ltd. (Auckland, New Zealand). Soya-oil was purchased from Davis Trading Company, Palmerston North, New Zealand. Deuterated toluene (*d*-toluene:  $\text{C}_6\text{D}_5\text{CD}_3$ ) was purchased from Sigma Aldrich (St. Louis, MO, USA). Milli-Q water (Millipore Corp., Bedford, MA, USA) and deuterium oxide ( $\text{D}_2\text{O}$ ) (Sigma Aldrich) were used to prepare emulsion samples for the SANS studies. All chemicals used were of analytical grade and were purchased from Sigma-Aldrich (St. Louis, MO, USA) or BDH Chemicals (BDH Ltd., Pooles, England).

### 5.2.2 Preparation of calcium cross-linked caseinate particle (Ca-CAS)

The method of preparing Ca-CAS was the same as Cheng et al. (2022). In brief, Ca-CAS were formed with 3.0% w/v sodium caseinate and 20 mM  $\text{CaCl}_2$  in Milli-Q water (resistivity

= 18.2 M $\Omega$ .cm) at pH 7.0 at room temperature. The resultant sample contains sodium azide at a final concentration of 0.04 wt% for preservation.

### 5.2.3 Emulsion preparation

#### 5.2.3.1 Primary emulsion

Emulsions with nano-sized droplets were prepared and used as the emulsifying agent for the droplet-stabilised emulsion and termed as primary emulsion. Ca-CAS dispersion (3.00 w/v % protein, 20.00 mM CaCl<sub>2</sub>, pH 7.0) was mixed with soya-oil, giving 30 v/v % soya-oil in the final primary. The mixture was prehomogenized using a handheld Ultra-Turrax (IKA T10 basic, Staufen, Germany) at 30,000 rev min<sup>-1</sup> for 30 s, then passed through a two-stage homogeniser (Homolab 2, FBF Italia, Italy) at pressures of 47 MPa (first stage)/5 MPa (second stage), resulting in a nano-sized primary emulsion. The outlet temperature of the two-stage homogeniser was controlled by using an ice bath to avoid excessive heating during high-pressure homogenisation.

The resultant primary emulsion was subsequently diluted with D<sub>2</sub>O and H<sub>2</sub>O to reach different D<sub>2</sub>O concentrations in the aqueous phase in a range from 12 to 89.5 % v/v D<sub>2</sub>O. The diluted primary emulsion contains 4.2 v/v % hydrogenated soya-oil and 0.3 w/v % proteins. The pH of the diluted primary was adjusted to pH 5.80  $\pm$  0.05 using 2M HCl under mild magnetic stirring.

#### 5.2.3.2 Droplet-stabilised emulsions

The diluted primary containing hydrogenated soya-oil was mixed with *d*-toluene to form droplet-stabilised emulsion (DSE). The final emulsion contains 10 v/v % *d*-toluene, 3.78 v/v % hydrogenated soya-oil, and 0.27 % w/v protein. Homogenisation of the concentrated DSE was

performed using a handheld Ultra-Turrax (IKA T10 basic, Staufen, Germany) at 24,000 rev min<sup>-1</sup> for 2 min. The resultant sample contains sodium azide at a final concentration of 0.04 wt% for preservation.

### 5.2.3.3 Mixed emulsions

Ca-CAS dispersion (3.00 w/v % protein, 20.00 mM CaCl<sub>2</sub>, pH 7.0) was diluted with D<sub>2</sub>O and H<sub>2</sub>O to reach 0.3 w/v % protein, and then mixed with *d*-toluene to form *d*-toluene emulsion. The final *d*-toluene emulsion contains 10 v/v % *d*-toluene and 0.27 % w/v protein. Homogenisation of the DSE was performed using a handheld Ultra-Turrax (IKA T10 basic, Staufen, Germany) at 24,000 rev min<sup>-1</sup> for 2 min. The resultant *d*-toluene emulsion was mixed with diluted primary emulsions at 1:1 volume ratio to obtain the mixed emulsion. Sodium azide at a final concentration of 0.04 wt% was also added for preservation.

### 5.2.4 Microstructure of the droplets

An optical microscope (Zeiss Axio, Jena, Germany) was used to capture the microstructure of the droplet. 40 μL of samples were transfer to a microscope slide with a cavity immediately after preparation. The edges of the cover slip were sealed with nail polish to prevent evaporation. All experiments were carried out at 40× magnifications.

### 5.2.5 Droplet size distributions

Emulsion droplet size were determined by static light scattering using a Malvern MasterSizer 2000 (Malvern Instruments Ltd, Malvern, UK). The refractive index of toluene was 1.49 and that of water (the dispersing medium) was 1.33. The absorbance value of the emulsion droplets was 0.001. Droplet size measurements are reported as the De Broukere mean ( $d_{4,3}$ ). Mean particle diameters were calculated as the average of duplicate measurements.

### 5.2.6 Ultra- small-angle neutron scattering (USANS) and small-angle neutron scattering (SANS)

USANS and SANS experiments were performed on the KOOKABURRA and QUOKKA instruments, respectively, at the OPAL reactor at ANSTO (Sydney, Australia). SANS was used to probe at a  $Q$  range from 0.003 to 0.4  $\text{\AA}^{-1}$ , corresponding to a length scale from  $\sim 6$  up to 628 nm. The  $Q = \frac{4\pi \sin \theta}{\lambda}$  is the magnitude of the scattering vector,  $\lambda$  is the wavelength ( $\text{\AA}$ ), and  $2\theta$  is the scattering angle. USANS was set up in the long-wavelength configuration (4.74  $\text{\AA}$ ), allowing a  $Q$  range of  $\sim 0.00004 - 0.01 \text{\AA}^{-1}$  extending the range of the experimentally measurable length scale from  $\sim 62.8$  nm up to 16  $\mu\text{m}$ .

A set of solvent contrast variation measurements were conducted to characterise the oil-exchange between the *d*-toluene (a neutron SLD corresponding to  $\sim 89\%$   $\text{D}_2\text{O}$  /  $11\%$   $\text{H}_2\text{O}$ ) and the soya-oil (a neutron SLD corresponding to  $\sim 10.4\%$   $\text{D}_2\text{O}$  /  $89.6\%$   $\text{H}_2\text{O}$ ). Emulsions prepared in 5 different solvents, namely, water containing 12%  $\text{D}_2\text{O}$  (contrast matching hydrogenated oil), 40%  $\text{D}_2\text{O}$  (contrast matching the proteins), 89%  $\text{D}_2\text{O}$  (contrast matching the deuterated oil), 60%  $\text{D}_2\text{O}$  and 70%  $\text{D}_2\text{O}$  (contrast matching the fully mixed deuterated and hydrogenated oil) were studied. It was noted that the droplet concentration of the mixed emulsions was half that of the DSE due to 1:1 volume ratio mixing. The droplet concentration of the mixed emulsion and the DSE will be kept consistent by solvent dilution, prior to USANS and SANS measurements.

To prevent emulsion creaming, a multi-position tumbler was used during the collection of the USANS and SANS data. The scattering backgrounds of each contrast were prepared by ultracentrifugation of the corresponding emulsions at 63,000 g at 4  $^\circ\text{C}$  for 60 min followed by 0.1  $\mu\text{m}$  syringe filtration. All the SANS data were collected at room temperature (20  $^\circ\text{C}$ ), and

were reduced according to standard procedures (Kline, 2006) using the Igor Pro software (Wavemetrics, USA) with the respective solvent background subtraction.

### 5.2.7 USANS and SANS data analysis

USANS and SANS data was analysed using power-law model,  $I(Q) \sim Q^\alpha$ , or unified fit model (Beaucage, 1995, 1996). The Guinier scattering representing particle size and the power-law exponent scattering indicating the presence of mass or surface fractals can be obtained from the unified fit model. The unified fit model is expressed as:

$$I(Q) = \sum_{i=1}^n \left[ G_i \exp\left(\frac{-Q^2 R_{gi}^2}{3}\right) + B_i \exp\left(\frac{-Q^2 R_{g(i+1)}^2}{3}\right) \right] \quad (5-1)$$

where  $n$  is the number of structural levels,  $G$  is the Guinier scale factor,  $Q$  is the scattering wave vector,  $R_g$  is the radius of gyration and  $B$  represents the scale factor for power-law scattering. The fits were conducted in the Irena SAS macro (Ilavsky & Jemian, 2009) embedded in Igor Pro (Ilavsky & Jemian, 2009), which can take the smearing conditions for USANS into account by setting the slit-height to  $0.0584 \text{ \AA}^{-1}$  (Yang et al., 2022).

### 5.3 Results and discussion

#### 5.3.1 DSE stability towards coalescence

Emulsions prepared in various D<sub>2</sub>O/H<sub>2</sub>O solutions had similar droplet size distributions and droplet diameters,  $d_{4,3}$ , of  $\sim 20 \mu\text{m}$  as measured by static light scattering (**Figure 5-1**). Oil droplet size distributions of freshly prepared and 72 hours aged DSE in 89% D<sub>2</sub>O were compared to examine the changes in droplet sizes as a function of time. As shown in **Figure 5-1**, the droplet size distribution of fresh DSE prepared in 89% D<sub>2</sub>O overlapped with that of the aged DSE; the  $d_{4,3}$  values for freshly made DSE and aged DSE were similar ( $\sim 20 \mu\text{m}$ ). These results suggested that DSE, where the *d*-toluene was stabilised with Ca-CAS-particle-coated-soya-oil emulsions, was stable against droplet coalescence during 72 h storage.

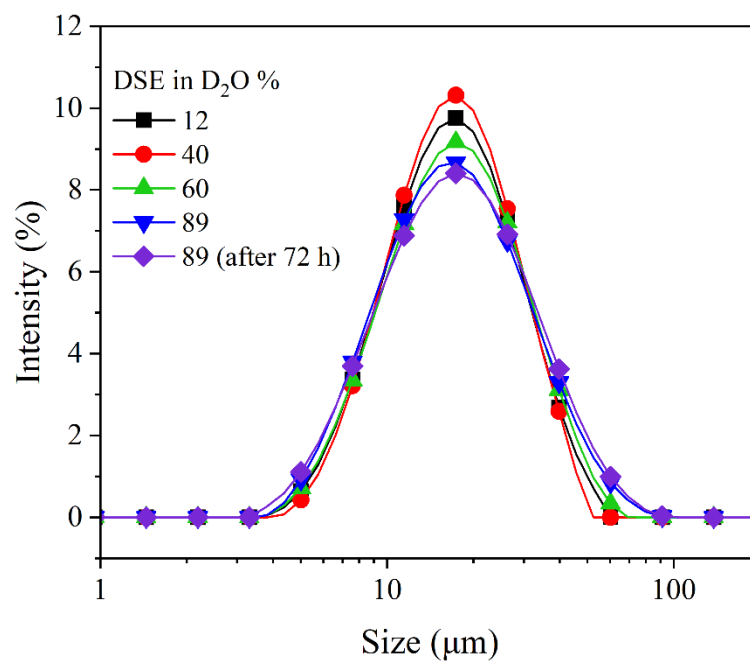


**Figure 5-1:** Droplet size distributions of freshly prepared droplet-stabilised emulsions (DSE) in 12% (—■—), 40% (—●—), 60% (—▲—), and 89% D<sub>2</sub>O (—▼—) and the DSE in 89% D<sub>2</sub>O (—◆—) after 72 hours.



### 5.3.2 Oil exchange in DSE

USANS and SANS scattering curves of DSE in various solvents with different D<sub>2</sub>O/H<sub>2</sub>O ratios are shown in **Figure 5-2a-b**. The scattering intensities of DSE in 12%, 40% and 89% D<sub>2</sub>O solvents were parallel to each other in the entire  $Q$ -range probed by either USANS or SANS. In addition, the DSE showed extremely low scattering intensity in the whole  $Q$  range in 60% D<sub>2</sub>O solvent, suggesting the neutron SLD of DSE was very close to that of the solvent, thus resulting in a significant reduction in scattering intensity. The parallel scattering pattern observed in 12%, 40% and 89% D<sub>2</sub>O implies that DSE may have a similar contrast match point and a similar oil composition at the whole  $Q$ -range since the scattering contrast is composition-dependent. Further, the contrast match points of DSE at different  $Q$  value (corresponding to various sizes) were determined to quantitatively evaluate the oil composition.

Contrast match points at different  $Q$  values were determined by a linearisation method (Heller, 2010; Richards, 2018) where the  $\sqrt{I(Q)}$  is plotted as a function of the volumetric concentration of D<sub>2</sub>O (D<sub>2</sub>O%) in the solvent and the contrast match point is determined at  $\sqrt{I(Q)} = 0$  (**Figure 5-2c**). The contrast match points of DSE obtained at different  $Q$  values were similar (~62.5 % D<sub>2</sub>O), confirming that the oil compositions of DSE at different length scale were similar. In addition, the contrast match point determined here is very close to the SLD of fully mixed *d*-toluene and hydrogenated soya-oil. Theoretically the contrast match point of the DSE scattering when the two oil phases are completely mixed can be calculated as ~ 67 % D<sub>2</sub>O based on the composition of 10 % *d*-toluene (equivalent to 89.3 % D<sub>2</sub>O), 3.78 % soya-oil (equivalent to 10.4 % D<sub>2</sub>O), and 0.27 % casein (equivalent to 40.9 % D<sub>2</sub>O). This finding indicates that the oil mixing in DSE occurred and completed during the emulsion preparation (e.g., homogenization).

To further understand the oil exchange kinetics in the DSE, the time-resolved CV-USANS was applied. In the kinetics experiment, USANS measurements of DSE were performed immediately after sample preparation. As shown in **Figure 5-2d**, the USANS scattering curves collected at different times from 3 min to 2301 min after DES preparations overlapped with each other. There were nearly no changes in scattering profiles with time. The kinetics results confirmed that oil exchange between *d*-toluene and hydrogenated soya oil in DSE was a very rapid process, which could be attributed to the low viscosity of toluene of 0.554 cP (Santos et al., 2006) and intermediate viscosity of soya oil of 5.4 cP (Noureddini et al., 1992). Previous study showed that the whey-protein-coated-solid-tripalmitin-particles-stabilised sunflower oil droplets were able to co-deliver dimethyl phthalate (DMP, encapsulated within sunflower oil droplet) and Sudan III (encapsulated within tripalmitin solid lipid particles), in which DMP had a faster release kinetics than Sudan III (Sakellari et al., 2021). The different release profiles of DMP and Sudan III indicated that they were released from different oil droplets; the solid tripalmitin particles and the core sunflower oil droplet were not homogeneously mixed with each other after homogenisation. The different oil mixing phenomena in low viscosity oil emulsions (the current soya-oil-droplet-stabilised-*d*-toluene emulsion) and the high viscosity oil emulsion (the solid tripalmitin-stabilised-sunflower-oil emulsion) suggested that the extent of oil mixing between the surface primary droplet and the core droplet could be controlled by varying the oil viscosity/molecular structures in the two droplet phases. This topic will be worth studying in the future.

In addition to the oil viscosity, the droplet collision during the ultra-turraxing and the direct contact between soya-oil and *d*-toluene droplets after the DSE formed could be due to other factors affecting the kinetics of oil exchange between the surface droplet and the core droplet. During the homogenisation process, significant oil transport can occur at different length and

time scales as the breakup of the dispersed phase (e.g., *d*-toluene), the adsorption of emulsifiers (e.g., soya oil droplet) to the newly generated oil surface, and the coalescence of droplets before the sufficient interface coverage (Jafari et al., 2008; Kotula & Anna, 2012). The coalescence mechanism could possibly explain the transfer of soya oil from the small droplet to the large *d*-toluene droplet, resulting in a decrease in the neutron contrast of the *d*-toluene droplet.

However, this assumption was not consistent with the experimental results of the current study. A surface fractal dimension value of 3.7 was determined in the  $Q$ -range between  $3.8 \times 10^{-5}$  and  $5 \times 10^{-4} \text{ \AA}^{-1}$  from the scattering curve at different times, suggesting a rough interfacial layer of DSE. A similar rough interfacial layer with a surface fractal dimension value of 3.0 was found in a previous USANS study of the DSE stabilised by whey-protein-microgel-(WPM-) coated-primary-droplets (Cheng et al., 2019). The rough interface of DSE was attributed to the adsorption of Ca-CAS-coated-primary-droplets onto the core droplet, which was confirmed by optical microscopy (**Figure 5-2d, inset**). At longer time, the same surface fractal dimension value of 3.7 for DSE indicating that the adsorbed primary droplet layer at the DSE interface did not coalesce with the core droplet. Combined with the findings from SLS measurements of DSE droplet size distribution, these results suggested that DSE were stable to droplet coalescence not only between DSE droplets but also between adsorbed primary droplets and the core droplet. The exchange of oil between surface oil droplets and core oil droplets did not promote or resulted in the coalescence between them. The fast exchange between the surface and the core oil droplets may occur via pathways other than droplet coalescence.

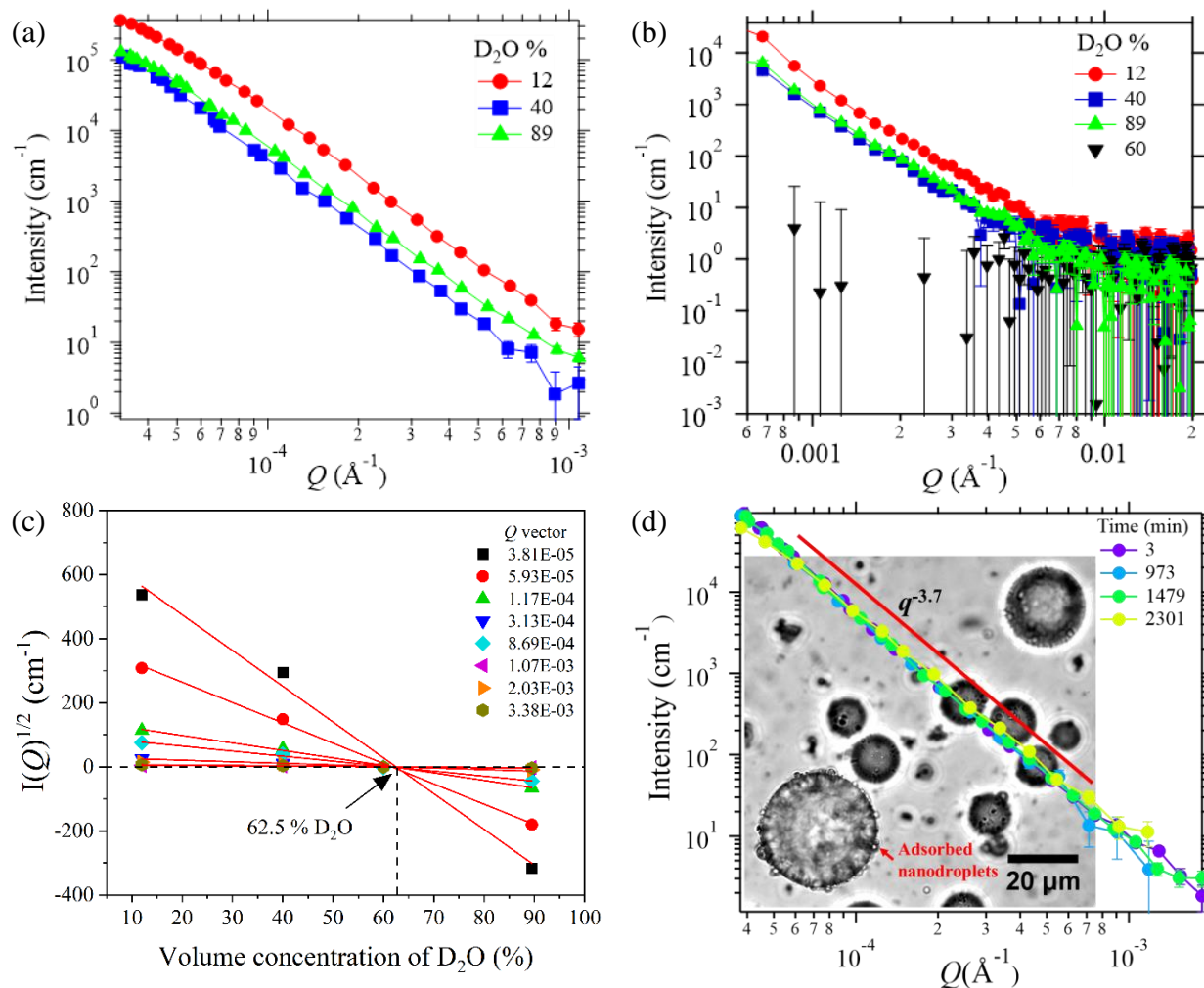


**Figure 5-2:** Scattering curves of the DSE measured by (a) USANS and (b) SANS in the solvent containing 12 % (—●—), 40 % (—■—), 89 % (—▲—), and 60 % (▼) D<sub>2</sub>O. (c) The intensity of DSE at selective  $Q$  as the function of D<sub>2</sub>O concentration; the solid red line represents the linear fit of the intensity value obtained at the fixed  $Q$  and various D<sub>2</sub>O concentration, the arrow guides the calculated contrast matching point (62.5 % D<sub>2</sub>O) of the DSE. (d) USANS kinetic scattering curves of DSE in 89 % D<sub>2</sub>O from 3 – to 2301 min after addition of the *d*-toluene into the aqueous phase, and the solid red line represents the power-law fit; inset is the optical microscopy image of the fresh DSE in 89 % D<sub>2</sub>O.

### 5.3.3 Oil exchange in the mixed emulsion

To further understand the oil exchange process in emulsion systems, two emulsions prepared from the two *d*-toluene /hydrogenated-soya-oils stabilised by the Ca-CAS were used. Since these simply mixed emulsions have a different structure compared to the DSE, different oil exchange kinetics would be expected. The mixed emulsion was similar to DSE in terms of oil composition, oil volume fraction and droplet size distribution, but without the adsorption of droplets onto the surface of *d*-toluene core droplet. As shown in **Figure 5-3a**, both emulsions show monomodal distributions; the hydrogenated-soya-oil emulsion was the primary emulsion used in DSE preparation that had a  $d_{4,3}$  of  $0.68 \pm 0.05 \mu\text{m}$ , while the *d*-toluene emulsion was controlled to a similar droplet size distribution to DSE with a  $d_{4,3}$  of  $16.6 \pm 0.5 \mu\text{m}$ .

Before monitoring the oil exchange process between the soya-oil emulsions and the *d*-toluene emulsion, it was necessary to characterise the structure of the two individual emulsions, as well as the kinetic stability of the *d*-toluene emulsion to exclude the contribution of droplet instability to the changes in scattering curves. A solvent of 70% D<sub>2</sub>O was chosen because its scattering contrast was close to the theoretically calculated contrast match point of the soya oil/toluene mixture (contrast match point ~67% D<sub>2</sub>O) but was significantly different from the scattering contrast of the two individual emulsions.

Scattering curves of the two individual emulsions measured by USANS are shown in **Figure 5-3b**. The scattering curve of soya-oil emulsion showed a Guinier feature at  $Q = 0.0004 \text{ \AA}^{-1}$ , indicating the presence of  $R_g$  of  $0.36 \pm 0.01 \mu\text{m}$ . This size was comparable with the size determined by SLS (**Figure 5-3a**). Due to the large size of the *d*-toluene emulsion, their scattering curves did not show any Guinier features but a steep power-law decay. The power-law exponent is 4.0 in the entire  $Q$  range, indicating a smooth interface of the droplet. This result agrees well with our previous study of emulsion stabilised with Ca-CAS (Cheng et al.,

2022b). It is known that *d*-toluene has certain extent of solubility in water (5.2 g/L at 20 °C); the loss and uptake of *d*-toluene molecules in the droplet due to transport of *d*-toluene molecules through the aqueous phase could result in changes in droplet size distribution and shifts in the scattering profile (Alvarez et al., 2009; Cheng et al., 2019). However, all scattering intensity curves of the pure *d*-toluene emulsion at different times overlapped. This observation suggested that transportation of *d*-toluene molecules via aqueous phase between droplets was very limited (**Figure 5-3b**). The Ca-CAS-layer can prevent *d*-toluene droplets from droplet coalescence and Ostwald ripening at least for 392 min.

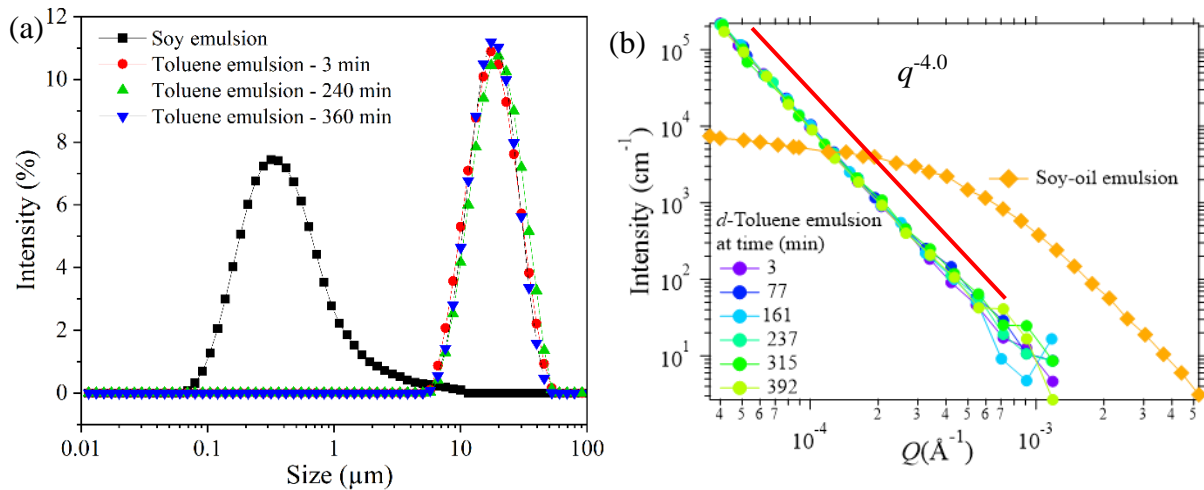


**Figure 5-3:** (a) Droplet size distribution of the Ca-CAS-stabilised soya-oil emulsion ( $\blacksquare$ ) and of the Ca-CAS-stabilised  $d$ -toluene emulsion at 3 min ( $\bullet$ ), 240 min ( $\blacktriangle$ ) and 360 min ( $\blacktriangledown$ ) after preparation. (b) USANS scattering curves of the Ca-CAS-stabilised soya-oil emulsion (diamond symbols) and Ca-CAS-stabilised  $d$ -toluene emulsion (circle symbols) during time from 3 to 392 min after addition of the  $d$ -toluene into the aqueous phase; the solid red line indicates the power-law fit.

To capture any oil-exchanges between two emulsions, the ultra-fast-USANS technique with a scanning time interval of 17 second was used to determine the scattering intensity at a single  $Q$ -vector. **Figure 5-4a** shows the scattered intensities at low  $Q = 9 \times 10^{-5} \text{ \AA}^{-1}$  of two individual emulsions ( $d$ -toluene navy circle and soya-oil red triangle) and the mixture emulsion (two emulsion mixing) (blue squares) for the first 15 min. In this time range, the emulsions of pure  $d$ -toluene and pure soya-oil emulsions showed a constant scattered intensity of 21285 and 5223  $\text{cm}^{-1}$ , respectively (**Figure 5-4a**), which were also verified in the extended time range in **Figure 5-3b**. Upon mixing the two emulsions, the scattering intensity decreased progressively from  $7940 \pm 254$  to  $6198 \pm 225 \text{ cm}^{-1}$  within 500 s and then plateaued around  $6200 \text{ cm}^{-1}$  for the next 400 s (**Figure 5-4a**). This indicated that a rapid mixing of  $d$ -toluene and soya-oil had taken place immediately and slowed down gradually.

Further, a fast scan USANS measurement covering a  $Q$  range from  $3.5 \times 10^{-5}$  to  $9.2 \times 10^{-4}$  was performed to track the kinetics of oil changes up to 493 min. It can be observed that the scattering intensity decreased progressively with time (**Figure 5-4b**). For example, the scattering intensity at  $Q (= 9 \times 10^{-5} \text{ \AA}^{-1})$  was markedly decreased from  $5685 \pm 174$  to  $1297 \pm 52 \text{ cm}^{-1}$  within 255 min before reaching a plateau at  $\sim 1190 \pm 50 \text{ cm}^{-1}$  after 320 min. An exponential decay function (Motulsky & Christopoulos, 2003) was used to fit the decrease of scattering intensity with time:

$$I_t = ae^{-kt} + I_p \quad (5-2)$$

where  $t$  is the time,  $I_t$  represents the intensity at time  $t$ ,  $I_p$  represents the asymptotic value of the plateau intensity,  $a$  represents the span between  $I_p$  and the initial scattering intensity value, and  $k$  is the intensity decay rate coefficient.



The  $k$  of the mixed emulsion at  $Q = 9 \times 10^{-5} \text{ \AA}^{-1}$  was calculated as  $0.0095 \pm 0.0003 \text{ min}^{-1}$  (**Figure 5-4c**), while at high  $Q = 3 \times 10^{-4} \text{ \AA}^{-1}$   $k$  was  $0.0075 \pm 0.0005 \text{ min}^{-1}$  (curve not shown). The different  $k$  values obtained at different  $Q$ -vector could be explained by the droplet size distribution of the mixed emulsion as the intensity is more sensitive to the change in droplet size for the large droplets ( $I(Q) \sim R_g^2$ ) (Alvarez et al., 2009; Cheng et al., 2019).

Further, a steep intensity decay was observed at  $3.8 \times 10^{-5} < Q (\text{ \AA}^{-1}) < 7.2 \times 10^{-5}$ , which was attributed to the surface scattering of the  $d$ -toluene droplet. As the time increased, the power law exponent in the low- $Q$  range gradually decreased from 2.6 to 0.6 within the first 120 min as shown in **Figure 5-4b**. The vanishing of the surface scattering features of the large  $d$ -toluene droplets may be attributed to (1) a reduction in scattering contrast due to the soya oil transferring to the  $d$ -toluene droplets, or (2) the collapse and shrinkage of the  $d$ -toluene droplets to a small size because the  $d$ -toluene molecules transfer from the large droplet to the small soya oil droplet, or (3) a combination of both.

Assumption (2) can be examined by SLS and optical microscope measurements. The freshly prepared mixed emulsion was sealed in glass bottles and droplet size distribution was measured at different times after preparation, as shown in **Figure 5-4d**. After mixing the large  $d$ -toluene droplets and the small soya oil droplets for 1 min, the mixed emulsion showed a bimodal distribution of the large  $d$ -toluene droplets and small soya oil droplets. The lower intensity of the  $d$ -toluene droplets might be the consequence of the evaporation of  $d$ -toluene due to the stirring during the SLS measurement. After mixing two emulsions for more than 10 min, the peak of  $d$ -toluene droplet could not be detected by SLS measurements. Simultaneously, the small size end of the small droplet peak shifted towards the larger size, the size range of the peak became narrower, while the intensity of the summit point became higher. The smallest droplet size increase could be due to the uptake of the  $d$ -toluene molecules by small soya-oil

droplets, while the narrowing of the droplet size distribution narrowed over time was consistent with the Ostwald ripening effect (Schmitt et al., 2004). This result supported the assumption (2) that *d*-toluene molecules transfer from the large droplet to the small soya oil droplet resulting in the shrinkage of the large *d*-toluene droplets and slight growth of the small soya oil droplets. However, the loss of droplet features of *d*-toluene droplet with time was not exactly consistent in the SLS and USANS determinations. This discrepancy may be due to the evaporation of *d*-toluene during the transfer of the sample from the container to the instrument in the SLS determination, whereas in the *in-situ* USANS determination the evaporation of *d*-toluene was restricted.

To visualise the droplet size and morphology at the limited evaporation state, the freshly prepared mixed emulsion was sealed in the cavity microscopic slide. The observation had conducted at the fixed X-Y position and the optimised focus. As shown in **Figure 5-4e-g**, at the well-sealed and resting conditions, both large (marked with a scale bar) and small droplets (marked with a red square) were presented over 120 mins. The change in droplet size of *d*-toluene droplet over time could be due to the loss of *d*-toluene from the large droplet and the creaming effect of the droplets in the sealed cavity slide. This set of results from SLS and optical microscopy results indicated that there was a mass-transport of *d*-toluene from the large droplets to the small soya-oil droplets narrowing the droplet size distribution with time. Therefore, the decay in scattering intensity of the mixed emulsion with time (**Figure 5-4c**) could be attributed to both the mixing of *d*-toluene and soya-oil in droplets and the change in the droplet size distribution.

Regarding assumption (1) and (3), it was difficult to draw a firm conclusion based on the current experimental results. Previous studies on the mixing of two emulsions containing different oils have shown that it is possible for insoluble oils to be transported from one droplet

to the other. Taylor (2003) had suggested that the transfer of the less soluble alkane (C13) from the small droplet to the large droplet containing more soluble alkane (C10) was driven by both the Kelvin effect of the small droplet due to its great surface curvature and the chemical potential differences in different droplets (Taylor, 2003). The greater the curvature of the smaller droplet surface, the amount of bonding that can go on between any one oil molecules on the surface and its neighbours is reduced; as a result, there is a greater probability that oil molecules can escape out of the droplet (Lewis, 2006). Besides, a high Laplace pressure in small droplets, which also known to be affected by the interfacial tension and the droplet radius, will drive the oil molecules out of the smaller droplets into larger ones as well (Bibette et al., 1992). Therefore, the high Laplace pressure or the Kelvin effect arising from the small droplets could drive the transport of the insoluble soya-oil molecules from the small droplet to the large droplet in the current mixed emulsion system. Moreover, Taylor (2003) also suggested that the more soluble oils have a faster diffusion rate than the less soluble oils (Taylor, 2003), which is consistent with other studies using *n*-alkanes of different chain-lengths (Lee & Pozzo, 2019; Moitzi et al., 2007). Thus, the shrinkage of the large *d*-toluene droplets could be the consequence of the rapid transfer of the *d*-toluene molecules from the large to small droplets that had not been mass balanced by the slow transfer of the soya-oil from the small to large droplets. However, the pathway underlying the oil molecules transportation between droplets in the current study could be different from previous studies because of the difference in the type of emulsifiers. In the previous study, the emulsifier was sodium dodecyl sulphate (SDS), which was known to form micelles and bind oil molecules to transport them through the aqueous phase (Lee & Pozzo, 2019; Taylor, 2003).

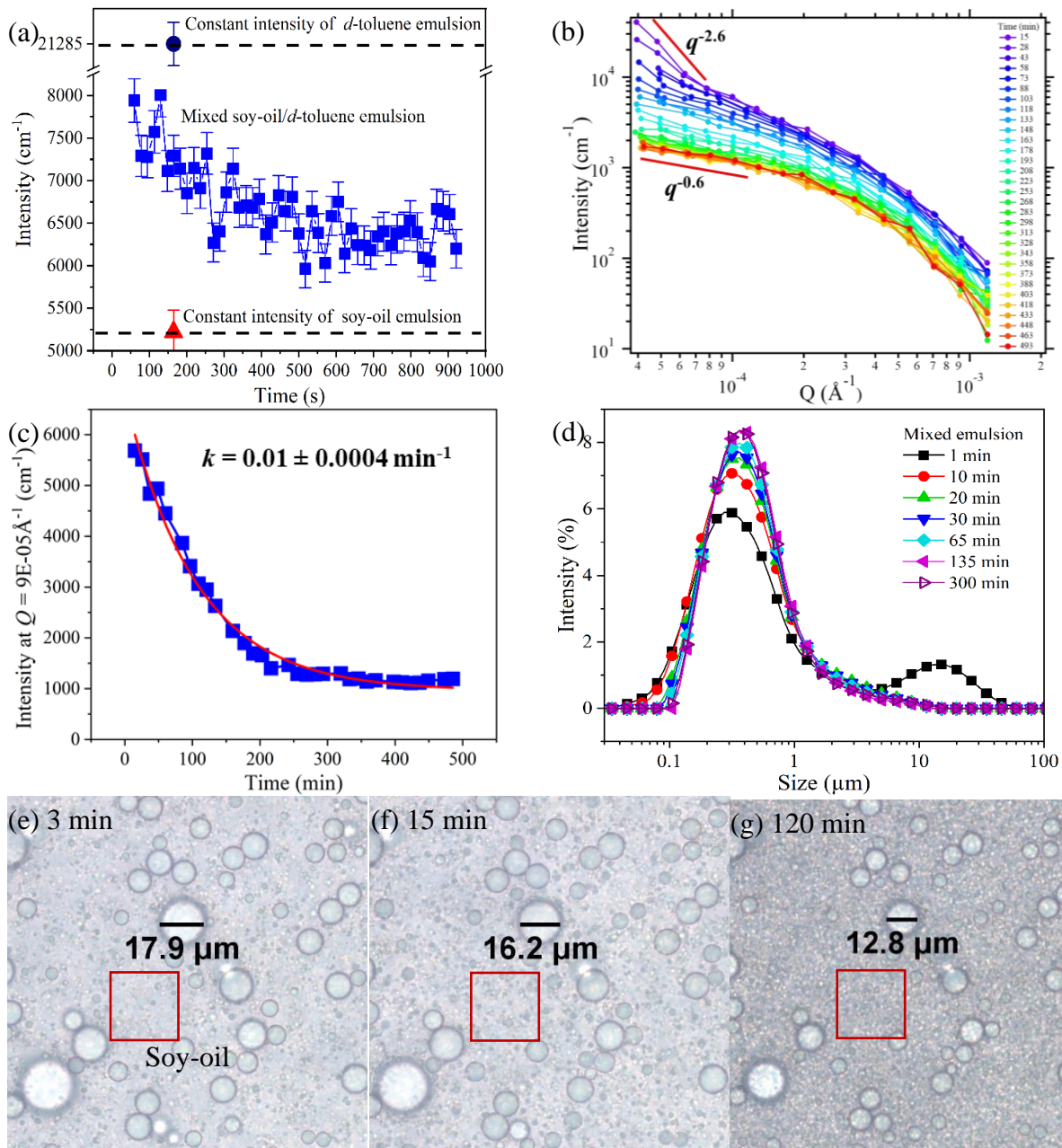


**Figure 5-4:** (a) Intensity at  $Q = 9 \times 10^{-5} \text{ \AA}^{-1}$  of pure *d*-toluene emulsion ( $\bullet$ ), pure soya-oil emulsion ( $\blacktriangle$ ) at 3 min after preparation, and intensity decay curve of the mixed soya-oil/*d*-toluene emulsion ( $\blacksquare$ ) as function of time at  $Q = 9 \times 10^{-5} \text{ \AA}^{-1}$  by USANS single-point method. (b) USANS kinetics scattering curves of the mixed soya-oil/*d*-toluene emulsion ( $\bullet$ ) for 15 – 493 min after mixing two emulsions. (c) the intensity decay curve of the mixed soya-oil/*d*-toluene emulsion ( $\blacksquare$ ) as function of time at  $Q = 9 \times 10^{-5} \text{ \AA}^{-1}$ ; the solid red lines indicate the power-law fit. (d) The droplet size distribution of mixed soya-oil/*d*-toluene emulsion for 1 – 300 min after mixing two emulsions. (e-g) Optical microscopy images of the mixed soya-oil/*d*-toluene emulsion for 3, 15 and 120 min after mixing two emulsions, scale marks the diameter of the selective *d*-toluene droplet, and the red square indicates the presence of soya-oil droplets.

**5.3.4 Possible pathways of oil exchange between droplets**

As discussed in the mixed emulsion system, there might be a mutual exchange of *d*-toluene and soya-oil between two distant droplets. This mutual exchange process was probably driven by the differences in chemical potentials of droplets; the diffusion rate of the oil molecules was being influenced by their solubility in the aqueous phase and the different Laplace pressure of droplets (Lee & Pozzo, 2019; Moitzi et al., 2007; Taylor, 2003). In the present study, in the absence of chemical potential differences between droplets, the Ca-CAS-coated *d*-toluene droplet did not coalesce over time at the expense of small droplets (**Figure 5-3b**). The oil exchange process was only observed in the mixed emulsion containing different oils and required a long time (250 min) to reach equilibrium, despite the relatively high solubility of *d*-toluene in the aqueous phase ( $C_7D_8$ , 5.2 g/L) (**Figure 5-4**). This equilibrium process (250 min) was much longer than that of the less soluble dodecane ( $C_{12}H_{26}/C_{12}D_{26}$ ) by surfactant solubilisation and transportation through aqueous phase (10 min) (Lee & Pozzo, 2019). These phenomena indicate that the pathway allowing the exchange of oil molecules across interfacial protein films was impossible to be due to spontaneous diffusion of oil molecules through the aqueous phase, or due to the solubilisation and transportation by the emulsifiers (proteins or surfactants) (Lee & Pozzo, 2019; McClements et al., 1992, 1993a). It is most likely to be due to collision-induced direct contact between droplets (Roger et al., 2015).

In a previous study of the oil exchange between milk protein stabilised emulsions, McClements et al. (1993) reported that the pathway of oil exchange was the solubilisation and transportation by milk protein molecules (whey protein or sodium caseinate), which is a process of reversible binding of hydrocarbons to protein molecules (either at a specific binding site or by incorporation into micelles), and their subsequent transport between separating droplets through the aqueous phase (McClements et al., 1993a). Our previous study on the

dynamic interfacial tension at the *d*-toluene-water interface also found that when casein was in the sodium caseinate state, there was an exchange of casein molecules between the interface and the aqueous phase (Dickinson, 1992a; Dickinson et al., 1988b); however, when casein was cross-linked by calcium ions, the protein exchange between the interface and the aqueous phase was largely reduced (Cheng et al., 2022). Thus, in emulsions stabilised with a thin layer of protein molecules, oil exchange may occur through protein solubilisation in the presence of excess milk protein in the aqueous phase. However, the exchange of Ca-CAS between the interface and the aqueous phase was found to be limited (Cheng et al., 2022b; Hunt et al., 1993). In the present case of emulsions stabilised with Ca-CAS particles, the solubilisation and transport by Ca-CAS particles was less likely responsible for the oil-exchange. In the same previous study by McClements et al. (1993), they also observed that when the effect of milk protein solubilisation was eliminated by the addition of 2.5 wt% NaCl to form emulsions, oil exchange between droplets was still observed (McClements et al., 1993a). This indicated that oil-molecules can cross the interfacial protein film between two adjacent droplets and this could be the pathway for the observed oil-exchange.

Roger et al. (2005) suggested that primary pathway for oil exchange between droplets was the local synchronous thinning of the interfacial film upon direct contact of droplet collisions, allowing oil molecule to pass through the layer. They had shown that the droplet coarsening rate was slowed down by inducing long-range repulsions and preventing droplet-contact, which suggested that the exchange mechanism is inconsistent with the Ostwald ripening. They also found that the oil exchange process between  $C_{16}H_{34}$  and  $C_{16}D_{34}$  had been completed before droplet size change at an applied high mixing entropy, which confirmed that the oil exchange between droplets was through the direct contact upon droplet collisions. In addition, by varying the chain length of either hydrophilic head ( $C_{12}E_{5-7}$ ) or hydrophobic chain ( $C_{12-16}E_6$ ) of the

surfactant ( $C_iE_j$ ), they found the growth rate of the droplets changed symmetrically with overall chain length of the surfactant. This growth rate was only consistent with the transport rate by the pathway of interfacial layer local thinning which was affected by the increasing both the hydrophobic and the hydrophilic chain length. For the pathway of permeation, the transport rate was determined by only the thickness of hydrophilic layer, and for the pathway of transient hole at the interfacial layer, the transport was weakly affected by the chain length of the surfactant. In the current sample, given the droplet collisions arising from the sample cell tumbling and Brownian motion of primary emulsion, the pathway of droplet direct contact could be responsible for oil molecule exchange between the droplets. Upon contact between two droplets, the chemical potential and the Laplace pressure in different droplet drive the oil molecule across the local thinning layer. The longer equilibrium process of oil exchange in emulsions stabilised by Ca-CAS particles than that in emulsions stabilised by surfactants (Lee & Pozzo, 2019) could be explained by the less local fluctuation of the adsorbed Ca-CAS particles due to their large particle size. However, a better comparison of the exchange rate in emulsion stabilised by different type of emulsifiers needs a control of the oil composition. This aspect requires further studies.

The pathway of interfacial layer local thinning is also relevant to our experimental results in DSE system that the oil exchange equilibrated immediately after preparation. In the DSE system, the primary droplets were in contact with the second oil under high-speed mixing. The protein layer at the primary droplet interface was very likely to experience vigorous interfacial fluctuations and local thinning during shearing as vigorous shear could accelerate the molecule movement (Frank & Evans, 1945). After shearing, the different oils reach a complete mixed state at different length scale of droplets, as supported by the experimental results of the equal scattering contrast match point obtained from different  $Q$ -vector in DSE **Figure 5-2c**.

Therefore, the high mixing entropy during homogenisation, in fact, facilitate the oil transport across the protein layer. In addition, this vigorous mixing also increased the contact between the *d*-toluene and air leading to an evaporation of *d*-toluene. As shown in **Figure 5-5**, the experimental contrast matching point of DSE corresponds to 7.6 % *d*-toluene in the system, which was less than the initial added 10 % *d*-toluene. The loss of the *d*-toluene probably be the consequence of the evaporation of *d*-toluene during homogenisation process.



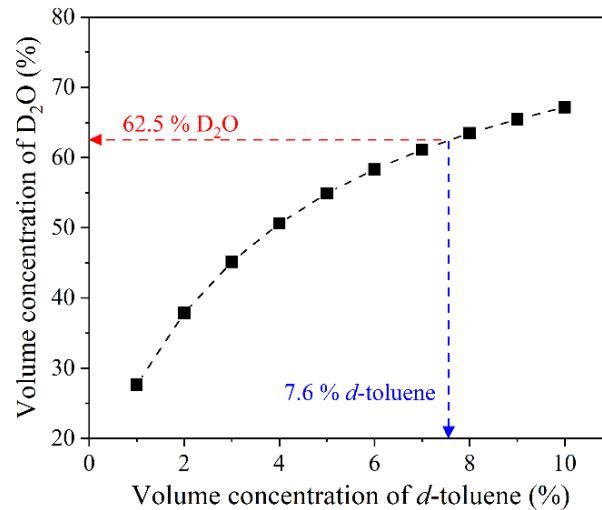


**Figure 5-5:** Theoretical calculated corresponding D<sub>2</sub>O volume concentration (%) used for contrast matching of DSE is plotted as a function of varying the volume concentration *d*-toluene (%) in DSE. The maximum volume concentration *d*-toluene (%) in DSE is the volume of *d*-toluene added into the emulsion prior to homogenisation. The horizontal red line indicates the experimentally determined contrast matching point of DSE after homogenisation, and the vertical blue line indicates the calculated volume concentration *d*-toluene (%) in DSE after homogenisation.

After the homogenisation process was completed, the fluctuation of protein films between the adsorbed primary droplet and the core droplets could be reduced as assuming the protein film was entrapped within the hierarchical DSE structure. Additionally, the chemical gradients arising from the oil composition were removed as either the primary droplet adsorbed at the interface or the core droplet of DSE containing the fully mixed oils. Therefore, the DSE structure destabilisation (the primary droplet coalescence into the core droplet) derived from the different Laplace pressure between adsorbed primary droplet and the core droplet will be expected to be a slow process.

### 5.4 Conclusions

In this study, we demonstrated that the time-resolved contrast variation USANS and SANS are powerful non-invasive tools in characterizing the droplet structure and monitoring the oil transfer between droplets. The homogenisation process in preparing the droplet-stabilised emulsion induced a rapid oil transfer/exchange between droplets, resulting in a homogenous mixed oil distributed at different length scale in the hierarchical emulsion. In an emulsion by simply mixing the droplet and large size droplet without external vigorous agitation, the collision between droplets was responsible for the oil transfer between droplets through inducing local synchronous interfacial thinning upon droplet contact. The oil transfer direction and rate were affected by the oil molecule chain-length, the shorter chain-length the faster transfer, resulting in the change of the droplet size distribution over time. In comparison to emulsion containing short-chain length oil stabilised by surfactant (Lee & Pozzo, 2019; Roger et al., 2015), the calcium-cross-linked casein particles appeared to slow down the oil exchange process. It will be interesting to extend this research to other emulsions stabilized by rigid particles or emulsions containing viscous oils, where oil mixing induced by the vigorous shearing during homogenisation and droplet collision may be hindered. This knowledge will

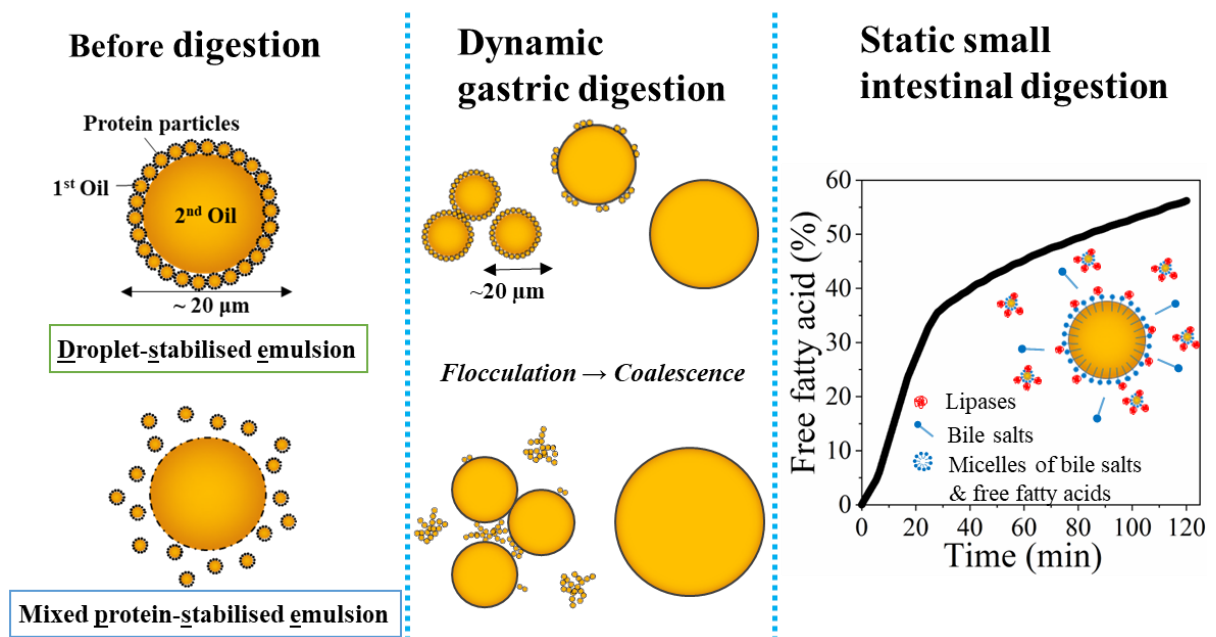
bring an array of new possibilities for different needs, such as the emulsions being used as delivery systems, the location of active compound in a hierarchical emulsion can be controlled by stopping or improving the transfer.

### **5.5 Acknowledgements**

This work was funded by the Riddet Institute, a National Centre of Research Excellence (CoRE), funded by the New Zealand Tertiary Education Commission. We acknowledge the grants and the support of the Australian Nuclear Science and Technology Organization, Australia, for access to the small-angle X-ray scattering (Bruker) and small-angle neutron scattering (QUOKKA) facilities under proposal P8623. We also thank the Manawatu Microscopy and Imaging Centre at Massey University for technical support.

## Chapter 6 Modification of the interfacial structure of droplet-stabilised emulsions during *in vitro* dynamic gastric digestion: impact on *in vitro* intestinal lipid digestion

### Graphic abstract



### Abstract

The *in-vitro* digestion behaviour of an oil-in-water emulsion with an interface consisting of nano-sized droplets coated with caseinate particles, referred to as a droplet-stabilised emulsion (DSE), was explored using the Human Gastric Simulator. A caseinate-particle-stabilised emulsion (PSE) was used as a control, with a similar droplet size distribution and the same composition as the DSE. The nanodroplet-stabilised interface of the DSE was preserved during the first 180 min of gastric digestion. During 240 min, the droplet sizes of the DSE and the PSE increased from  $22.71 \pm 1.14$  to  $63.34 \pm 6.57 \mu\text{m}$  and from  $17.98 \pm 1.16$  to  $85.11 \pm 9.35 \mu\text{m}$  respectively. The small droplet size of the DSE that was released from the gastric phase

contributed to slightly higher total free fatty acid (FFA) release ( $56.18 \pm 3.55\%$ ) than that from the PSE ( $49.4 \pm 2.67\%$ ). The FFA release rate of the DSE ( $1.21\% \text{ min}^{-1}$ ) was greater than that of the PSE ( $1.06\% \text{ min}^{-1}$ ) during the first 30 min of small intestinal digestion; similar FFA release rates ( $0.5 \mu\text{mol s}^{-1} \text{ m}^{-2} \times 10^{-4}$ ) were obtained for both emulsions beyond 30 min of digestion. This study provides new information on lipid digestion using a novel interfacial layer that was stabilised with nanodroplets.

### 6.1 Introduction

Lipids are an essential nutrient in the human diet as they are a source of energy and help to improve the lubricity, palatability and taste of food; however, excessive lipid intake is associated with an increased risk of certain chronic diseases, such as obesity, heart disease and hypertension (Blundell & Macdiarmid, 1997; Daniels & Greer, 2008). For people with digestive disorders, who have difficulty obtaining adequate calories or essential fat-soluble nutrients, e.g. vitamins A, D, E and K,  $\omega$ -3 fatty acids, carotenoids and phytosterols, better lipid digestion and absorption from the diet are needed (Bauer et al., 2005; Favé et al., 2004; McClements et al., 2007; Pafumi et al., 2002). In contrast, in some cases, e.g. humans who are at risk of cardiovascular disease, it is necessary to decrease the absorption of specific food lipids (Bauer et al., 2005; Favé et al., 2004).

In most processed foods, such as coffee whiteners, whipped toppings, soups, dressings, liquid nutritional products and medical foods, lipids are present in the form of emulsions. There has been considerable research on lipid digestion in emulsion systems. The digestibility of lipids has been found to be affected by several factors, including the type of emulsifier, the size of the lipid droplets and the type and structure of the triacylglycerols. The droplet size and the nature of the droplet interfacial layer have been highlighted in the control of lipid digestion (Golding & Wooster, 2010; McClements et al., 2009; Mun et al., 2007; Salvia-Trujillo et al.,

2013; Singh et al., 2009). It has been reported that the amount of free fatty acids (FFAs) released per unit of time is inversely related to the mean oil droplet diameter, which is attributed to the larger surface area available to lipid digestion in smaller sized emulsions droplets (Borel et al., 1994; McClements & Li, 2010b; Salvia-Trujillo et al., 2013). However, this influence of droplet size can be altered by the nature of the emulsifier and its structure at the oil-water interface. A faster rate of FFA release was obtained for conventional emulsions (200 nm droplet diameter size) than for a nanoemulsion (60 nm droplet diameter size) stabilised by  $\beta$ -lactoglobulin; this was attributed to the compact structure of the  $\beta$ -lactoglobulin layer at the nanodroplet interface after emulsion preparation by solvent evaporation (McClements & Li, 2010b). This study emphasises the importance of the structure of the interfacial layer in controlling the digestion of lipids in emulsion systems.

The design of novel interfaces to enhance the functionalities of emulsions, including digestion and the delivery of lipophilic compounds, is a challenge. More and more interfacial structures are being developed using Pickering emulsion technologies, such as emulsions stabilised with protein particles (soy protein nanoparticles, nanocrystals, modified starch, whey protein microgels etc.), rather than traditional inorganic or synthetic particles (Lin et al., 2018; Murray & Phisarnchananan, 2016; Sarkar et al., 2016a; Zhao et al., 2021a), for example, multilayer interfaces made of a mixture of proteins and polysaccharides (Wei et al., 2021) or protein-polysaccharide (Ding et al., 2021; Guzey & McClements, 2006; Mun et al., 2005; Wang et al., 2020b) and soft nanodroplet-stabilised emulsions (Chen et al., 2017; Cheng et al., 2019; Okubanjo et al., 2019, 2021; Ye et al., 2013b). Based on the *in vitro* digestion investigation, some structured interfaces have reduced the rate and extent of lipolysis in the intestinal tract (Ding et al., 2021; Guzey & McClements, 2006; Mun et al., 2005; Wang et al., 2020b; Wei et al., 2021). For example, recent work on Pickering emulsions showed that the

interfacial layers of emulsions that were stabilised by enzymatically modified soy protein particles (Zhao et al., 2021a) or whey protein microgels (Sarkar et al., 2016a) reduced the degree of lipolysis during *in vitro* small intestinal digestion because the protein-particle-laden interface resisted the displacement of bile salts. The bioavailability of lipids from multilayer emulsions is decreased because the thick and impermeable interfacial layer of biopolymers (proteins and polysaccharides) is resistant to enzymatic degradation (Mun et al., 2007; Wei et al., 2021). However, the effect of a droplet-stabilised emulsion with a structured interface on the droplet stability and the lipid digestion during gastrointestinal digestion of the emulsion has not yet been investigated. The thick nanodroplet interface may improve the lipid digestion in the intestinal tract by reducing the coalescence of emulsion droplets during gastric digestion and transporting enzymatically degradable and small-sized emulsion droplets for intestinal digestion.

The present study investigated the structural stability of a droplet-stabilised emulsion (DSE) during gastric digestion and the kinetics of FFA release during intestinal digestion. The dynamic human gastric simulator (HGS) model was used for gastric digestion, and a pH-stat model was used for intestinal digestion. A protein-stabilised conventional emulsion (PSE) with a similar droplet size distribution to the DSE was used as a control.

## 6.2 Materials and methods

### 6.2.1 Materials

Sodium caseinate (#A180: 92.7 wt% protein, 4.3 wt% moisture, 0.7 wt% fat and 0.2 wt% carbohydrates) was purchased from Fonterra Co-operative Group Ltd., Auckland, New Zealand. Soybean oil was purchased from Davis Trading Company, Palmerston North, New Zealand. Pepsin from porcine gastric mucosa (#P7000: 625 U mg solid<sup>-1</sup>), pancreatin from porcine pancreas (#P7545: 8 × UPS, trypsin of 5 U mg<sup>-1</sup> and lipase of 150 U mg solid<sup>-1</sup>) and

bile extract porcine (#B8631) were purchased from Sigma Aldrich (St. Louis, MO, USA). Milli-Q water (Millipore Corp., Bedford, MA, USA) was used in all experiments. All chemicals used in this study were of analytical grade and were purchased from Sigma Chemical Co. (St. Louis, MO, USA) or BDH Chemicals (BDH Ltd., Poole, England) unless otherwise specified.

The electrolytes of the simulated gastric fluid (SGF) and the simulated intestinal fluid (SIF) are listed in SM Table 1; they were prepared according to the formulation described by Brodkorb et al. (Brodkorb et al., 2019), with a slight modification. This study used the pH-stat approach with a not-fully-sealed vessel to simulate the small intestinal digestion. Carbon dioxide ( $\text{CO}_2$ ) will release from sodium bicarbonate ( $\text{NaHCO}_3$ ) and the pH will progressively increase with time. Hence,  $\text{NaHCO}_3$  in the SIF was replaced with  $\text{NaCl}$  at the same molar ratio to maintain the ionic strength of the SIF. In addition,  $\text{CaCl}_2$  was added just before use. The stock simulated electrolyte fluids at a concentration of 1.25 times ( $1.25\times$ ) were prepared by diluting the stock salt solutions with Milli-Q water and 6 M  $\text{HCl}/\text{NaOH}$ . The pHs of the stock SGF ( $1.25\times$ ) and the stock SIF ( $1.25\times$ ) was set to 2.0 and 7.0 respectively. The stock simulated electrolyte fluids ( $1.25\times$ ) were stored at 4 °C, warmed to room temperature in a 37 °C water bath before use and used within 1 month after preparation. Before use, the stock simulated electrolyte fluids ( $1.25\times$ ) were mixed with enzyme dispersions, resulting in a  $1.0\times$  concentration of the working digestion fluid. The formulations of the enzyme dispersions are given in Sections 2.2.3 and 2.2.6 for digestion in the stomach and digestion in the small intestine, respectively.

### **6.2.2 Preparation of calcium caseinate (Ca-CAS) particles**

Sodium caseinate dispersion was prepared by dissolving sodium caseinate powder in Milli-Q water (18.2 M $\Omega$  cm) at 50 °C and stirring for 2 h, followed by overnight storage at room



temperature to ensure complete hydration. Ca-CAS particles containing 3 wt% protein and 20 mM CaCl<sub>2</sub> were prepared by adding an appropriate amount of stock CaCl<sub>2</sub> solution (1 M) dropwise into the sodium caseinate dispersion (3.1 wt% protein) under mild stirring. The calcium–casein reaction was equilibrated for 30 min under mild stirring. The pH of the Ca-CAS dispersions was adjusted to  $7.00 \pm 0.02$  by 2 M NaOH. Following mixing for 1 h, the dispersions were stored at room temperature overnight to ensure complete equilibration.

Ca-CAS dispersions containing lower protein content were obtained by diluting Ca-CAS dispersions containing 3 wt% protein and 20 mM CaCl<sub>2</sub> with Milli-Q water; they were used to prepare the conventional PSEs with small droplet size and large droplet size.

### 6.2.3 Emulsion preparation

#### 6.2.3.1 DSE preparation

Ca-CAS particle dispersion (3.00 wt% protein, 20.00 mM CaCl<sub>2</sub>, pH 7.0) was mixed with soybean oil to give 20 wt% soybean oil in the primary emulsion. Mixtures were pre-homogenised using a handheld Ultra-Turrax (IKA T10 basic, Staufen, Germany) at 30,000 rev min<sup>-1</sup> for 30 s, followed by a two-stage homogenisation (Homolab 2, FBF Italia, Italy) at pressures of 47 MPa (first stage)/5 MPa (second stage) with six passes, resulting in a primary emulsion with small size. The outlet temperature was controlled at about 32 °C by using an ice bath to avoid the heating from the high-pressure homogenisation. Subsequently, the primary emulsion was diluted 6.25 times with Milli-Q water, and the pH was adjusted to 5.6 with 2 M HCl under mild magnetic stirring. The diluted primary emulsion contained 0.38 wt% protein, 2.56 mM CaCl<sub>2</sub> and 3.20 wt% soybean oil.

The diluted primary emulsion was used as the aqueous phase to mix with the second oil phase (soybean oil) in a weight ratio of 80:20 to produce the DSE, giving 0.31 wt% protein,

2.05 mM CaCl<sub>2</sub> and 22.56 wt% soybean oil in the final DSE. Homogenisation of the DSE was performed using a handheld Ultra-Turrax (IKA T10 basic, Staufen, Germany) at 30,000 rev min<sup>-1</sup> for 5 min. Sodium azide was added at a final concentration of 0.02 wt% as a preservative.

### 6.2.3.2 Conventional PSE preparations

Conventional PSEs with small and large droplet sizes were prepared separately and were then mixed to obtain a droplet size distribution similar to that of the DSE.

The large PSE was prepared by homogenising an appropriate amount of soybean oil with Ca-CAS dispersion of 0.34 wt% protein and 2.28 mM CaCl<sub>2</sub> at pH 7.0 using an Ultra-Turrax (IKA T10 basic, Staufen, Germany) at 30,000 rev min<sup>-1</sup> for 5 min. The final large PSE contained 0.20 wt% protein, 1.37 mM CaCl<sub>2</sub> and 40.00 wt% soybean oil.

The small PSE was prepared by homogenising an appropriate amount of soybean oil with Ca-CAS dispersion of 2.00 wt% protein and 13.33 mM CaCl<sub>2</sub> at pH 7.0 using a two-stage homogenisation (Homolab 2, FBF Italia, Italy) at pressures of 47 MPa (first stage)/5 MPa (second stage) with six passes, giving 20.00 wt% soybean oil in the small PSE. Before passing through the two-stage homogeniser, the soybean oil and the Ca-CAS dispersion were pre-homogenised using a handheld Ultra-Turrax (IKA T10 basic, Staufen, Germany) at 30,000 rev min<sup>-1</sup> for 30 s. Subsequently, the small PSE was diluted 3.91 times with Milli-Q water, and the pH was adjusted to 5.6 with 2 M HCl under mild magnetic stirring. The diluted small PSE contained 0.41 wt% protein, 2.73 mM CaCl<sub>2</sub> and 5.12 wt% soybean oil.

The large and small PSEs were mixed at a volume ratio of 1:1. The final mixed PSE contained 0.31 wt% protein, 2.05 mM CaCl<sub>2</sub> and 22.56 wt% soybean oil, the same composition as the DSE. Sodium azide was added at a final concentration of 0.02 wt% as a preservative.

**6.2.4 Dynamic *in vitro* gastric digestion**

A dynamic HGS, designed by (Kong & Singh, 2010), was used for *in vitro* gastric digestion. The digestion procedure was based on the method described previously by (Ye et al., 2016) with some modifications. In brief, a 200 g sample was prewarmed in a water bath at 37 °C and fed into the HGS for 4 h of digestion by mixing with SGF and pepsin solution (**Figure S 6-1**). A 4× concentrated enzyme dispersion containing pepsin (10000 U mL<sup>-1</sup>) and CaCl<sub>2</sub> (0.75 mM) was prepared using Milli-Q water. The stock SGF (1.25×) and the enzyme solution were added in separately using two pumps during the simulated gastric digestion; the injection rates were 2 mL min<sup>-1</sup> for the stock SGF and 0.5 mL min<sup>-1</sup> for the enzyme dispersion, resulting in a final 1.0× concentrated electrolyte (as shown in SM Table 1) with 2000 U mL<sup>-1</sup> of pepsin and a 0.15 mM CaCl<sub>2</sub> working digestive fluid. The temperature of the HGS was set and maintained at 37 °C by a heater during digestion. The gastric contraction frequency was 3 times min<sup>-1</sup>, to simulate stomach contractions (Marciani et al., 2001).

For further analyses, digesta were collected from the bottom of the HGS (SM Fig. 1) at 20 min intervals during 4 hours of gastric digestion for mimicking the human gastric emptying from the gastric compartment to the small intestine compartment. At each time point, 66 mL of digesta was removed from the bottom of the stomach chamber, equalling a gastric emptying rate of 3.3 mL min<sup>-1</sup>. The remaining sample in the simulative gastric chamber was defined as gastric chyme. Gastric digestion experiments of 5 min, 20 min, 1 h, 2 h and 3 h were performed to collect gastric chyme for further analyses. At the set time points, gastric digestion was stopped, and gastric chyme was collected from the bottom of the HGS after taking out the gastric digesta. For the 5 min gastric digestion, 16.5 mL of gastric digesta (= 5 min x emptying rate) was collected firstly; the remaining sample was fully emptied from the bottom of HGS subsequently as the gastric chyme. In the other short-duration experiments (≥ 20 min), gastric

digesta was removed every 20 min with a volume of 66 mL; the remained sample at the given time points was the gastric chyme and being fully emptied from the bottom of HGS.

Immediately after emptying from the HGS, the pH of the emptied gastric digesta was adjusted to 7.0 using 2 M NaOH to inhibit pepsin activity, followed by storage of part of the sample in an ice bath and the remaining part in a  $-80\text{ }^{\circ}\text{C}$  freezer for short-term and long-term storage, respectively.

### 6.2.5 pH measurement

The initial pH in the HGS refers to the pH of the freshly prepared emulsions. As access into the HGS was prevented by the simulated gastric contraction (roller movement), the pH in the HGS at different times was assumed to be that of the emptied digesta.

### 6.2.6 Measurement of oil content

Emptied digesta samples were collected at selected time points during gastric digestion to determine their crude oil content. The gastric digestion was terminated by increasing the pH to above 7.0 using 1 M NaOH. The total oil contents of the initial emulsion and the emptied digesta were measured using the Mojonnier ether extraction method, as prescribed for dairy products (AACC 30–10) and as previously described by Wang et al. (Wang et al., 2019). The oil content was reported as grams of oil per 100 millilitres of digesta.

### 6.2.7 *In vitro* intestinal digestion

Portions (5 mL) of each gastric digesta sample (pH 7.0) collected at each 20 min interval (total of 12 time points) were mixed well, and 50 mL of the gastric digesta mixture was used for the subsequent *in vitro* small intestinal digestion. Small intestinal digestive fluid, consisting of four parts of 1.25× concentrated SIF (SM Table 1) and one part of bile extract solution containing pancreatin and  $\text{CaCl}_2$ , was added to this 50 mL of gastric digestion mixture at a

volume ratio of 1:1. The concentrations of bile extract, pancreatin and  $\text{CaCl}_2$  in the total digesta were  $12.5 \text{ mg mL}^{-1}$  (30.6 mM),  $100 \text{ U mL}^{-1}$  of trypsin activity (including  $\sim 3000 \text{ U mL}^{-1}$  of lipase activity) and 0.3 mM, respectively. The small intestinal digestion was conducted for 2 h at pH 7.00 and  $37 \text{ }^\circ\text{C}$  using a pH-stat (TitraLab 856; Radiometer Analytical, Villeurbanne, France) according to the method described in Wang et al. (Wang et al., 2019). The volume of 0.05 M NaOH used to neutralise the FFAs released during the lipid hydrolysis was recorded.

### 6.2.8 Static light scattering

Static light scattering (MasterSizer Hydro 2000, Malvern Instruments Ltd, Malvern, Worcestershire, UK) was used to determine the average diameters of the emulsion droplets. The refractive indices of the aqueous phase and the dispersion phase (soybean oil) were set to 1.33 and 1.47 respectively. Measurements were performed at room temperature and were repeated three times for each sample. Average droplet sizes were reported as the Sauter mean diameters ( $d_{32}$ ) and as the De Broukere mean diameters ( $d_{4,3}$ ).

### 6.2.9 Confocal laser scanning microscopy (CLSM)

The microstructures of the samples and the gastric and intestinal digesta were examined using a confocal microscope (Leica, Heidelberg, Germany) equipped with a  $40\times$  oil immersion lens. The samples for microscopic examination were not pre-treated (i.e., heating or pH adjustment); they were placed into an ice bath to minimise the enzymatic action temporarily before analysis. The imaging was completed within 5 min after the sample removed from the ice bath. The fluorescent dyes Nile Red and Fast Green were dissolved in acetone ( $1 \text{ mg mL}^{-1}$ ) and Milli-Q water ( $10 \text{ mg mL}^{-1}$ ) respectively. Aliquots of  $3 \mu\text{L}$  of Nile Red and  $3 \mu\text{L}$  of Fast Green were added to  $50 \mu\text{L}$  of digesta. Then,  $44 \mu\text{L}$  of 5 wt% agarose solution was mixed with the digesta at a final 1:1 (v/v) ratio for sample fixing. Nile Red was excited by an argon laser at 488 nm and the emitted fluorescence between 494 and 605 nm was measured. Fast Green

was excited by a helium-neon laser at 633 nm and the emission between 638 and 750 nm was measured. To enhance image quality, sequential scanning was used. Images were captured with LAS AF software (version 2.7.3.9723) at room temperature. They were analysed using ImageJ software (ImageJ, National Institutes of Health, Bethesda, MD, USA).

### 6.2.10 Kinetics of lipolysis

The percentage of FFAs released per gram of oil from the small intestinal digesta mixture was calculated according to **equation (6-1)**:

$$total\ FFAs\ released\ (\%) = \frac{V_{NaOH}(t) \times C_{NaOH} \times m_w\ lipid}{2m_{lipid}} \times 100 \quad (6-1)$$

where  $V_{NaOH}(t)$  is the volume of NaOH added into the reaction mixture at digestion time  $t$ ,  $C_{NaOH}$  is the molar concentration of the NaOH solution (0.05 M) used,  $m_w\ lipid$  is the average molecular weight of the lipid (881 g mol<sup>-1</sup>) and  $m_{lipid}$  is the total mass of oil in the reaction mixture. The volume of NaOH titrated into the small intestinal digestive fluid without sample was subtracted as a background.

The kinetic parameters for the initial FFA release were calculated using **equations (6-2)** and **(6-3)** (Ye et al., 2013a):

$$\varphi(t) = \varphi_{Max} (1 - \exp(-k_1 t)) \quad (6-2)$$

where  $t$  is the intestinal digestion time (min),  $\varphi_{Max}$  is the maximum total FFA level (%) and  $k_1$  (s<sup>-1</sup>) is the first-order rate constant of FFA release (%FFA min<sup>-1</sup>), which can be calculated as

$$k_1 = 6M_w k / (d_0 \rho_0) \quad (6-3)$$

where  $M_w$  is the molecular weight of lipid,  $d_0$  is the initial average diameter of the emulsion ( $d_{4,3}$ ),  $\rho_0$  is the density of the lipid and  $k$  (mol s<sup>-1</sup> m<sup>-2</sup>) is the lipid conversion rate per unit area

of the droplet surface, occurring at maximum lipase surface coverage  $\Gamma^{Max}$  (typically  $2.66 \times 10^{-7} \text{ mol m}^{-2}$ ) (Pignol et al., 2000).

**Equations (6-2)** and **(6-3)** were used as mathematical models to give the best fits to the experimental data.

### 6.2.11 Statistical analysis

Each experiment was performed at least three times using freshly prepared samples. The results are reported as the calculated means and standard deviations. A one-way analysis and independent sample T-test of variance were used to compare samples in the SPSS 19.0 package (IBM, Armonk, NY, USA). The significant difference was at a *P*-level of 0.05.

## 6.3 Results and discussion

### 6.3.1 Size and microstructure of emulsions before digestion

The droplet size and the microstructure of the DSE and the PSE before digestion were characterised by static light scattering and CLSM, respectively, as shown in **Figure 6-1**. **Figure 6-1A** shows the size distributions of emulsions including the small-sized emulsion, the large emulsion (for PSE only) and the final DSE and PSE. The individual droplet size distribution was obtained by mixing emulsions with 2 wt% sodium dodecyl sulphate (SDS) solution at volume ratio of 1:4 before the static light scattering measurements. It has been suggested that SDS is capable of disrupting hydrophobic interactions and displacing protein molecules/protein-coated droplets from the oil–water interface (Cheng et al., 2019; Dickinson & Ritzoulis, 2000; Mackie et al., 2000). Due to insufficient signal of protein particles with SDS addition during static light scattering measurement, the independent size of protein particles with SDS was not available.

As shown in **Figure 6-1A**, the droplet size of the small-sized emulsion was between  $\sim 0.03$ – $5 \mu\text{m}$ , and the large-sized emulsion was at  $\sim 20 \mu\text{m}$ . As expected, the bimodal size distribution of PSE had two prominent peaks, which corresponded to the independent droplet distribution of the small- and large-sized emulsions. The droplet size distribution of PSE overlapped with the one with SDS, suggesting that all droplets dispersed separately in PSE without flocculation or aggregation.

Bimodal size distribution of DSE with two prominent peaks was also observed, corresponding to the size distributions of nanoemulsion and the core droplets (**Figure 6-1A**). The peak area of nano-sized droplets in DSE with the absence of SDS is small, probably attributed to the adsorption of most nanodroplets at the interfaces of the core droplets. The peak area of the nano-sized droplets in the DSE increased in the presence of SDS compared with in



its absence (**Figure 6-1A**). In the presence of SDS, the droplet size distributions of the DSE and the PSE largely overlapped, and the average sizes ( $d_{4,3}$ ) were almost identical:  $16.91 \pm 1.39$  and  $17.01 \pm 1.03 \mu\text{m}$  for the DSE and the PSE respectively. These results confirm that the small droplets adsorbed at the interface stabilised the large (core) droplets in the DSE, whereas the large and small droplets in the PSE dispersed separately.

The morphologies of the droplets in the DSE and the PSE were observed using CLSM. The confocal images (**Figure 6-1A** and **1C**) clearly show that nanodroplets stabilised the large oil droplets in the DSE as a thick dense layer; this was different from the conventional emulsion stabilised by a thin layer of protein particles (PSE). In the PSE, no nano-sized droplets had adsorbed at the interface of the large oil droplets; they were well dispersed in the aqueous phase. The weak signal of oil (in red) from the nano-sized droplets in PSE is attributed to the

Thus, the DSE and the PSE had similar droplet size distributions but different interfacial structures, which meant that the effect of the interfacial structure on the stability of the emulsion and lipid degradation during *in vitro* digestion could be investigated.

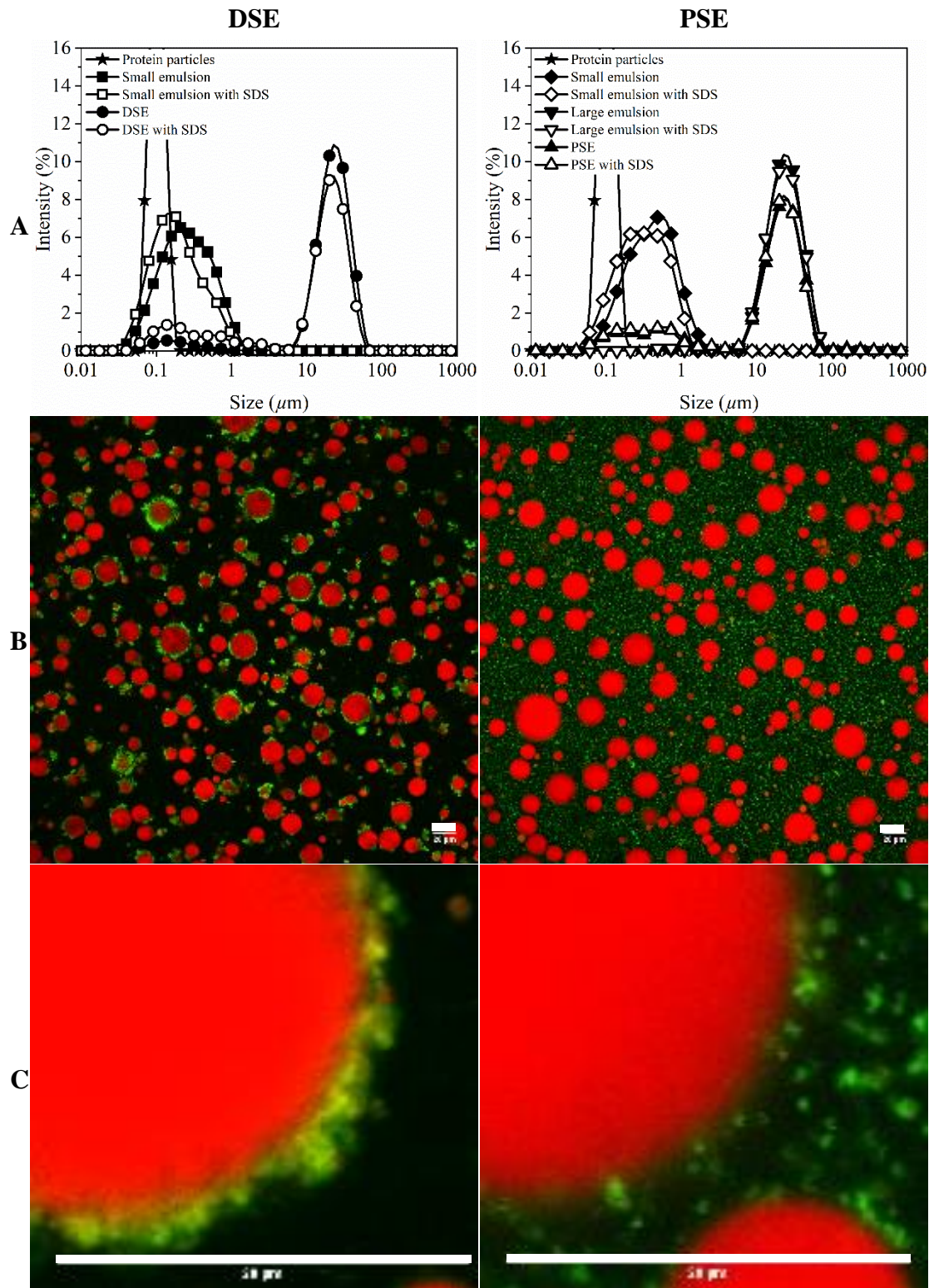


**Figure 6-1:** (A) The representative particle size distribution of  $\text{Ca}^{2+}$  cross-linked caseinate particles (protein particles, ★) were measured by static light scattering and droplet size distributions of different emulsions before gastric digestion: the protein particle-stabilised small-sized emulsion (Small emulsion, ■), protein particle-stabilised large-sized emulsion

(Large emulsion, ▼), small droplet-stabilised emulsion (DSE, ●) and the protein-stabilised emulsion containing small- and large-sized emulsion (PSE, ▲). The solid symbols represent the emulsion in the absence of sodium dodecyl sulphate (SDS), and the open symbols represent the emulsion in the presence of SDS. Confocal images of (B) 40×-magnification and (C) high-magnification of the DSE (left row) and the PSE (right row); red colour represents the oils and green colour represents the proteins. The scale bar is 20  $\mu\text{m}$ .

### 6.3.2 *In vitro* gastric digestion of emulsions

#### 6.3.2.1 Change in droplet size of emulsions during *in vitro* gastric digestion

The average sizes ( $d_{4,3}$ ) of the gastric digesta and the gastric chyme (sample remaining in the stomach) obtained from the DSE and the PSE during gastric digestion were measured using static light scattering in the absence and the presence of SDS (**Figure 6-2**). In general, the  $d_{4,3}$  values of the gastric digesta (**Figure 6-2A**) and the gastric chyme (**Figure 6-2B**) increased with increasing digestion time.

As shown in **Figure 6-2A**, except for the first 5 min and at 240 min of gastric digestion, the droplet sizes of the gastric digesta in the absence and the presence of SDS were similar in the DSE and the PSE at a given time during the gastric digestion. At 5 min of gastric digestion, the droplet size of the gastric digesta from the DSE was  $31.04 \pm 2.58 \mu\text{m}$ , much smaller than that from the PSE at  $84.34 \pm 1.14 \mu\text{m}$ . In the presence of SDS in the gastric digesta at 5 min of digestion, the  $d_{4,3}$  values decreased to  $17.53 \pm 2.74$  and  $20.52 \pm 3.25 \mu\text{m}$  for the DSE and the PSE respectively, i.e., similar to the sizes of the emulsion droplets in the DSE and the PSE before gastric digestion. This indicated that the large droplet size of the gastric digesta after 5 min of digestion was due to droplet flocculation, with the PSE showing more extensive droplet flocculation than the DSE. At 240 min of gastric digestion, the droplet sizes of both the DSE and the PSE were significantly higher than before gastric digestion ( $P < 0.05$ ), increasing from  $22.71 \pm 1.14$  to  $63.34 \pm 6.57 \mu\text{m}$  for the DSE and from  $17.98 \pm 1.16$  to  $85.11 \pm 9.35 \mu\text{m}$  for the PSE. The PSE had a greater increase in droplet size than the DSE because of droplet flocculation and droplet coalescence during gastric digestion. In the presence of SDS, the droplet size of the PSE decreased slightly to  $71.32 \pm 17.78 \mu\text{m}$ , whereas that the DSE remained constant ( $62.82 \pm 4.99 \mu\text{m}$ ). The slight decrease in the size of PSE at 240 min of gastric

digestion with SDS addition could be due to the dissociation of the flocculated droplets by SDS.

As shown in **Figure 6-2B**, the differences in the droplet sizes between the DSE and the PSE during gastric digestion (20–180 min) were more pronounced in the gastric chyme than in the gastric digesta. The droplet size of the gastric chyme of the PSE, with and without the presence of SDS, was larger than that of the DSE at a given digestion time, suggesting that PSE droplets tended to flocculate and coalesce more than DSE droplets during gastric digestion. For example, at 20 min, the droplet sizes of the gastric chyme in the absence of SDS were  $45.11 \pm 10.03$  and  $108.59 \pm 18.04$   $\mu\text{m}$  for the DSE and the PSE respectively; in the presence of SDS, these droplet sizes decreased to  $22.71 \pm 3.83$  and  $31.03 \pm 4.86$   $\mu\text{m}$  for the DSE and the PSE respectively. However, these droplet sizes in the presence of SDS were larger than those before gastric digestion ( $\sim 17$   $\mu\text{m}$ ), suggesting that droplet coalescence occurred in both emulsions after 20 min of gastric digestion and that the PSE had a greater extent of droplet flocculation and coalescence than the DSE. After 180 min of gastric digestion, the droplet sizes of the DSE in the presence and absence of SDS were similar, indicating that the increase in droplet size was mainly due to droplet coalescence. In contrast, the increase in droplet size in the PSE after 180 min of gastric digestion was caused by both droplet flocculation and droplet coalescence. Overall, this result suggested that the DSE was more stable than the PSE against droplet flocculation and droplet coalescence during gastric digestion.

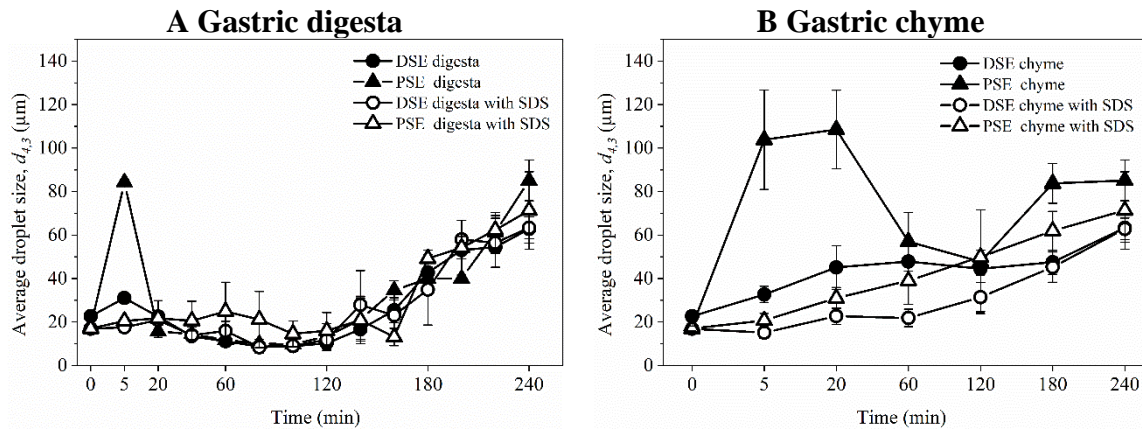


**Figure 6-2:** Droplet size ( $d_{4,3}$ ) of (A) the gastric digesta and (B) the gastric chyme of the droplet-stabilised emulsion (DSE, ●) and the protein-stabilised emulsion (PSE, ▲). The solid symbols represent the samples in the absence of sodium dodecyl sulphate (SDS) and the open symbols represent the samples in the presence of SDS. Error bars represent standard deviations from triplicates.

### 6.3.2.2 Morphology of emulsions during gastric digestion

CLSM was used to observe the morphologies of the gastric digesta and the gastric chyme of the DSE and the PSE, as shown in **Figure 6-3**. At 5 min of gastric digestion, the droplet size and the interfacial structure in the gastric digesta and the gastric chyme of the DSE were retained without a significant size increase. At longer gastric digestion times, fewer droplets were found in the gastric digesta than in the gastric chyme, which was the result of droplet creaming due to the large initial droplet size and droplet flocculation during gastric digestion. With an increase in the digestion time, the interfacial layer (the adsorbed nanodroplets) in the gastric digesta of the DSE gradually disintegrated and became thinner. However, the nanodroplet-stabilised interface remained relatively intact until 180 min of gastric digestion. In the gastric chyme of the DSE, clusters of droplets formed by flocculation between DSE droplets were observed. At a given gastric digestion time, the interfacial layer of the DSE droplets was thicker in the gastric chyme than in the gastric digesta, although there was also a gradual disintegration of the interfacial layer in the gastric chyme. At 240 min of gastric digestion, most droplets were surrounded by a thin layer of protein or peptides, and their size increased because of droplet coalescence.

In contrast, clusters of droplets and large individual droplets were found in both the gastric digesta and the gastric chyme of the PSE at 5 min of gastric digestion, although fewer droplets were present in the gastric digesta because of droplet creaming. The clusters of droplets were formed by the flocculation of small droplets or large droplets bridged by small droplets. Large droplets of approximately 100  $\mu\text{m}$  in size were formed through droplet coalescence as the proteins at the droplet interfaces were hydrolysed by pepsin. With an increase in the digestion time, the droplet clusters gradually disintegrated because of protein hydrolysis and more large droplets were formed because of coalescence. At 240 min of gastric digestion, some droplets

had coalesced into lipid pools of a few hundred microns or larger in size. These changes in the droplet structure, as observed by CLSM, were consistent with the droplet size as measured by light scattering. The PSE droplets were more likely to flocculate and coalesce than the DSE droplets during gastric digestion.

The droplet flocculation of milk-protein-coated emulsions during gastric digestion has been demonstrated widely as being the result of dynamic gastric acidification and protein hydrolysis (Singh et al., 2009; Wang et al., 2019; Ye et al., 2020). In the present study, the pH values of both emulsions decreased from 5.6 to 2.3 with increasing digestion time, passing the isoelectric point of casein ( $pI$  4.6) at 5–20 min of gastric digestion (**Supplementary materials, Figure S 6-2**). When the pH decreases to the isoelectric point of casein, the negative charges of the caseins are neutralised, and thus there is a loss of electrostatic repulsion (Wang et al., 2019). Hydrolysis by pepsin has also been reported to decrease the electrostatic interaction by cleaving the peptides carrying positively charged residues from the proteins adsorbed at the droplet interfaces (Sarkar et al., 2009; Singh et al., 2009).

Furthermore, the disappearance of nanodroplets at the DSE interface may be caused by gradual pepsin hydrolysis. A previous study on dynamic gastric digestion of emulsions suggested that the hydrolysis of adsorbed caseins by pepsin at the interface leads to the disintegration of the droplet flocs and the droplet coalescence (Wang et al., 2019). In the absence of a protein layer acting as a mechanical barrier, it is possible for droplets to coalesce or detach from each other. The resulting small peptides generally have less electrostatic repulsion and less steric barrier than intact proteins (Caessens et al., 1999; Li et al., 2012; Sarkar et al., 2009; van Aken et al., 2003). Therefore, coalescence of the droplets occurred in the emulsions when their adsorbed proteins were hydrolysed to small peptides.



As indicated above, the nature of the adsorbed layer will determine the stability behaviour of the emulsion droplets upon exposure to the low gastric pH and to hydrolysis by pepsin. The thick interfacial layer of the DSE, in the form of the small droplet network, may slow the hydrolytic action of pepsin on the adsorbed proteins. In the DSE, with the interfacial arrangement of the protein particles adsorbed onto the surfaces of both small droplet and core droplet, the effective binding site of the protein for pepsin could be somewhat restricted. In contrast, the interface made of casein particles in PSE is exposed to the aqueous phase, allowing fast pepsin binding and hydrolysis. In addition, most of the protein in the emulsion was brought to the surface layer of the core droplet by the adsorbed small droplets in the DSE, which contributed to a higher protein surface load. Bearing the assumption of a higher protein load at the interface of core droplets in the DSE, the hydrolysis of interfacial protein could be delayed, leading to the slower destabilisation of DSE. In summary, the difference in the interfacial structure, i.e., a small droplet interfacial layer versus a caseinate interfacial layer, resulted in different behaviours, i.e., flocculation and coalescence of the droplets during gastric digestion. However, the underlying mechanism of the improved stability of DSE under gastric conditions required further systematic investigations.

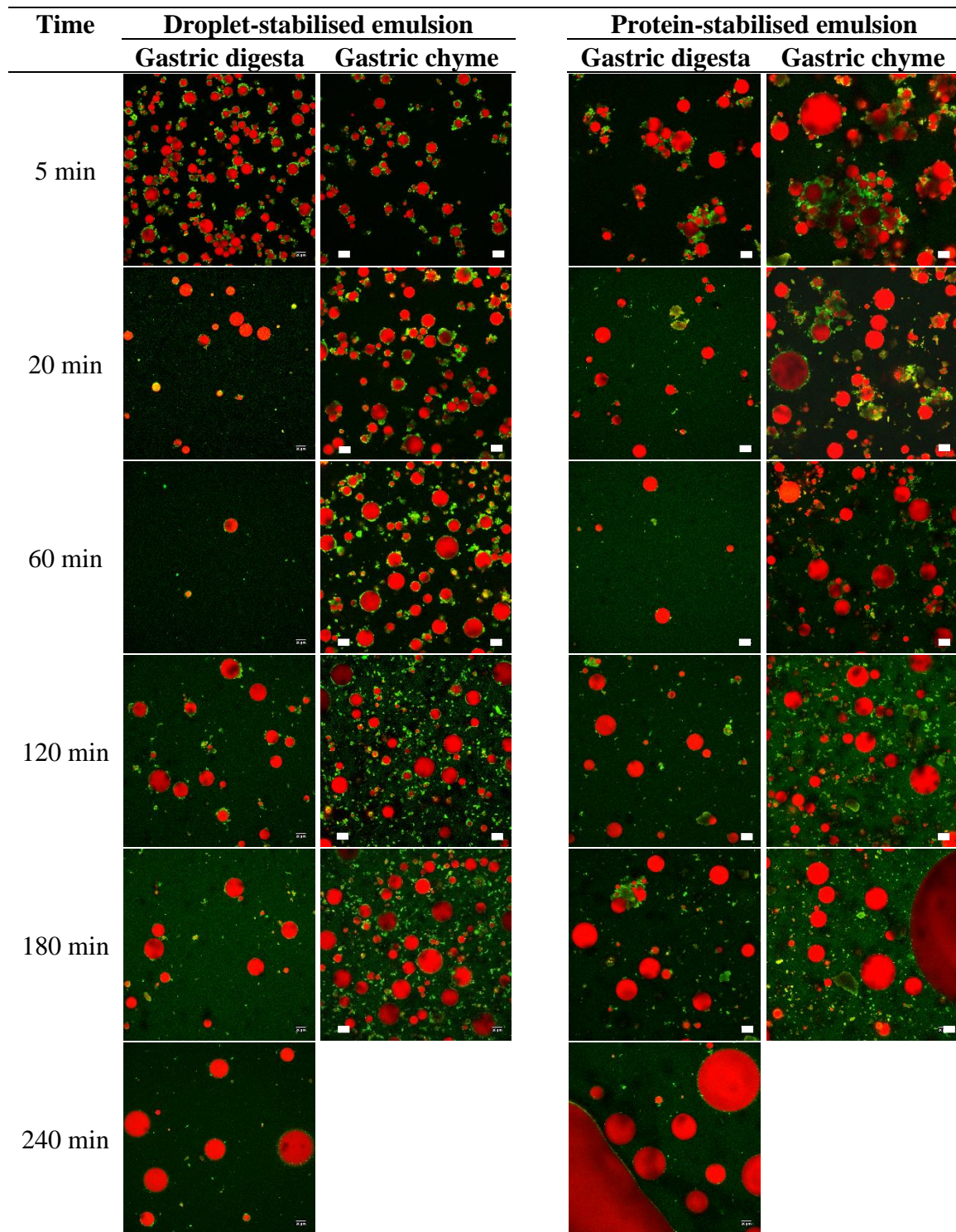


**Figure 6-3:** Confocal images of the gastric digesta and the gastric chyme of the droplet-stabilised emulsion (DSE) and the protein-stabilised emulsion (PSE) after 5–240 min of gastric digestion. Red colour represents the oils and green colour represents the proteins. The scale bar is 20  $\mu\text{m}$ .

**6.3.2.3 Oil content of the emptied digesta**

The oil contents of the gastric digesta of the emulsions as a function of the digestion time are shown in **Figure 6-4**. They represent the amount of oil delivered to the small intestine at different times. In both emulsions, a small amount of oil was released in the early stages of gastric emptying, and larger amounts of oil were released in the latter stages. This can be attributed to the creaming of the emulsions, when large droplets migrated to the top layer in the gastric chamber. Thus, the aqueous phase consisting of the digestive fluid was emptied first.

In the first 120 min of gastric digestion, the oil content released from the PSE was lower than that from the DSE at any given time point. At 60 min of gastric digestion, the oil released from both emulsions reached the lowest values ( $0.27 \pm 0.06\%$  w/w for the DSE and  $0.06 \pm 0.01\%$  w/w for the PSE). The lower amount of oil released from the PSE suggests that this emulsion was more prone to creaming and phase separation than the DSE during gastric digestion. This result is supported by the large droplet size and the extensive droplet flocculation/coalescence observed in the PSE during early-stage gastric digestion, as determined by light scattering and CLSM (**Figure 6-2** and **Figure 6-3**). That is, the gastric chyme of the PSE contained less water and more oil droplets than that of the DSE.

During the latter stages of gastric digestion, the PSE tended to release higher oil content than the DSE at the given time point. For example, at 180 min of gastric digestion, approximately 2.8 times more oil was released from the PSE than from the DSE ( $2.93 \pm 0.19\%$  w/w and  $8.21 \pm 0.34\%$  w/w for the DSE and the PSE respectively). However, lower oil content in the PSE was found at 240 min, which was probably the consequence of the droplet destabilisation (droplet coalescence) (**Figure 6-3**). The large droplets (or free oil) on the top of cream layer could not be recovered at the final time point because they were attached to the

simulated gastric chamber wall. Thus, current results suggested that the oil release profile of the emulsions during gastric digestion was affected by the structure of the interfacial layer of the emulsion (nanodroplet interfacial layer versus caseinate interfacial layer).

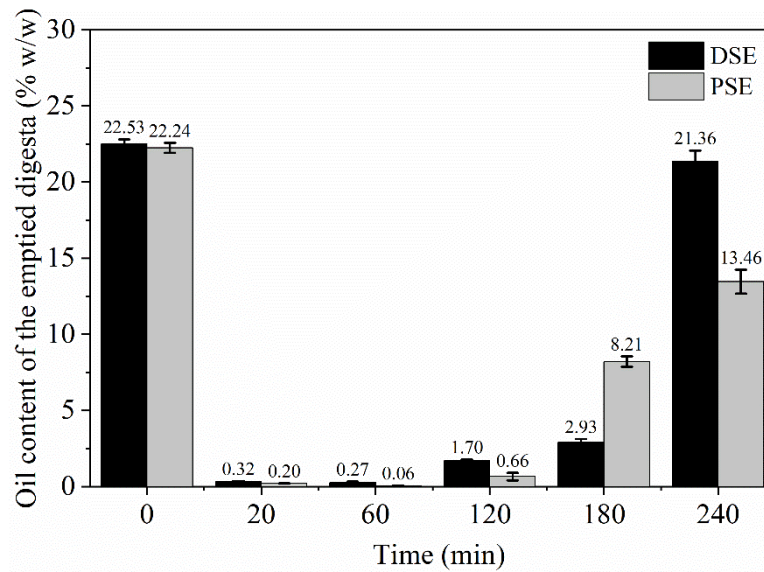


**Figure 6-4:** Oil contents of the droplet-stabilised emulsion (DSE) and the protein-stabilised emulsion (PSE) before digestion (0 min) and of the gastric digesta at different digestion times (20–240 min). Error bars represent standard deviations from triplicates.

### 6.3.3 *In vitro* small intestinal digestion of emulsions

#### 6.3.3.1 Microstructure of emulsions during *in vitro* small intestinal digestion

Immediately after the gastric digesta had been mixed with the small intestinal digestive fluid (0 min of small intestinal digestion), the droplet size distributions were measured by light scattering. As shown in **Figure 6-5A**, at the onset of the small intestinal digestion, both the DSE and the PSE were polydisperse and had two groups of droplets: one with small droplets distributed in the  $\sim 0.03$ – $2 \mu\text{m}$  range and one with large droplets centred at  $\sim 30$  and  $\sim 50 \mu\text{m}$  in the DSE and the PSE respectively. The smaller size of the large droplets and the greater proportion of small droplets in the DSE were due to less droplet coalescence after gastric digestion. After 3 min of small intestinal digestion, most of the small droplets in both samples had disappeared, resulting in a large average droplet size (SM Fig. 3). Small droplets tend to be hydrolysed by lipase more rapidly than large droplets because their larger specific surface area allows more lipase molecules to bind to and hydrolyse the lipids (Armand et al., 1992, 1999). With further small intestinal digestion ( $\geq 15$  min), the average droplet size ( $d_{4,3}$ ) decreased with an increase in the digestion time (SM Fig. 3). A small peak of between  $0.03$  and  $0.40 \mu\text{m}$  in size appeared after 15 min of digestion in the small intestine; this may have been micelles of bile salts and lipolysis products that were generated during the digestion.

The CLSM images (**Figure 6-5B**) show that there was no droplet flocculation in both emulsions, and that the nanodroplets had detached from the interface of the larger droplets in the DSE. This was possible because bile salts replaced the original adsorbed emulsifier from the interface, allowing the lipase/colipase complex to act on the bile-salt-coated interface (Bellesi et al., 2014; Sarkar et al., 2016b). At 0 min of small intestinal digestion, the droplets present in the DSE were smaller than those in the PSE, confirming the light scattering results (**Figure 6-5A**). At 3 min of small intestinal digestion, the number of droplets had decreased

dramatically (**Figure 6-5B**), and a layer of digestive enzyme and other material from pancreatin had adsorbed onto and surrounded the large droplets. At 15 min of small intestinal digestion, the interfaces of the droplets became fragmented (zoom-in image of **Figure 6-5B**), which indicated that intensive lipolysis had occurred; lipolysis is an interfacial process (Sarkar et al., 2019; Wilde & Chu, 2011). In addition, droplet coalescence occurred during the small intestinal digestion (**Figure 6-5B**). For example, at 3 and 15 min of small intestinal digestion, the size of the DSE droplets was larger than that prior to the small intestinal digestion.

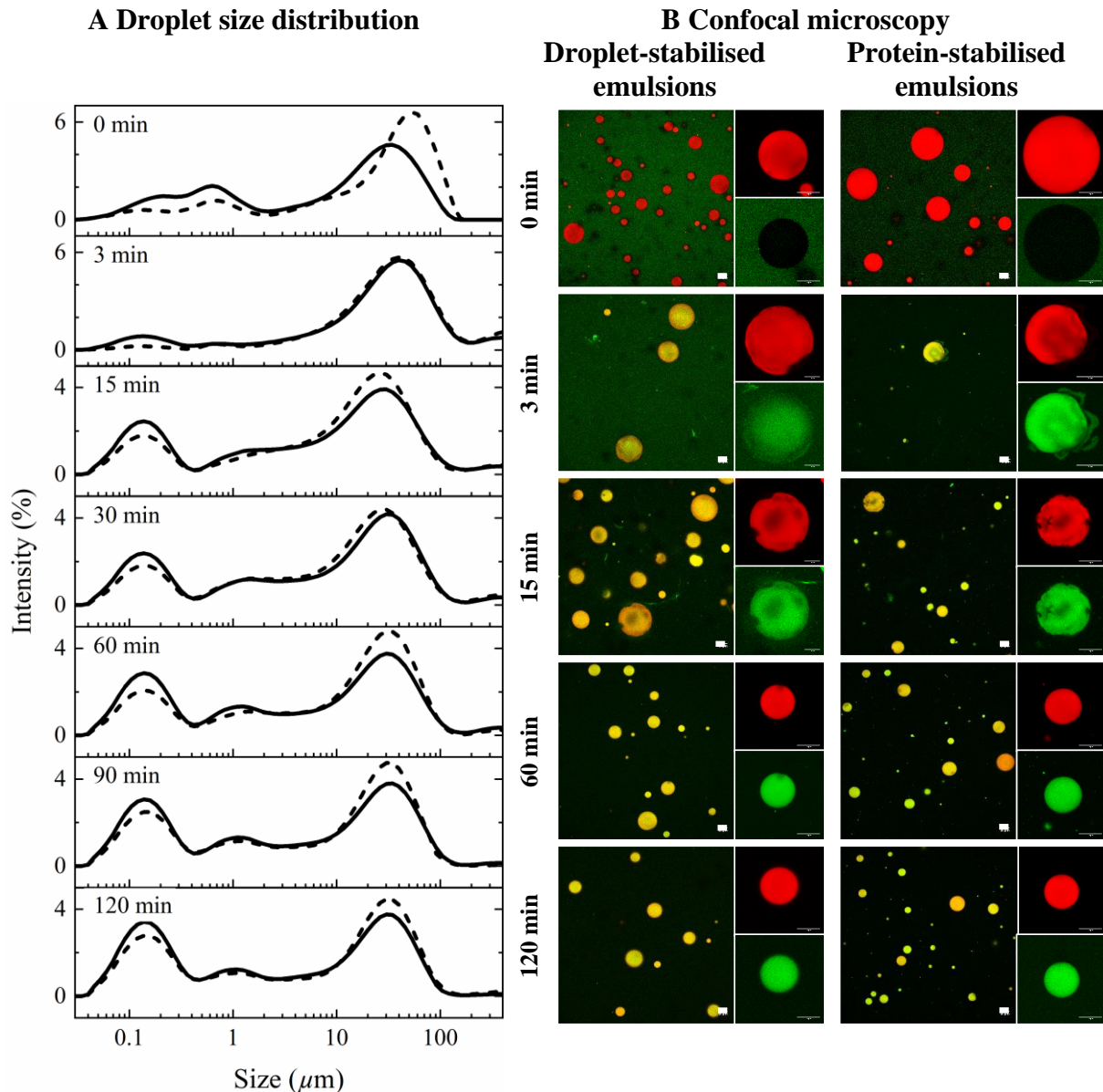


**Figure 6-5:** (A) Droplet size distributions of the droplet-stabilised emulsion (DSE, —) and the protein-stabilised emulsion (PSE, ---) during *in vitro* small intestinal digestion. (B) Confocal images of the DSE (left-hand column) and the PSE (right-hand column) during *in vitro* small intestinal digestion. Red colour represents the oils and green colour represents the proteins. The scale bar is 20  $\mu\text{m}$ .



### 6.3.3.2 Modelling of the kinetics of lipolysis

The total FFAs released from the emulsions as a function of the digestion time are shown in **Figure 6-6**. Two regions can be clearly distinguished. The emulsions exhibited a rapid release of FFAs in the early stages of small intestinal digestion and slow release in the later stages. The duration of the rapid FFA release for the two emulsions was ~28 min for the DSE and ~20 min for the PSE, respectively. The rapid FFA release probably resulted from fast lipolysis of small droplets due to the larger oil-water interfacial area for lipase action (Li & McClements, 2010; McClements, 2018; Riquelme et al., 2020). In addition, the fast rate of FFA release in the early stages could also be attributed to the fast adsorption of the lipase at the oil droplet surface and the less inhibitory lipolysis products (e.g. long-chain fatty acids and monoacylglycerols) accumulated at the surface (Golding & Wooster, 2010; Porter et al., 2007; Sek et al., 2002).

Initially, an attempt was made to calculate the kinetic parameters for the initial FFA release from the two emulsions using **equations (6-2)** and **(6-3)**. This kinetic model describes the release of FFAs by lipolysis under conditions of rapid lipase adsorption at the interface and independent of the change in droplet size during digestion (Sarkar et al., 2019; Ye et al., 2013a). However, the first-order relationship for FFA release with time could not be obtained, implying that the rate of lipid digestion in the early stages of small intestinal digestion was affected by factors such as the dynamics of enzyme adsorption and the droplet size. A mathematical model,  $\varphi(t) = \varphi_{Max} \left[ 1 - \left( 1 - \frac{2M_w k}{d_0 \rho_0} t \right)^3 \right]$ , was first proposed by McClements and Li (Li & McClements, 2010; McClements & Li, 2015) and later solved by Gaucel et al. (Gaucel et al., 2015) to describe the impact of droplet size on the rate of lipid digestion; it assumed that individual lipid droplets shrank during digestion because some of the triacylglycerols were hydrolysed and lost. However, in this study, the size of the emulsion droplets did not simply

decrease over time (**Figure 6-5B**). There was an increase in the size of the droplets after 3 min of digestion and a decrease in size after 30 min of digestion (**Supplementary material, Figure S 6-3**). The model (Gaucel et al., 2015; Li & McClements, 2010; McClements & Li, 2015), which assumes that the droplet size simply decreases with the digestion time, may not explain the FFA release kinetics in this study. Therefore, the best description of the initial FFA release kinetics would be the increase in FFAs released per unit of time ( $r$ , %FFA  $\text{min}^{-1}$ ), calculated as  $\varphi_t - \varphi_0 = rt$ , which was  $1.21\% \text{ min}^{-1}$  and  $1.06\% \text{ min}^{-1}$  for the DSE and the PSE respectively (**Supplementary material, Table S 6-2**).

The slower release of FFAs occurred after about 30 min of intestinal digestion. The accumulation of lipolysis products at the interfaces could have decreased the interface area available for lipase action, contributing to the slow release of FFAs (Mun et al., 2007; Pafumi et al., 2002). Moreover, a real plateau was not reached after 120 min for both emulsions, which is a classical result for the digestion of long-chain triacylglycerols (Giang et al., 2016; Golding et al., 2011; Williams et al., 2012). At the end of this experiment,  $56.19 \pm 3.55$  and  $49.40 \pm 2.67\%$  of the FFAs had been released from the DSE and the PSE, respectively. The order of magnitude of the final percentage of FFA release was in good agreement with the results from the lipid digestion of long-chain fatty acids in the literature. During the stage of slow FFA release, similar  $k$  values ( $0.5 \mu\text{mol s}^{-1} \text{ m}^{-2} \times 10^{-4}$ ) were obtained for the DSE and the PSE, as the droplet sizes ( $d_{4,3}$ ) of the DSE ( $28.31 \mu\text{m}$ ) and the PSE ( $29.34 \mu\text{m}$ ) were similar after 30 min of digestion (**Supplementary material, Table S 6-2**). The similar lipolysis kinetic parameters suggested that the efficiencies of the interfacial process of lipolysis in the two emulsions were comparable. The size of the emulsions released from gastric digestion into the intestine may have been the crucial factor in determining the rate of lipolysis in the present study.

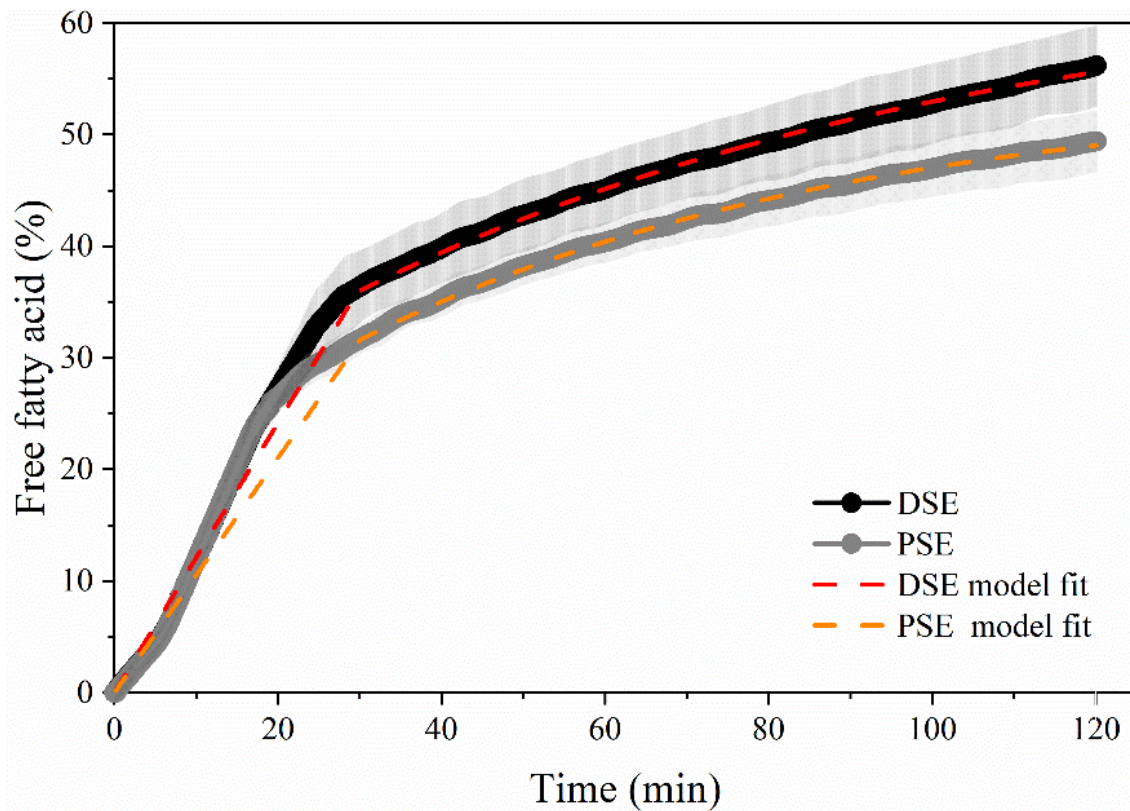


**Figure 6-6:** Free fatty acid release profiles of the droplet-stabilised emulsion (DSE, solid black line) and the protein-stabilised emulsion (PSE, solid grey line) during *in vitro* small intestinal digestion. The solid lines represent the experimental data determined by pH-stat titration and the dashed lines represent the model data that were superimposed on the experimental data. Error bars represent the standard deviations from triplicate.

### 6.4 Conclusions

In this study, a novel oil-in-water emulsion stabilised by small primary droplets was compared to conventional protein-stabilised emulsion in their behaviours in the *in vitro* gastrointestinal digestion. This study demonstrated that under gastric pH close to the isoelectric point of caseins (~ pH 4.6), the dense and thick interface layer composed of nanoemulsion droplets prevented the emulsions from flocculation and coalescence. In contrast, the polydisperse emulsion stabilized by casein particles showed extensive droplet flocculation and coalescence which was similar to conventional casein-stabilized emulsions (Wang et al., 2019) (Ye et al., 2020). The nanodroplet-stabilised interface of the emulsion contributed to a smaller droplet size after gastric digestion. The extent of the lipid digestion was mainly associated with the droplet size distribution in the emulsions emptied from the stomach, thus leading to a slightly greater amount of FFA release from the DSE during the small intestinal digestion. In addition, the polydisperse droplets resulted in different rates of FFA release during the intestinal digestion, with the smaller droplets having a faster rate of FFA release at the beginning of the digestion. The droplet-stabilised interfaces of DSE were disassembled and resulted in polydisperse emulsion droplets in the small intestinal phase. This study provides useful information for designing novel food structures with controlled digestibility, while promoting the understanding on the digestion of the polydisperse emulsion systems consisting of a broad range of droplet sizes, such as milk and infant formula.

## 6.5 Supplementary material

**Table S 6-1:** Formulae of electrolyte solutions for the simulated gastric fluid (SGF) and the simulated intestinal fluid (SIF)

Salts	Concentration of stock solutions		SGF (pH 2.0)		SIF (pH 7.0)	
			Salt concentration in stock (1.25x)	Salt concentration in final SGF (1.0x)	Salt concentration in stock (1.25x)	Salt concentration in final SIF (1.0x)
	(mM)	(g/L)	(mM)	(mM)	(mM)	(mM)
KCl	1000.00	74.55	8.63	6.90	8.50	6.80
KH <sub>2</sub> PO <sub>4</sub>	500.00	68.04	1.13	0.90	1.00	0.80
NaCl	3000.00	175.32	59.00	47.20	154.25	123.40
MgCl <sub>2</sub> (H <sub>2</sub> O) <sub>6</sub>	100.00	20.33	0.15	0.12	0.41	0.33
NaHCO <sub>3</sub>	500.00	43.50	31.25	25.00	–	–
(NH <sub>4</sub> ) <sub>2</sub> CO <sub>3</sub>	100.00	9.61	0.63	0.50	–	–
CaCl <sub>2</sub> *	1000.00	110.98	–	0.15	–	0.60

\*CaCl<sub>2</sub> is absent in the stock simulated digestion fluids but is added immediately before use.

**Table S 6-2:** Kinetic parameters of the emulsions during the *in vitro* intestinal digestion

	DSE	PSE
$d_{4,3}$ ( $\mu\text{m}$ ) at 0 min	25.16 (4.45)	39.81 (4.69)
$d_{4,3}$ ( $\mu\text{m}$ ) at 30 min	28.31 (2.48)	29.34 (4.11)
$\varphi_{Max}$ (%)	56.19 (3.55)	49.40 (2.67)
$r$ (%FFA $\text{min}^{-1}$ )	1.21 (0.036)	1.06 (0.052)
$k$ ( $\mu\text{mol s}^{-1} \text{m}^{-2} \times 10^{-4}$ )	0.5 (0.004)	0.5 (0.007)

DSE, droplet-stabilized emulsion; PSE, particle-stabilized emulsion.

$r$ , percentage of free fatty acids (FFAs) released per unit of time; kinetic parameter for the initial 0–30 min of small intestinal digestion.

$k$ , lipid conversion rate per unit area of the droplet surface; kinetic parameter calculated from  $k_l$  [equation (6-3)] for 30–120 min of small intestinal digestion.

Standard deviation from triplicates were included in brackets.

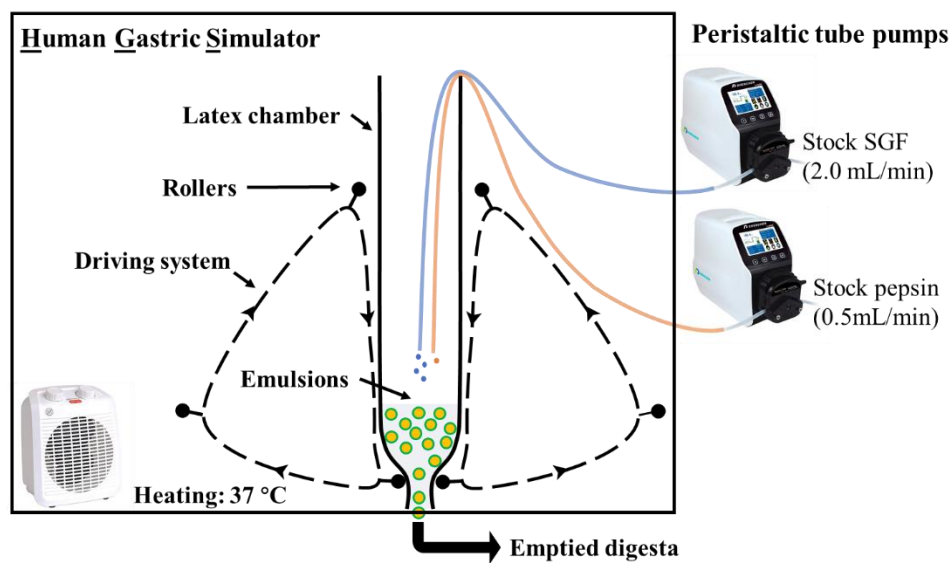


**Figure S 6-1:** Illustration of the set-up for the human gastric simulator.

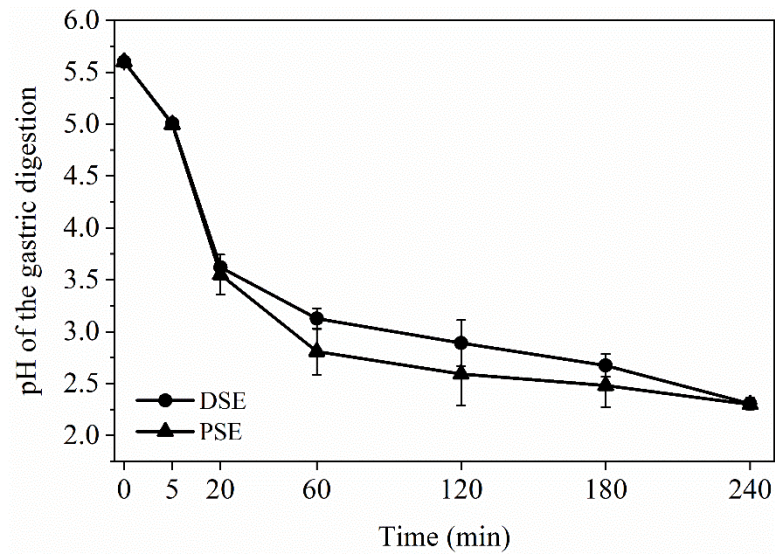


**Figure S 6-2:** Changes in pH during gastric digestion of the droplet-stabilised emulsion (DSE, ●) and the protein-stabilised emulsion (PSE, ▲). Error bars represent standard deviations from triplicates.



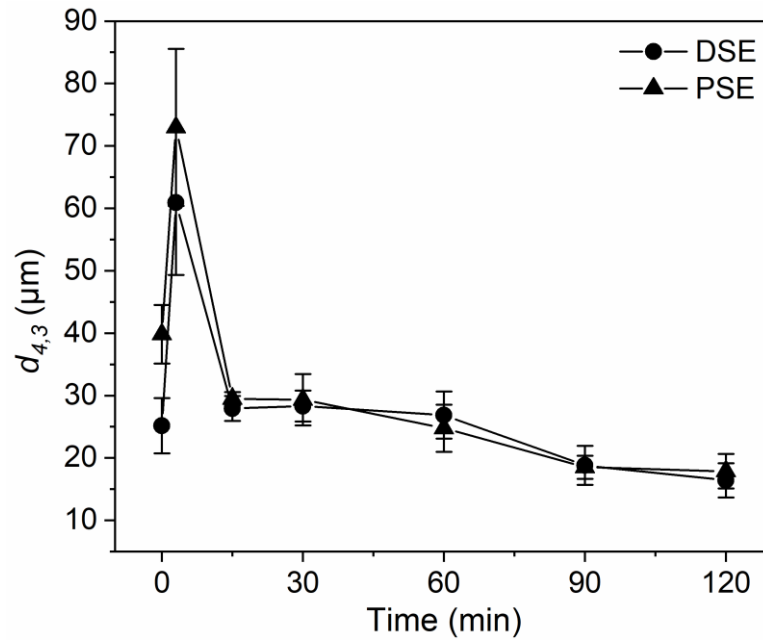


**Figure S 6-3:** Average droplet size ( $d_{4,3}$ ) of the droplet-stabilised emulsion (DSE, ●) and the protein-stabilised emulsion (PSE, ▲) during *in vitro* small intestinal digestion. Error bars represent standard deviations from triplicates.

### 6.6 Acknowledgements

This work was funded by the Riddet Institute, a National Centre of Research Excellence, and by the New Zealand Tertiary Education Commission. We also thank the Manawatu Microscopy and Imaging Centre at Massey University for technical support.

### CRediT authorship contribution statement

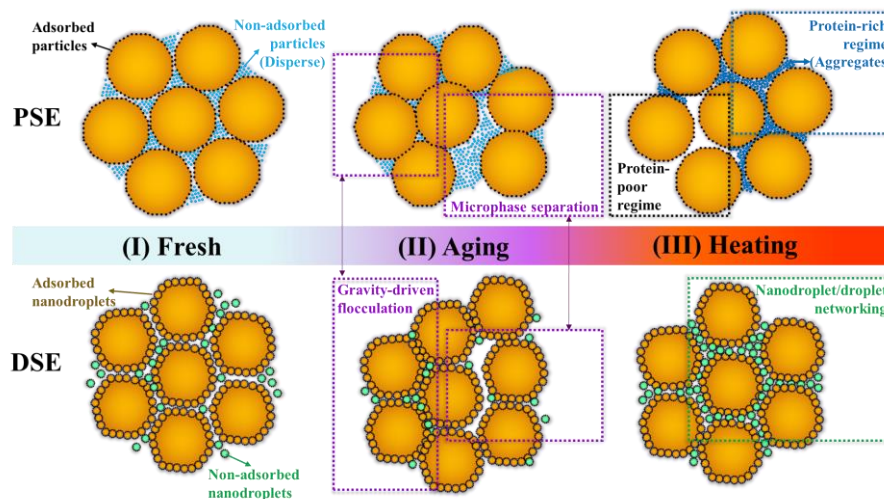
**Lirong Cheng:** Conceptualisation, Methodology, Software, Validation, Investigation, Formal analysis, Data Curation, Visualization, Writing - original draft. **Aiqian Ye:** Conceptualisation, Methodology, Resources, Funding acquisition, Supervision, Project administration, Writing - review & editing. **Yacine Hemar:** Writing - review & editing, Supervision. **Harjinder Singh:** Conceptualisation, Funding acquisition, Writing - review & editing, Supervision.

### Declaration of Competing Interest

The authors declare no conflict of interest.

## Chapter 7 Formation and properties of highly concentrated oil-in-water emulsions stabilised by emulsion droplets

### Graphic abstract



### Abstract

Food-graded caseinate particles (Ca-CAS) were prepared by mixing sodium caseinate and calcium chloride. Ca-CAS (~110~140 nm in diameter) and the Ca-CAS coated primary emulsion droplets (400 nm in average diameter) exhibited good dispersion at both pH 7.0 and 5.8 with charges between -6 and -9 mV, and they were used as emulsifiers in the subsequent 70 % (v/v) concentrated emulsion preparation. The emulsion stabilised by primary droplets (DSE) was compared with conventional emulsion stabilised by Ca-CAS (PSE) in terms of viscoelasticity as affected by aging (30 days) and heating (80 °C, 30 min). All emulsions exhibited exceptional resistance to droplet coalescence for 30 days of aging and to heating. Storage moduli of all emulsions were higher than the loss moduli under all conditions, suggesting gel-like properties. The emulsion with full coverage of primary droplets (DSE at pH 5.8) showed the highest complex modulus ( $1174 \pm 39$  Pa) approximately six-times higher

than other emulsions ( $\leq \sim 250$  Pa) due to the thick primary droplet layer increasing the effective volume fraction by a factor of  $\sim 1.21$ . The complex moduli of DSE at pH 5.8 increased to  $1685 \pm 68$  Pa after 30 days aging and to  $1801 \pm 69$  Pa after heating at  $80^\circ\text{C}$  for 30 min; while the complex moduli of PSE increased to  $\sim 400$  Pa and  $\sim 600$  Pa after aging and heating, respectively. The possible mechanism for aging-induced gelation was the gravity-driven microphase separation, in which the droplet flocs together with the entrapped aqueous phase increasing the effective volume fraction. The heat-induced gelation was attributed to the increase in droplet interactions at elevated temperature, in which the touching droplets were associated together through protein aggregates and/or primary droplets forming three-dimensional networks. This study suggests that the mechanical strength of food-graded concentrated emulsions can be effectively improved using nano-sized primary emulsions as emulsifiers and can be further modulated by aging or heating, which will be useful for developing semi-solid emulsion-based products.

### 7.1 Introduction

Oil-in-water (O/W) emulsion is a mixture of two immiscible liquid phases, with one oil phase dispersed as droplets in another aqueous continuous phase. When the volume fraction of the disperse phase ( $\phi$ ) is high, the droplets are packed very closely, conferring the emulsion a yield-stress and viscoelastic properties. Typically, they appear to flow at high shear rates but solidify at low shear rates, exhibiting high stability with a self-supporting texture (Li et al., 2020). Owing to the unique gel-like rheological properties, special texture and long-term stability, concentrated emulsions have attracted increasing attention from both academic research and industry (Li et al., 2018; Patel & Dewettinck, 2016). The advantages of concentrated emulsion rely on their adjustable viscoelastic properties (Tan et al., 2020; Wang

et al., 2016). Many studies have indicated that the rheological properties of concentrated emulsion depend on  $\varphi$  (Hemar & Horne, 2000; Lacasse et al., 1996; Mason et al., 1996; Princen & Kiss, 1986), droplet size distribution (Desmond & Weeks, 2014; Foudazi et al., 2012; Pal, 1996), droplet coalescence and aggregation state (Berli, 2007; Chuang et al., 2020; Zhang et al., 2021a), as well as continuous phase viscosity (Geremias-Andrade et al., 2017; Zhu et al., 2019). These factors can be manipulated prior to emulsification by adjusting different parameters such as emulsifiers, oil fraction, pH, ionic strength, additives, etc., to obtain a concentrated emulsion with desirable processibility, physicochemical and functional properties. For instance, a reduced disperse phase volume fraction of emulsion could be designed to have the same rheological properties than that made with a higher disperse phase volume fraction.

The viscoelasticity of concentrated emulsions could change over long-term storage, due to droplets coalescence (Chuang et al., 2020; Dimitrova & Leal-Calderon, 2004; Hu et al., 2016). To improve the long-term stability towards coalescence of concentrated emulsions, strategies using large amount of surfactants (e.g., Tweens and Spans) (Barbetta & Cameron, 2004; Cameron & Sherrington, 1996; Wijaya et al., 2017) or colloidal particles (e.g., silica particles) (Abdullah et al., 2020; Zheng et al., 2014) are often employed. It is well established that emulsions stabilised by colloidal particles often possess better stability to droplet coalescence than those stabilised by surfactants through Pickering mechanism (Binks, 2002). Therefore, the application of food-grade particles (e.g., starch, cellulose, chitin, proteins, and polysaccharides) has attracted increased interest in the manufacture of edible concentrated emulsion-based products (Huang et al., 2019; Zhang et al., 2021a; Zhu et al., 2019). However, a low viscoelasticity of about 10 – 500 Pa at 1 Hz has been usually reported for Pickering concentrated emulsions ( $\varphi > 0.75$ ) that are stabilised by food-grade particles, such as gliadin-

based particles (Zeng et al., 2017), zein-based particles (Jiang et al., 2019), whey protein microgel (Su et al., 2018), and pH-modified casein particles (Guo et al., 2021).

Recently, several studies have been carried out to improve the mechanical strength of concentrated emulsions through modifying the interfacial structure by increasing the size of the particles and improving the amount of the adsorbed particles at the interface (Guo et al., 2021; Yan et al., 2019). For example, concentrated emulsions stabilised with OSA starch/chitosan complex particles showed the highest viscoelasticity at pH 6 as compared to emulsions formed at pH below 6. At pH 6, the OSA starch/chitosan particle had a large size and formed a thick interfacial layer at the droplet surfaces, which promote the formation of a percolation network structure in the emulsion (Yan et al., 2019). Similar results have been found in zein/pectin hybrid particle (ZPHP)-stabilised Pickering emulsions (Zhou et al., 2018). A well-ordered interfacial layer of the droplet formed with ZPHP at pH 3.0 led to high interfacial coverage and a better stability and higher viscoelasticity compared to emulsions formed at higher pH. It has been suggested that the protective well-ordered and thick interfacial layer contribute to the formation of a percolating network of droplets and thus to the viscoelastic properties of concentrated emulsions (Yan et al., 2019; Zhou et al., 2018). This type of interfacial layer has been previously observed in dilute emulsion ( $\phi = 0.2$ ) formed with small primary droplets as stabilisers (Cheng et al., 2019). This leads one to hypothesise that the viscoelasticity of the concentrated emulsion will be improved by the formation of a thick interfacial layer consisting of small primary droplets.

The aim of this study was therefore to develop an oil-in-water concentrated emulsion (70% v/v) stabilised by primary droplets coated with calcium cross-linked caseinate particles (Ca-CAS) with different interfacial structures. The concentrated emulsions stabilised by Ca-CAS coated primary droplets were compared to emulsions solely stabilised by Ca-CAS in terms of

their rheological properties at controlled compositions (e.g., same oil volume fraction and protein concentration). The effects of aging (30 days) and heating (80 °C, 30 min) on the rheological properties were also investigated. The rheological measurements were supported with droplet size measurements and confocal laser scanning microscopy observation.

## 7.2 Materials and methods

### 7.2.1 Materials

Sodium caseinate (Alanate 180: 92.7 % w/w protein, 4.3 % w/w moisture, 0.7 % w/w fat and 0.2 % w/w carbohydrate) was purchased from Fonterra Co-operative Group Ltd. (Auckland, New Zealand). Soybean oil was purchased from Davis Trading Company, Palmerston North, New Zealand. Milli-Q water (Millipore Corp., Bedford, MA, USA) was used for all experiments. All chemicals used were of analytical grade and were purchased from Sigma-Aldrich (St. Louis, MO, USA) or BDH Chemicals (BDH Ltd., Pooles, England) unless otherwise specified.

### 7.2.2 Preparation of calcium cross-linked caseinate particle

Stock sodium caseinate (CAS) dispersion with protein concentration of 3.1 w/v% was prepared by dissolving sodium caseinate powder in ultrapure Milli-Q water (18.2 M $\Omega$ ) at 50 °C and stirring for 2h, followed by overnight storage at the room temperature to ensure complete hydration. The pH of this sodium caseinate dispersion is  $6.90 \pm 0.2$ . Ca-CAS dispersions were prepared by adding an appropriate amount of stock CaCl<sub>2</sub> solution (1 M, 0.22  $\mu$ m filtration) drop-wisely into the stock CAS dispersion under mild stirring for half-hour equilibrium, followed by adjusting the pH to  $7.00 \pm 0.05$  using 2 M NaOH or 2M HCl and equilibrating at room temperature overnight. The final Ca-CAS dispersion contains 3.0% w/v protein and 20 mM CaCl<sub>2</sub>, which is close to the concentration of protein and colloidal calcium found in casein micelles. Sodium azide was added at a final concentration of 0.04 % (w/w) as a preservative.

### 7.2.3 Emulsion preparations

#### 7.2.3.1 Concentrated droplet-stabilized emulsion preparations

Nano-sized primary emulsion was firstly prepared as the emulsifying agent for the droplet-stabilised emulsion. Ca-CAS dispersion (3.00 w/v % protein, 20.00 mM CaCl<sub>2</sub>, pH 7.0) was mixed with soybean oil, giving 20 v/v % soy oil of the final primary emulsion. The mixture was prehomogenized using a handheld Ultra-Turrax (IKA T10 basic, Staufen, Germany) at 30,000 rev min<sup>-1</sup> for 30 s, then passes through a two-stage homogenisation (Homolab 2, FBF Italia, Italy) at pressures of 47 MPa (first stage)/5 MPa (second stage), resulting in a primary emulsion. The outlet temperature of the two-stage homogeniser was controlled by using an ice bath to avoid the heating from the high-pressure homogenisation. The pH of the primary emulsion is the same as the pH of its aqueous phase.

Primary emulsions were subsequently used as the aqueous phase to mix with the secondary oil phase (soybean oil) in volume ratio of 6:10 to prepare 16 mL of droplet-stabilised emulsion (DSE). In the final emulsion, the total oil volume fraction reached to 70 v/v %, in which the primary emulsion contributed 7.5 v/v % and the secondary oil phase contributed 62.5 v/v %. The secondary oil phase was adding drop by drop. Prior to adding the secondary oil phase, the pH of the primary emulsion was checked as  $7.00 \pm 0.05$  and adjusted to  $\text{pH } 5.80 \pm 0.05$  for the acidic emulsion using 2M HCl under mild magnetic stirring. Homogenisation of the concentrated DSE was performed using a handheld Ultra-Turrax (IKA T10 basic, Staufen, Germany) at 10,000 rev min<sup>-1</sup> for 5 min. Sodium azide was added at a final concentration of 0.04 wt% as a preservative. Emulsions were prepared in duplicate for each pH value.

#### 7.2.3.2 Concentrated CAS particle-stabilised emulsion preparation



Ca-CAS dispersion (3.00 w/v % protein, 20.00 mM CaCl<sub>2</sub>, pH 7.0) mixed with soybean oil in ratio of 3:7 to prepare the 16 mL of high concentrated Ca-CAS particle-stabilized emulsion (PSE). Prior to adding the oil phase, the pH of the Ca-CAS dispersion was checked as  $7.00 \pm 0.05$  or adjusted to  $\text{pH } 5.80 \pm 0.05$  for the acidic emulsion using 2M HCl under mild magnetic stirring. Homogenisation of the concentrated PSE was performed using a handheld Ultra-Turrax (IKA T10 basic, Staufen, Germany) at  $10,000 \text{ rev min}^{-1}$  for 5 min. Sodium azide was added at a final concentration of 0.04 wt% as a preservative. Emulsions were prepared in duplicate for each pH value.

### 7.2.4 Emulsion stability during storage and heat treatment

All emulsion samples were stored in temperature-controlled lab (22 °C) at dark place for 30 days. The bottle caps were tightened and sealed with parafilm (PARAFILM<sup>®</sup> M) to prevent moisture loss.

### 7.2.5 Particle size measurement

The  $z$ -average hydrodynamic diameter Ca-CAS were measured by dynamic light scattering (DLS) at 20 °C using a ZetaSizer Ultra (Malvern Instruments Ltd, Malvern, UK). The instrument used a backscattering configuration with detection at a scattering angle of 173° using an avalanche photodiode and a helium-neon laser at  $\lambda = 633 \text{ nm}$ ; refractive indices of 1.50 and 1.33 were used for protein and water, respectively.

The droplet size of emulsions with and without sodium dodecyl sulphate (SDS) was determined by static light scattering using (SLS) using a Malvern MasterSizer 2000 (Malvern Instruments Ltd, Malvern, UK). Emulsion in the absence of SDS was directly added into the MasterSizer dispersion tank under stirring at 2500 rpm during measurements. The size of individual droplets was obtained by dispersing the emulsion in 2 wt% SDS solution at volume

ratio of 1:10 before SLS measurements, because SDS is capable of disrupting hydrophobic interactions and displacing protein molecules and the protein-coated droplets from the oil–water interface without changing the oil droplet size (Cheng et al., 2019, 2022a; Dickinson & Ritzoulis, 2000; Mackie et al., 2000; Tomas et al., 1994).

The refractive index of soy oil was 1.47 and water (the dispersing medium) was 1.33. Droplet size measurements are reported as De Broukere mean ( $d_{4,3}$ ). Mean particle diameters were calculated as the average of duplicate measurements.

### 7.2.6 Zeta-potential measurements

The zeta-potentials of Ca-CAS particles, and associated emulsions, were determined by DLS at 20 °C using a ZetaSizer Ultra instrument (Malvern Instruments Ltd, Malvern, UK). The dispersions of Ca-CAS were measured at pH 7.0 and 5.8; the Ca-CAS coated primary emulsion was diluted 100 times with 20 mM CaCl<sub>2</sub> buffer before measurements to avoid multiple scattering effects. The pH of the diluted emulsions was adjusted to 7.0 and 5.8 using 0.1 M NaOH or 0.1M HCl.

### 7.2.7 Characterisations of rheological properties

The rheological characterisations of the emulsions were conducted using AR-G2 stress-controlled rheometer (TA Instruments, Crawley, West Sussex, UK) equipped with a stainless-steel plate and plate geometry (40mm diameter) set to a gap of 1.0 mm. The sample for rheological characterisations was transferred by a flat end stainless-steel spatula from a sample vial to the rheometer's bottom plate set at 25 °C. The geometry plate was lowered to the gap position of 1 mm. Excess emulsion was carefully trimmed out and a thin layer of mineral oil was used to seal the edge of the geometry to prevent water evaporation during the measurement. All the samples were relaxed on the rheometer following a time-sweep for 60 min at 25 °C

with constant strain amplitude of 1% and constant frequency of 1 Hz before further rheological characterisations.

To measure the rheological properties of the emulsion storage at different times, a range of oscillatory experiment were performed at 25 °C: (1) the frequency sweep measurement was carried out at a constant strain of 1% for frequencies ranging from  $10^{-2}$  Hz to  $10^2$  Hz; (2) the strain sweep measurement was performed at a constant frequency of 1 Hz for strain amplitude ranging from  $10^{-1}$  % to  $10^3$  %.

The rheological properties of freshly prepared emulsion with heat-treatment were characterised as well. After time sweep measurements, a temperature sweep measurement was performed at fixed strain of 1% and fixed frequency of 1 Hz with four stages: (1) temperature was increased from 20 to 80 °C with a heating rate of 1°C/min; (2) held at 80°C for 30 min; (3) cooled from 80 to 20 °C with a cooling rate of 1°C/min; and (4) held at 20 °C for 15 min. After that, the frequency-sweep and strain-sweep were performed as described above.

### **7.2.8 Confocal laser scanning microscopy (CLSM)**

The microstructures of the emulsions were examined using a confocal laser scanning microscope (Leica, Heidelberg, Germany) equipped with a 40× magnification oil immersion lens. Fast green and Nile red powder were added to the protein dispersion and soy oil at concentration of 0.05 mg/mL prior to emulsification. The stained emulsion was transferred onto a concave confocal microscope slide with a coverslip. Fast green was excited by a helium–neon laser at 633 nm and the emission between 638 and 750 nm was measured. Nile Red was excited by an argon laser at 488 nm and the emitted fluorescence between 494 and 605 nm was measured. To enhance image quality, sequential scanning was used. Images were captured with

LAS AF software (version 2.7.3.9723) at room temperature. They were analysed using ImageJ software (ImageJ, National Institutes of Health, Bethesda, MD, USA).

### **7.2.9 Statistical analysis**

Each experiment was performed in duplicate using freshly prepared samples. The results are reported as the means and standard deviations. Independent sample T-test of variance were used to compare samples in the SPSS 19.0 package (IBM, Armonk, NY, USA). The significant difference was set at a P-level of 0.05.

### **7.3 Results and discussion**

#### **7.3.1 Formation of DSE concentrated emulsions**

Ca-CAS or nano-sized primary emulsions coated with Ca-CAS were used as emulsifying agents to stabilise the concentrated emulsions in the present study. The particle size and zeta-potential of Ca-CAS and primary emulsions are shown in **Figure 7-1a**. Size distributions of Ca-CAS dispersions and the primary emulsions were monomodal at both pH conditions as shown in **Figure 7-1b**. The  $z$ -average hydrodynamic diameter of Ca-CAS was  $141 \pm 3$  and  $110 \pm 2$  nm at pH 7.0 and 5.8, respectively. The Ca-CAS-coated emulsions were well dispersed at both pH conditions by the electrostatic stabilisation of the Ca-CAS layer. The average diameters,  $d_{4,3}$ , of primary emulsion were  $400 \pm 10$  nm at both pHs. The surface charges of Ca-CAS and the droplets were similar at a given pH, and the zeta-potential value was  $\sim -9$  mV at pH 7.0 and  $\sim -6$  mV at pH 5.8, respectively. The low net charge of Ca-CAS and its droplets was due to the binding and charge screening effect of calcium ions. (Cheng et al., 2022b; Guo et al., 2021; Ma et al., 2009; McCarthy et al., 2014; Sosa-Herrera et al., 2012; Zittle et al., 1958).

#### **7.3.2 Droplet size distribution of the concentrated emulsions**

The droplet size distributions of concentrated emulsions ( $\varphi = 70\%$ ) stabilised by Ca-CAS (PSE) or by primary emulsion (DSE) are shown in **Figure 7-1c-d**. The droplet size distributions of PSE at pH 7.0 and 5.8 were similar, with a prominent peak at  $\sim 20 \mu\text{m}$  (**Figure 7-1c**) and a polydisperse index (PDI) of 0.4. The average droplet diameter ( $d_{4,3}$ ) for PSE at pH 7.0 and pH 5.8 was  $20.06 \pm 1.14$  and  $19.35 \pm 0.36$ , respectively. These droplet size distributions of PSE in the absence of SDS overlapped with those in the presence of SDS, indicating that there was no droplet aggregation in the fresh PSE.

For DSE at pH 5.8, a prominent peak centred at  $\sim 20 \mu\text{m}$  was observed, with a  $d_{4,3}$  of  $14.12 \pm 0.85 \mu\text{m}$  and PDI of 0.5 (**Figure 7-1d**). The slightly smaller  $d_{4,3}$  and larger PDI of DSE at pH

5.8 compared to PSE was due to the present of small size droplets of  $0.2 - 2 \mu\text{m}$ . The  $0.2 - 2 \mu\text{m}$  size droplets could be the mixture of excess primary emulsions and newly formed small size DSE. After dispersing the DSE in the SDS solution, the peak of the small sized droplet population expanded into the smaller size range and between  $\sim 0.1 - 2 \mu\text{m}$  (**Figure 7-1d**), which corresponded to the droplet size distribution of primary emulsion only (**Figure 7-1b**). Note also that SDS will disintegrate the Ca-CAS particles, by suppressing the hydrophobic interactions. The expansion of the peak area of small sized droplet population indicated that the adsorbed primary droplets had been detached by SDS molecules from the interface of the core droplet in DSE (Cheng et al., 2019, 2022a). This result confirmed that the primary droplets have assembled at the interface of the core droplets.

In contrast, DSE at pH 7.0 showed peaks of both the primary emulsion and the core droplets, resulting in the smaller average  $d_{4,3}$  of  $12.08 \pm 0.12 \mu\text{m}$  and the larger PDI of 0.6 than that for DSE at pH 5.8. The droplet size distributions of the DSE at pH 7.0 with and without addition of SDS overlapped.

The average  $d_{4,3}$  of DSE at pH 7.0 and 5.8 with addition of SDS was  $11.89 \pm 0.68 \mu\text{m}$  and  $10.16 \pm 1.35 \mu\text{m}$ , respectively. These results suggested that the adsorption of primary droplets at the interface of the core droplets in DSE was promoted by lowering the pH. Previous studies suggested that for casein-coating layers, bringing the pH down towards the isoelectric point (IEP = 4.6) lead to reducing the strength and range of the interlayer repulsion (Dickinson, 1999; Dickinson et al., 1997). The pH-responsive adsorption of particles have also been widely found in Pickering emulsion stabilized by different proteins or polysaccharides (Cui et al., 2022; Luo et al., 2012; Yang et al., 2007; Zhang et al., 2020a).

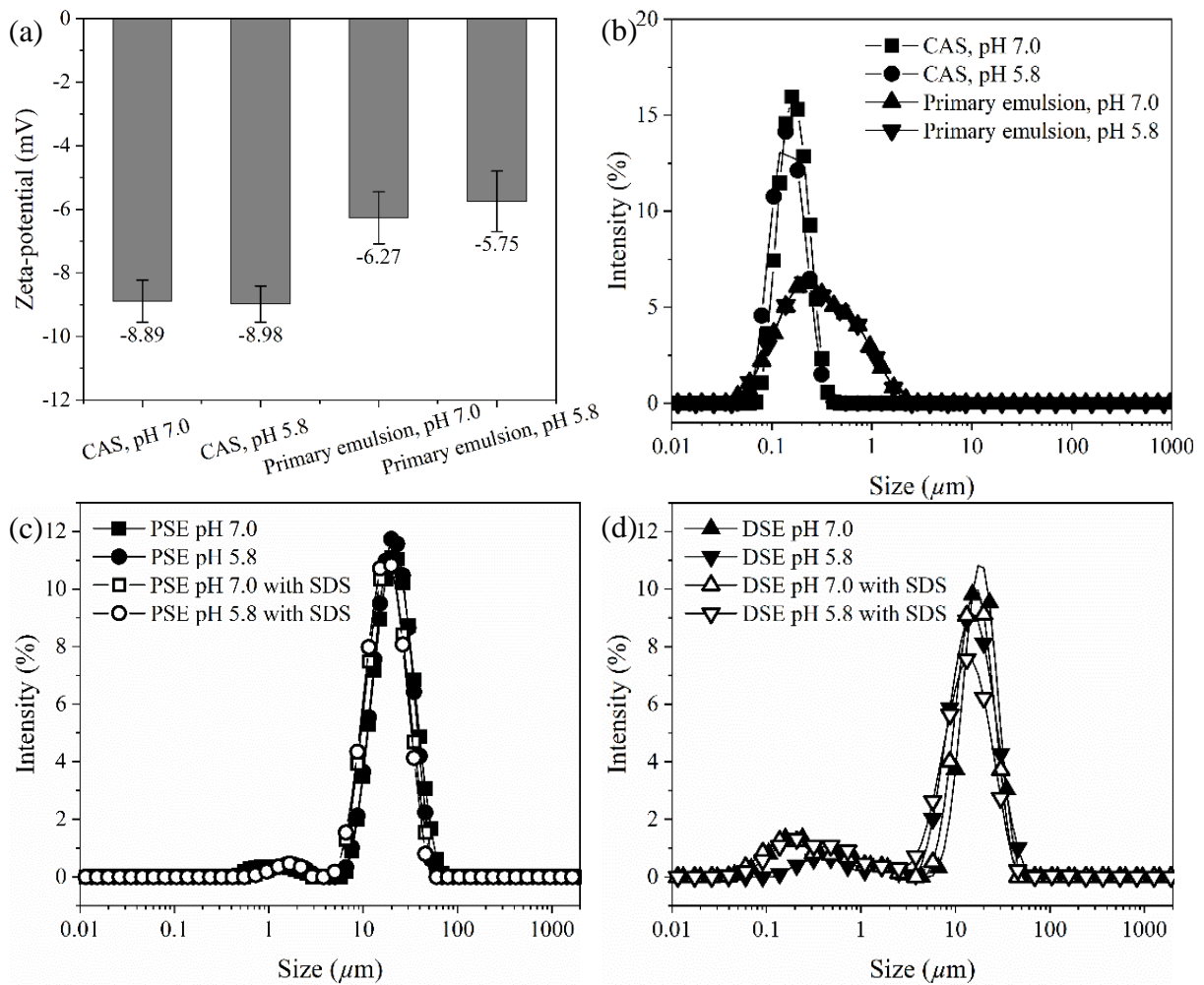


**Figure 7-1:** (a) The zeta-potential of Ca-CAS dispersions and Ca-CAS-stabilized nano-sized primary emulsions at pH 7.0 and 5.8; (b) particles size distributions of Ca-CAS dispersions and Ca-CAS-stabilized nano-sized primary emulsions at pH 7.0 and 5.8; (c) droplet size distributions of Ca-CAS particle stabilized-emulsion (PSE) at pH 7.0 and 5.8 in the absence and presence of SDS; (d) droplet size distributions of droplet stabilized-emulsion (DSE) at pH 7.0 and 5.8 in the absence and presence of SDS.

### 7.3.3 Properties and stability of the concentrated emulsions

As showed in **Figure 7-2 a-d-1**, all emulsions exhibited a good stability without phase separation or oiling-off over 30 days. Except for the fresh DSE at pH 7.0 (**Figure 7-2c-1**), the other three fresh emulsions did not flow when the glass vials were inverted (**Figure 7-2a-1, b-1, & d-1**). This phenomenon indicated that the  $\phi$  as close to the maximum volume fraction of the dispersed phase  $\phi_{max}$  for DSE at pH 5.8, PSE at pH 7.0 and PSE at 5.8, but this was not the case for DSE at pH 7.0. It has been suggested that when the  $\phi$  approaches or exceeds a critical value of  $\phi_{max}$ , droplets are caged by their neighbouring droplets and do not flow, the emulsion thereby transition from a viscous liquid to a viscoelastic material (Mason, 1999). The  $\phi_{max}$  has been well-established as 0.74 for the undeformable spheres with a narrow PDI of 0.1 reaching the hexagonal packing (Mason, 1999; Scott & Kilgour, 1969). However, in a polydisperse emulsion, the  $\phi_{max}$  can be greater than 0.74 because the small droplets can fill the interstitial space between the large droplets (Lubachevsky & Stillinger, 1990; Scott & Kilgour, 1969; Tadros, 1994).

After aging for 30 days, all emulsions did not flow when the glass vials were inverted (**Figure 7-2a-d-2**). To examine the droplet-droplet interactions, the size of the emulsions at different storage times were measured. Except for DSE at pH 7.0, the rest of the emulsions showed an increase in size with storage time, and the droplet flocs in the aged emulsions did not dissociate during the MasterSizer measurements, as shown in **Figure 7-2e**. After dispersing the aged emulsion in SDS solution, the droplet flocs disassociated into the individual droplets of similar size to the fresh droplets (**Figure 7-2f**). These results suggested that (1) all types of emulsions were stable towards droplet coalescence for 30 days; (2) irreversible flocculation or aggregation of droplets developed with time, except for DSE at pH 7.0.



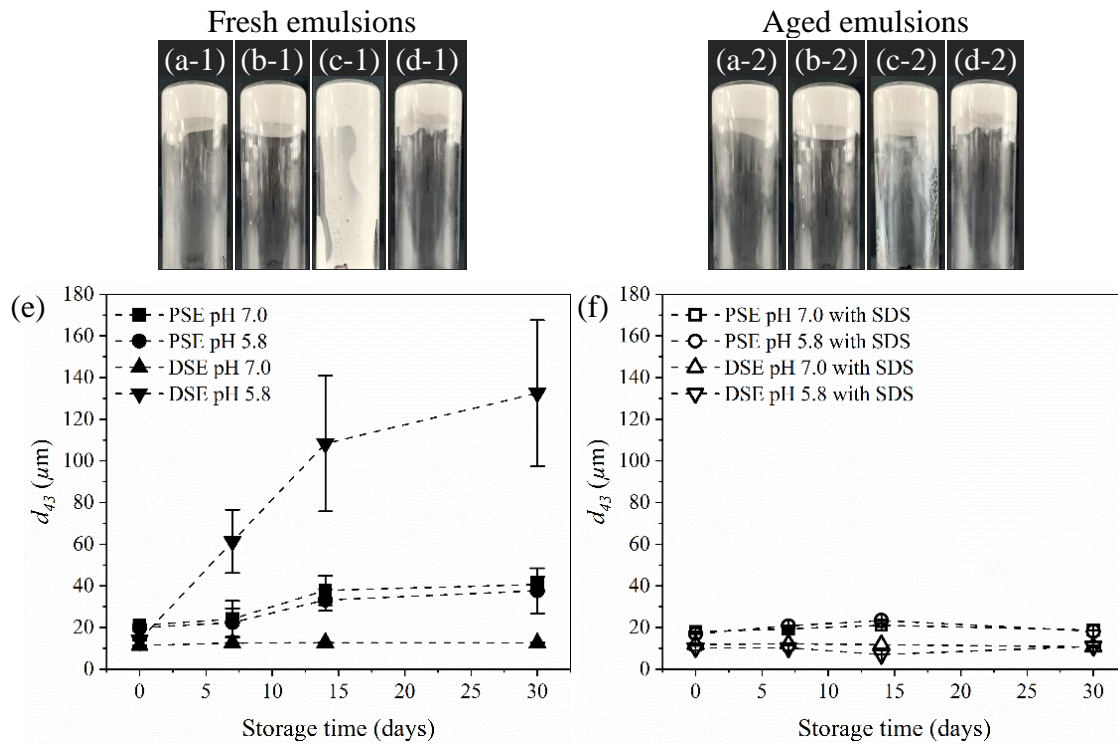


**Figure 7-2:** Appearance of concentrated emulsion with 70% of oil volume fraction in the sealed inverted glass vials for (-1) 0 day and (-2) 30 days. Emulsion stabilized by (a) Ca-CAS at pH 7.0, (b) Ca-CAS at pH 5.8, (c) primary emulsion at pH 7.0, and (d) primary emulsion at pH 5.8. (e) The average droplet size ( $d_{4,3}$ ) of PSE and DSE at pH 7.0 and 5.8 as a function of a storage time for 0, 7, 14 and 30 days. (f) The average droplet size ( $d_{4,3}$ ) of PSE and DSE at pH 7.0 and 5.8 as a function of a storage time for 0, 7, 14 and 30 days in the presence of SDS.

### 7.3.4 Microstructure of concentrated emulsions during aging

CLSM images showed that freshly prepared emulsions had large size droplets of  $\sim 15 \mu\text{m}$  in diameter packed closely and distributed uniformly throughout the field of view (**Figure 7-3a-d-1**). With increasing storage time, the size of individual droplets did not appear to change significantly for all the emulsions (**Figure 7-3a-d-2&3**). These results indicated that droplets stabilised with Ca-CAS or Ca-CAS-coated primary droplets were stable against coalescence over 30 days. The signal in the aqueous phase of PSE suggested the existence of an excess proteins (**Figure 7-3a-b**), while in the aqueous phase of DSE at pH 7.0 suggested the existence of non-adsorbed Ca-CAS-coated droplets (**Figure 7-3c**). The excess proteins in the aqueous phase indicated that the interface of the core droplet in PSE or DSE at pH 7.0 was saturated with Ca-CAS particles. In contrast, there was a lack of signal in the continuous phase of DSE at pH 5.8, indicating that most droplets adsorbed at the interface of the core droplets (**Figure 7-3d**). A thick interfacial layer consisting of nano-sized droplets was observed for all the DSEs at pH 5.8 at different storage times, indicating that interfacial layer of primary droplets also provided long-term stability to the DSE.

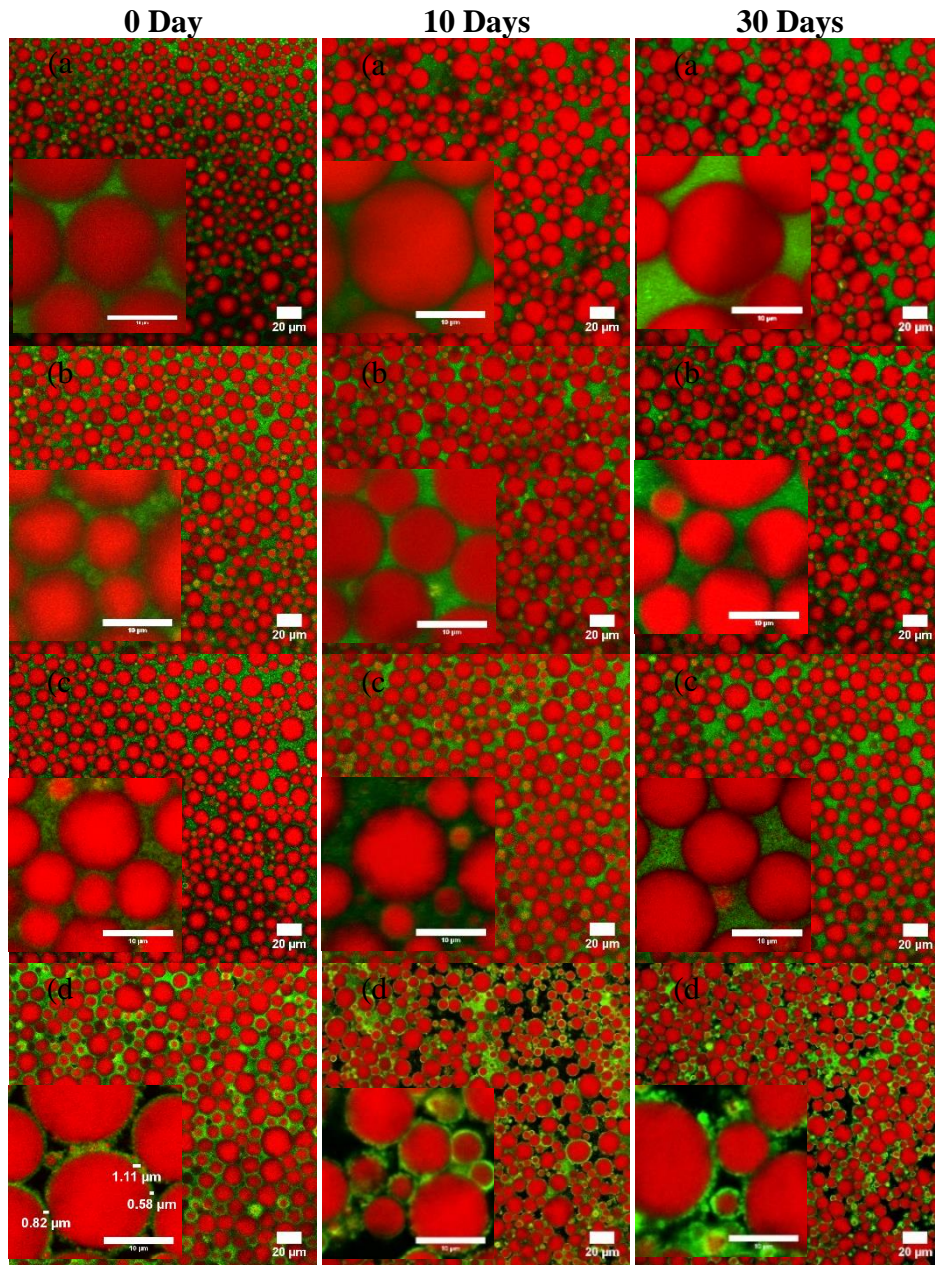


**Figure 7-3:** 63× Magnification confocal images of concentrated emulsion with 70 % of oil volume fraction that stabilized by (a) Ca-CAS at pH 7.0, (b) Ca-CAS at pH 5.8, (c) primary emulsion droplets at pH 7.0, and (d) primary emulsion droplets at pH 5.8 for (-1) 0, (-2) 10 and (-3) 30 days aging. Red colour represents the oil phase stained by Nile red and green colour represents the protein stained by fast green. Scale bar is 20 μm. Insets are associated zoom-in images with scale bar of 10 μm.

**7.3.5 Viscoelasticity of concentrated DSE emulsions during aging**

The frequency sweep test was performed at a fixed strain of 1%, the strain was well within the linear viscoelastic region (LVR) as shown in **Figure 7-4 b-1&-2**. The dependence of storage modulus ( $G'$ ) and loss modulus ( $G''$ ) with frequency for 0 day and 30 days was plotted in **Figure 7-4 a-1&-2**, respectively. For the whole frequency range, both  $G'$  and  $G''$  of all emulsions showed a weak frequency dependence; the  $G'$  of all emulsions was in parallel with and about 9 times higher than the  $G''$ , which suggested that these emulsions were weak gels before and after aging (Gabriele et al., 2001; Ross-Murphy et al., 1993). Similar dynamic weak gel characteristic had been reported for many high internal phase Pickering emulsions stabilized by food-grade particles, such as transglutaminase cross-linked gelatine (Du et al., 2021), casein and casein-hemp protein particles (Chuang et al., 2020), and soy protein/cellulose nanofibrils (Zhang et al., 2020b). The frequency dependence of aging emulsion decreased (**Figure 7-4 a-2**), indicating that inter-droplet motion was reduced after 30 days (Tang & Ghosh, 2021).

To better compare the viscoelasticity of various emulsions at different aging times, the complex modulus  $G^*$  at 1 Hz of emulsions was summarized in **Figure 7-4c** and **Table 7-1**, where  $G^* = (G'^2 + G''^2)^{1/2}$  combining the contribution from both  $G'$  and  $G''$ . In freshly prepared emulsions, the values of  $G^*$  for the PSE at both pH 7.0 ( $238 \pm 15$  Pa) and 5.8 ( $215 \pm 25$  Pa) were not significantly different. As expected, the fresh DSE showed the lowest  $G^*$  ( $126 \pm 15$  Pa) at pH 7.0 due to the high polydispersity, but the highest  $G^*$  ( $1174 \pm 28$  Pa) at pH 5.8. The high  $G^*$  in DSE at pH 5.8 than other emulsions ( $P > 0.05$ ) could suggest that there were DSE droplet-droplet networking through the primary droplets that were entrapped within two interfaces. However, this droplet-droplet network could be weak and reversible, as it can be

broken up by dilution and stirring. This was rejected as no significant change in particle size during SLS measurements (**Figure 7-2e**).

**Table 7-1** Complex moduli  $G^*$  at 1 Hz (Pa) of PSE and DSE at pH 7.0 and 5.8 after 0 day, 30 days aging, and heating at 80 °C for 30 min.

	$G^*$ at 1 Hz (Pa)		
	0 D	30 D	80 °C
PSE, pH 7.0	238 ± 21 <sup>Aa</sup>	403 ± 68 <sup>Ba</sup>	583 ± 76 <sup>Ca</sup>
PSE, pH 5.8	215 ± 35 <sup>Aa</sup>	354 ± 79 <sup>Ba</sup>	653 ± 20 <sup>Ca</sup>
DSE, pH 7.0	126 ± 21 <sup>Ab</sup>	443 ± 127 <sup>Ba</sup>	1312 ± 205 <sup>Cb</sup>
DSE, pH 5.8	1174 ± 39 <sup>Ac</sup>	1685 ± 68 <sup>Bb</sup>	1801 ± 69 <sup>Bc</sup>

Different letters in capitals represent significant differences between different storage time and temperature of the same sample according to SPSS T-test ( $P < 0.05$ ); different letters in lower case represent significant differences between samples at same storage time and temperature. Experimental data are the means of duplicate samples. Numbers in parentheses represent the standard error from duplicates.

Another possible contributor for the high  $G^*$  of DSE at pH 5.8 was the thick interfacial layer for DSE at pH 5.8, which resulted in an increase in the effective volume fraction of the emulsion. When taking a thickness of the interfacial layer,  $h$ , into account, the effective volume fraction,  $\varphi_{eff}$  can be calculated using **equation ((7-1))** (Mason, 1999):

$$\varphi_{eff} \approx \varphi_{core} \left[ 1 + \frac{2h}{D} \right]^3 \quad (7-1)$$

where  $\varphi_{core}$  is oil volume fraction of the large core droplet,  $D$  is the mean droplet diameter ( $D \approx 15 \mu\text{m}$ , given by the emulsion with addition of SDS measured by SLS after excluding the contribution from small droplets), which is valid for  $2h \ll d$  (Erramreddy & Ghosh, 2015; Mason, 1999; Princen et al., 1980; Wilking & Mason, 2007).

For DSE at pH 5.8, the primary droplet layer at the core droplet surface,  $h$ , was contributed to  $\sim 0.87 \mu\text{m}$  thickness as estimated by the difference in large droplet diameter before ( $14.59 \pm 0.17 \mu\text{m}$ ) and after adding SDS ( $12.85 \pm 0.41 \mu\text{m}$ ). The  $\varphi_{eff}$  was calculated as 0.87 which was 1.39 times higher than the set  $\varphi_{core}$  of 0.625 (the primary emulsion accounted for oil volume fraction of 0.075). Similar results have been reported previously that an increase of  $\varphi_{eff}$  by increasing the size ratio of emulsifier to the droplet has led to the dramatic increase in the elasticity of the concentrated emulsion ( $\varphi = 0.3 - 0.9$ ) (Chanamai & McClements, 2000; Erramreddy & Ghosh, 2015; Hemar & Horne, 2000). For DSE at pH 7.0, the difference in the large droplet size before ( $15.44 \pm 0.29 \mu\text{m}$ ) and after adding SDS ( $15.44 \pm 0.34 \mu\text{m}$ ) was not significant. The  $\varphi_{eff}$  of DSE at pH 7.0 should then be similar to the set  $\varphi_{core}$  ( $= 0.625$ ) and was probably below or near to its  $\varphi_{RCP}$  ( $> 0.64$ , due to its polydispersity). Therefore, the highest  $G^*$  of the DSE at pH 5.8 could be attributed to the large  $\varphi_{eff}$  caused by the thick interfacial layer consisting of primary emulsion droplets, while the lowest  $G^*$  of DSE at pH 7.0 among all emulsions could be attributed to its lowest  $\varphi_{eff}$  and high polydispersity.

For PSE, the previous study showed that the thickness of Ca-CAS-particle layer,  $h$ , at the oil-water interfaces is  $\sim 30$  nm (Cheng et al., 2022b). Taking the  $2h$  by Ca-CAS-particles as  $0.06 \mu\text{m}$  ( $h = 0.03 \mu\text{m}$ ), the calculated  $\varphi_{\text{eff}}$  was 0.71 and slightly higher than the  $\varphi_{\text{core}}$  of 0.7 of PSE. This result was consistent with other studies that have used nano-sized protein particles (soy  $\beta$ -conglycinin and ovalbumin) as emulsifier in concentrated emulsions where the thickness of the interfacial layer had a negligible effect on the viscoelasticity of the emulsion (Xu et al., 2018, 2019).

During aging, the  $G^*$  of PSE increased to  $\sim 400$  Pa after 7 days at both pH values and then did not change during further storage. The  $G^*$  of DSE at pH 7.0 were  $13 \pm 3$ ,  $32 \pm 20$  and  $443 \pm 184$  Pa for 7, 14 and 30 days, respectively, which were significantly lower or higher than that of the fresh sample. In contrast to DSE at pH 7.0, the  $G^*$  of DSE at pH 5.8 steadily increased with aging time. The  $G^*$  of DSE at pH 5.8 increased from  $1174 \pm 28$  at fresh state to  $1430 \pm 18$  Pa after 7 days of aging. The subsequent increase in  $G^*$  was not significant between 14 ( $1650 \pm 127$  Pa) and 30 days ( $1686 \pm 68$  Pa) of aging. The trend of the increase in  $G^*$  was similar between DSE at pH 5.8 and PSE at both pH values, suggesting that the three emulsions may follow the same mechanism of re-structuring during aging. The fluctuation of  $G^*$  from DSE at pH 7.0 was possibly a result from the weak and inhomogeneous spatial structure during aging for 0-14 days which formed a stable network after 30 days.

A possible mechanism accounting for the increase in  $G^*$  of emulsion during storage could be the gravity-driven microphase separation and protein-protein aggregation in order to reduce the Gibbs free energy in the emulsion (Tadros, 2004). Tadros (2004) suggested that the contraction of the droplet network during the storage could be driven by gravity force if the droplet size is larger than  $1 \mu\text{m}$ , resulting in phase separation. Between the close contact droplets, the droplet-droplet aggregation might occur, resulting in irreversible increase in



droplet size as shown in SLS measurements **Figure 7-2e**. Due to the low zeta potential (6 - 9 mV absolute) and high electrolyte concentration (20 mM CaCl<sub>2</sub>) in these emulsions, irreversible aggregation between the adsorbed proteins may be caused by calcium ion cross-linking, electrostatic and/or hydrophobic interactions. Nevertheless, the positive relationship between the droplet flocculation and the  $G'$  of emulsions with storage time has been previously reported; this is because the droplet clusters with the entrapped aqueous phase enhance the effective volume fraction of emulsion, resulting in a greater  $G'$  (Anton et al., 2001; Hayati et al., 2007; Tadros, 2004). The  $G^*$  of DSE at pH 5.8 after 30 days was significantly higher, which might be attributed to both the gravity-driven microphase separation and its initial high viscoelasticity.

The stability of emulsion under the large deformation oscillation is shown in **Figure 7-4 b-1&-2**, in which  $G'$  and  $G''$  were plotted against the applied strain amplitude at a fixed frequency of 1 Hz. Within the LVR, all emulsions exhibited a gel-like behaviour, in which  $G'$  was higher than  $G''$ , with both  $G'$  and  $G''$  being independent of the applied strain until a certain critical strain point. The critical strain point could be defined as both  $G'$  and  $G''$  started to deviate from the LVR, which suggested that the sample started to flow. For fresh emulsions (**Figure 7-4 b-1**), the maximum strain of the LVR was in the order DSE at pH 5.8 ( $9.95 \pm 0.16\%$ ) > PSE at both pH ( $7.34 \pm 1.00\%$ ) > DSE at pH 7.0 ( $1.60 \pm 0.00\%$ ). After 30 days (**Figure 7-4 b-2**), the maximum strain of the LVR of all emulsions was increased as DSE at pH 5.8 ( $25.57 \pm 0.79\%$ )  $\approx$  PSE at both pH ( $25.55 \pm 0.12\%$ ) > DSE at pH 7.0 ( $4.55 \pm 0.48\%$ ). Compared to the other three emulsions, DSE at pH 7.0 had a weaker inter-droplet interaction at a given storage time that was attributed to its broad distribution and low  $\varphi_{\text{eff}}$ .

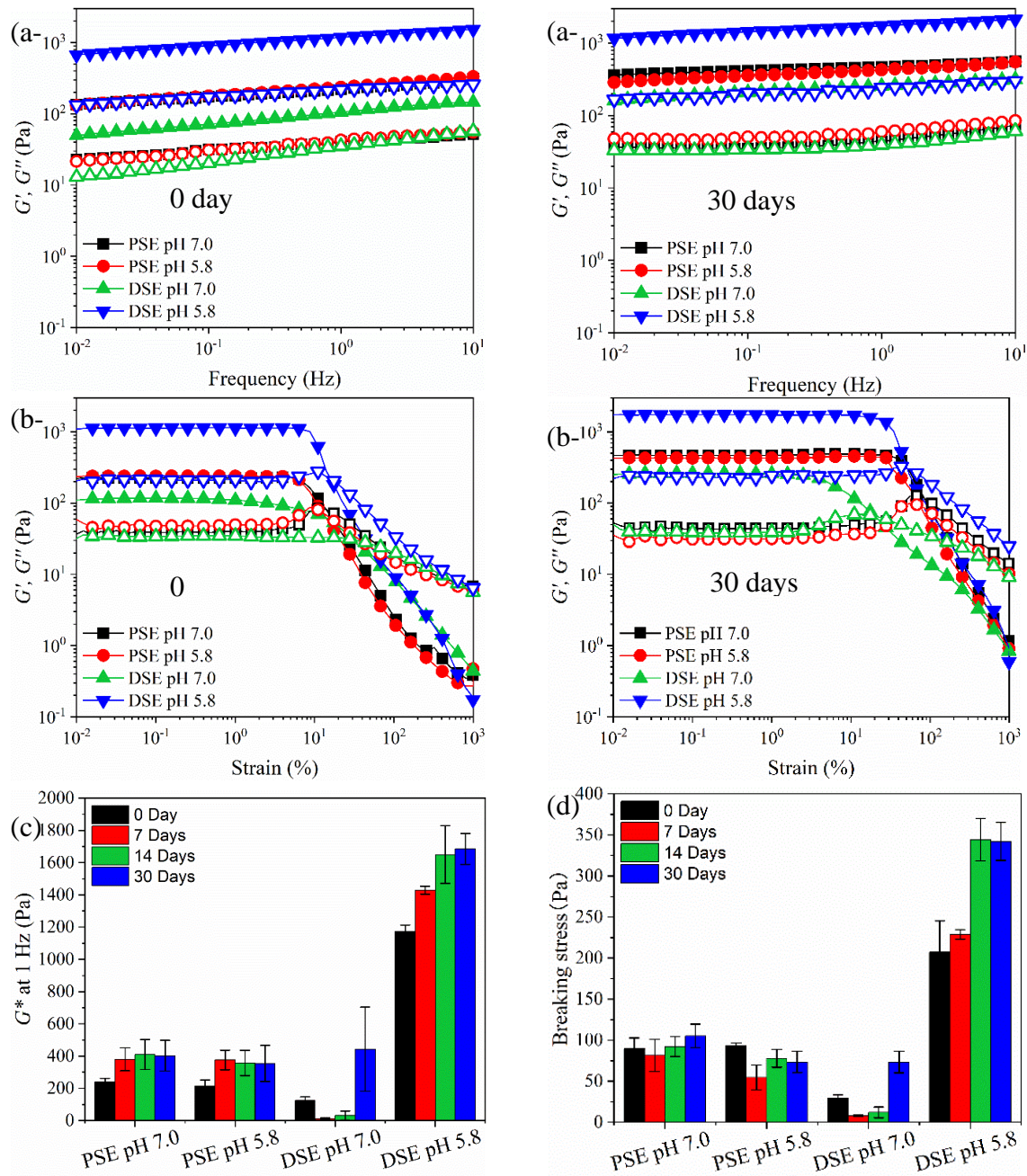


**Figure 7-4:**  $G'$  (solid symbols) and  $G''$  (open symbols) as (a) a function of frequency and (b) as a function of the strain for concentrated emulsion PSE (stabilized by Ca-CAS) and DSE (stabilised by primary emulsion) at pH 5.8 and pH 7.0 at (1) 0 day and (2) 30 days aging. (c) Complex modulus  $G^*$  (1Hz) and (d) breaking stress of PSE and DSE at pH 7.0 and 5.8 as the function of aging time.

**7.3.6 Stability of concentrated emulsions against heating**

After heating at 80 °C for 30 min, all the freshly made concentrated emulsions gelled, without phase separation, and did not flow when the glass vials were inverted (**Figure 7-5a-d**). The droplet size of heated emulsions in the absence or the presence of SDS is shown in **Figure 7-5e-f**. There was no significant difference ( $P > 0.05$ ) in the size of emulsion droplets both in the presence and the absence of SDS before and after heating. This result indicated that emulsions coated with Ca-CAS layer or primary droplet layer were stable against coalescence during heating.

The microstructures of the heated emulsion observed by CLSM are shown in **Figure 7-5 g-j**. As shown in the confocal images, the size of the core droplets after heating remained similar to the size of the fresh emulsion (**Figure 7-3a-d-1**), confirming that there was no droplet coalescence of core droplets stabilized by either the Ca-CAS layer or primary droplet layer during heating process.

For PSE after heating, the droplet network was consisted of the protein-rich and protein-poor regions (**Figure 7-5g-h, insets**). In the protein-rich region, two droplet interfaces were connected by protein aggregates, or in another words, the protein aggregates were entrapped among the droplets. In the protein-poor region, interfaces of the droplets lacked of protein signals because these areas were covered by small size protein particles. Some of the droplet network of PSE was disconnected in the protein-poor region due to the lack of the large protein aggregates to fill the gaps between the droplets. In contrast, the network of DSE was continuous and tight. The core droplets was embedded in the matrix and were made up of aggregated primary droplets (**Figure 7-5i-j, insets**). The different network structures for PSE and DSE were probably affected by the concentration of the free protein in the continuous phase. As compared to that in PSE, the total specific surface area of DSE was larger due to the presence

of the primary droplets. The large surface area in DSE, hence, had used most of the Ca-CAS for the interface stabilization and a small amount of non-adsorbed Ca-CAS was left in the aqueous phase. Upon heating, the non-adsorbed Ca-CAS in PSE could move through the crowded droplets and aggregate together due to their small original size about one hundred nanometres, resulting in protein aggregates randomly distributed throughout the emulsion. For DSE, as most of Ca-CAS had initially adsorbed to the interfaces of the primary droplets, the heat-induced aggregation was mainly attributed to the adsorbed protein layers and the free non-adsorbed Ca-CAS. Given the size of primary droplets was large, the movement of the primary droplets in the DSE was hindered by crowded droplets, so that the protein aggregation mainly occurred locally between the adsorbed protein layers and non-adsorbed Ca-CAS. Consequently, the non-adsorbed Ca-CAS particles and primary droplets formed a matrix which entrapped the core droplets. Herewith, the heated emulsion would be seen as an emulsion gel due to the coherent three-dimensional network in DSE and in the protein-rich regime of PSE (Nishinari, 2009).

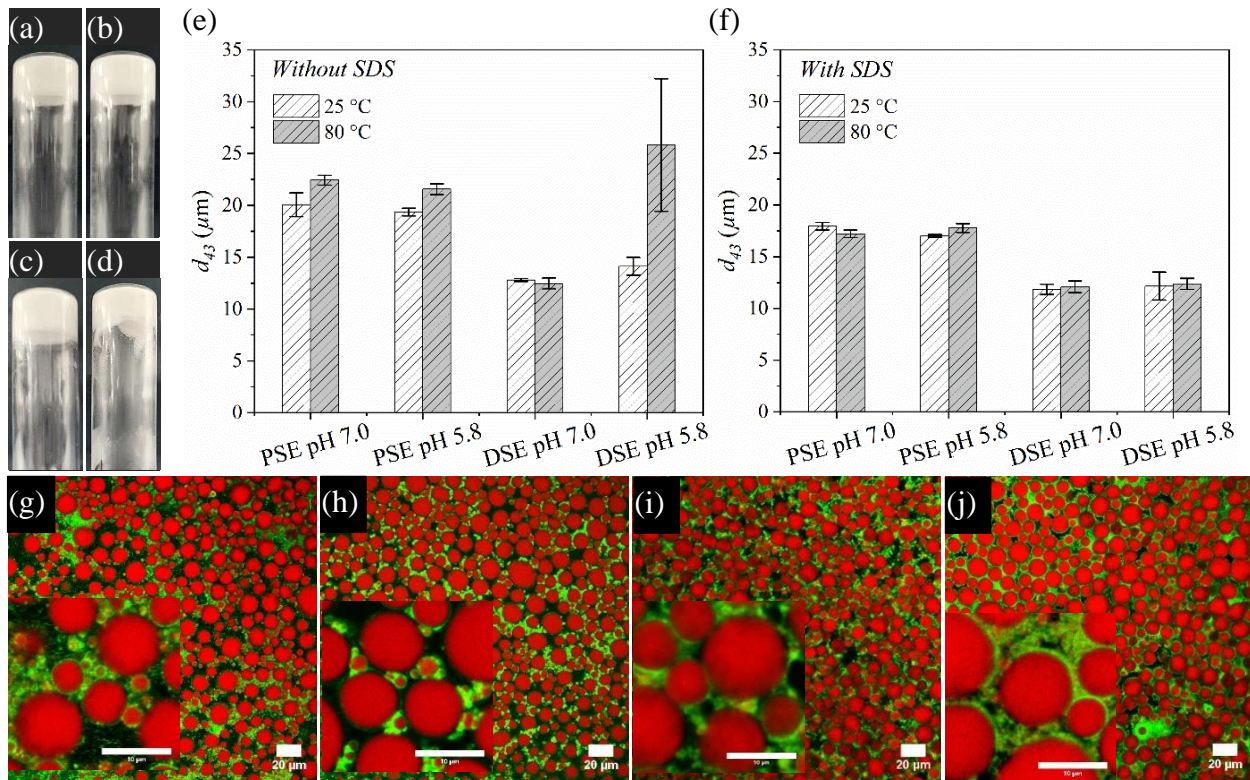


**Figure 7-5:** Appearance (left panel) of 70 % concentrated emulsions stabilized by (a) Ca-CAS at pH 7.0, (b) Ca-CAS at pH 5.8, (c) primary emulsion at pH 7.0, and (d) primary emulsion at pH 5.8 in the inverted seal glass vials after heating in oven at 80 °C for 30 min. The average droplet size ( $d_{4,3}$ ) of PSE and DSE at pH 7.0 and 5.8 before and after heating (e) with the absence of SDS and (f) with the presence of SDS. 63 $\times$  Magnification confocal images of concentrated emulsion that stabilized by (G) Ca-CAS at pH 7.0, (h) Ca-CAS at pH 5.8, (i) primary emulsion droplets at pH 7.0, and (j) primary emulsion droplets at pH 5.8 after heating. Scale bar is 20  $\mu\text{m}$ . Insets are associated zoom-in images with scale bar of 10  $\mu\text{m}$ .

**7.3.7 Viscoelasticity of concentrated emulsions after heating**

The changes in the elasticity of the emulsions with the heating temperature were monitored by the temperature ramp (**Figure 7-6a, inset**). The rapid increase in  $G'$  with the increasing temperature indicated that the emulsion converted into an emulsion gel. The rapid increase in  $G'$  in all the emulsions started at  $\sim 40$  °C, which was consistent with the previously reported gelation temperature ( $\sim 40$  °C) of caseinate-stabilized emulsions or casein micelles solutions in the presence of  $\text{Ca}^{2+}$  (Balakrishnan et al., 2018; Dickinson & Casanova, 1999; McCarthy et al., 2014). When the temperature arrived to 80 °C, the  $G'$  of all emulsion gels reached a plateau level over the time sweep at 80 °C for 30 min. The stable  $G'$  of the emulsion over the holding time confirmed that the structure of emulsion gels resisted to heat-induced destabilization, such as droplet coalescence, phase separation or syneresis. The gel strength further increased during the cooling step, which was possibly attributed to the increase in the strength of hydrogen bonds at low temperatures (Cordier & Grzesiek, 2002).

The subsequent frequency-dependent  $G'$  and  $G''$  of PSE and DSE is plotted in **Figure 7-6a**. The weak frequency dependence of both  $G'$  and  $G''$  suggested that all the heated emulsions were weak gels (Gabriele et al., 2001; Ross-Murphy et al., 1993). As compared to the unheated emulsion (**Figure 7-4a-1**), the frequency dependence of the heated emulsion was less pronounced (**Figure 7-6a**) (Tang & Ghosh, 2021). This result was consistent with the observations that all emulsions did not flow in the inverted tube after heating (**Figure 7-5a-d**) and the droplets were bridged together after heating (**Figure 7-5g-j**).

The gel strength of unheated emulsion and heated emulsions was represented by the complex modulus  $G^*$  at 1 Hz as presented in **Figure 7-6b** and **Table 7-1**. The  $G^*$  of the emulsion was significantly increased after heat-treatment compared to that of the unheated

emulsions. The gel strength of heated PSE did not show a significant dependency on the pH, whereas the gel strength of heated DSE did (**Table 7-1**).

The large deformation rheological properties of heat-induced emulsion gels were measured by strain sweep as shown in **Figure 7-6c**, in which  $G'$  and  $G''$  were plotted against the applied strain amplitude. All the samples exhibited a gel like behaviours in the LVR, both  $G'$  and  $G''$  were independent of the applied strain up to the critical strain point. For all the heated emulsions, at a strain close to the critical strain point, the  $G''$  showed the over-shoot feature, indicating the presence of droplet compression in the heated emulsion causing the high energy dissipation before the breakdown of network (Seth et al., 2011).

The breaking stress of the unheated and heated emulsions was summarized in **Figure 7-6d**. As shown in **Figure 7-6d**, the breaking stress of emulsion was significantly increased by the heat-treatment, indicating that the heated emulsions had a higher stability towards large deformation than the unheated emulsions. The breaking stress of emulsions shared a similar trend to their  $G^*$  suggesting their large deformation behaviour correlated well with the small deformation viscoelastic behaviour. It was clear that the greater average  $G^*$  and breaking stress in heated emulsions resulted from the heated-induced protein-protein aggregation (**Figure 7-5g-j**) and droplet flocculation (**Figure 7-5e-f**). Since the heat-induced interactions were superimposed on the droplet interactions provided by the adsorbed primary droplet layer, the  $G^*$  and breaking stress of DSE at pH 5.8 were significantly higher than that at pH 7.0.

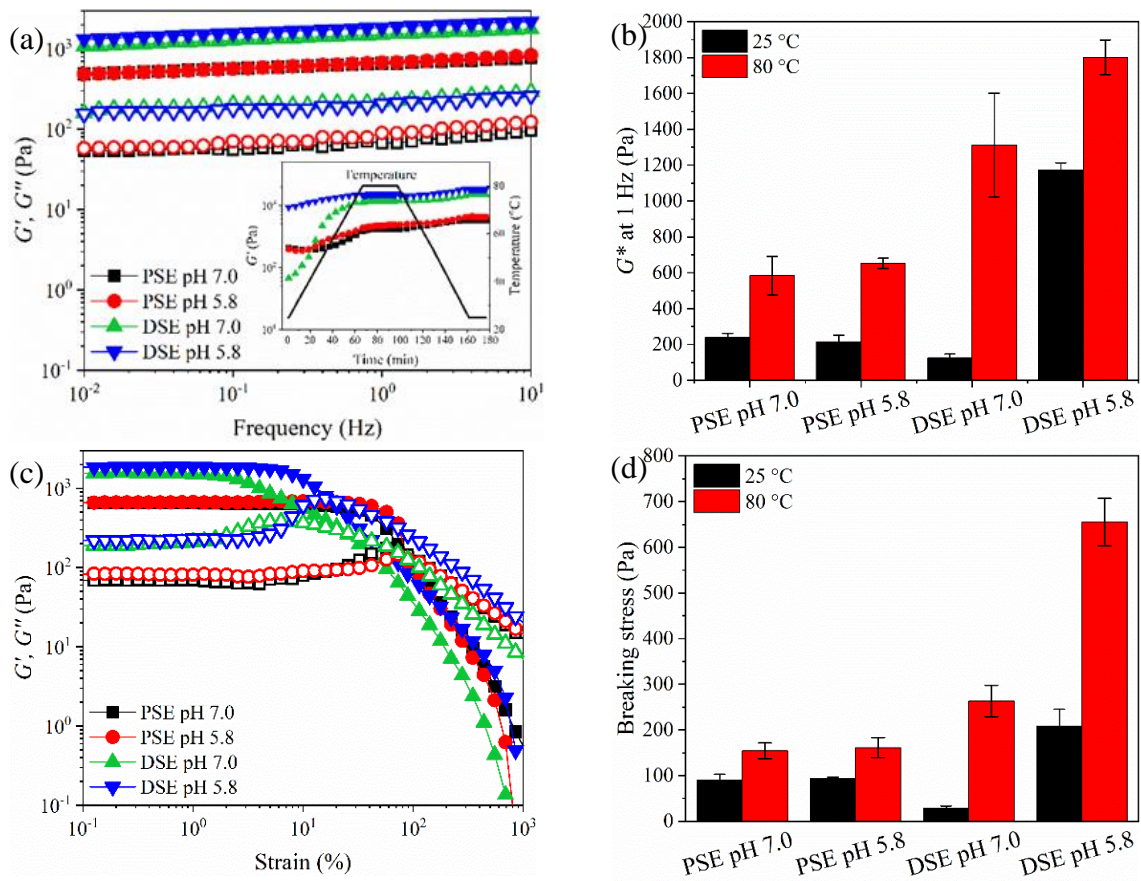


**Figure 7-6:** (a) The frequency dependence, (c) strain amplitude behaviour, and (e) viscosity of  $G'$  (solid symbols) and  $G''$  (open symbols) for concentrated emulsion stabilized by Ca-CAS and primary emulsion at pH 5.8 and pH 7.0 after heating at 80 °C for 30 min. (b) The complex moduli  $G^*$  (1Hz), (d) breaking stress and (f) intermediate shear rate ( $1 \text{ s}^{-1}$ ) viscosity for PSE and DSE at pH 7.0 and 5.8 as the function of temperature at 25 and 80 °C.



## 7.4 Conclusions

In this study, Ca-CAS particles and Ca-CAS coated nano-sized primary emulsions exhibited good dispersion at both pH 7.0 and 5.8, and they were used as emulsifying agents in the subsequent 70% oil-in-water emulsion preparation. The viscoelasticity of the concentrated emulsion stabilized by Ca-CAS (PSE) was insensitive to pH in the range between 7.0 and 5.8. When the primary emulsion was used as the emulsifier to stabilise emulsion (DSE), the viscoelasticity of the concentrated emulsion was altered. By lowering the pH from 7.0 to 5.8, the adsorption of primary emulsion droplets at the oil-water interfaces was promoted, wgcg reduced polydispersity. The thick droplet layer at the surface of the core droplet in DSE formed at pH 5.8 increased the effective volume fraction of the core droplet phase by a factor of 1.39, whereas the Ca-CAS layer of PSE increase the effective volume fraction of the core droplet phase by a factor of 1.01, leading to a ~6-fold higher viscoelasticity of DSE compared to PSE in the fresh state.

After the long-term storage (30 days) and heat-treatment (80°C for 30 min), all concentrated emulsions showed excellent stability against droplet coalescence, and transformed into self-supporting gels. Compared to the other three emulsions, DSE at pH 5.8 exhibited the highest viscoelasticity, because the positive effects of aging and heating superimposed on its initially high viscoelasticity. The significant increase in the viscoelasticity in the aged emulsions was attributed to the gravity-driven microphase separation and droplet flocculation. The droplet flocs together with the entrapped aqueous phase led to the increase in effective volume fraction. Heating the emulsions to 80 °C led to a dramatic increase in the rheological properties with the highest viscoelasticity. With increasing temperature, the hydrophobic interactions between proteins increased resulting in protein aggregation between the non-adsorbed proteins themselves and/or between the non-adsorbed proteins and adsorbed proteins. The touching

droplets were associated together through the protein aggregates or primary droplets, forming a three-dimensional droplet network. This study provided us with a clear picture of using droplet-stabilised interface in improving the mechanical strength of food-graded concentrated emulsion.

### **7.5 Acknowledgements**

This work was funded by the Riddet Institute, a National Centre of Research Excellence, and by the New Zealand Tertiary Education Commission. We also thank the Manawatu Microscopy and Imaging Centre at Massey University for technical support.

---

## Chapter 8 Overall conclusions, discussion and future recommendations

### 8.1 Overall conclusions and discussion

In this project, the overall aim was to understand the formation, stability, and functionality of DSE as affected by the type of emulsifier and the environmental stresses. A series of experiments were conducted to characterise the physico-chemical properties and structures of the material comprising the droplet-stabilised emulsion (DSE), from the protein particles, primary emulsion (coated with protein particles) and the resultant DSE (stabilised by primary emulsion droplets), as well as to study the stability of DSE at various conditions, such as the oil mixing between the surface and core droplet, the droplet destabilisation under simulated physiological conditions, and the droplet interaction during long-term storage and heating.

This research demonstrated that DSE was an oil-in-water emulsion in which the emulsifier comprised of nano-sized primary emulsion droplet coated with protein particles, such as whey protein microgel (WPM) and  $\text{Ca}^{2+}$  cross-linked sodium caseinate (Ca-CAS) particles. The WPM particles were obtained by heating 10 wt% whey protein isolate at pH 5.9 with z-average hydrodynamic diameters ( $D_h$ ) of  $270.9 \pm 4.7$  nm. The interfacial tension of WPM particle at the oil-water interfaces was approximately 13 mN/m. The WPM particles did not exhibit flattening and penetration at the oil-water interface as observed by transmission electron microscope. Compared to WPM, Ca-CAS particles can be formed at lower protein concentrations and result in smaller particle sizes, which was obtained by mixing the 3 % w/w sodium caseinate with 20 mM  $\text{CaCl}_2$  with a  $D_h$  of  $132.6 \pm 5.0$  nm. As measured by small-angle X-ray scattering (SAXS), the Ca-CAS particles were self-assembled from the small  $\text{Ca}^{2+}$ -cross-linked particles ( $R_g \sim 6.5\text{--}8.0$  nm). The Ca-CAS particles showed a fast adsorption at the oil-

water interface, giving an interfacial tension value of  $9.54 \pm 0.14$  mN/m, lower than the interfacial tension value of WPM at the oil-water interface. The oil–water interface stabilised by Ca-CAS particles was  $\sim 30$  nm thick as analysed by small angle neutron scattering with contrast variation technique (CV-SANS), which was smaller than their corresponding  $D_h$  in solution  $\sim 133$  nm for Ca-CAS. It was suggesting Ca-CAS particles were flexible and can adjust their conformation to cover the interface, leading to efficient film formation. The deformation and the spreading of Ca-CAS were similar to that of the flexible casein micelles reported in previous studies (Robson & Dalgleish, 1987; Ye et al., 2013b). The interfacial properties of protein particles subsequently influenced the structure of the primary emulsion droplets as well as the roughness of the DSE interfacial layer.

The primary emulsions coated by WPM were flocculated with a Sauter mean diameter ( $d_{32}$ ) of  $\sim 15$   $\mu\text{m}$  and a mass fractal dimension of  $\sim 2.75$ , as determined by static light scattering (SLS), SANS and ultra-SANS (USANS). As probed by USANS, the DSE interface formed by the primary emulsion droplets was extremely rough and had a surface fractal dimension value of 3.0. The extreme rough interface of DSE was probably due to the formation of a multilayer structure by the adsorbed primary emulsion droplets which flocculated with each other prior to adsorption. In contrast, the primary emulsions coated by Ca-CAS particles were well-dispersed monomodal with a De Broukere mean diameter ( $d_{4,3}$ ) of  $< 0.68$   $\mu\text{m}$  or a gyration radius  $R_g$  of  $0.37$   $\mu\text{m}$  as measured by USANS. The subsequent formed DSE was also monomodal distribution with a  $d_{4,3}$  values of  $\sim 21$   $\mu\text{m}$ , which was smaller than that stabilised with WPM-coated primary emulsion with a  $d_{4,3}$  values of  $\sim 32$   $\mu\text{m}$ . The soft and flexible protein particles, hence, was able to improve the emulsification capability of primary emulsions. The surface fractal dimension value was 3.7 for the DSE stabilised by droplets coated with Ca-CAS,

indicating a rough interfacial layer; however, it was more compact and smoother than the interfacial layer of DSE stabilised by droplets coated with WPM.

The oil mixing between the surface adsorbed droplets and the core droplet were investigated using time-resolved CV-USANS and CV-SANS and the DSE containing *d*-toluene stabilised with Ca-CAS coated soy-oil droplets. The homogenisation process in preparing the DSE induced a rapid oil mixing between droplets, resulting in a homogenous mixed oil distributed at different length scale in the hierarchical emulsion. In an emulsion by simply mixing the primary droplet and large size droplet without external vigorous agitation, the oil mixing process was slow down. The droplet collision was responsible for the oil transfer between droplets through inducing local synchronous interfacial thinning upon droplet contact. In comparison to emulsion containing short-chain length oil stabilised by surfactant (Lee & Pozzo, 2019; Roger et al., 2015), the protein layer of Ca-CAS particles appeared to slow down oil mixing process. It would be interesting to extend this study to the DSE containing long-chain length oils to understand the control of oil mixing in DSE preparation and prepared by varying the degrees of homogenisation pressure. This knowledge will bring an array of possibilities for using emulsions as delivery carriers and controlling the location of active compound in a hierarchical emulsion.

The effect of the droplet layer (consisted of Ca-CAS and soy oil) on the structural stability and on the FFA release of DSE was studied using *in-vitro* simulated digestion models consisting of dynamic stomach digestion and static intestinal digestion. A Ca-CAS-stabilised emulsion (PSE) was used as a control, with a similar droplet size distribution and the same composition as the DSE. This study demonstrated that under gastric pH close to the isoelectric point of caseins (~ pH 4.6), the dense and thick interface layer composed of small emulsion droplets prevented the emulsions from flocculation and coalescence. In contrast, the

polydisperse emulsion stabilized by CA-CAS particles showed extensive droplet flocculation and coalescence which was similar to conventional casein-stabilized emulsions (Wang et al., 2019; Ye et al., 2020). The droplet-stabilised interface of the emulsion contributed to a smaller droplet size after gastric digestion. The extent of the lipid digestion was mainly associated with the droplet size distribution in the emulsions emptied from the stomach, thus leading to a slightly greater amount of FFA release from the DSE during the small intestinal digestion. In addition, the polydisperse droplets resulted in different rates of FFA release during the intestinal digestion, with the smaller droplets having a faster rate of FFA release at the beginning of the digestion. The droplet-stabilised interfaces of DSE were disassembled and resulted in polydisperse emulsion droplets in the small intestinal phase. This study provides useful information for designing novel food structures with controlled digestibility, while promoting the understanding on the digestion of the polydisperse emulsion systems consisting of a broad range of droplet sizes.

The modification of the interfacial layer from the conventional protein layer to droplet layer has also affected the rheological properties of emulsion. Meanwhile, environmental conditions including pH, storage time and temperature can further modulate the rheological properties of emulsions. In this study, Ca-CAS particles and Ca-CAS coated primary emulsions were used as emulsifiers in the 70% oil-in-water emulsion preparation at both pH 7.0 and 5.8. The viscoelasticity of the concentrated emulsion stabilized by Ca-CAS (PSE) were insensitive to pH in the range between 7.0 and 5.8. In contrast, the viscoelasticity of the concentrated DSE was improved with increasing adsorption of primary emulsion by lowering the pH from 7.0 to 5.8. The thick droplet layer of DSE formed at pH 5.8 increased the effective volume fraction of the core droplet phase by a factor of 1.39, whereas the Ca-CAS layer of PSE was thin and increased the effective volume fraction of the core droplet phase by a factor of 1.01. The greater

effective volume fraction of DSE resulted in the higher viscoelasticity of DSE, which was ~6-fold higher compared to PSE at fresh state. After the long-term storage (30 days) and heat-treatment (80°C for 30 min), all concentrated emulsions were self-supporting gels and showed excellent stability against droplet coalescence. The significant increase in the viscoelasticity in the aged emulsion was attributed to the gravity-driven microphase separation and droplet flocculation. The droplet flocs together with the entrapped aqueous phase led to the increase in effective volume fraction. Heating the emulsions to 80 °C led to a dramatic increase in the rheological properties. At the increasing temperature, the hydrophobic interactions between proteins were increased, resulting in protein aggregation between the non-adsorbed proteins themselves and/or between the non-adsorbed proteins and adsorbed proteins. The touching droplets were associated together through the protein aggregates or primary droplets, forming a three-dimensional droplet network. The highest viscoelasticity of DSE at pH 5.8 after aging and heating was because the positive effects of aging and heating superimposed on its initially high viscoelasticity. This study provided a clear picture of how droplet-stabilised interface can be used in improving the mechanical strength of food-graded concentrated emulsion.

Overall, the structure and interfacial properties of the protein particles played a crucial role in the formation and structure of the primary emulsion and the DSE. By controlling the excess, non-adsorbed protein, and pH in the aqueous phase of the primary emulsion, the adsorption of primary emulsion droplets onto the surface of DSE core droplets was tuneable, and thus the digestion behaviour and rheological properties of DSE was adjustable. In addition, in this project the oil molecules transportation between the surface and the core droplets of DSE was investigated, extending the length scale of the study of oil-exchange from the conventional nanoscale to the micron scale by improving the methodology of CV-USANS. The information

gained from this project will contribute to the development of various functional foods using structured emulsions with new and adjustable interface design.

### 8.2 Recommendations for future work

#### 8.2.1 Protein particles

Protein particles derived from other animal sources (e.g., egg and fish), or plant and microbial based sources can be considered to use to form the droplet-stabilised emulsion as the alternative to milk-protein-based emulsion foods. By controlling the density of the cross-linking (e.g., Maillard glycation, pH, divalent ions, cross-linkers) within the protein particles, the adsorption behaviour of protein particle-coated primary emulsion droplets and the interfacial layer structure of DSE will be altered. A relationship between the interfacial rheology of the protein particles/primary emulsion droplets and the bulk rheology of the DSE would be of interest.

#### 8.2.2 Oil mixing study

In Chapter 5, we established a method for *in-situ* monitoring of the exchange of oil molecules between different droplets. As the chain-length of the oil affect to the kinetics of oil transportation, it is recommended to use isotopic (D/H) long-chain *n*-alkanes with chain-lengths comparable to those of edible oils to further validate the mixing process between surface and core oils in DSE. It is recommended to consider the effect of factors such as input energy, temperature, type of protein particles, concentration of primary emulsions, and viscosity of the continuous phase of primary emulsions on the extent of oil mixing.

#### 8.2.3 Emulsion rheology

DSE has been demonstrated to form an emulsion gel after heating, with an enhanced gel strength than traditional protein-stabilised emulsion at given compositions. It is recommended



to compare the rheological properties of the DSE gel formed with different concentration of primary emulsion, as well as formed with different types of proteins (rigid vs. soft). Moreover, the polysaccharides, such as charged pectin or neutral starch, could be involved in the gel system. The interactions and concentration ratio between the DSE droplet and polysaccharides could modulate the gel strength and affect sensory perception, gel breakdown, protein hydrolysis, lipid digestion and bioaccessibility of bioactive compounds.

### **8.2.4 Emulsion digestion**

In the current study, the emulsion digestions had been conducted on the liquid emulsion. It is recommended to extend the digestion study to semi-solid emulsion gels that consisting of different compositions (e.g., proteins, oils, and polysaccharides) and structures. In the digestion of semi-solid samples, it is recommended to use an integrated digestion model that includes oral, gastric, and intestinal phase, because the digestion behaviour is affected by the breakdown of the structure since the oral phase.

**Bibliography**

- Abdullah, Weiss, J., Ahmad, T., Zhang, C., & Zhang, H. (2020). A review of recent progress on high internal-phase Pickering emulsions in food science. *Trends in Food Science and Technology*, *106*, 91–103. <https://doi.org/10.1016/j.tifs.2020.10.016>
- Acevedo-Fani, A., & Singh, H. (2022). Biophysical insights into modulating lipid digestion in food emulsions. *Progress in Lipid Research*, *85*, 101129. <https://doi.org/10.1016/j.plipres.2021.101129>
- Akbari, S., & Nour, A. H. (2018). Emulsion types, stability mechanisms and rheology: A review. *International Journal of Innovative Research and Scientific Studies*, *1*(1), 11–17. <https://doi.org/10.53894/ijirss.v1i1.4>
- Ako, K., Nicolai, T., & Durand, D. (2010). Salt-induced gelation of globular protein aggregates: Structure and kinetics. *Biomacromolecules*, *11*(4), 864–871. <https://doi.org/10.1021/bm9011437>
- Alvarez, G., Jestin, J., Argillier, J. F., & Langevin, D. (2009). Small-angle neutron scattering study of crude oil emulsions: structure of the oil–water interfaces. *Langmuir*, *25*(7), 3985–3990. <https://doi.org/10.1021/la802736c>
- Amagliani, L., O'Regan, J., Kelly, A. L., & O'Mahony, J. A. (2022). Influence of low molecular weight surfactants on the stability of model infant formula emulsions based on hydrolyzed rice protein. *LWT*, *154*, 112544. <https://doi.org/10.1016/j.lwt.2021.112544>
- Anton, M., Chapleau, N., Beaumal, V., Delépine, S., & De Lamballerie-Anton, M. (2001). Effect of high-pressure treatment on rheology of oil-in-water emulsions prepared with hen

- egg yolk. *Innovative Food Science and Emerging Technologies*, 2(1), 9–21.  
[https://doi.org/10.1016/S1466-8564\(00\)00036-9](https://doi.org/10.1016/S1466-8564(00)00036-9)
- Araiza-Calahorra, A., & Sarkar, A. (2019). Pickering emulsion stabilized by protein nanogel particles for delivery of curcumin: effects of pH and ionic strength on curcumin retention. *Food Structure*, 21, 100113. <https://doi.org/10.1016/j.foostr.2019.100113>
- Arditty, S., Schmitt, V., Lequeux, F., & Leal-Calderon, F. (2005). Interfacial properties in solid-stabilized emulsions. *European Physical Journal B*, 44(3), 381–393.  
<https://doi.org/10.1140/epjb/e2005-00137-0>
- Armand, M., Borel, P., Ythier, P., Dutot, G., Melin, C., Senft, M., Lafont, H., & Lairon, D. (1992). Effects of droplet size, triacylglycerol composition, and calcium on the hydrolysis of complex emulsions by pancreatic lipase: an in vitro study. *The Journal of Nutritional Biochemistry*, 3(7), 333–341. [https://doi.org/10.1016/0955-2863\(92\)90024-D](https://doi.org/10.1016/0955-2863(92)90024-D)
- Armand, M., Pasquier, B., André, M., Borel, P., Senft, M., Peyrot, J., Salducci, J., Portugal, H., Jaussan, V., & Lairon, D. (1999). Digestion and absorption of 2 fat emulsions with different droplet sizes in the human digestive tract. *American Journal of Clinical Nutrition*, 70(6), 1096–1106. <https://doi.org/10.1093/ajcn/70.6.1096>
- Asakura, S., & Oosawa, F. (1954). On interaction between two bodies immersed in a solution of macromolecules. *The Journal of Chemical Physics*, 22(7), 1255–1256.  
<https://doi.org/10.1063/1.1740347>
- Ashby, N. P., & Binks, B. P. (2000). Pickering emulsions stabilised by Laponite clay particles. *Physical Chemistry Chemical Physics*, 2(24), 5640–5646.  
<https://doi.org/10.1039/b007098j>

- Aveyard, R., Binks, B. P., Clark, S., & Mead, J. (1986). Interfacial tension minima in oil-water-surfactant systems. *J. Chem. Soc. Faraday Trans. 1*, 82(1), 125–142.
- Aveyard, R., Binks, B. P., & Clint, J. H. (2003). Emulsions stabilised solely by colloidal particles. *Advances in Colloid and Interface Science*, 100–102, 503–546.  
[https://doi.org/10.1016/S0001-8686\(02\)00069-6](https://doi.org/10.1016/S0001-8686(02)00069-6)
- Bai, L., Huan, S., Rojas, O. J., & McClements, D. J. (2021). Recent innovations in emulsion science and technology for food applications. *Journal of Agricultural and Food Chemistry*, 69(32), 8944–8963. <https://doi.org/10.1021/acs.jafc.1c01877>
- Balakrishnan, G., Silva, J. V. C., Nicolai, T., Chassenieux, C., Bovay, C., Buczkowski, J., & Schmitt, C. (2018). Specific effect of calcium ions on thermal gelation of aqueous micellar casein suspensions. *Colloids and Surfaces B: Biointerfaces*, 163, 218–224.  
<https://doi.org/10.1016/j.colsurfb.2017.12.029>
- Barbetta, A., & Cameron, N. R. (2004). Morphology and surface area of emulsion-derived (PolyHIPE) solid foams prepared with oil-phase soluble porogenic solvents: Three-component surfactant system. *Macromolecules*, 37(9), 3202–3213.  
<https://doi.org/10.1021/ma035944y>
- Barnett, C. E. (1942). Some applications of wave-length turbidimetry in the infrared. *The Journal of Physical Chemistry*, 46(1), 69–75. <https://doi.org/10.1021/j150415a009>
- Bauer, E., Jakob, S., & Mosenthin, R. (2005). Principles of physiology of lipid digestion. *Asian-Australasian Journal of Animal Sciences*, 18(2), 282–295.  
<https://doi.org/10.5713/ajas.2005.282>
- Beaucage, G. (1995). Approximations leading to a unified exponential/power-law approach to

- small-angle scattering. *Journal of Applied Crystallography*, 28(6), 717–728.  
<https://doi.org/10.1107/S0021889895005292>
- Beaucage, G. (1996). Small-angle scattering from polymeric mass fractals of arbitrary mass-fractal dimension. *Journal of Applied Crystallography*, 29(2), 134–146.  
<https://doi.org/10.1107/S0021889895011605>
- Bellesi, F. A., Pizones Ruiz-Henestrosa, V. M., & Pilosof, A. M. R. (2014). Behavior of protein interfacial films upon bile salts addition. *Food Hydrocolloids*, 36, 115–122.  
<https://doi.org/10.1016/j.foodhyd.2013.09.010>
- Berli, C. L. A. (2007). Rheology and phase behavior of aggregating emulsions related to droplet-droplet interactions. *Brazilian Journal of Chemical Engineering*, 24(2), 203–210.  
<https://doi.org/10.1590/S0104-66322007000200005>
- Berton-Carabin, C. C., Ropers, M.-H., & Genot, C. (2014). Lipid oxidation in oil-in-water emulsions: involvement of the interfacial layer. *Comprehensive Reviews in Food Science and Food Safety*, 13(5), 945–977. <https://doi.org/10.1111/1541-4337.12097>
- Berton-Carabin, C. C., & Schroën, K. (2015). Pickering emulsions for food applications: background, trends, and challenges. *Annual Review of Food Science and Technology*, 6(1), 263–297. <https://doi.org/10.1146/annurev-food-081114-110822>
- Berton-Carabin, C., Genot, C., Gaillard, C., Guibert, D., & Ropers, M. H. (2013). Design of interfacial films to control lipid oxidation in oil-in-water emulsions. *Food Hydrocolloids*, 33(1), 99–105. <https://doi.org/10.1016/j.foodhyd.2013.02.021>
- Berton-Carabin, C., & Schroën, K. (2019). Towards new food emulsions: designing the interface and beyond. *Current Opinion in Food Science*, 27, 74–81.

<https://doi.org/10.1016/j.cofs.2019.06.006>

Beverung, C. J., Radke, C. J., & Blanch, H. W. (1999). Protein adsorption at the oil/water interface: Characterization of adsorption kinetics by dynamic interfacial tension measurements. *Biophysical Chemistry*, *81*(1), 59–80. [https://doi.org/10.1016/S0301-4622\(99\)00082-4](https://doi.org/10.1016/S0301-4622(99)00082-4)

Bi, A. Q., Xu, X. B., Guo, Y., Du, M., Yu, C. P., & Wu, C. (2020). Ultrasound pre-fractured casein and in-situ formation of high internal phase emulsions. *Ultrasonics Sonochemistry*, *64*(1), 1–6. <https://doi.org/10.1016/j.ultsonch.2019.104916>

Bibette, J., Morse, D. C., Witten, T. A., & Weitz, D. A. (1992). Stability criteria for emulsions. *Physical Review Letters*, *69*(16), 2439–2442. <https://doi.org/10.1103/PhysRevLett.69.2439>

Binks, B. P. (2002). Particles as surfactants—similarities and differences. *Current Opinion in Colloid & Interface Science*, *7*(1–2), 21–41. [https://doi.org/10.1016/S1359-0294\(02\)00008-0](https://doi.org/10.1016/S1359-0294(02)00008-0)

Binks, B. P., & Lumsdon, S. O. (1999). Stability of oil-in-water emulsions stabilised by silica particles. *Physical Chemistry Chemical Physics*, *1*(12), 3007–3016. <https://doi.org/10.1039/a902209k>

Binks, B. P., & Rodrigues, J. A. (2007). Enhanced stabilization of emulsions due to surfactant-induced nanoparticle flocculation. *Langmuir*, *23*(14), 7436–7439. <https://doi.org/10.1021/la700597k>

Blundell, J. E., & Macdiarmid, J. I. (1997). Fat as a risk factor for overconsumption: satiation, satiety, and patterns of eating. *Journal of the American Dietetic Association*, *97*(7), S63–

S69. [https://doi.org/10.1016/S0002-8223\(97\)00733-5](https://doi.org/10.1016/S0002-8223(97)00733-5)

Bohn, T., Carriere, F., Day, L., Deglaire, A., Egger, L., Freitas, D., Golding, M., Le Feunteun, S., Macierzanka, A., Menard, O., Miralles, B., Moscovici, A., Portmann, R., Recio, I., Rémond, D., Santé-Lhoutelier, V., Wooster, T. J., Lesmes, U., Mackie, A. R., & Dupont, D. (2018). Correlation between in vitro and in vivo data on food digestion. What can we predict with static in vitro digestion models? *Critical Reviews in Food Science and Nutrition*, 58(13), 2239–2261. <https://doi.org/10.1080/10408398.2017.1315362>

Borel, P., Armand, M., Ythier, P., Dutot, G., Melin, C., Senft, M., Lafont, H., & Lairon, D. (1994). Hydrolysis of emulsions with different triglycerides and droplet sizes by gastric lipase in vitro. Effect on pancreatic lipase activity. *The Journal of Nutritional Biochemistry*, 5(3), 124–133. [https://doi.org/10.1016/0955-2863\(94\)90083-3](https://doi.org/10.1016/0955-2863(94)90083-3)

Bos, M. A., & Vliet, T. van. (2001). Interfacial rheological properties of adsorbed protein layers and surfactants: a review. *Advances in Colloid and Interface Science*, 91(3), 437–471. [https://doi.org/10.1016/S0001-8686\(00\)00077-4](https://doi.org/10.1016/S0001-8686(00)00077-4)

Bouchoux, A., Gésan-Guiziu, G., Pérez, J., & Cabane, B. (2010). How to squeeze a sponge: casein micelles under osmotic stress, a SAXS study. *Biophysical Journal*, 99(11), 3754–3762. <https://doi.org/10.1016/j.bpj.2010.10.019>

Boyd, J., Parkinson, C., & Sherman, P. (1972). Factors affecting emulsion stability, and the HLB concept. *Journal of Colloid and Interface Science*, 41(2), 359–370. [https://doi.org/10.1016/0021-9797\(72\)90122-1](https://doi.org/10.1016/0021-9797(72)90122-1)

Brodkorb, A., Egger, L., Alminger, M., Alvito, P., Assunção, R., Ballance, S., Bohn, T., Bourlieu-Lacanal, C., Boutrou, R., Carrière, F., Clemente, A., Corredig, M., Dupont, D.,

- Dufour, C., Edwards, C., Golding, M., Karakaya, S., Kirkhus, B., Le Feunteun, S., ... Recio, I. (2019). INFOGEST static in vitro simulation of gastrointestinal food digestion. *Nature Protocols*, *14*(4), 991–1014. <https://doi.org/10.1038/s41596-018-0119-1>
- Brugger, B., & Richtering, W. (2008). Emulsions stabilized by stimuli-sensitive poly (N-isopropylacrylamide)-co-methacrylic acid polymers: microgels versus low molecular weight polymers. *Langmuir*, *24*(15), 7769–7777.
- Brugger, B., Rosen, B. A., & Richtering, W. (2008). Microgels as stimuli-responsive stabilizers for emulsions. *Langmuir*, *24*(21), 12202–12208. <https://doi.org/10.1021/la8015854>
- Brugger, B., Vermant, J., & Richtering, W. (2010). Interfacial layers of stimuli-responsive poly-(N-isopropylacrylamide-co-methacrylic acid) (PNIPAM-co-MAA) microgels characterized by interfacial rheology and compression isotherms. *Physical Chemistry Chemical Physics*, *12*(43), 14573. <https://doi.org/10.1039/c0cp01022g>
- Burchard, W. (1999). Solution properties of branched macromolecules. In *Branched Polymers II* (Vol. 143, pp. 113–194). Springer Berlin Heidelberg. [https://doi.org/10.1007/3-540-49780-3\\_3](https://doi.org/10.1007/3-540-49780-3_3)
- Burdette-Trofimov, M. K., Armstrong, B. L., Rogers, A. M., Heroux, L., Doucet, M., Yang, G., Phillip, N. D., Kidder, M. K., & Veith, G. M. (2020). Understanding binder-silicon interactions during slurry processing. *Journal of Physical Chemistry C*, *124*(24), 13479–13494. <https://doi.org/10.1021/acs.jpcc.0c03660>
- Caessens, P. W. J. R., Visser, S., Gruppen, H., Van Aken, G. A., & Voragen, A. G. J. (1999). Emulsion and foam properties of plasmin derived  $\beta$ -casein peptides. *International Dairy Journal*, *9*(3–6), 347–351. [https://doi.org/10.1016/S0958-6946\(99\)00086-2](https://doi.org/10.1016/S0958-6946(99)00086-2)



- Camacho, S., Den Hollander, E., Van De Velde, F., & Stieger, M. (2015). Properties of oil/water emulsions affecting the deposition, clearance, and after-feel sensory perception of oral coatings. *Journal of Agricultural and Food Chemistry*, 63(8), 2145–2153. <https://doi.org/10.1021/jf505653t>
- Camargo-Perea, A. L., Rubio-Clemente, A., & Peñuela, G. A. (2020). Use of ultrasound as an advanced oxidation process for the degradation of emerging pollutants in water. *Water*, 12(4), 1068. <https://doi.org/10.3390/w12041068>
- Cameron, N. R., & Sherrington, D. C. (1996). High internal phase emulsions (HIPEs) — structure, properties and use in polymer preparation. In *Advances in polymer science* (Vol. 126, pp. 163–214). [https://doi.org/10.1007/3-540-60484-7\\_4](https://doi.org/10.1007/3-540-60484-7_4)
- Chanamai, R., & McClements, D. J. (2000). Dependence of creaming and rheology of monodisperse oil-in-water emulsions on droplet size and concentration. *Colloids and Surfaces A: Physicochemical and Engineering Aspects*, 172(1–3), 79–86. [https://doi.org/10.1016/S0927-7757\(00\)00551-3](https://doi.org/10.1016/S0927-7757(00)00551-3)
- Chemat, F., Grondin, I., Costes, P., Moutoussamy, L., Sing, A. S. C., & Smadja, J. (2004). High power ultrasound effects on lipid oxidation of refined sunflower oil. *Ultrasonics Sonochemistry*, 11(5), 281–285. <https://doi.org/10.1016/j.ultsonch.2003.07.004>
- Chen, S., & Zhang, L.-M. (2019). Casein nanogels as effective stabilizers for Pickering high internal phase emulsions. *Colloids and Surfaces A: Physicochemical and Engineering Aspects*, 579, 123662. <https://doi.org/10.1016/j.colsurfa.2019.123662>
- Chen, X. W., Wang, J. M., Guo, J., Wan, Z. L., Yin, S. W., & Yang, X. Q. (2017). Hierarchical high internal phase emulsions and transparent oleogels stabilized by quillaja saponin-

- coated nanodroplets for color performance. *Food and Function*, 8(2), 823–831.  
<https://doi.org/10.1039/c6fo01752e>
- Cheng, L., Ye, A., Hemar, Y., Gilbert, E. P., de Campo, L., Whitten, A. E., & Singh, H. (2019). Interfacial structures of droplet-stabilized emulsions formed with whey protein microgel particles as revealed by small- and ultra-small-angle neutron scattering. *Langmuir*, 35(37), 12017–12027. <https://doi.org/10.1021/acs.langmuir.9b01966>
- Cheng, L., Ye, A., Hemar, Y., & Singh, H. (2022a). Modification of the interfacial structure of droplet-stabilised emulsions during in vitro dynamic gastric digestion: impact on in vitro intestinal lipid digestion. *Journal of Colloid and Interface Science*, 608, 1286–1296. <https://doi.org/10.1016/j.jcis.2021.10.075>
- Cheng, L., Ye, A., Yang, Z., Gilbert, E. P., Knott, R., de Campo, L., Storer, B., Hemar, Y., & Singh, H. (2022b). Small-angle X-ray scattering (SAXS) and small-angle neutron scattering (SANS) study on the structure of sodium caseinate in dispersions and at the oil-water interface: effect of calcium ions. *Food Structure*, 32, 100276. <https://doi.org/10.1016/j.foostr.2022.100276>
- Chevalier, Y., & Bolzinger, M. A. (2013). Emulsions stabilized with solid nanoparticles: Pickering emulsions. *Colloids and Surfaces A: Physicochemical and Engineering Aspects*, 439, 23–34. <https://doi.org/10.1016/j.colsurfa.2013.02.054>
- Chu, B., Zhou, Z., Wu, G., & Farrell, H. M. (1995). Laser light scattering of model casein solutions: effects of high temperature. *Journal of Colloid and Interface Science*, 170(1), 102–112. <https://doi.org/10.1006/jcis.1995.1077>
- Chuang, C., Ye, A., Anema, S. G., & Loveday, S. M. (2020). Concentrated Pickering emulsions

- stabilised by hemp globulin–caseinate nanoparticles: tuning the rheological properties by adjusting the hemp globulin : caseinate ratio. *Food & Function*, *11*(11), 10193–10204. <https://doi.org/10.1039/D0FO01745K>
- Cordier, F., & Grzesiek, S. (2002). Temperature-dependence of protein hydrogen bond properties as studied by high-resolution NMR. *Journal of Molecular Biology*, *317*(5), 739–752. <https://doi.org/10.1006/jmbi.2002.5446>
- Corstens, M. N., Berton-Carabin, C. C., de Vries, R., Troost, F. J., Masclee, A. A. M., & Schroën, K. (2017a). Food-grade micro-encapsulation systems that may induce satiety via delayed lipolysis: a review. *Critical Reviews in Food Science and Nutrition*, *57*(10), 2218–2244. <https://doi.org/10.1080/10408398.2015.1057634>
- Corstens, M. N., Berton-Carabin, C. C., Kester, A., Fokkink, R., van den Broek, J. M., de Vries, R., Troost, F. J., Masclee, A. A. M., & Schroën, K. (2017b). Destabilization of multilayered interfaces in digestive conditions limits their ability to prevent lipolysis in emulsions. *Food Structure*, *12*, 54–63. <https://doi.org/10.1016/j.foostr.2016.07.004>
- Cui, F., McClements, D. J., Liu, X., Liu, F., & Ngai, T. (2022). Development of pH-responsive emulsions stabilized by whey protein fibrils. *Food Hydrocolloids*, *122*, 107067. <https://doi.org/10.1016/j.foodhyd.2021.107067>
- Dalgleish, D. G. (1993). The sizes and conformations of the proteins in adsorbed layers of individual caseins on latices and in oil-in-water emulsions. *Colloids and Surfaces B: Biointerfaces*, *1*(1), 1–8. [https://doi.org/10.1016/0927-7765\(93\)80011-M](https://doi.org/10.1016/0927-7765(93)80011-M)
- Dalgleish, D. G. (1997). Adsorption of protein and the stability of emulsions. *Trends in Food Science & Technology*, *8*(1), 1–6. [https://doi.org/10.1016/S0924-2244\(97\)01001-7](https://doi.org/10.1016/S0924-2244(97)01001-7)

- Dalgleish, D. G., & Hallett, F. R. (1995). Dynamic light scattering: applications to food systems. *Food Research International*, 28(3), 181–193. [https://doi.org/10.1016/0963-9969\(94\)00053-B](https://doi.org/10.1016/0963-9969(94)00053-B)
- Dalgleish, D. G., & Parker, T. G. (1980). Binding of calcium ions to bovine  $\alpha$ 1-casein and precipitability of the protein-calcium ion complexes. *Journal of Dairy Research*, 47(1), 113–122. <https://doi.org/10.1017/S002202990002094X>
- Dalgleish, D. G., Srinivasan, M., & Singh, H. (1995). Surface properties of oil-in-water emulsion droplets containing casein and Tween 60. *Journal of Agricultural and Food Chemistry*, 43(9), 2351–2355. <https://doi.org/10.1021/jf00057a007>
- Dammak, I., Sobral, P. J. do A., Aquino, A., Neves, M. A. das, & Conte-Junior, C. A. (2020). Nanoemulsions: using emulsifiers from natural sources replacing synthetic ones—a review. *Comprehensive Reviews in Food Science and Food Safety*, 19(5), 2721–2746. <https://doi.org/10.1111/1541-4337.12606>
- Damodaran, S. (2006). Protein stabilization of emulsions and foams. *Journal of Food Science*, 70(3), R54–R66. <https://doi.org/10.1111/j.1365-2621.2005.tb07150.x>
- Dan, N. (2016). Transport and release in nano-carriers for food applications. *Journal of Food Engineering*, 175, 136–144. <https://doi.org/10.1016/j.jfoodeng.2015.12.017>
- Daniels, S. R., & Greer, F. R. (2008). Lipid screening and cardiovascular health in childhood. *Pediatrics*, 122(1), 198–208. <https://doi.org/10.1542/peds.2008-1349>
- Danov, K. D., Denkov, N. D., Petsev, D. N., Ivanov, I. B., & Borwankar, R. (1993). Coalescence dynamics of deformable Brownian emulsion droplets. *Langmuir*, 9(7), 1731–1740. <https://doi.org/10.1021/la00031a021>

- Davidov-Pardo, G., Joye, I. J., & McClements, D. J. (2015). Food-grade protein-based nanoparticles and microparticles for bioactive delivery. In *Advances in Protein Chemistry and Structural Biology* (1st ed., Vol. 98, pp. 293–325). Elsevier Inc. <https://doi.org/10.1016/bs.apcsb.2014.11.004>
- de Kruif, C. G., Tuinier, R., Holt, C., Timmins, P. A., & Rollema, H. S. (2002). Physicochemical study of  $\kappa$ - and  $\beta$ -Casein dispersions and the effect of cross-linking by transglutaminase. *Langmuir*, *18*(12), 4885–4891. <https://doi.org/10.1021/la025543w>
- de la Fuente, M. A., Singh, H., & Hemar, Y. (2002). Recent advances in the characterisation of heat-induced aggregates and intermediates of whey proteins. *Trends in Food Science and Technology*, *13*(8), 262–274. [https://doi.org/10.1016/S0924-2244\(02\)00133-4](https://doi.org/10.1016/S0924-2244(02)00133-4)
- Delahaije, R. J. B. M., Wierenga, P. A., Van Nieuwenhuijzen, N. H., Giuseppin, M. L. F., & Gruppen, H. (2013). Protein concentration and protein-exposed hydrophobicity as dominant parameters determining the flocculation of protein-stabilized oil-in-water emulsions. *Langmuir*, *29*(37), 11567–11574. <https://doi.org/10.1021/la401314a>
- Demetriades, K., Coupland, J. N., & McClements, D. J. (1997a). Physical properties of whey protein stabilized emulsions as related to pH and NaCl. *Journal of Food Science*, *62*(2), 342–347. <https://doi.org/10.1111/j.1365-2621.1997.tb03997.x>
- Demetriades, K., Coupland, J. N., & McClements, D. J. (1997b). Physicochemical properties of whey protein-stabilized emulsions as affected by heating and ionic strength. *Journal of Food Science*, *62*(3), 462–467. <https://doi.org/10.1111/j.1365-2621.1997.tb04407.x>
- Derkach, S. R. (2009). Rheology of emulsions. *Advances in Colloid and Interface Science*, *151*(1–2), 1–23. <https://doi.org/10.1016/j.cis.2009.07.001>

- Deroubaix, A., Moahla, B., & Penny, C. (2020). *Monitoring of intracellular localization of Hepatitis B virus P22 protein using Laser Scanning Confocal Microscopy and Airyscan*. *July 2019*, 499–506. <https://doi.org/10.1002/jemt.23438>
- Deshmukh, O. S., van den Ende, D., Stuart, M. C., Mugele, F., & Duits, M. H. G. (2015). Hard and soft colloids at fluid interfaces: adsorption, interactions, assembly & rheology. *Advances in Colloid and Interface Science*, 222, 215–227. <https://doi.org/10.1016/j.cis.2014.09.003>
- Desmond, K. W., & Weeks, E. R. (2014). Influence of particle size distribution on random close packing of spheres. *Physical Review E*, 90(2), 022204. <https://doi.org/10.1103/PhysRevE.90.022204>
- Destribats, M., Rouvet, M., Gehin-Delval, C., Schmitt, C., & Binks, B. P. (2014). Emulsions stabilised by whey protein microgel particles: towards food-grade Pickering emulsions. *Soft Matter*, 10(36), 6941–6954. <https://doi.org/10.1039/C4SM00179F>
- Dickinson, E. (1992a). Adsorption of sticky hard spheres: relevance to protein competitive adsorption. *Journal of the Chemical Society, Faraday Transactions*, 88(24), 3561. <https://doi.org/10.1039/ft9928803561>
- Dickinson, E. (1992b). *Introduction to food colloids*. Oxford University Press.
- Dickinson, E. (1994a). Emulsion Stability. In K. Nishinari & E. Doi (Eds.), *Food Hydrocolloids* (pp. 387–398). Springer US. [https://doi.org/10.1007/978-1-4615-2486-1\\_61](https://doi.org/10.1007/978-1-4615-2486-1_61)
- Dickinson, E. (1994b). Protein-stabilized emulsions. *Journal of Food Engineering*, 22(1–4), 59–74. [https://doi.org/10.1016/0260-8774\(94\)90025-6](https://doi.org/10.1016/0260-8774(94)90025-6)

- Dickinson, E. (1999). Adsorbed protein layers at fluid interfaces: interactions, structure and surface rheology. *Colloids and Surfaces B: Biointerfaces*, 15(2), 161–176. [https://doi.org/10.1016/S0927-7765\(99\)00042-9](https://doi.org/10.1016/S0927-7765(99)00042-9)
- Dickinson, E. (2003). Hydrocolloids at interfaces and the influence on the properties of dispersed systems. *Food Hydrocolloids*, 17(1), 25–39. [https://doi.org/https://doi.org/10.1016/S0268-005X\(01\)00120-5](https://doi.org/https://doi.org/10.1016/S0268-005X(01)00120-5)
- Dickinson, E. (2009). Hydrocolloids as emulsifiers and emulsion stabilizers. *Food Hydrocolloids*, 23(6), 1473–1482. <https://doi.org/10.1016/j.foodhyd.2008.08.005>
- Dickinson, E. (2010a). Flocculation of protein-stabilized oil-in-water emulsions. *Colloids and Surfaces B: Biointerfaces*, 81(1), 130–140. <https://doi.org/10.1016/j.colsurfb.2010.06.033>
- Dickinson, E. (2010b). Food emulsions and foams: stabilization by particles. *Current Opinion in Colloid & Interface Science*, 15(1–2), 40–49. <https://doi.org/10.1016/j.cocis.2009.11.001>
- Dickinson, E. (2011). Mixed biopolymers at interfaces: competitive adsorption and multilayer structures. *Food Hydrocolloids*, 25(8), 1966–1983. <https://doi.org/10.1016/j.foodhyd.2010.12.001>
- Dickinson, E., & Casanova, H. (1999). A thermoreversible emulsion gel based on sodium caseinate. *Food Hydrocolloids*, 13(4), 285–289. [https://doi.org/10.1016/S0268-005X\(99\)00010-7](https://doi.org/10.1016/S0268-005X(99)00010-7)
- Dickinson, E., & James, J. D. (1999). Influence of competitive adsorption on flocculation and rheology of high-pressure-treated milk protein-stabilized emulsions. *Journal of Agricultural and Food Chemistry*, 47(1), 25–30. <https://doi.org/10.1021/jf980724i>

- Dickinson, E., Murray, B. S., & Stainsby, G. (1988a). Coalescence stability of emulsion-sized droplets at a planar oil-water interface and the relationship to protein film surface rheology. *Journal of the Chemical Society, Faraday Transactions 1: Physical Chemistry in Condensed Phases*, 84(3), 871–883. <https://doi.org/10.1039/F19888400871>
- Dickinson, E., Owusu, R. K., & Williams, A. (1993). Orthokinetic destabilization of a protein-stabilized emulsion by a water-soluble surfactant. *Journal of the Chemical Society, Faraday Transactions*, 89(5), 865. <https://doi.org/10.1039/ft9938900865>
- Dickinson, E., Pinfield, V. J., Horne, D. S., & Leermakers, F. A. M. (1997). Self-consistent-field modelling of adsorbed casein: interaction between two protein-coated surfaces. *Journal of the Chemical Society, Faraday Transactions*, 93(9), 1785–1790. <https://doi.org/10.1039/a608417f>
- Dickinson, E., & Ritzoulis, C. (2000). Creaming and rheology of oil-in-water emulsions containing sodium dodecyl sulfate and sodium caseinate. *Journal of Colloid and Interface Science*, 224(1), 148–154. <https://doi.org/10.1006/jcis.1999.6682>
- Dickinson, E., Rolfe, S. E., & Dalgleish, D. G. (1988b). Competitive adsorption of  $\alpha$ 1-casein and  $\beta$ -casein in oil-in-water emulsions. *Food Hydrocolloids*, 2(5), 397–405. [https://doi.org/10.1016/S0268-005X\(88\)80004-3](https://doi.org/10.1016/S0268-005X(88)80004-3)
- Dickinson, E., Rolfe, S. E., & Dalgleish, D. G. (1989). Competitive adsorption in oil-in-water emulsions containing  $\alpha$ -lactalbumin and  $\beta$ -lactoglobulin. *Food Hydrocolloids*, 3(3), 193–203. [https://doi.org/10.1016/S0268-005X\(89\)80003-7](https://doi.org/10.1016/S0268-005X(89)80003-7)
- Dickinson, E., Semenova, M. G., Belyakova, L. E., Antipova, A. S., Il'in, M. M., Tsapkina, E. N., & Ritzoulis, C. (2001). Analysis of light scattering data on the calcium ion sensitivity



- of caseinate solution thermodynamics: relationship to emulsion flocculation. *Journal of Colloid and Interface Science*, 239(1), 87–97. <https://doi.org/10.1006/jcis.2001.7480>
- Dimitrova, T. D., & Leal-Calderon, F. (2004). Rheological properties of highly concentrated protein-stabilized emulsions. *Advances in Colloid and Interface Science*, 108–109, 49–61. <https://doi.org/10.1016/j.cis.2003.10.002>
- Ding, M., Liu, L., Zhang, T., Tao, N., Wang, X., & Zhong, J. (2021). Effect of interfacial layer number on the storage stability and in vitro digestion of fish oil-loaded multilayer emulsions consisting of gelatin particle and polysaccharides. *Food Chemistry*, 336, 127686. <https://doi.org/10.1016/j.foodchem.2020.127686>
- Dinsmore, A. D., Hsu, M. F., Nikolaidis, M. G., Marquez, M., Bausch, A. R., & Weitz, D. A. (2002). Colloidosomes: selectively permeable capsules composed of colloidal particles. *Science*, 298(5595), 1006–1009. <https://doi.org/10.1126/science.1074868>
- Doudiès, F., Arsène, A.-S., Garnier-Lambrouin, F., Famelart, M.-H., Bouchoux, A., Pignon, F., & Gésan-Guiziou, G. (2019). Major role of voluminosity in the compressibility and sol–gel transition of casein micelle dispersions concentrated at 7 °C and 20 °C. *Foods*, 8(12), 652. <https://doi.org/10.3390/foods8120652>
- Du, J., Dai, H., Wang, H., Yu, Y., Zhu, H., Fu, Y., Ma, L., Peng, L., Li, L., Wang, Q., & Zhang, Y. (2021). Preparation of high thermal stability gelatin emulsion and its application in 3D printing. *Food Hydrocolloids*, 113, 106536. <https://doi.org/10.1016/j.foodhyd.2020.106536>
- Du, M., Sun, Z., Liu, Z., Yang, Y., Liu, Z., Wang, Y., Jiang, B., Feng, Z., & Liu, C. (2022). High efficiency desalination of wasted salted duck egg white and processing into food-

- grade pickering emulsion stabilizer. *LWT*, 161, 113337.  
<https://doi.org/10.1016/j.lwt.2022.113337>
- Dudkiewicz, A., Tiede, K., Loeschner, K., Jensen, L. H. S., Jensen, E., Wierzbicki, R., Boxall, A. B. A., & Molhave, K. (2011). Characterization of nanomaterials in food by electron microscopy. *Trends in Analytical Chemistry*, 30(1), 28–43.  
<https://doi.org/10.1016/j.trac.2010.10.007>
- Eberle, A. P. R., & Porcar, L. (2012). Flow-SANS and Rheo-SANS applied to soft matter. *Current Opinion in Colloid & Interface Science*, 17(1), 33–43.  
<https://doi.org/10.1016/j.cocis.2011.12.001>
- Echlin, P. (1992). *Low-temperature microscopy and analysis*. Springer US.  
<https://doi.org/10.1007/978-1-4899-2302-8>
- Erramreddy, V. V., & Ghosh, S. (2015). Influence of droplet size on repulsive and attractive nanoemulsion gelation. *Colloids and Surfaces A: Physicochemical and Engineering Aspects*, 484, 144–152. <https://doi.org/10.1016/j.colsurfa.2015.07.027>
- Evans, D. F., & Wennerström, H. (1999). *The colloidal domain: Where physics, chemistry, biology, and technology meet*. (2nd Editio). New York: Wiley-VHC.
- Fang, Y., & Dalgleish, D. G. (1993). Dimensions of the adsorbed layers in oil-in-water emulsions stabilized by caseins. *Journal of Colloid and Interface Science*, 156(2), 329–334. <https://doi.org/10.1006/jcis.1993.1120>
- Farr, R. S., & Groot, R. D. (2009). Close packing density of polydisperse hard spheres. *Journal of Chemical Physics*, 131(24). <https://doi.org/10.1063/1.3276799>

- Farrer, D., & Lips, A. (1999). On the self-assembly of sodium caseinate. *International Dairy Journal*, 9(3–6), 281–286. [https://doi.org/10.1016/S0958-6946\(99\)00075-8](https://doi.org/10.1016/S0958-6946(99)00075-8)
- Favé, G., Coste, T. C., & Armand, M. (2004). Physicochemical properties of lipids: new strategies to manage fatty acid bioavailability. *Cellular and Molecular Biology (Noisy-Le-Grand, France)*, 50(7), 815–831. <https://doi.org/10.1170/T575>
- Feigin, L. A., & Svergun, D. I. (1987). *Structure analysis by small-angle X-ray and neutron scattering* (G. W. Taylor (ed.)). Springer US. <https://doi.org/10.1007/978-1-4757-6624-0>
- Félix, M., Carrera, C., Romero, A., Bengoechea, C., & Guerrero, A. (2020). Rheological approaches as a tool for the development and stability behaviour of protein-stabilized emulsions. *Food Hydrocolloids*, 104, 105719. <https://doi.org/10.1016/j.foodhyd.2020.105719>
- Finkle, P., Draper, H. D., & Hildebrand, J. H. (1923). The theory of emulsification. *Journal of the American Chemical Society*, 45(12), 2780–2788. <https://doi.org/10.1021/ja01665a002>
- Foudazi, R., Masalova, I., & Malkin, A. Y. (2012). The rheology of binary mixtures of highly concentrated emulsions: Effect of droplet size ratio. *Journal of Rheology*, 56(5), 1299. <https://doi.org/10.1122/1.4736556>
- Foudazi, R., Qavi, S., Masalova, I., & Malkin, A. Y. (2015). Physical chemistry of highly concentrated emulsions. *Advances in Colloid and Interface Science*, 220, 78–91. <https://doi.org/10.1016/j.cis.2015.03.002>
- Frank, H. S., & Evans, M. W. (1945). Free volume and entropy in condensed systems III. Entropy in binary liquid mixtures; partial molal entropy in dilute solutions; structure and thermodynamics in aqueous electrolytes. *The Journal of Chemical Physics*, 13(11), 507–

532. <https://doi.org/10.1063/1.1723985>

Frasch-Melnik, S., Norton, I. T., & Spyropoulos, F. (2010). Fat-crystal stabilised w/o emulsions for controlled salt release. *Journal of Food Engineering*, 98(4), 437–442. <https://doi.org/10.1016/j.jfoodeng.2010.01.025>

Gabriele, D., de Cindio, B., & D'Antona, P. (2001). A weak gel model for foods. *Rheologica Acta*, 40(2), 120–127. <https://doi.org/10.1007/s003970000139>

Gallet, J.-C., Domine, F., Zender, C. S., & Picard, G. (2009). Measurement of the specific surface area of snow using infrared reflectance in an integrating sphere at 1310 and 1550 nm. *The Cryosphere*, 3(2), 167–182. <https://doi.org/10.5194/tc-3-167-2009>

Gaucel, S., Trelea, I. C., & Le Feunteun, S. (2015). Comment on new mathematical model for interpreting pH-stat digestion profiles: impact of lipid droplet characteristics on in vitro digestibility. *Journal of Agricultural and Food Chemistry*, 63(47), 10352–10353. <https://doi.org/10.1021/acs.jafc.5b03573>

Gautier, F., Destribats, M., Perrier-Cornet, R., Dechezelles, J.-F., Giermanska, J., Heroguez, V., Ravaine, S., Leal-Calderon, F., & Schmitt, V. (2007). Pickering emulsions with stimuable particles: from highly- to weakly-covered interfaces. *Physical Chemistry Chemical Physics*, 9(48), 6455–6462. <https://doi.org/10.1039/B710226G>

Geremias-Andrade, I. M., Souki, N. P. D. B. G., Moraes, I. C. F., & Pinho, S. C. (2017). Rheological and mechanical characterization of curcumin-loaded emulsion-filled gels produced with whey protein isolate and xanthan gum. *LWT*, 86, 166–173. <https://doi.org/10.1016/j.lwt.2017.07.063>

Giang, T. M., Gaucel, S., Brestaz, P., Anton, M., Meynier, A., Trelea, I. C., & Le Feunteun, S.

- (2016). Dynamic modeling of in vitro lipid digestion: individual fatty acid release and bioaccessibility kinetics. *Food Chemistry*, *194*, 1180–1188. <https://doi.org/10.1016/j.foodchem.2015.08.125>
- Gilbert, E. P. (2019). Small angle X-ray and neutron scattering in food colloids. *Current Opinion in Colloid and Interface Science*, *42*, 55–72. <https://doi.org/10.1016/j.cocis.2019.03.005>
- Gilbert, E. P., Schulz, J. C., & Noakes, T. J. (2006). ‘Quokka’—the small-angle neutron scattering instrument at OPAL. *Physica B: Condensed Matter*, *385–386*, 1180–1182. <https://doi.org/10.1016/j.physb.2006.05.385>
- Golding, M., & Wooster, T. J. (2010). The influence of emulsion structure and stability on lipid digestion. *Current Opinion in Colloid and Interface Science*, *15*(1–2), 90–101. <https://doi.org/10.1016/j.cocis.2009.11.006>
- Golding, M., Wooster, T. J., Day, L., Xu, M., Lundin, L., Keogh, J., & Cliftonx, P. (2011). Impact of gastric structuring on the lipolysis of emulsified lipids. *Soft Matter*, *7*(7), 3513–3523. <https://doi.org/10.1039/c0sm01227k>
- Grigoriev, D. O., & Miller, R. (2009). Mono- and multilayer covered drops as carriers. *Current Opinion in Colloid and Interface Science*, *14*(1), 48–59. <https://doi.org/10.1016/j.cocis.2008.03.003>
- Gudipati, V., Sandra, S., McClements, D. J., & Decker, E. A. (2010). Oxidative stability and in vitro digestibility of fish oil-in-water emulsions containing multilayered membranes. *Journal of Agricultural and Food Chemistry*, *58*(13), 8093–8099. <https://doi.org/10.1021/jf101348c>

- Guida, C., Aguiar, A. C., & Cunha, R. L. (2021). Green techniques for starch modification to stabilize Pickering emulsions: a current review and future perspectives. *Current Opinion in Food Science*, *38*, 52–61. <https://doi.org/10.1016/j.cofs.2020.10.017>
- Guo, Y., Wu, C., Du, M., Lin, S., Xu, X., & Yu, P. (2021). In-situ dispersion of casein to form nanoparticles for Pickering high internal phase emulsions. *LWT*, *139*(1), 110538. <https://doi.org/10.1016/j.lwt.2020.110538>
- Gupta, R., & Rousseau, D. (2012). Surface-active solid lipid nanoparticles as Pickering stabilizers for oil-in-water emulsions. *Food & Function*, *3*(3), 302. <https://doi.org/10.1039/c2fo10203j>
- Guzey, D., & McClements, D. J. (2006). Formation, stability and properties of multilayer emulsions for application in the food industry. *Advances in Colloid and Interface Science*, *128–130*(2006), 227–248. <https://doi.org/10.1016/j.cis.2006.11.021>
- HadjSadok, A., Pitkowski, A., Nicolai, T., Benyahia, L., & Moulai-Mostefa, N. (2008). Characterisation of sodium caseinate as a function of ionic strength, pH and temperature using static and dynamic light scattering. *Food Hydrocolloids*, *22*(8), 1460–1466. <https://doi.org/10.1016/j.foodhyd.2007.09.002>
- Hammouda, B. (2016). *Probing nanoscale structures - the SANS toolbox*. [https://www.ncnr.nist.gov/staff/hammouda/the\\_SANS\\_toolbox.pdf](https://www.ncnr.nist.gov/staff/hammouda/the_SANS_toolbox.pdf)
- Hansen, J., & Hayter, J. B. (1982). A rescaled MSA structure factor for dilute charged colloidal dispersions. *Molecular Physics*, *46*(3), 651–656. <https://doi.org/10.1080/00268978200101471>
- Hayati, I. N., Che Man, Y. Bin, Tan, C. P., & Aini, I. N. (2007). Stability and rheology of

- concentrated O/W emulsions based on soybean oil/palm kernel olein blends. *Food Research International*, 40(8), 1051–1061. <https://doi.org/10.1016/j.foodres.2007.05.008>
- Hayter, J. B., & Penfold, J. (1981). An analytic structure factor for macroion solutions. *Molecular Physics*, 42(1), 109–118. <https://doi.org/10.1080/00268978100100091>
- Heller, W. T. (2010). Small-angle neutron scattering and contrast variation: a powerful combination for studying biological structures. *Acta Crystallographica Section D: Biological Crystallography*, 66(11), 1213–1217. <https://doi.org/10.1107/S0907444910017658>
- Heller, W. T., & Littrell, K. C. (2009). Small-angle neutron scattering for molecular biology: basics and instrumentation. In R. S. Foote & J. W. Lee (Eds.), *Micro and Nano Technologies in Bioanalysis: Methods and Protocols* (pp. 293–305). Humana Press. [https://doi.org/10.1007/978-1-59745-483-4\\_19](https://doi.org/10.1007/978-1-59745-483-4_19)
- Hemar, Y., Banjar, W., Otter, D., & Yang, Z. (2021). Viscosity, size, structural and interfacial properties of sodium caseinate obtained from A2 milk. *Colloids and Surfaces A: Physicochemical and Engineering Aspects*, 614, 126163. <https://doi.org/10.1016/j.colsurfa.2021.126163>
- Hemar, Y., & Horne, D. S. (2000). Dynamic rheological properties of highly concentrated protein-stabilized emulsions. *Langmuir*, 16(7), 3050–3057. <https://doi.org/10.1021/la9908440>
- Hennig, S., & Manstein, D. J. (2021). Improvement of image resolution by combining enhanced confocal microscopy and quantum dot triexciton imaging. *FEBS Open Bio*, 11, 3324–3330. <https://doi.org/10.1002/2211-5463.13246>

- Hettiarachchi, K., Zhang, S., Feingold, S., Lee, A. P., & Dayton, P. A. (2009). Controllable microfluidic synthesis of multiphase drug-carrying lipospheres for site-targeted therapy. *Biotechnology Progress*, 25(4), 938–945. <https://doi.org/10.1002/btpr.214>
- Hoffmann, M. A. M., Roefs, S. P. F. M., Verheul, M., van Mil, P. J. J. M., & De Kruif, K. G. (1996). Aggregation of  $\beta$ -lactoglobulin studied by in situ light scattering. *Journal of Dairy Research*, 63(3), 423–440. <https://doi.org/10.1017/S0022029900031939>
- Hu, M., McClements, D. J., & Decker, E. A. (2003). Lipid oxidation in corn oil-in-water emulsions stabilized by casein, whey protein isolate, and soy protein isolate. *Journal of Agricultural and Food Chemistry*, 51(6), 1696–1700. <https://doi.org/10.1021/jf020952j>
- Hu, Y. Q., Yin, S. W., Zhu, J. H., Qi, J. R., Guo, J., Wu, L. Y., Tang, C. H., & Yang, X. Q. (2016). Fabrication and characterization of novel Pickering emulsions and Pickering high internal emulsions stabilized by gliadin colloidal particles. *Food Hydrocolloids*, 61, 300–310. <https://doi.org/10.1016/j.foodhyd.2016.05.028>
- Huang, X.-N., Zhu, J.-J., Xi, Y.-K., Yin, S.-W., Ngai, T., & Yang, X.-Q. (2019). Protein-based Pickering high internal phase emulsions as nutraceutical vehicles of and the template for advanced materials: a perspective paper. *Journal of Agricultural and Food Chemistry*, 67(35), 9719–9726. <https://doi.org/10.1021/acs.jafc.9b03356>
- Hunt, J. A., & Dalgleish, D. G. (1994). Effect of pH on the stability and surface composition of emulsions made with whey protein isolate. *Journal of Agricultural and Food Chemistry*, 42(10), 2131–2135. <https://doi.org/10.1021/jf00046a011>
- Hunt, J. A., Dickinson, E., & Horne, D. S. (1993). Competitive displacement of proteins in oil-in-water emulsions containing calcium ions. *Colloids and Surfaces A: Physicochemical*



*and Engineering Aspects*, 71(2), 197–203. [https://doi.org/10.1016/0927-7757\(93\)80344-](https://doi.org/10.1016/0927-7757(93)80344-)

E

Ilavsky, J., & Jemian, P. R. (2009). Irena: tool suite for modeling and analysis of small-angle scattering. *Journal of Applied Crystallography*, 42(2), 347–353. <https://doi.org/10.1107/S0021889809002222>

Ingham, B., Smialowska, A., Erlangga, G. D., Matia-Merino, L., Kirby, N. M., Wang, C., Haverkamp, R. G., & Carr, A. J. (2016). Revisiting the interpretation of casein micelle SAXS data. *Soft Matter*, 12(33), 6937–6953. <https://doi.org/10.1039/c6sm01091a>

Jafari, S. M., Assadpoor, E., He, Y., & Bhandari, B. (2008). Re-coalescence of emulsion droplets during high-energy emulsification. *Food Hydrocolloids*, 22(7), 1191–1202. <https://doi.org/10.1016/j.foodhyd.2007.09.006>

Jarvie, H. P., & King, S. M. (2007). Small-angle neutron scattering study of natural aquatic nanocolloids. *Environmental Science and Technology*, 41(8), 2868–2873. <https://doi.org/10.1021/es061912p>

Jeffries, C. M., Ilavsky, J., Martel, A., Hinrichs, S., Meyer, A., Pedersen, J. S., Sokolova, A. V, & Svergun, D. I. (2021). Small-angle X-ray and neutron scattering. *Nature Reviews Methods Primers*, 1(1), 70. <https://doi.org/10.1038/s43586-021-00064-9>

Jenkins, P., & Snowden, M. (1996). Depletion flocculation in colloidal dispersions. *Advances in Colloid and Interface Science*, 68, 57–96. [https://doi.org/10.1016/S0001-8686\(96\)90046-9](https://doi.org/10.1016/S0001-8686(96)90046-9)

Jestin, J., Simon, S., Zupancic, L., & Barré, L. (2007). A small angle neutron scattering study of the adsorbed asphaltene layer in water-in-hydrocarbon emulsions: structural

- description related to stability. *Langmuir*, 23(21), 10471–10478.  
<https://doi.org/10.1021/la701193f>
- Jiang, Y., Zhang, C., Yuan, J., Wu, Y., Li, F., Li, D., & Huang, Q. (2019). Effects of pectin polydispersity on zein/pectin composite nanoparticles (ZAPs) as high internal-phase Pickering emulsion stabilizers. *Carbohydrate Polymers*, 219, 77–86.  
<https://doi.org/10.1016/j.carbpol.2019.05.025>
- Jiao, B., Shi, A., Wang, Q., & Binks, B. P. (2018). High-internal-phase Pickering emulsions stabilized solely by peanut-protein-isolate microgel particles with multiple potential applications. *Angewandte Chemie*, 130(30), 9418–9422.  
<https://doi.org/10.1002/ange.201801350>
- Kaz, D. M., McGorty, R., Mani, M., Brenner, M. P., & Manoharan, V. N. (2012). Physical ageing of the contact line on colloidal particles at liquid interfaces. *Nature Materials*, 11(2), 138–142. <https://doi.org/10.1038/nmat3190>
- Kenmogne-Domguia, H. B., Meynier, A., Viau, M., Llamas, G., & Genot, C. (2012). Gastric conditions control both the evolution of the organization of protein-stabilized emulsions and the kinetic of lipolysis during in vitro digestion. *Food and Function*, 3(12), 1302–1309. <https://doi.org/10.1039/c2fo30031a>
- Kharlamova, A., Inthavong, W., Nicolai, T., & Chassenieux, C. (2016). The effect of aggregation into fractals or microgels on the charge density and the isoionic point of globular proteins. *Food Hydrocolloids*, 60, 470–475.  
<https://doi.org/10.1016/j.foodhyd.2016.04.013>
- Kim, H. S., & Mason, T. G. (2017). Advances and challenges in the rheology of concentrated

- emulsions and nanoemulsions. *Advances in Colloid and Interface Science*, 247, 397–412.  
<https://doi.org/10.1016/j.cis.2017.07.002>
- Klang, V., Matsko, N. B., Valenta, C., & Hofer, F. (2012). Electron microscopy of nanoemulsions: an essential tool for characterisation and stability assessment. *Micron*, 43(2–3), 85–103. <https://doi.org/10.1016/j.micron.2011.07.014>
- Kline, S. R. (2006). Reduction and analysis of SANS and USANS data using IGOR Pro. *Journal of Applied Crystallography*, 39(6), 895–900.  
<https://doi.org/10.1107/S0021889806035059>
- Kong, F., & Singh, R. P. (2010). A human gastric simulator (HGS) to study food digestion in human stomach. *Journal of Food Science*, 75(9), E627–E635.  
<https://doi.org/10.1111/j.1750-3841.2010.01856.x>
- Kotula, A. P., & Anna, S. L. (2012). Probing timescales for colloidal particle adsorption using slug bubbles in rectangular microchannels. *Soft Matter*, 8(41), 10759–10772.  
<https://doi.org/10.1039/c2sm25970b>
- Kralova, I., & Sjöblom, J. (2009). Surfactants used in food industry: a Review. *Journal of Dispersion Science and Technology*, 30(9), 1363–1383.  
<https://doi.org/10.1080/01932690902735561>
- Kumosinski, T. F., Pessen, H., Farrell, H. M., & Brumberger, H. (1988). Determination of the quaternary structural states of bovine casein by small-angle X-ray scattering: submicellar and micellar forms. *Archives of Biochemistry and Biophysics*, 266(2), 548–561.  
[https://doi.org/10.1016/0003-9861\(88\)90288-3](https://doi.org/10.1016/0003-9861(88)90288-3)
- Lacasse, M. D., Grest, G. S., Levine, D., Mason, T. G., & Weitz, D. A. (1996). Model for the

- elasticity of compressed emulsions. *Physical Review Letters*, 76(18), 3448–3451.  
<https://doi.org/10.1103/PhysRevLett.76.3448>
- Laguerre, M., Bily, A., Roller, M., & Birtić, S. (2017). Mass transport phenomena in lipid oxidation and antioxidation. *Annual Review of Food Science and Technology*, 8, 391–411.  
<https://doi.org/10.1146/annurev-food-030216-025812>
- Larson-Smith, K., & Pozzo, D. C. (2012). Pickering emulsions stabilized by nanoparticle surfactants. *Langmuir*, 28(32), 11725–11732. <https://doi.org/10.1021/la301896c>
- Leal-Calderon, F. (2012). Emulsified lipids: formulation and control of end-use properties. *OCL - Oleagineux Corps Gras Lipides*, 19(2), 111–119.  
<https://doi.org/10.1684/ocl.2012.0438>
- Leal-Calderon, F., & Schmitt, V. (2008). Solid-stabilized emulsions. *Current Opinion in Colloid and Interface Science*, 13(4), 217–227.  
<https://doi.org/10.1016/j.cocis.2007.09.005>
- Lee, Y.-T., & Pozzo, L. D. (2019). Contrast-variation time-resolved small-angle neutron scattering analysis of oil-exchange kinetics between oil-in-water emulsions stabilized by anionic surfactants. *Langmuir*, 35(47), 15192–15203.  
<https://doi.org/10.1021/acs.langmuir.9b02423>
- Lee, Y. T., Li, D. S., Ilavsky, J., Kuzmenko, I., Jeng, G. S., O'Donnell, M., & Pozzo, L. D. (2019). Ultrasound-based formation of nano-Pickering emulsions investigated via in-situ SAXS. *Journal of Colloid and Interface Science*, 536, 281–290.  
<https://doi.org/10.1016/j.jcis.2018.10.047>
- Leonard, P., & Harold M, F. (1982). Interactions leading to formation of casein submicelles.

- Journal of Dairy Science*, 65(12), 2259–2266. [https://doi.org/10.3168/jds.S0022-0302\(82\)82495-8](https://doi.org/10.3168/jds.S0022-0302(82)82495-8)
- Lewis, E. R. (2006). The effect of surface tension (Kelvin effect) on the equilibrium radius of a hygroscopic aqueous aerosol particle. *Journal of Aerosol Science*, 37(11), 1605–1617. <https://doi.org/10.1016/j.jaerosci.2006.04.001>
- Li, J., Ye, A., Lee, S. J., & Singh, H. (2012). Influence of gastric digestive reaction on subsequent in vitro intestinal digestion of sodium caseinate-stabilized emulsions. *Food and Function*, 3(3), 320–326. <https://doi.org/10.1039/c2fo10242k>
- Li, J., Ye, A., Lee, S. J., & Singh, H. (2013a). Physicochemical behaviour of WPI-stabilized emulsions in in vitro gastric and intestinal conditions. *Colloids and Surfaces B: Biointerfaces*, 111, 80–87. <https://doi.org/10.1016/j.colsurfb.2013.05.034>
- Li, X., Xu, X., Song, L., Bi, A., Wu, C., Ma, Y., Du, M., & Zhu, B. (2020). High internal phase emulsion for food-grade 3D printing materials. *ACS Applied Materials & Interfaces*, 12(40), 45493–45503. <https://doi.org/10.1021/acsami.0c11434>
- Li, Y., & McClements, D. J. (2010). New mathematical model for interpreting pH-stat digestion profiles: impact of lipid droplet characteristics on in vitro digestibility. *Journal of Agricultural and Food Chemistry*, 58(13), 8085–8092. <https://doi.org/10.1021/jf101325m>
- Li, Z., Dai, L., Wang, D., Mao, L., & Gao, Y. (2018). Stabilization and rheology of concentrated emulsions using the natural emulsifiers quillaja saponins and rhamnolipids. *Journal of Agricultural and Food Chemistry*, 66(15), 3922–3929. <https://doi.org/10.1021/acs.jafc.7b05291>
- Li, Z., Harbottle, D., Pensini, E., Ngai, T., Richtering, W., & Xu, Z. (2015). Fundamental study

- of emulsions stabilized by soft and rigid particles. *Langmuir*, 31(23), 6282–6288.  
<https://doi.org/10.1021/acs.langmuir.5b00039>
- Li, Z., & Ngai, T. (2013). Microgel particles at the fluid-fluid interfaces. *Nanoscale*, 5(4), 1399–1410. <https://doi.org/10.1039/c2nr33503d>
- Li, Z., Xiao, M., Wang, J., & Ngai, T. (2013b). Pure protein scaffolds from pickering high internal phase emulsion template. *Macromolecular Rapid Communications*, 34(2), 169–174. <https://doi.org/10.1002/marc.201200553>
- Lim, H., Jo, M., Ban, C., & Choi, Y. J. (2020). Interfacial and colloidal characterization of oil-in-water emulsions stabilized by interface-tunable solid lipid nanoparticles. *Food Chemistry*, 306, 125619. <https://doi.org/10.1016/j.foodchem.2019.125619>
- Lin, Q., Liang, R., Zhong, F., Ye, A., & Singh, H. (2018). Effect of degree of octenyl succinic anhydride (OSA) substitution on the digestion of emulsions and the bioaccessibility of  $\beta$ -carotene in OSA-modified-starch-stabilized-emulsions. *Food Hydrocolloids*, 84, 303–312. <https://doi.org/10.1016/j.foodhyd.2018.05.056>
- Liu, F., & Tang, C. H. (2014). Phytosterol colloidal particles as pickering stabilizers for emulsions. *Journal of Agricultural and Food Chemistry*, 62(22), 5133–5141. <https://doi.org/10.1021/jf404930c>
- Liu, W., Gao, H., McClements, D. J., Zhou, L., Wu, J., & Zou, L. (2019). Stability, rheology, and  $\beta$ -carotene bioaccessibility of high internal phase emulsion gels. *Food Hydrocolloids*, 88(October 2018), 210–217. <https://doi.org/10.1016/j.foodhyd.2018.10.012>
- Lopez-Rubio, A., & Gilbert, E. P. (2009). Neutron scattering: a natural tool for food science and technology research. *Trends in Food Science and Technology*, 20(11–12), 576–586.

<https://doi.org/10.1016/j.tifs.2009.07.008>

Lu, P. J., & Weitz, D. A. (2013). Colloidal particles: crystals, glasses, and gels. *Annual Review of Condensed Matter Physics*, 4(1), 217–233. <https://doi.org/10.1146/annurev-conmatphys-030212-184213>

Lubachevsky, B. D., & Stillinger, F. H. (1990). Geometric properties of random disk packings. *Journal of Statistical Physics*, 60(5–6), 561–583. <https://doi.org/10.1007/BF01025983>

Lucey, J. A., Srinivasan, M., Singh, H., & Munro, P. A. (2000). Characterization of commercial and experimental sodium caseinates by multiangle laser light scattering and size-exclusion chromatography. *Journal of Agricultural and Food Chemistry*, 48(5), 1610–1616. <https://doi.org/10.1021/jf990769z>

Luo, Z., Murray, B. S., Ross, A. L., Povey, M. J. W., Morgan, M. R. A., & Day, A. J. (2012). Effects of pH on the ability of flavonoids to act as Pickering emulsion stabilizers. *Colloids and Surfaces B: Biointerfaces*, 92, 84–90. <https://doi.org/10.1016/j.colsurfb.2011.11.027>

Lv, P., Wang, D., Dai, L., Wu, X., Gao, Y., & Yuan, F. (2020). Pickering emulsion gels stabilized by high hydrostatic pressure-induced whey protein isolate gel particles: characterization and encapsulation of curcumin. *Food Research International*, 132, 109032. <https://doi.org/10.1016/j.foodres.2020.109032>

Ma, H., Forssell, P., Partanen, R., Seppänen, R., Buchert, J., & Boer, H. (2009). Sodium caseinates with an altered isoelectric point as emulsifiers in oil/water systems. *Journal of Agricultural and Food Chemistry*, 57(9), 3800–3807. <https://doi.org/10.1021/jf803104s>

Mackie, A. R., Gunning, A. P., Wilde, P. J., & Morris, V. J. (2000). Competitive displacement of  $\beta$ -lactoglobulin from the air/water interface by sodium dodecyl sulfate. *Langmuir*,

16(21), 8176–8181. <https://doi.org/10.1021/la0003950>

Mackie, A. R., Nativel, S., Wilson, D. R., Ladha, S., & Clark, D. C. (1996). Process-induced changes in molecular structure that alter adsorbed layer properties in oil-in-water emulsions stabilised by  $\beta$ -casein/ tween20 mixtures. *Journal of the Science of Food and Agriculture*, 70(4), 413–421. [https://doi.org/10.1002/\(SICI\)1097-0010\(199604\)70:4<413::AID-JSFA507>3.3.CO;2-R](https://doi.org/10.1002/(SICI)1097-0010(199604)70:4<413::AID-JSFA507>3.3.CO;2-R)

MacKie, A. R., Wilde, P. J., Wilson, D. R., & Clark, D. C. (1993). Competitive effects in the adsorbed layer of oil-in-water emulsions stabilised by  $\beta$ -lactoglobulin-Tween 20 mixtures. *Journal of the Chemical Society, Faraday Transactions*, 89(15), 2755–2759. <https://doi.org/10.1039/FT9938902755>

Malassagne-Bulgarelli, N., & McGrath, K. M. (2009). Dynamics of oil transfer in oil-in-water emulsions. *Soft Matter*, 5(23), 4804–4813. <https://doi.org/10.1039/b912742a>

Maldonado-Valderrama, J. (2019). Probing in vitro digestion at oil–water interfaces. *Current Opinion in Colloid and Interface Science*, 39, 51–60. <https://doi.org/10.1016/j.cocis.2019.01.004>

Mao, L., & Miao, S. (2015). Structuring food emulsions to improve nutrient delivery during digestion. *Food Engineering Reviews*, 7(4), 439–451. <https://doi.org/10.1007/s12393-015-9108-0>

Mao, L., Xu, D., Yang, J., Yuan, F., Gao, Y., & Zhao, J. (2009). Effects of Small and Large Molecule Emulsifiers on the Characteristics of  $\beta$ -Carotene Nanoemulsions Prepared by High Pressure Homogenization. *Food Technology and Biotechnology*, 47(3), 336–342.

Marciani, L., Young, P., Wright, J., Moore, R., Coleman, N., Gowland, P. A., & Spiller, R. C.



- (2001). Antral motility measurements by magnetic resonance imaging. *Neurogastroenterology and Motility*, 13(5), 511–518. <https://doi.org/10.1046/j.1365-2982.2001.00285.x>
- Martin, J. E., & Schaefer, D. W. (1984). Dynamics of fractal colloidal aggregates. *Physical Review Letters*, 53(26), 2457–2460. <https://doi.org/10.1103/PhysRevLett.53.2457>
- Mason, T. G. (1999). New fundamental concepts in emulsion theology. *Current Opinion in Colloid and Interface Science*, 4(3), 231–238. [https://doi.org/10.1016/S1359-0294\(99\)00035-7](https://doi.org/10.1016/S1359-0294(99)00035-7)
- Mason, T. G., Bibette, J., & Weitz, D. A. (1996). Yielding and flow of monodisperse emulsions. *Journal of Colloid and Interface Science*, 179(2), 439–448. <https://doi.org/10.1006/jcis.1996.0235>
- Mason, T. G., Bibette, J., Weitz, D. A., Guerra, R. E., Weitz, D. A., Mason, T. G., Bibette, J., & Weitz, D. A. (1995). Elasticity of compressed emulsions. *Physical Review Letters*, 75(10), 2051–2054. <https://doi.org/10.1103/PhysRevLett.75.2051>
- Mason, T. G., Wilking, J. N., Meleson, K., Chang, C. B., & Graves, S. M. (2006). Nanoemulsions: formation, structure, and physical properties. *Journal of Physics Condensed Matter*, 18(41). <https://doi.org/10.1088/0953-8984/18/41/R01>
- McCarthy, N. A., Kelly, A. L., O'Mahony, J. A., & Fenelon, M. A. (2014). Sensitivity of emulsions stabilised by bovine  $\beta$ -casein and lactoferrin to heat and CaCl<sub>2</sub>. *Food Hydrocolloids*, 35, 420–428. <https://doi.org/10.1016/j.foodhyd.2013.06.021>
- McClements, D. J. (2000). Comments on viscosity enhancement and depletion flocculation by polysaccharides. *Food Hydrocolloids*, 14(2), 173–177. <https://doi.org/10.1016/S0268->

005X(99)00065-X

- McClements, D. J. (2004). Protein-stabilized emulsions. *Current Opinion in Colloid & Interface Science*, 9(5), 305–313. <https://doi.org/10.1016/j.cocis.2004.09.003>
- McClements, D. J. (2009). Biopolymers in Food Emulsions. In *Modern Biopolymer Science* (First Edit, pp. 129–166). Elsevier. <https://doi.org/10.1016/B978-0-12-374195-0.00004-5>
- McClements, D. J. (2015a). Encapsulation, protection, and release of hydrophilic active components: Potential and limitations of colloidal delivery systems. *Advances in Colloid and Interface Science*, 219, 27–53. <https://doi.org/10.1016/j.cis.2015.02.002>
- McClements, D. J. (2015b). *Food Emulsions* (3rd edn). CRC Press. <https://doi.org/10.1201/b18868>
- McClements, D. J. (2018). Enhanced delivery of lipophilic bioactives using emulsions: a review of major factors affecting vitamin, nutraceutical, and lipid bioaccessibility. *Food and Function*, 9(1), 22–41. <https://doi.org/10.1039/c7fo01515a>
- McClements, D. J., & Decker, E. (2018). Interfacial antioxidants: a review of natural and synthetic emulsifiers and coemulsifiers that can inhibit lipid oxidation. *Journal of Agricultural and Food Chemistry*, 66(1), 20–35. <https://doi.org/10.1021/acs.jafc.7b05066>
- McClements, D. J., Decker, E. A., & Park, Y. (2009). Controlling lipid bioavailability through physicochemical and structural approaches. *Critical Reviews in Food Science and Nutrition*, 49(1), 48–67. <https://doi.org/10.1080/10408390701764245>
- McClements, D. J., Decker, E. A., & Weiss, J. (2007). Emulsion-based delivery systems for lipophilic bioactive components. *Journal of Food Science*, 72(8), 109–124.

<https://doi.org/10.1111/j.1750-3841.2007.00507.x>

McClements, D. J., & Dungan, S. R. (1993). Factors that affect the rate of oil exchange between oil-in-water emulsion droplets stabilized by a nonionic surfactant: droplet size, surfactant concentration, and ionic strength. *Journal of Physical Chemistry*, *97*(28), 7304–7308. <https://doi.org/10.1021/j100130a030>

McClements, D. J., Dungan, S. R., German, J. B., & Kinsella, J. E. (1993a). Evidence of oil exchange between oil-in-water emulsion droplets stabilized by milk proteins. *Journal of Colloid and Interface Science*, *156*(2), 425–429. <https://doi.org/10.1006/jcis.1993.1133>

McClements, D. J., & Gumus, C. E. (2016). Natural emulsifiers — biosurfactants, phospholipids, biopolymers, and colloidal particles: molecular and physicochemical basis of functional performance. *Advances in Colloid and Interface Science*, *234*, 3–26. <https://doi.org/10.1016/j.cis.2016.03.002>

McClements, D. J. J., Dungan, S. R. R., German, J. B. B., & Kinsella, J. E. E. (1992). Oil exchange between oil-in-water emulsion droplets stabilised with a non-ionic surfactant. *Food Hydrocolloids*, *6*(5), 415–422. [https://doi.org/10.1016/S0268-005X\(09\)80027-1](https://doi.org/10.1016/S0268-005X(09)80027-1)

McClements, D. J. J., MONAHAN, F. J. J., & Kinsella, J. E. E. (1993b). Disulfide bond formation affects stability of whey protein isolate emulsions. *Journal of Food Science*, *58*(5), 1036–1039. <https://doi.org/10.1111/j.1365-2621.1993.tb06106.x>

McClements, D. J., & Li, Y. (2010a). Review of in vitro digestion models for rapid screening of emulsion-based systems. *Food and Function*, *1*(1), 32–59. <https://doi.org/10.1039/c0fo00111b>

McClements, D. J., & Li, Y. (2010b). Structured emulsion-based delivery systems: controlling

- the digestion and release of lipophilic food components. *Advances in Colloid and Interface Science*, 159(2), 213–228. <https://doi.org/10.1016/j.cis.2010.06.010>
- McClements, D. J., & Li, Y. (2015). Response to comment on new mathematical model for interpreting pH-stat digestion profiles: impact of lipid droplet characteristics on in vitro digestibility. *Journal of Agricultural and Food Chemistry*, 63(47), 10354–10354. <https://doi.org/10.1021/acs.jafc.5b05219>
- Mehalebi, S., Nicolai, T., & Durand, D. (2008). Light scattering study of heat-denatured globular protein aggregates. *International Journal of Biological Macromolecules*, 43(2), 129–135. <https://doi.org/10.1016/j.ijbiomac.2008.04.002>
- Mertz, J. (2019). *Introduction to optical microscopy* (2nd edn). Cambridge University Press. <https://doi.org/10.1017/9781108552660>
- Moitzi, C., Guillot, S., Fritz, G., Salentinig, S., & Glatter, O. (2007). Phase reorganization in self-assembled systems through interparticle material transfer. *Advanced Materials*, 19(10), 1352–1358. <https://doi.org/10.1002/adma.200601679>
- Monahan, F. J., McClements, D. J., & German, J. B. (1996). Disulfide-mediated polymerization reactions and physical properties of heated WPI-stabilized emulsions. *Journal of Food Science*, 61(3), 504–509. <https://doi.org/10.1111/j.1365-2621.1996.tb13143.x>
- Motulsky, H., & Christopoulos, A. (2003). *Fitting models to biological data using linear and nonlinear regression: a practical guide to curve fitting*. GraphPad Software, Inc. [www.graphpad.com](http://www.graphpad.com)
- Mougel, J., Alvarez, O., Baravian, C., Caton, F., Marchal, P., Stébé, M.-J., & Choplin, L.

- (2006). Aging of an unstable w/o gel emulsion with a nonionic surfactant. *Rheologica Acta*, 45(5), 555–560. <https://doi.org/10.1007/s00397-006-0089-z>
- Mulvihill, D. M., & Murphy, P. C. (1991). Surface active and emulsifying properties of caseins/caseinates as influenced by state of aggregation. *International Dairy Journal*, 1(1), 13–37. [https://doi.org/10.1016/0958-6946\(91\)90025-4](https://doi.org/10.1016/0958-6946(91)90025-4)
- Mun, S., Decker, E. A., & McClements, D. J. (2007). Influence of emulsifier type on in vitro digestibility of lipid droplets by pancreatic lipase. *Food Research International*, 40(6), 770–781. <https://doi.org/10.1016/j.foodres.2007.01.007>
- Mun, S., Decker, E. A., McClements, D. J., A. Decker, E., Julian McClements, D., Decker, E. A., McClements, D. J., A. Decker, E., Julian McClements, D., Decker, E. A., & McClements, D. J. (2005). Influence of droplet characteristics on the formation of oil-in-water emulsions stabilized by surfactant-chitosan layers. *Langmuir*, 21(14), 6228–6234. <https://doi.org/10.1021/la050502w>
- Murphy, D. B., & Davidson, M. W. (2012). Fundamentals of light microscopy and electronic imaging. In *Fundamentals of Light Microscopy and Electronic Imaging: Second Edition* (2nd edn). John Wiley & Sons, Inc. <https://doi.org/10.1002/9781118382905>
- Murray, B. S., Durga, K., Yusoff, A., & Stoyanov, S. D. (2011). Stabilization of foams and emulsions by mixtures of surface active food-grade particles and proteins. *Food Hydrocolloids*, 25(4), 627–638. <https://doi.org/10.1016/j.foodhyd.2010.07.025>
- Murray, B. S., & Phisarnchananan, N. (2016). Whey protein microgel particles as stabilizers of waxy corn starch + locust bean gum water-in-water emulsions. *Food Hydrocolloids*, 56, 161–169. <https://doi.org/10.1016/j.foodhyd.2015.11.032>

- Nambam, J. S., & Philip, J. (2012). Competitive adsorption of polymer and surfactant at a liquid droplet interface and its effect on flocculation of emulsion. *Journal of Colloid and Interface Science*, *366*(1), 88–95. <https://doi.org/10.1016/j.jcis.2011.07.100>
- Nash, W., Pinder, D. N., Hemar, Y., & Singh, H. (2002). Dynamic light scattering investigation of sodium caseinate and xanthan mixtures. *International Journal of Biological Macromolecules*, *30*(5), 269–271. [https://doi.org/10.1016/S0141-8130\(02\)00041-7](https://doi.org/10.1016/S0141-8130(02)00041-7)
- Neeson, M. J., Chan, D. Y. C., & Tabor, R. F. (2014). Compound pendant drop tensiometry for interfacial tension measurement at zero bond number. *Langmuir*, *30*(51), 15388–15391. <https://doi.org/10.1021/la504406m>
- Nishinari, K. (2009). Some thoughts on the definition of a gel. *Progress in Colloid and Polymer Science*, *136*, 87–94. [https://doi.org/10.1007/2882\\_2009\\_12](https://doi.org/10.1007/2882_2009_12)
- Nöbel, S., Weidendorfer, K., & Hinrichs, J. (2012). Apparent voluminosity of casein micelles determined by rheometry. *Journal of Colloid and Interface Science*, *386*(1), 174–180. <https://doi.org/10.1016/j.jcis.2012.07.075>
- Norde, W. (1986). Adsorption of proteins from solution at the solid-liquid interface. *Advances in Colloid and Interface Science*, *25*(C), 267–340. [https://doi.org/10.1016/0001-8686\(86\)80012-4](https://doi.org/10.1016/0001-8686(86)80012-4)
- Noureddini, H., Teoh, B. C., & Davis Clements, L. (1992). Viscosities of vegetable oils and fatty acids. *Journal of the American Oil Chemists' Society*, *69*(12), 1189–1191. <https://doi.org/10.1007/BF02637678>
- Okubanjo, S. S., Loveday, S. M., Ye, A. M., Wilde, P. J., & Singh, H. (2019). Droplet-stabilized oil-in-water emulsions protect unsaturated lipids from oxidation. *Journal of*

- Agricultural and Food Chemistry*, 67(9), acs.jafc.8b02871.  
<https://doi.org/10.1021/acs.jafc.8b02871>
- Okubanjo, S. S., Ye, A., Wilde, P. J., Singh, H., & Loveday, S. M. (2021). Antioxidant performance in droplet-stabilized oil-in-water emulsions. *LWT*, 139(November 2020), 110541. <https://doi.org/10.1016/j.lwt.2020.110541>
- Pafumi, Y., Lairon, D., De La Porte, P. L., Juhel, C., Storch, J., Hamosh, M., & Armand, M. (2002). Mechanisms of inhibition of triacylglycerol hydrolysis by human gastric lipase. *Journal of Biological Chemistry*, 277(31), 28070–28079. <https://doi.org/10.1074/jbc.M202839200>
- Pal, R. (1996). Effect of droplet size on the rheology of emulsions. *AIChE Journal*, 42(11), 3181–3190. <https://doi.org/10.1002/aic.690421119>
- Pal, R. (2011). Rheology of simple and multiple emulsions. *Current Opinion in Colloid and Interface Science*, 16(1), 41–60. <https://doi.org/10.1016/j.cocis.2010.10.001>
- Panouillé, M., Benyahia, L., Durand, D., & Nicolai, T. (2005). Dynamic mechanical properties of suspensions of micellar casein particles. *Journal of Colloid and Interface Science*, 287(2), 468–475. <https://doi.org/10.1016/j.jcis.2005.02.007>
- Parker, T. G., & Dalgleish, D. G. (1981). Binding of calcium ions to bovine  $\beta$ -casein. *Journal of Dairy Research*, 48(1), 71–76. <https://doi.org/10.1017/S0022029900021476>
- Patel, A. R., & Dewettinck, K. (2016). Edible oil structuring: an overview and recent updates. *Food & Function*, 7(1), 20–29. <https://doi.org/10.1039/C5FO01006C>
- Paunov, V. N., Cayre, O. J., Noble, P. F., Stoyanov, S. D., Velikov, K. P., & Golding, M.

- (2007). Emulsions stabilised by food colloid particles: role of particle adsorption and wettability at the liquid interface. *Journal of Colloid and Interface Science*, 312(2), 381–389. <https://doi.org/10.1016/j.jcis.2007.03.031>
- Pawlik, A., Kurukji, D., Norton, I., & Spyropoulos, F. (2016). Food-grade Pickering emulsions stabilised with solid lipid particles. *Food & Function*, 7(6), 2712–2721. <https://doi.org/10.1039/C6FO00238B>
- Pedersen, J. S. (1997). Analysis of small-angle scattering data from colloids and polymer solutions: modeling and least-squares fitting. *Advances in Colloid and Interface Science*, 70(1–3), 171–210. [https://doi.org/10.1016/S0001-8686\(97\)00312-6](https://doi.org/10.1016/S0001-8686(97)00312-6)
- Pickering, S. U. (1907). Emulsions. *J. Chem. Soc., Trans.*, 91, 2001–2021. <https://doi.org/10.1039/CT9079102001>
- Pignol, D., Ayvazian, L., Kerfelec, B., Timmins, P., Crenon, I., Hermoso, J., Fontecilla-Camps, J. C., & Chapus, C. (2000). Critical role of micelles in pancreatic lipase activation revealed by small angle neutron scattering. *Journal of Biological Chemistry*, 275(6), 4220–4224. <https://doi.org/10.1074/jbc.275.6.4220>
- Pitkowski, A., Durand, D., & Nicolai, T. (2008). Structure and dynamical mechanical properties of suspensions of sodium caseinate. *Journal of Colloid and Interface Science*, 326(1), 96–102. <https://doi.org/10.1016/j.jcis.2008.07.003>
- Pitkowski, A., Nicolai, T., & Durand, D. (2009). Stability of caseinate solutions in the presence of calcium. *Food Hydrocolloids*, 23(4), 1164–1168. <https://doi.org/10.1016/j.foodhyd.2008.07.016>
- Porter, C. J. H., Trevaskis, N. L., & Charman, W. N. (2007). Lipids and lipid-based



- formulations: optimizing the oral delivery of lipophilic drugs. *Nature Reviews Drug Discovery*, 6(3), 231–248. <https://doi.org/10.1038/nrd2197>
- Princen, H. ., Aronson, M. ., & Moser, J. . (1980). Highly concentrated emulsions: II. Real systems. The effect of film thickness and contact angle on the volume fraction in creamed emulsions. *Journal of Colloid and Interface Science*, 75(1), 246–270. [https://doi.org/10.1016/0021-9797\(80\)90367-7](https://doi.org/10.1016/0021-9797(80)90367-7)
- Princen, H. ., & Kiss, A. . (1986). Rheology of foams and highly concentrated emulsions. *Journal of Colloid and Interface Science*, 112(2), 427–437. [https://doi.org/10.1016/0021-9797\(86\)90111-6](https://doi.org/10.1016/0021-9797(86)90111-6)
- Qiu, D., Cosgrove, T., Howe, A. M., & Dreiss, C. A. (2006). A small-angle X-ray scattering study of the interactions in concentrated silica colloidal dispersions. *Langmuir*, 22(2), 546–552. <https://doi.org/10.1021/la052061m>
- Quansah, J. K., Udenigwe, C. C., Saalia, F. K., & Yada, R. Y. (2013). The effect of thermal and ultrasonic treatment on amino acid composition, radical scavenging and reducing potential of hydrolysates obtained from simulated gastrointestinal digestion of cowpea proteins. *Plant Foods for Human Nutrition*, 68(1), 31–38. <https://doi.org/10.1007/s11130-013-0334-4>
- Radford, S. J., & Dickinson, E. (2004). Depletion flocculation of caseinate-stabilised emulsions: what is the optimum size of the non-adsorbed protein nano-particles? *Colloids and Surfaces A: Physicochemical and Engineering Aspects*, 238(1–3), 71–81. <https://doi.org/10.1016/j.colsurfa.2004.02.020>
- Ramírez-García, G., Trapiella-Alfonso, L., D’Orlyé, F., & D’Orlyé, A. (2018). Electrophoretic

- methods for characterizing nanoparticles and evaluating their bio-interactions for their further use as diagnostic, imaging, or therapeutic tools. *Capillary Electromigration Separation Methods*, 397–421. <https://doi.org/10.1016/B978-0-12-809375-7.00019-8>
- Ramsden, W. (1904). Separation of solids in the surface-layers of solutions and ‘suspensions’ (observations on surface-membranes, bubbles, emulsions, and mechanical coagulation).—Preliminary account. *Proceedings of the Royal Society of London*, 72(477–486), 156–164. <https://doi.org/10.1098/rspl.1903.0034>
- Rao, Y., Yang, H., Xue, D., Guo, Y., Qi, F., & Ma, J. (2016). Sonolytic and sonopholytic degradation of Carbamazepine: kinetic and mechanisms. *Ultrasonics Sonochemistry*, 32, 371–379. <https://doi.org/10.1016/j.ultsonch.2016.04.005>
- Raya, S. A., Mohd Saaïd, I., Abbas Ahmed, A., & Abubakar Umar, A. (2020). A critical review of development and demulsification mechanisms of crude oil emulsion in the petroleum industry. *Journal of Petroleum Exploration and Production Technology*, 10(4), 1711–1728. <https://doi.org/10.1007/s13202-020-00830-7>
- Rehm, C., Brûlé, A., Freund, A. K., & Kennedy, S. J. (2013). Kookaburra: the ultra-small-angle neutron scattering instrument at OPAL. *Journal of Applied Crystallography*, 46(6), 1699–1704. <https://doi.org/10.1107/S0021889813025788>
- Rehm, C., & de Campo, L. (2016). KOOKABURRA: the ultra-small-angle neutron scattering instrument at ANSTO. *Neutron News*, 27(2), 30–32. <https://doi.org/10.1080/10448632.2016.1165063>
- Reynolds, P. A., Gilbert, E. P., & White, J. W. (2000). High internal phase water-in-oil emulsions studied by small-angle neutron scattering. *Journal of Physical Chemistry B*,

104(30), 7012–7022. <https://doi.org/10.1021/jp000327m>

Richards, J. J. (2018). *Contrast variation small angle neutron scattering-identifying the unique fingerprints for the structure of proteins*. <https://www.nist.gov/system/files/documents/2018/06/15/ng7sansc2.pdf>

Richtering, W. (2012). Responsive emulsions stabilized by stimuli-sensitive microgels: Emulsions with special non-pickering properties. *Langmuir*, 28(50), 17218–17229. <https://doi.org/10.1021/la302331s>

Riquelme, N., Robert, P., Troncoso, E., & Arancibia, C. (2020). Influence of the particle size and hydrocolloid type on lipid digestion of thickened emulsions. *Food and Function*, 11(7), 5955–5964. <https://doi.org/10.1039/d0fo01202e>

Robins, M. M., Watson, A. D., & Wilde, P. J. (2002). Emulsions—creaming and rheology. *Current Opinion in Colloid & Interface Science*, 7(5–6), 419–425. [https://doi.org/10.1016/S1359-0294\(02\)00089-4](https://doi.org/10.1016/S1359-0294(02)00089-4)

Robson, E. W., & Dalgleish, D. G. D. G. D. G. (1987). Interfacial composition of sodium caseinate emulsions. *Journal of Food Science*, 52(6), 1694–1698. <https://doi.org/10.1111/j.1365-2621.1987.tb05908.x>

Roger, K., Olsson, U., Schweins, R., & Cabane, B. (2015). Emulsion ripening through molecular exchange at droplet contacts. *Angewandte Chemie*, 127(5), 1472–1475. <https://doi.org/10.1002/ange.201407858>

Romero, I. C., Urban, M. A., & Punyasena, S. W. (2020). Review of palaeobotany and palynology Airyscan superresolution microscopy: a high-throughput alternative to electron microscopy for the visualization and analysis of fossil pollen. *Review of*

---

*Palaeobotany and Palynology*, 276, 104192.  
<https://doi.org/10.1016/j.revpalbo.2020.104192>

Ross-Murphy, S. B. B., Shatwell, K. P. P., SB, R.-M., & KP., S. (1993). Polysaccharide strong and weak gels. *Biorheology*, 30(3–4), 217–227. <https://doi.org/10.3233/BIR-1993-303-407>

Rousseau, D. (2000). Fat crystals and emulsion stability — a review. *Food Research International*, 33(1), 3–14. [https://doi.org/10.1016/S0963-9969\(00\)00017-X](https://doi.org/10.1016/S0963-9969(00)00017-X)

Rousseau, D. (2013). Trends in structuring edible emulsions with Pickering fat crystals. *Current Opinion in Colloid and Interface Science*, 18(4), 283–291. <https://doi.org/10.1016/j.cocis.2013.04.009>

Saiki, Y., & Prestidge, C. A. (2005). Droplet deformability and emulsion rheology: steady and dynamic behavior. *Korea Australia Rheology Journal*, 17(4), 191–198.

Sakellari, G. I., Zafeiri, I., Pawlik, A., Kurukji, D., Taylor, P., Norton, I. T., & Spyropoulos, F. (2021). Independent co-delivery of model actives with different degrees of hydrophilicity from oil-in-water and water-in-oil emulsions stabilised by solid lipid particles via a Pickering mechanism: a-proof-of-principle study. *Journal of Colloid and Interface Science*, 587, 644–649. <https://doi.org/10.1016/j.jcis.2020.11.021>

Salari, J. W. O., Mutsaers, G., Meuldijk, J., & Klumperman, B. (2014). Deformation of the water/oil interface during the adsorption of sterically stabilized particles. *Langmuir*, 30(25), 7327–7333. <https://doi.org/10.1021/la501334p>

Salis, A., Boström, M., Medda, L., Cugia, F., Barse, B., Parsons, D. F., Ninham, B. W., & Monduzzi, M. (2011). Measurements and theoretical interpretation of points of zero

- charge/potential of BSA protein. *Langmuir*, 27(18), 11597–11604.  
<https://doi.org/10.1021/la2024605>
- Salvia-Trujillo, L., Qian, C., Martín-Belloso, O., & McClements, D. J. (2013). Influence of particle size on lipid digestion and  $\beta$ -carotene bioaccessibility in emulsions and nanoemulsions. *Food Chemistry*, 141(2), 1472–1480.  
<https://doi.org/10.1016/j.foodchem.2013.03.050>
- Santos, T. P., Okuro, P. K., & Cunha, R. L. (2021). Pickering emulsions as a platform for structures design: cutting-edge strategies to engineer digestibility. *Food Hydrocolloids*, 116(December 2020), 106645. <https://doi.org/10.1016/j.foodhyd.2021.106645>
- Santos, F. J. V, Nieto de Castro, C. A., Dymond, J. H., Dalaouti, N. K., Assael, M. J., & Nagashima, A. (2006). Standard reference data for the viscosity of toluene. *Journal of Physical and Chemical Reference Data*, 35(1), 1–8. <https://doi.org/10.1063/1.1928233>
- Sarkar, A., & Dickinson, E. (2020). Sustainable food-grade Pickering emulsions stabilized by plant-based particles. *Current Opinion in Colloid and Interface Science*, 49, 69–81.  
<https://doi.org/10.1016/j.cocis.2020.04.004>
- Sarkar, A., Goh, K. K. T., Singh, R. P., & Singh, H. (2009). Behaviour of an oil-in-water emulsion stabilized by  $\beta$ -lactoglobulin in an in vitro gastric model. *Food Hydrocolloids*, 23(6), 1563–1569. <https://doi.org/10.1016/j.foodhyd.2008.10.014>
- Sarkar, A., Kanti, F., Gulotta, A., Murray, B. S., & Zhang, S. (2017). Aqueous lubrication, structure and rheological properties of whey protein microgel Particles. *Langmuir*, 33(51), 14699–14708. <https://doi.org/10.1021/acs.langmuir.7b03627>
- Sarkar, A., Murray, B., Holmes, M., Ettelaie, R., Abdalla, A., & Yang, X. (2016a). In vitro

- digestion of Pickering emulsions stabilized by soft whey protein microgel particles: Influence of thermal treatment. *Soft Matter*, 12(15), 3558–3569. <https://doi.org/10.1039/c5sm02998h>
- Sarkar, A., Ye, A., & Singh, H. (2016b). On the role of bile salts in the digestion of emulsified lipids. *Food Hydrocolloids*, 60, 77–84. <https://doi.org/10.1016/j.foodhyd.2016.03.018>
- Sarkar, A., Zhang, S., Holmes, M., & Ettelaie, R. (2019). Colloidal aspects of digestion of Pickering emulsions: Experiments and theoretical models of lipid digestion kinetics. *Advances in Colloid and Interface Science*, 263, 195–211. <https://doi.org/10.1016/j.cis.2018.10.002>
- Schaefer, D. W. (1989). Polymers, fractals, and ceramic materials. *Science*, 243(4894), 1023–1027. <https://doi.org/10.1126/science.243.4894.1023>
- Schaefer, D. W., Zhao, J., Brown, J. M., Anderson, D. P., & Tomlin, D. W. (2003). Morphology of dispersed carbon single-walled nanotubes. *Chemical Physics Letters*, 375(3–4), 369–375. [https://doi.org/10.1016/S0009-2614\(03\)00867-4](https://doi.org/10.1016/S0009-2614(03)00867-4)
- Schmitt, C., Moitzi, C., Bovay, C., Rouvet, M., Bovetto, L., Donato, L., Leser, M. E., Schurtenberger, P., & Stradner, A. (2010). Internal structure and colloidal behaviour of covalent whey protein microgels obtained by heat treatment. *Soft Matter*, 6(19), 4876. <https://doi.org/10.1039/c0sm00220h>
- Schmitt, V., Cattelet, C., & Leal-Calderon, F. (2004). Coarsening of alkane-in-water emulsions stabilized by nonionic poly(oxyethylene) surfactants: the role of molecular permeation and coalescence. *Langmuir*, 20(1), 46–52. <https://doi.org/10.1021/la034747p>
- Schröder, A., Berton-Carabin, C., Venema, P., & Cornacchia, L. (2017). Interfacial properties

- of whey protein and whey protein hydrolysates and their influence on O/W emulsion stability. *Food Hydrocolloids*, *73*, 129–140.  
<https://doi.org/10.1016/j.foodhyd.2017.06.001>
- Schröder, A., Sprakel, J., Schroën, K., Spaen, J. N., & Berton-Carabin, C. C. (2018). Coalescence stability of Pickering emulsions produced with lipid particles: a microfluidic study. *Journal of Food Engineering*, *234*, 63–72.  
<https://doi.org/10.1016/j.jfoodeng.2018.04.007>
- Scott, G. D., & Kilgour, D. M. (1969). The density of random close packing of spheres. *Journal of Physics D: Applied Physics*, *2*(6), 863–866. <https://doi.org/10.1088/0022-3727/2/6/311>
- Sek, L., Porter, C. J. H., Kaukonen, A. M., & Charman, W. N. (2002). Evaluation of the in-vitro digestion profiles of long and medium chain glycerides and the phase behaviour of their lipolytic products. *Journal of Pharmacy and Pharmacology*, *54*(1), 29–41.  
<https://doi.org/10.1211/0022357021771896>
- Seth, J. R., Mohan, L., Locatelli-Champagne, C., Cloitre, M., & Bonnecaze, R. T. (2011). A micromechanical model to predict the flow of soft particle glasses. *Nature Materials*, *10*(11), 838–843. <https://doi.org/10.1038/nmat3119>
- Shi, A., Feng, X., Wang, Q., & Adhikari, B. (2020). Pickering and high internal phase Pickering emulsions stabilized by protein-based particles: a review of synthesis, application and prospective. *Food Hydrocolloids*, *109*(June), 106117.  
<https://doi.org/10.1016/j.foodhyd.2020.106117>
- Singh, B., & Indra, A. (2020). Surface and interface engineering in transition metal-based catalysts for electrochemical water oxidation. *Materials Today Chemistry*, *16*, 100239.

<https://doi.org/10.1016/j.mtchem.2019.100239>

Singh, H. (2011). Aspects of milk-protein-stabilised emulsions. *Food Hydrocolloids*, 25(8), 1938–1944. <https://doi.org/10.1016/j.foodhyd.2011.02.022>

Singh, H., & Ye, A. (2013). Structural and biochemical factors affecting the digestion of protein-stabilized emulsions. *Current Opinion in Colloid and Interface Science*, 18(4), 360–370. <https://doi.org/10.1016/j.cocis.2013.04.006>

Singh, H., Ye, A., & Horne, D. (2009). Structuring food emulsions in the gastrointestinal tract to modify lipid digestion. *Progress in Lipid Research*, 48(2), 92–100. <https://doi.org/10.1016/j.plipres.2008.12.001>

Smalowska, A., Matia-Merino, L., Ingham, B., & Carr, A. J. J. (2017). Effect of calcium on the aggregation behaviour of caseinates. *Colloids and Surfaces A: Physicochemical and Engineering Aspects*, 522, 113–123. <https://doi.org/10.1016/j.colsurfa.2017.02.074>

Sokolova, A., Christoforidis, J., Eltobaji, A., Barnes, J., Darmann, F., Whitten, A. E., & de Campo, L. (2016). BILBY: time-of-flight small angle scattering instrument. *Neutron News*, 27(2), 9–13. <https://doi.org/10.1080/10448632.2016.1163980>

Sokolova, A., Whitten, A. E., de Campo, L., Christoforidis, J., Eltobaji, A., Barnes, J., Darmann, F., & Berry, A. (2019). Performance and characteristics of the BILBY time-of-flight small-angle neutron scattering instrument. *Journal of Applied Crystallography*, 52(1), 1–12. <https://doi.org/10.1107/s1600576718018009>

Sosa-Herrera, M. G., Berli, C. L. A., & Martínez-Padilla, L. P. (2008). Physicochemical and rheological properties of oil-in-water emulsions prepared with sodium caseinate/gellan gum mixtures. *Food Hydrocolloids*, 22(5), 934–942.



<https://doi.org/10.1016/j.foodhyd.2007.05.003>

Sosa-Herrera, M. G. G., Lozano-Esquivel, I. E. E., Ponce de León-Ramírez, Y. R. R., & Martínez-Padilla, L. P. P. (2012). Effect of added calcium chloride on the physicochemical and rheological properties of aqueous mixtures of sodium caseinate/sodium alginate and respective oil-in-water emulsions. *Food Hydrocolloids*, 29(1), 175–184. <https://doi.org/10.1016/j.foodhyd.2012.02.017>

Sriamornsak, P., Thirawong, N., Cheewatanakornkool, K., Burapapadh, K., & Sae-Ngow, W. (2008). Cryo-scanning electron microscopy (cryo-SEM) as a tool for studying the ultrastructure during bead formation by ionotropic gelation of calcium pectinate. *International Journal of Pharmaceutics*, 352(1–2), 115–122. <https://doi.org/10.1016/j.ijpharm.2007.10.038>

Srinivasan, M., Singh, H., & Munro, P. A. (1996). Sodium caseinate-stabilized emulsions: factors affecting coverage and composition of surface proteins. *Journal of Agricultural and Food Chemistry*, 44(12), 3807–3811. <https://doi.org/10.1021/jf960135h>

Stetefeld, J., McKenna, S. A., & Patel, T. R. (2016). Dynamic light scattering: a practical guide and applications in biomedical sciences. *Biophysical Reviews*, 8(4), 409–427. <https://doi.org/10.1007/s12551-016-0218-6>

Stothart, P. H., & Cebula, D. J. (1982). Small-angle neutron scattering study of bovine casein micelles and sub-micelles. *Journal of Molecular Biology*, 160(2), 391–395. [https://doi.org/10.1016/0022-2836\(82\)90185-1](https://doi.org/10.1016/0022-2836(82)90185-1)

Su, J., & Cavaco-Paulo, A. (2021). Effect of ultrasound on protein functionality. *Ultrasonics Sonochemistry*, 76, 105653. <https://doi.org/10.1016/j.ultsonch.2021.105653>

- Su, J., Wang, X., Li, W., Chen, L., Zeng, X., Huang, Q., & Hu, B. (2018). Enhancing the Viability of *Lactobacillus plantarum* as Probiotics through Encapsulation with High Internal Phase Emulsions Stabilized with Whey Protein Isolate Microgels. *Journal of Agricultural and Food Chemistry*, 66(46), 12335–12343. <https://doi.org/10.1021/acs.jafc.8b03807>
- Swaisgood, H. E. (2003). Chemistry of the Caseins. In P. F. Fox & P. L. H. McSweeney (Eds.), *Advanced Dairy Chemistry—1 Proteins* (3rd edn, pp. 139–201). Springer US. [https://doi.org/10.1007/978-1-4419-8602-3\\_3](https://doi.org/10.1007/978-1-4419-8602-3_3)
- Tadros, T. (2004). Application of rheology for assessment and prediction of the long-term physical stability of emulsions. *Advances in Colloid and Interface Science*, 108–109, 227–258. <https://doi.org/10.1016/j.cis.2003.10.025>
- Tadros, T. F. (1994). Fundamental principles of emulsion rheology and their applications. *Colloids and Surfaces A: Physicochemical and Engineering Aspects*, 91, 39–55. [https://doi.org/10.1016/0927-7757\(93\)02709-N](https://doi.org/10.1016/0927-7757(93)02709-N)
- Tadros, T. F. (2013a). *Emulsion formation and stability*. John Wiley & Sons.
- Tadros, T. F. (2013b). Emulsion formation, stability, and rheology. In *Emulsion Formation and Stability* (pp. 1–75). Wiley. <https://doi.org/10.1002/9783527647941.ch1>
- Tan, C., & McClements, D. J. (2021). Application of advanced emulsion technology in the food industry: A review and critical evaluation. *Foods*, 10(4). <https://doi.org/10.3390/foods10040812>
- Tan, Y., Xu, K., Niu, C., Liu, C., Li, Y., Wang, P., & Binks, B. P. (2014). Triglyceride-water emulsions stabilised by starch-based nanoparticles. *Food Hydrocolloids*, 36, 70–75.

<https://doi.org/10.1016/j.foodhyd.2013.08.032>

Tan, Y., Zhang, Z., Muriel Mundo, J., & McClements, D. J. (2020). Factors impacting lipid digestion and nutraceutical bioaccessibility assessed by standardized gastrointestinal model (INFOGEST): emulsifier type. *Food Research International*, 137, 109739. <https://doi.org/10.1016/j.foodres.2020.109739>

Taneja, A., Ye, A., & Singh, H. (2015). Influence of protein concentration on the stability of oil-in-water emulsions formed with aggregated milk proteins during spray drying. *Dairy Science and Technology*, 95(3), 279–293. <https://doi.org/10.1007/s13594-014-0208-z>

Tang, Y. R., & Ghosh, S. (2021). Stability and rheology of canola protein isolate-stabilized concentrated oil-in-water emulsions. *Food Hydrocolloids*, 113(October 2020), 106399. <https://doi.org/10.1016/j.foodhyd.2020.106399>

Taylor, P. (2003). Ostwald ripening in emulsions: Estimation of solution thermodynamics of the disperse phase. *Advances in Colloid and Interface Science*, 106(1–3), 261–285. [https://doi.org/10.1016/S0001-8686\(03\)00113-1](https://doi.org/10.1016/S0001-8686(03)00113-1)

Tcholakova, S., Denkov, N. D., & Lips, A. (2008). Comparison of solid particles, globular proteins and surfactants as emulsifiers. *Phys. Chem. Chem. Phys.*, 10(12), 1608–1627. <https://doi.org/10.1039/b715933c>

Tomas, A., Paquet, D., Courthaudon, J. L., & Lorient, D. (1994). Effect of fat and protein contents on droplet size and surface protein coverage in dairy emulsions. *Journal of Dairy Science*, 77(2), 413–417. [https://doi.org/10.3168/jds.S0022-0302\(94\)76967-8](https://doi.org/10.3168/jds.S0022-0302(94)76967-8)

van Aken, G. A. (2003). Coalescence Mechanisms in Protein-Stabilized Emulsions. In J. S. S.E. Friberg, K. Larsson (Ed.), *Food Emulsions* (4th edn, pp. 299–325). CRC press.

<https://doi.org/10.1201/9780203913222.ch8>

van Aken, G. A., Blijdenstein, T. B. J., & Hotrum, N. E. (2003). Colloidal destabilisation mechanisms in protein-stabilized emulsions. *Current Opinion in Colloid and Interface Science*, 8(4–5), 371–379. [https://doi.org/10.1016/S1359-0294\(03\)00098-0](https://doi.org/10.1016/S1359-0294(03)00098-0)

van Aken, G. A., Vingerhoeds, M. H., & de Wijk, R. A. (2011). Textural perception of liquid emulsions: role of oil content, oil viscosity and emulsion viscosity. *Food Hydrocolloids*, 25(4), 789–796. <https://doi.org/10.1016/j.foodhyd.2010.09.015>

Verruto, V. J., & Kilpatrick, P. K. (2008). Water-in-model oil emulsions studied by small-angle neutron scattering: interfacial film thickness and composition. *Langmuir*, 24(22), 12807–12822. <https://doi.org/10.1021/la802095m>

Walstra, P., Walstra, P., Wouters, J. T. M., & Geurts, T. J. (2005). *Dairy science and technology* (2nd edn). CRC Press. <https://doi.org/10.1201/9781420028010>

Wang, A. J., Paterson, T., Owen, R., Sherborne, C., Dugan, J., Li, J. M., & Claeysens, F. (2016). Photocurable high internal phase emulsions (HIPEs) containing hydroxyapatite for additive manufacture of tissue engineering scaffolds with multi-scale porosity. *Materials Science and Engineering C*, 67, 51–58. <https://doi.org/10.1016/j.msec.2016.04.087>

Wang, K., Hong, Y., Gu, Z., Cheng, L., Li, Z., & Li, C. (2020a). Stabilization of Pickering emulsions using starch nanocrystals treated with alkaline solution. *International Journal of Biological Macromolecules*, 155, 273–285. <https://doi.org/10.1016/j.ijbiomac.2020.03.219>

Wang, P., Chen, C., Guo, H., Zhang, H., Yang, Z., & Ren, F. (2018). Casein gel particles as

- novel soft Pickering stabilizers: the emulsifying property and packing behaviour at the oil-water interface. *Food Hydrocolloids*, 77, 689–698. <https://doi.org/10.1016/j.foodhyd.2017.11.010>
- Wang, S., Shao, G., Yang, J., Zhao, H., Qu, D., Zhang, D., Zhu, D., He, Y., & Liu, H. (2020b). Contribution of soybean polysaccharides in digestion of oil-in-water emulsion-based delivery system in an in vitro gastric environment. *Food Science and Technology International*, 26(5), 444–452. <https://doi.org/10.1177/1082013219894145>
- Wang, X., Lin, Q., Ye, A., Han, J., & Singh, H. (2019). Flocculation of oil-in-water emulsions stabilised by milk protein ingredients under gastric conditions: impact on in vitro intestinal lipid digestion. *Food Hydrocolloids*, 88, 272–282. <https://doi.org/10.1016/j.foodhyd.2018.10.001>
- Webster, A. J., & Cates, M. E. (1998). Stabilization of emulsions by trapped species. *Langmuir*, 14(8), 2068–2079. <https://doi.org/10.1021/la9712597>
- Wei, Y., Tong, Z., Dai, L., Wang, D., Lv, P., Liu, J., Mao, L., Yuan, F., & Gao, Y. (2020). Influence of interfacial compositions on the microstructure, physiochemical stability, lipid digestion and  $\beta$ -carotene bioaccessibility of Pickering emulsions. *Food Hydrocolloids*, 104(17), 105738. <https://doi.org/10.1016/j.foodhyd.2020.105738>
- Wei, Y., Zhou, D., Mackie, A., Yang, S., Dai, L., Zhang, L., Mao, L., & Gao, Y. (2021). Stability, interfacial structure, and gastrointestinal digestion of  $\beta$ -carotene-loaded Pickering emulsions co-stabilized by particles, a biopolymer, and a surfactant. *Journal of Agricultural and Food Chemistry*, 69(5), 1619–1636. <https://doi.org/10.1021/acs.jafc.0c06409>

- Weiss, J., Cancelliere, C., & McClements, D. J. (2000). Mass transport phenomena in oil-in-water emulsions containing surfactant micelles: Ostwald ripening. *Langmuir*, *16*(17), 6833–6838. <https://doi.org/10.1021/la991477v>
- Weiss, J., Herrmann, N., & McClements, D. J. (1999). Ostwald ripening of hydrocarbon emulsion droplets in surfactant solutions. *Langmuir*, *15*(20), 6652–6657. <https://doi.org/10.1021/la981739d>
- Weng, J., Lin, R., Jiang, C., Wei, W., Wang, X., & Jin, Q. (2021). O/W emulsion stabilized by bovine milk phospholipid-protein nanoemulsions: preparation, stability, and in vitro digestion. *Journal of Agricultural and Food Chemistry*, *69*(17), 5003–5012. <https://doi.org/10.1021/acs.jafc.0c05617>
- Wijaya, W., Patel, A. R., Setiowati, A. D., & Van der Meeren, P. (2017). Functional colloids from proteins and polysaccharides for food applications. *Trends in Food Science and Technology*, *68*, 56–69. <https://doi.org/10.1016/j.tifs.2017.08.003>
- Wijayanti, H. B., Bansal, N., & Deeth, H. C. (2014). Stability of whey proteins during thermal processing: a Review. *Comprehensive Reviews in Food Science and Food Safety*, *13*(6), 1235–1251. <https://doi.org/10.1111/1541-4337.12105>
- Wilde, P. J., & Chu, B. S. (2011). Interfacial & colloidal aspects of lipid digestion. *Advances in Colloid and Interface Science*, *165*(1), 14–22. <https://doi.org/10.1016/j.cis.2011.02.004>
- Wilde, P., Mackie, A., Husband, F., Gunning, P., & Morris, V. (2004). Proteins and emulsifiers at liquid interfaces. *Advances in Colloid and Interface Science*, *108–109*, 63–71. <https://doi.org/10.1016/j.cis.2003.10.011>
- Wilking, J. N., & Mason, T. G. (2007). Irreversible shear-induced vitrification of droplets into

- elastic nanoemulsions by extreme rupturing. *Physical Review E*, 75(4), 041407. <https://doi.org/10.1103/PhysRevE.75.041407>
- Williams, H. D., Sassene, P., Kleberg, K., Bakala-N’Goma, J.-C., Calderone, M., Jannin, V., Igonin, A., Partheil, A., Marchaud, D., Jule, E., Vertommen, J., Maio, M., Blundell, R., Benameur, H., Carrière, F., Müllertz, A., Porter, C. J. H., & Pouton, C. W. (2012). Toward the establishment of standardized in vitro tests for lipid-based formulations, part 1: method parameterization and comparison of in vitro digestion profiles across a range of representative formulations. *Journal of Pharmaceutical Sciences*, 101(9), 3360–3380. <https://doi.org/10.1002/jps.23205>
- Witten, T. A., Witten, T., Pincus, P. A., & Pincus, P. (2004). *Structured fluids: polymers, colloids, surfactants*. Oxford University Press on Demand.
- Wood, K., Mata, J. P., Garvey, C. J., Wu, C. M., Hamilton, W. A., Abbeywick, P., Bartlett, D., Bartsch, F., Baxter, P., Booth, N., Brown, W., Christoforidis, J., Clowes, D., D’Adam, T., Darmann, F., Deura, M., Harrison, S., Hauser, N., Horton, G., ... Gilbert, E. P. (2018). QUOKKA, the pinhole small-angle neutron scattering instrument at the OPAL Research Reactor, Australia: design, performance, operation and scientific highlights. *Journal of Applied Crystallography*, 51(2), 294–314. <https://doi.org/10.1107/S1600576718002534>
- Wooster, T. J., & Augustin, M. A. (2006).  $\beta$ -lactoglobulin–dextran Maillard conjugates: their effect on interfacial thickness and emulsion stability. *Journal of Colloid and Interface Science*, 303(2), 564–572. <https://doi.org/10.1016/j.jcis.2006.07.081>
- Wu, X., & Hammer, J. A. (2022). *ZEISS Airyscan: Optimizing usage for fast, gentle, super-resolution imaging*. 1–18. <https://doi.org/10.1007/978-1-0716-1402-0>

- Xu, D., Yuan, F., Gao, Y., Panya, A., McClements, D. J., & Decker, E. A. (2014). Influence of whey protein-beet pectin conjugate on the properties and digestibility of  $\beta$ -carotene emulsion during in vitro digestion. *Food Chemistry*, *156*, 374–379. <https://doi.org/10.1016/j.foodchem.2014.02.019>
- Xu, T., Yang, J., Hua, S., Hong, Y., Gu, Z., Cheng, L., Li, Z., & Li, C. (2020a). Characteristics of starch-based Pickering emulsions from the interface perspective. *Trends in Food Science and Technology*, *105*, 334–346. <https://doi.org/10.1016/j.tifs.2020.09.026>
- Xu, Y.-T., Tang, C.-H., & Binks, B. P. (2020b). High internal phase emulsions stabilized solely by a globular protein glycosylated to form soft particles. *Food Hydrocolloids*, *98*, 105254. <https://doi.org/10.1016/j.foodhyd.2019.105254>
- Xu, Y. T., Liu, T. X., & Tang, C. H. (2019). Novel pickering high internal phase emulsion gels stabilized solely by soy  $\beta$ -conglycinin. *Food Hydrocolloids*, *88*, 21–30. <https://doi.org/10.1016/j.foodhyd.2018.09.031>
- Xu, Y. T., Tang, C. H., Liu, T. X., & Liu, R. (2018). Ovalbumin as an outstanding Pickering nanostabilizer for high internal phase emulsions. *Journal of Agricultural and Food Chemistry*, *66*(33), 8795–8804. <https://doi.org/10.1021/acs.jafc.8b02183>
- Xue, J., & Zhong, Q. (2014). Thyme oil nanoemulsions coemulsified by sodium caseinate and lecithin. *Journal of Agricultural and Food Chemistry*, *62*(40), 9900–9907. <https://doi.org/10.1021/jf5034366>
- Yan, C., McClements, D. J., Zhu, Y., Zou, L., Zhou, W., & Liu, W. (2019). Fabrication of OSA starch/chitosan polysaccharide-based high internal phase emulsion via altering interfacial behaviors. *Journal of Agricultural and Food Chemistry*, *67*(39), 10937–10946.



<https://doi.org/10.1021/acs.jafc.9b04009>

Yan, X., Ma, C., Cui, F., McClements, D. J., Liu, X., & Liu, F. (2020). Protein-stabilized Pickering emulsions: formation, stability, properties, and applications in foods. *Trends in Food Science and Technology*, *103*, 293–303. <https://doi.org/10.1016/j.tifs.2020.07.005>

Yang, F., Niu, Q., Lan, Q., & Sun, D. (2007). Effect of dispersion pH on the formation and stability of Pickering emulsions stabilized by layered double hydroxides particles. *Journal of Colloid and Interface Science*, *306*(2), 285–295. <https://doi.org/10.1016/j.jcis.2006.10.062>

Yang, H., Liu, D., Ju, J., Li, J., Wang, Z., Yan, G., Ji, Y., Zhang, W., Sun, G., & Li, L. (2016). Chain deformation on the formation of shish nuclei under extension flow: an in situ SANS and SAXS study. *Macromolecules*, *49*(23), 9080–9088. <https://doi.org/10.1021/acs.macromol.6b01945>

Yang, Y., Fang, Z., Chen, X., Zhang, W., Xie, Y., Chen, Y., Liu, Z., & Yuan, W. (2017). An overview of Pickering emulsions: solid-particle materials, classification, morphology, and applications. *Frontiers in Pharmacology*, *8*, 1–20. <https://doi.org/10.3389/fphar.2017.00287>

Yang, Z., Chen, M., Xia, M., Wang, M., & Wang, X. (2019a). An effective and durable interface structure design for oxygen reduction and methanol oxidation electrocatalyst. *Applied Surface Science*, *487*, 655–663. <https://doi.org/10.1016/j.apsusc.2019.04.237>

Yang, Z., de Campo, L., Gilbert, E. P., Knott, R., Cheng, L., Storer, B., Lin, X., Luo, L., Patole, S., & Hemar, Y. (2022). Effect of NaCl and CaCl<sub>2</sub> concentration on the rheological and structural characteristics of thermally-induced quinoa protein gels. *Food Hydrocolloids*,

124, 107350. <https://doi.org/10.1016/j.foodhyd.2021.107350>

Yang, Z., Xu, X., Hemar, Y., Mo, G., de Campo, L., & Gilbert, E. P. (2020). Effect of porous waxy rice starch addition on acid milk gels: Structural and physicochemical functionality. *Food Hydrocolloids*, *109*, 106092. <https://doi.org/10.1016/j.foodhyd.2020.106092>

Yang, Z., Xu, X., Singh, R., de Campo, L., Gilbert, E. P., Wu, Z., & Hemar, Y. (2019b). Effect of amyloglucosidase hydrolysis on the multi-scale supramolecular structure of corn starch. *Carbohydrate Polymers*, *212*, 40–50. <https://doi.org/10.1016/j.carbpol.2019.02.028>

Ye, A. (2010). Surface protein composition and concentration of whey protein isolate-stabilized oil-in-water emulsions: Effect of heat treatment. *Colloids and Surfaces B: Biointerfaces*, *78*(1), 24–29. <https://doi.org/10.1016/j.colsurfb.2010.02.001>

Ye, A. (2021). Gastric colloidal behaviour of milk protein as a tool for manipulating nutrient digestion in dairy products and protein emulsions. *Food Hydrocolloids*, *115*(November 2020), 106599. <https://doi.org/10.1016/j.foodhyd.2021.106599>

Ye, A., Cui, J., Dalgleish, D., & Singh, H. (2016). The formation and breakdown of structured clots from whole milk during gastric digestion. *Food and Function*, *7*(10), 4259–4266. <https://doi.org/10.1039/c6fo00228e>

Ye, A., Cui, J., Zhu, X., & Singh, H. (2013a). Effect of calcium on the kinetics of free fatty acid release during in vitro lipid digestion in model emulsions. *Food Chemistry*, *139*(1–4), 681–688. <https://doi.org/10.1016/j.foodchem.2013.02.014>

Ye, A., & Singh, H. (2001). Interfacial composition and stability of sodium caseinate emulsions as influenced by calcium ions. *Food Hydrocolloids*, *15*(2), 195–207. [https://doi.org/10.1016/S0268-005X\(00\)00065-5](https://doi.org/10.1016/S0268-005X(00)00065-5)

- Ye, A., Wang, X., Lin, Q., Han, J., & Singh, H. (2020). Dynamic gastric stability and in vitro lipid digestion of whey-protein-stabilised emulsions: effect of heat treatment. *Food Chemistry*, 318, 126463. <https://doi.org/10.1016/j.foodchem.2020.126463>
- Ye, A., Zhu, X., & Singh, H. (2013b). Oil-in-water emulsion system stabilized by protein-coated nanoemulsion droplets. *Langmuir*, 29(47), 14403–14410. <https://doi.org/10.1021/la403493y>
- Yesiltas, B., Torkkeli, M., Almásy, L., Dudás, Z., Wacha, A. F., Dalglish, R., García-Moreno, P. J., Sørensen, A.-D. D. M., Jacobsen, C., & Knaapila, M. (2019). Interfacial structure of 70% fish oil-in-water emulsions stabilized with combinations of sodium caseinate and phosphatidylcholine. *Journal of Colloid and Interface Science*, 554, 183–190. <https://doi.org/10.1016/j.jcis.2019.06.103>
- Yu, H., Seow, Y.-X., Ong, P. K. C., & Zhou, W. (2018). Effects of high-intensity ultrasound and oil type on the Maillard reaction of d-glucose and glycine in oil-in-water systems. *Npj Science of Food*, 2(1). <https://doi.org/10.1038/s41538-017-0010-4>
- Yukuyama, M. N., Ghisleni, D. D. M., Pinto, T. J. A., & Bou-Chacra, N. A. (2016). Nanoemulsion: process selection and application in cosmetics - a review. *International Journal of Cosmetic Science*, 38(1), 13–24. <https://doi.org/10.1111/ics.12260>
- Zank, J., Reynolds, P. A., Jackson, A. J., Baranyai, K. J., Perriman, A. W., Barker, J. G., Kim, M.-H., & White, J. W. (2006). Aggregation in a high internal phase emulsion observed by SANS and USANS. *Physica B: Condensed Matter*, 385–386, 776–779. <https://doi.org/10.1016/j.physb.2006.06.081>
- Zemb, T., & Lindner, P. (2002). *Neutron, X-rays and light: scattering methods applied to soft*

*condensed matter*. North Holland.

- Zembyla, M., Murray, B. S., & Sarkar, A. (2020). Water-in-oil emulsions stabilized by surfactants, biopolymers and/or particles: a review. *Trends in Food Science and Technology*, *104*(July), 49–59. <https://doi.org/10.1016/j.tifs.2020.07.028>
- Zeng, T., Wu, Z. ling, Zhu, J. Y., Yin, S. W., Tang, C. H., Wu, L. Y., & Yang, X. Q. (2017). Development of antioxidant Pickering high internal phase emulsions (HIPEs) stabilized by protein/polysaccharide hybrid particles as potential alternative for PHOs. *Food Chemistry*, *231*, 122–130. <https://doi.org/10.1016/j.foodchem.2017.03.116>
- Zhai, J., Wooster, T. J., Hoffmann, S. V., Lee, T. H., Augustin, M. A., & Aguilar, M. I. (2011). Structural rearrangement of  $\beta$ -lactoglobulin at different oil-water interfaces and its effect on emulsion stability. *Langmuir*, *27*(15), 9227–9236. <https://doi.org/10.1021/la201483y>
- Zhang, F., Skoda, M. W. A. A., Jacobs, R. M. J. J., Martin, R. A., Martin, C. M., & Schreiber, F. (2007). Protein interactions studied by SAXS: effect of ionic strength and protein concentration for BSA in aqueous solutions. *Journal of Physical Chemistry B*, *111*(1), 251–259. <https://doi.org/10.1021/jp0649955>
- Zhang, R., Cheng, L., Luo, L., Hemar, Y., & Yang, Z. (2021a). Formation and characterisation of high-internal-phase emulsions stabilised by high-pressure homogenised quinoa protein isolate. *Colloids and Surfaces A: Physicochemical and Engineering Aspects*, *631*, 127688. <https://doi.org/10.1016/j.colsurfa.2021.127688>
- Zhang, S., Holmes, M., Ettelaie, R., & Sarkar, A. (2020a). Pea protein microgel particles as Pickering stabilisers of oil-in-water emulsions: responsiveness to pH and ionic strength. *Food Hydrocolloids*, *102*, 105583. <https://doi.org/10.1016/j.foodhyd.2019.105583>

- Zhang, T., Xu, J., Chen, J., Wang, Z., Wang, X., & Zhong, J. (2021b). Protein nanoparticles for Pickering emulsions: a comprehensive review on their shapes, preparation methods, and modification methods. *Trends in Food Science and Technology*, *113*, 26–41. <https://doi.org/10.1016/j.tifs.2021.04.054>
- Zhang, X., Luo, X., Wang, Y., Li, Y., Li, B., & Liu, S. (2020b). Concentrated O/W Pickering emulsions stabilized by soy protein/cellulose nanofibrils: influence of pH on the emulsification performance. *Food Hydrocolloids*, *108*, 106025. <https://doi.org/10.1016/j.foodhyd.2020.106025>
- Zhao, M., Shen, P., Zhang, Y., Zhong, M., Zhao, Q., & Zhou, F. (2021a). Fabrication of soy protein nanoparticles via partial enzymatic hydrolysis and their role in controlling lipid digestion of oil-in-water emulsions. *ACS Food Science & Technology*, *1*(2), 193–204. <https://doi.org/10.1021/acfoodscitech.0c00005>
- Zhao, Q., Gu, Q., Hong, X., Liu, Y., & Li, J. (2021b). Novel protein-based nanoparticles from perilla oilseed residues as sole Pickering stabilizers for high internal phase emulsions. *LWT*, *145*, 111340. <https://doi.org/10.1016/j.lwt.2021.111340>
- Zheng, X., Zhang, Y., Wang, H., & Du, Q. (2014). Interconnected macroporous polymers synthesized from silica particle stabilized high internal phase emulsions. *Macromolecules*, *47*(19), 6847–6855. <https://doi.org/10.1021/ma501253u>
- Zhou, F.-Z., Huang, X.-N., Wu, Z., Yin, S.-W., Zhu, J., Tang, C.-H., & Yang, X.-Q. (2018). Fabrication of zein/pectin hybrid particle-stabilized Pickering high internal phase emulsions with robust and ordered interface architecture. *Journal of Agricultural and Food Chemistry*, *66*(42), 11113–11123. <https://doi.org/10.1021/acs.jafc.8b03714>

- Zhou, L., Zhang, J., Xing, L., & Zhang, W. (2021). Applications and effects of ultrasound assisted emulsification in the production of food emulsions: a review. *Trends in Food Science and Technology*, *110*(1), 493–512. <https://doi.org/10.1016/j.tifs.2021.02.008>
- Zhu, F. (2019). Starch based Pickering emulsions: fabrication, properties, and applications. *Trends in Food Science & Technology*, *85*, 129–137. <https://doi.org/10.1016/j.tifs.2019.01.012>
- Zhu, Y., Gao, H., Liu, W., Zou, L., & McClements, D. J. (2019). A review of the rheological properties of dilute and concentrated food emulsions. *Journal of Texture Studies*, *51*(1), jtxs.12444. <https://doi.org/10.1111/jtxs.12444>
- Zittle, C. A., DellaMonica, E. S., Rudd, R. K., & Custer, J. H. (1958). Binding of calcium to casein: influence of pH and calcium and phosphate concentrations. *Archives of Biochemistry and Biophysics*, *76*(2), 342–353. [https://doi.org/10.1016/0003-9861\(58\)90159-0](https://doi.org/10.1016/0003-9861(58)90159-0)

## Appendix A: Permissions for reuse published articles

---

### Appendices

#### Appendix A: Permissions for reuse published articles

##### Permission from for reprinting Figure 2-1a-b

---

##### ELSEVIER LICENSE TERMS AND CONDITIONS

---

Jun 16, 2022

---

This Agreement between Riddet Institute, Massey University -- Lirong Cheng ("You") and Elsevier ("Elsevier") consists of your license details and the terms and conditions provided by Elsevier and Copyright Clearance Center.

---

License Number	5330651432031
License date	Jun 16, 2022
Licensed Content Publisher	Elsevier
Licensed Content Publication	Current Opinion in Colloid & Interface Science
Licensed Content Title	Particles as surfactants—similarities and differences
Licensed Content Author	Bernard P. Binks
Licensed Content Date	Mar 1, 2002
Licensed Content Volume	7
Licensed Content Issue	1-2
Licensed Content Pages	21
Start Page	21
End Page	41
Type of Use	reuse in a thesis/dissertation
Portion	figures/tables/illustrations
Number of figures/tables/illustrations	1
Format	both print and electronic
Are you the author of this Elsevier article?	No
Will you be translating?	No
Title	Physico-chemical properties and stability of droplet-stabilised emulsions
Institution name	Riddet Institute, Massey University
Expected presentation date	Jul 2022
Portions	Figure 1
Requestor Location	Riddet Institute, Massey University University Avenue, Fitzherbert Palmerston North, Manawatu-Wanganui 0632 New Zealand Attn: Riddet Institute, Massey University
Publisher Tax ID	GB 494 6272 12

---

## Appendix A: Permissions for reuse published articles

### Permission from for reprinting Figure 2-1c



This is a License Agreement between Lirong Cheng ("User") and Copyright Clearance Center, Inc. ("CCC") on behalf of the Rightsholder identified in the order details below. The license consists of the order details, the CCC Terms and Conditions below, and any Rightsholder Terms and Conditions which are included below.

All payments must be made in full to CCC in accordance with the CCC Terms and Conditions below.

<b>Order Date</b>	17-Jun-2022	<b>Type of Use</b>	Republish in a thesis/dissertation
<b>Order License ID</b>	1237473-1	<b>Publisher</b>	Annual Reviews
<b>ISSN</b>	1941-1421	<b>Portion</b>	Image/photo/illustration

#### LICENSED CONTENT

<b>Publication Title</b>	Annual review of food science and technology	<b>Country</b>	United States of America
<b>Author/Editor</b>	Annual Reviews, Inc.	<b>Rightsholder</b>	Annual Reviews, Inc.
<b>Date</b>	01/01/2010	<b>Publication Type</b>	e-Journal
<b>Language</b>	English	<b>URL</b>	<a href="http://www.annualreviews.org/loi/food">http://www.annualreviews.org/loi/food</a>

#### REQUEST DETAILS

<b>Portion Type</b>	Image/photo/illustration	<b>Distribution</b>	Worldwide
<b>Number of images / photos / illustrations</b>	1	<b>Translation</b>	Original language of publication
<b>Format (select all that apply)</b>	Print, Electronic	<b>Copies for the disabled?</b>	No
<b>Who will republish the content?</b>	Academic institution	<b>Minor editing privileges?</b>	Yes
<b>Duration of Use</b>	Life of current and all future editions	<b>Incidental promotional use?</b>	No
<b>Lifetime Unit Quantity</b>	Up to 499	<b>Currency</b>	USD
<b>Rights Requested</b>	Main product		

#### NEW WORK DETAILS

<b>Title</b>	Physico-chemical properties and stability of droplet-stabilised emulsions	<b>Institution name</b>	Ridder Institute, Massey University
<b>Instructor name</b>	Lirong Cheng	<b>Expected presentation date</b>	2022-06-17

#### ADDITIONAL DETAILS

<b>Order reference number</b>	N/A	<b>The requesting person / organization to appear on the license</b>	Lirong Cheng
-------------------------------	-----	--	--------------

#### REUSE CONTENT DETAILS

<b>Title, description or numeric reference of the portion(s)</b>	Figure 3	<b>Title of the article/chapter the portion is from</b>	Pickering Emulsions for Food Applications: Background, Trends, and Challenges
<b>Editor of portion(s)</b>	Clair C. Berton-Carabin and Karin Schroën	<b>Author of portion(s)</b>	Clair C. Berton-Carabin and Karin Schroën
<b>Volume of serial or monograph</b>	6	<b>Issue, if republishing an article from a serial</b>	1
		<b>Publication date of portion</b>	2015-02-20



## *Appendix A: Permissions for reuse published articles*

---

### Permission from for reprinting Figure 2-2a-b

---

#### ELSEVIER LICENSE TERMS AND CONDITIONS

---

Jun 16, 2022

---

This Agreement between Riddet Institute, Massey University -- Lirong Cheng ("You") and Elsevier ("Elsevier") consists of your license details and the terms and conditions provided by Elsevier and Copyright Clearance Center.

---

License Number	5330690726489
License date	Jun 16, 2022
Licensed Content Publisher	Elsevier
Licensed Content Publication	Food Hydrocolloids
Licensed Content Title	High internal phase emulsions stabilized solely by a globular protein glycated to form soft particles
Licensed Content Author	Yan-Teng Xu, Chuan-He Tang, Bernard P. Binks
Licensed Content Date	Jan 1, 2020
Licensed Content Volume	98
Licensed Content Issue	n/a
Licensed Content Pages	1
Start Page	105254
End Page	0
Type of Use	reuse in a thesis/dissertation
Portion	figures/tables/illustrations
Number of figures/tables/illustrations	1
Format	both print and electronic
Are you the author of this Elsevier article?	No
Will you be translating?	No
Title	Physico-chemical properties and stability of droplet-stabilised emulsions
Institution name	Riddet Institute, Massey University
Expected presentation date	Jul 2022
Portions	Figure 4
Requestor Location	Riddet Institute, Massey University University Avenue, Fitzherbert Palmerston North, Manawatu-Wanganui 0632 New Zealand Attn: Riddet Institute, Massey University
Publisher Tax ID	GB 494 6272 12

---

## *Appendix A: Permissions for reuse published articles*

---

### Permission from for reprinting Figure 2-2c-d

---

#### ELSEVIER LICENSE TERMS AND CONDITIONS

---

Jun 16, 2022

---

This Agreement between Riddet Institute, Massey University -- Lirong Cheng ("You") and Elsevier ("Elsevier") consists of your license details and the terms and conditions provided by Elsevier and Copyright Clearance Center.

---

License Number	5330700836030
License date	Jun 16, 2022
Licensed Content Publisher	Elsevier
Licensed Content Publication	Food Structure
Licensed Content Title	Pickering emulsion stabilized by protein nanogel particles for delivery of curcumin: Effects of pH and ionic strength on curcumin retention
Licensed Content Author	Andrea Araiza-Calahorra, Anwesha Sarkar
Licensed Content Date	Jul 1, 2019
Licensed Content Volume	21
Licensed Content Issue	n/a
Licensed Content Pages	1
Start Page	100113
End Page	0
Type of Use	reuse in a thesis/dissertation
Portion	figures/tables/illustrations
Number of figures/tables/illustrations	1
Format	both print and electronic
Are you the author of this Elsevier article?	No
Will you be translating?	No
Title	Physico-chemical properties and stability of droplet-stabilised emulsions
Institution name	Riddet Institute, Massey University
Expected presentation date	Jul 2022
Portions	Figure 2
Requestor Location	Riddet Institute, Massey University University Avenue, Fitzherbert Palmerston North, Manawatu-Wanganui 0632 New Zealand Attn: Riddet Institute, Massey University
Publisher Tax ID	GB 494 6272 12

---

## Appendix A: Permissions for reuse published articles

### Permission from for reprinting Figure 2-3a and Figure 2-8a-b



This is a License Agreement between Lirong Cheng ("User") and Copyright Clearance Center, Inc. ("CCC") on behalf of the Rights holder identified in the order details below. The license consists of the order details, the CCC Terms and Conditions below, and any Rights holder Terms and Conditions which are included below.

All payments must be made in full to CCC in accordance with the CCC Terms and Conditions below.

Order Date	16-Jun-2022	Type of Use	Republish in a
Order License ID	1236371-1	Publisher	thesis/dissertation
ISSN	1744-6848	Portion	ROYAL SOCIETY OF CHEMISTRY Chart/graph/table/figure

#### LICENSED CONTENT

Publication Title	Soft matter	Publication Type	e-Journal
Article Title	Emulsions stabilised by whey protein microgel particles: towards food-grade Pickering emulsions.	Start Page	6941
Author/Editor	Royal Society of Chemistry (Great Britain)	End Page	6954
Date	06/01/2005	Issue	36
Language	English	Volume	10
Country	United Kingdom of Great Britain and Northern Ireland	URL	<a href="http://www.rsc.org/Publishing/journals/sm/index.asp">http://www.rsc.org/Publishing/journals/sm/index.asp</a>
Rights holder	Royal Society of Chemistry		

#### REQUEST DETAILS

Portion Type	Chart/graph/table/figure	Distribution	Worldwide
Number of charts / graphs / tables / figures requested	3	Translation	Original language of publication
Format (select all that apply)	Print, Electronic	Copies for the disabled?	No
Who will republish the content?	Academic institution	Minor editing privileges?	Yes
Duration of Use	Life of current edition	Incidental promotional use?	No
Lifetime Unit Quantity	Up to 499	Currency	USD
Rights Requested	Main product		

#### NEW WORK DETAILS

Title	Physico-chemical properties and stability of droplet-stabilised emulsions	Institution name	Riddet Institute, Massey University
Instructor name	Lirong Cheng	Expected presentation date	2022-06-16

#### ADDITIONAL DETAILS

Order reference number	N/A	The requesting person / organization to appear on the license	Lirong Cheng
------------------------	-----	---	--------------

#### REUSE CONTENT DETAILS

Title, description or numeric reference of the portion(s)	Figure 2, Figure 9, Figure 12	Title of the article/chapter the portion is from	Emulsions stabilised by whey protein microgel particles: towards food-grade Pickering emulsions.
Editor of portion(s)	Destribats, Mathieu; Rouvet, Martine; Gehin-Delval, Cécile; Schmitt, Christophe; Binks, Bernard P.	Author of portion(s)	Destribats, Mathieu; Rouvet, Martine; Gehin-Delval, Cécile; Schmitt, Christophe; Binks, Bernard P.
Volume of serial or monograph	10	Issue, if republishing an article from a serial	36
Page or page range of portion	6941-6954	Publication date of portion	2014-09-28

## *Appendix A: Permissions for reuse published articles*

---

### Permission from for reprinting Figure 2-3b

---

#### ELSEVIER LICENSE TERMS AND CONDITIONS

---

Jun 16, 2022

---

This Agreement between Riddet Institute, Massey University -- Lirong Cheng ("You") and Elsevier ("Elsevier") consists of your license details and the terms and conditions provided by Elsevier and Copyright Clearance Center.

---

License Number	5330710033632
License date	Jun 16, 2022
Licensed Content Publisher	Elsevier
Licensed Content Publication	LWT - Food Science and Technology
Licensed Content Title	In-situ dispersion of casein to form nanoparticles for Pickering high internal phase emulsions
Licensed Content Author	Yu Guo,Chao Wu,Ming Du,Songyi Lin,Xianbing Xu,Pei Yu
Licensed Content Date	Mar 1, 2021
Licensed Content Volume	139
Licensed Content Issue	n/a
Licensed Content Pages	1
Start Page	110538
End Page	0
Type of Use	reuse in a thesis/dissertation
Portion	figures/tables/illustrations
Number of figures/tables/illustrations	1
Format	both print and electronic
Are you the author of this Elsevier article?	No
Will you be translating?	No
Title	Physico-chemical properties and stability of droplet-stabilised emulsions
Institution name	Riddet Institute, Massey University
Expected presentation date	Jul 2022
Portions	Figure 7
Requestor Location	Riddet Institute, Massey University University Avenue, Fitzherbert Palmerston North, Manawatu-Wanganui 0632 New Zealand Attn: Riddet Institute, Massey University
Publisher Tax ID	GB 494 6272 12

---

## Appendix A: Permissions for reuse published articles

### Permission from for reprinting Figure 2-3c

---

#### ELSEVIER LICENSE TERMS AND CONDITIONS

---

Jun 16, 2022

---

This Agreement between Riddet Institute, Massey University -- Lirong Cheng ("You") and Elsevier ("Elsevier") consists of your license details and the terms and conditions provided by Elsevier and Copyright Clearance Center.

---

License Number	5330710250824
License date	Jun 16, 2022
Licensed Content Publisher	Elsevier
Licensed Content Publication	Food Hydrocolloids
Licensed Content Title	Casein gel particles as novel soft Pickering stabilizers: The emulsifying property and packing behaviour at the oil-water interface
Licensed Content Author	Pengjie Wang,Chong Chen,Huiyuan Guo,Hao Zhang,Zibiao Yang,Fazheng Ren
Licensed Content Date	Apr 1, 2018
Licensed Content Volume	77
Licensed Content Issue	n/a
Licensed Content Pages	10
Start Page	689
End Page	698
Type of Use	reuse in a thesis/dissertation
Portion	figures/tables/illustrations
Number of figures/tables/illustrations	1
Format	both print and electronic
Are you the author of this Elsevier article?	No
Will you be translating?	No
Title	Physico-chemical properties and stability of droplet-stabilised emulsions
Institution name	Riddet Institute, Massey University
Expected presentation date	Jul 2022
Portions	Figure 8
Requestor Location	Riddet Institute, Massey University University Avenue, Fitzherbert Palmerston North, Manawatu-Wanganui 0632 New Zealand Attn: Riddet Institute, Massey University
Publisher Tax ID	GB 494 6272 12

---

## Appendix A: Permissions for reuse published articles

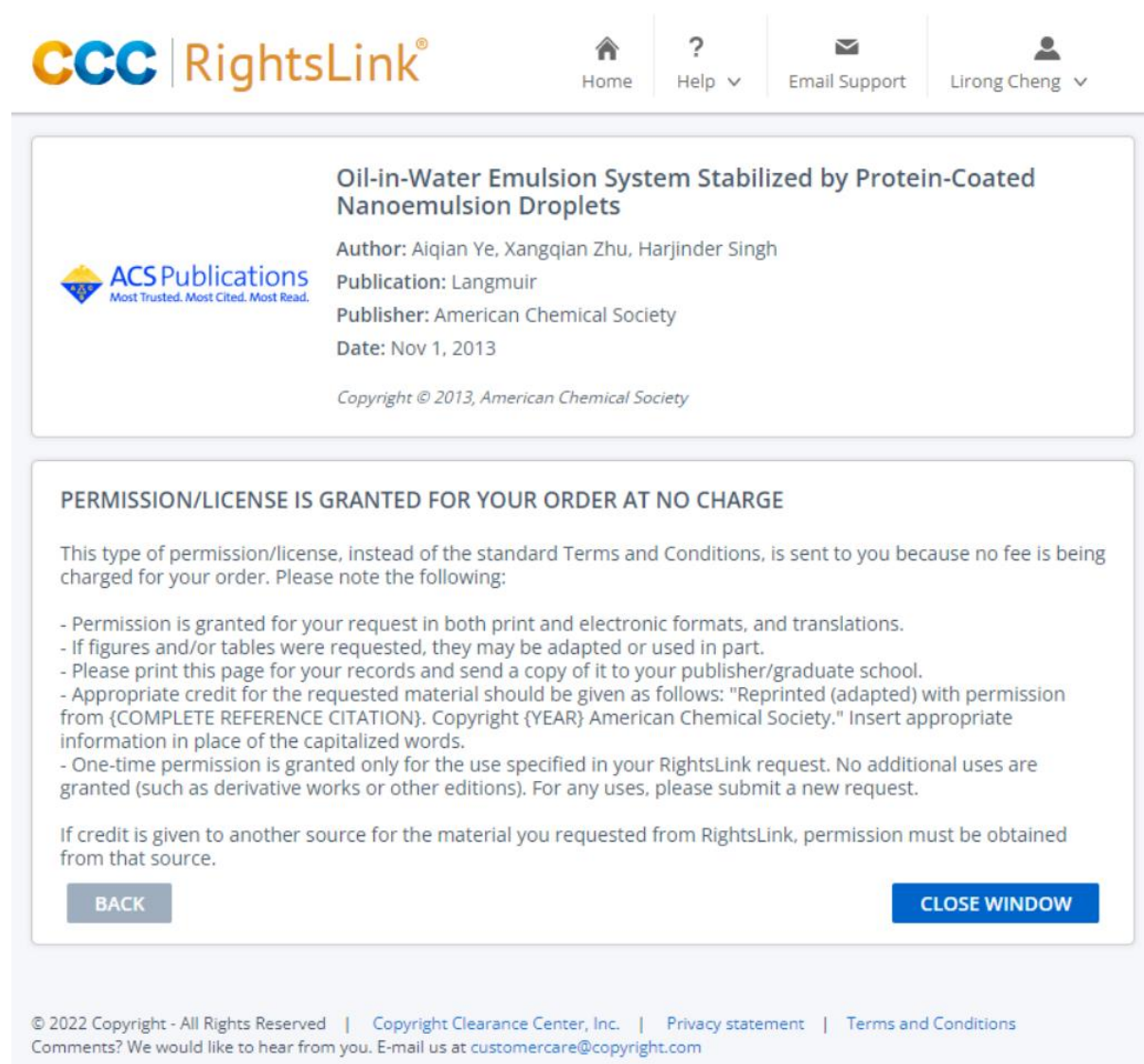
### Permission from for reprinting Figure 2-4a

#### Food-grade Pickering emulsions stabilised with solid lipid particles

A. Pawlik, D. Kurukji, I. Norton and F. Spyropoulos, *Food Funct.*, 2016, **7**, 2712  
DOI: 10.1039/C6FO00238B

This article is licensed under a [Creative Commons Attribution 3.0 Unported Licence](#). You can use material from this article in other publications without requesting further permissions from the RSC, provided that the correct acknowledgement is given.

### Permission from for reprinting Figure 2-4b



The screenshot shows the RightsLink interface. At the top, there is a navigation bar with the CCC RightsLink logo, and icons for Home, Help, Email Support, and a user profile for Lirong Cheng. Below the navigation bar, the article details for "Oil-in-Water Emulsion System Stabilized by Protein-Coated Nanoemulsion Droplets" are displayed, including the author (Aiqian Ye, Xangqian Zhu, Harjinder Singh), publication (Langmuir), publisher (American Chemical Society), and date (Nov 1, 2013). A prominent message states: "PERMISSION/LICENSE IS GRANTED FOR YOUR ORDER AT NO CHARGE". Below this message, a paragraph explains that this type of permission is sent because no fee is being charged. A list of conditions follows: permission is granted in both print and electronic formats; figures and tables may be adapted; users should print the page for records and send a copy to their publisher; appropriate credit should be given; and one-time permission is granted only for the specified use. At the bottom of the message box, there are "BACK" and "CLOSE WINDOW" buttons. The footer of the page contains copyright information for 2022, including links to the Copyright Clearance Center, Inc., Privacy statement, Terms and Conditions, and a contact email for customer care.

CCC RightsLink® Home Help Email Support Lirong Cheng

**Oil-in-Water Emulsion System Stabilized by Protein-Coated Nanoemulsion Droplets**

Author: Aiqian Ye, Xangqian Zhu, Harjinder Singh  
Publication: Langmuir  
Publisher: American Chemical Society  
Date: Nov 1, 2013  
Copyright © 2013, American Chemical Society

**PERMISSION/LICENSE IS GRANTED FOR YOUR ORDER AT NO CHARGE**

This type of permission/license, instead of the standard Terms and Conditions, is sent to you because no fee is being charged for your order. Please note the following:

- Permission is granted for your request in both print and electronic formats, and translations.
- If figures and/or tables were requested, they may be adapted or used in part.
- Please print this page for your records and send a copy of it to your publisher/graduate school.
- Appropriate credit for the requested material should be given as follows: "Reprinted (adapted) with permission from {COMPLETE REFERENCE CITATION}. Copyright {YEAR} American Chemical Society." Insert appropriate information in place of the capitalized words.
- One-time permission is granted only for the use specified in your RightsLink request. No additional uses are granted (such as derivative works or other editions). For any uses, please submit a new request.

If credit is given to another source for the material you requested from RightsLink, permission must be obtained from that source.

BACK CLOSE WINDOW

© 2022 Copyright - All Rights Reserved | Copyright Clearance Center, Inc. | Privacy statement | Terms and Conditions  
Comments? We would like to hear from you. E-mail us at [customer care@copyright.com](mailto:customer care@copyright.com)

## Appendix A: Permissions for reuse published articles

### Permission from for reprinting Figure 2-6a-b



This is a License Agreement between Lirong Cheng ("User") and Copyright Clearance Center, Inc. ("CCC") on behalf of the Rightsholder identified in the order details below. The license consists of the order details, the CCC Terms and Conditions below, and any Rightsholder Terms and Conditions which are included below.

All payments must be made in full to CCC in accordance with the CCC Terms and Conditions below.

Order Date	16-Jun-2022	Type of Use	Republish in a thesis/dissertation
Order License ID	1236387-1	Publisher	ROYAL SOCIETY OF CHEMISTRY
ISSN	1463-9084	Portion	Chart/graph/table/figure

#### LICENSED CONTENT

Publication Title	Physical chemistry chemical physics	Publication Type	e-Journal
Article Title	Interfacial layers of stimuli-responsive poly-(N-isopropylacrylamide-co-methacrylic acid) (PNIPAM-co-MAA) microgels characterized by interfacial rheology and compression isotherms.	Start Page	14573
Author/Editor	Royal Society of Chemistry (Great Britain)	End Page	14578
Date	01/01/1999	Issue	43
Language	English	Volume	12
Country	United Kingdom of Great Britain and Northern Ireland	URL	<a href="http://firstsearch.oclc.org/journal=1463-9076;screen=info;ECOIP">http://firstsearch.oclc.org/journal=1463-9076;screen=info;ECOIP</a>
Rightsholder	Royal Society of Chemistry		

#### REQUEST DETAILS

Portion Type	Chart/graph/table/figure	Distribution	Worldwide
Number of charts / graphs / tables / figures requested	2	Translation	Original language of publication
Format (select all that apply)	Print, Electronic	Copies for the disabled?	No
Who will republish the content?	Academic institution	Minor editing privileges?	No
Duration of Use	Life of current edition	Incidental promotional use?	No
Lifetime Unit Quantity	Up to 499	Currency	USD
Rights Requested	Main product		

#### NEW WORK DETAILS

Title	Physico-chemical properties and stability of droplet-stabilised emulsions	Institution name	Riddet Institute
Instructor name	Lirong Cheng	Expected presentation date	2022-06-16

#### ADDITIONAL DETAILS


Order reference number	N/A	The requesting person / organization to appear on the license	Lirong Cheng
------------------------	-----	---	--------------


#### REUSE CONTENT DETAILS

Title, description or numeric reference of the portion(s)	Figure 1, Figure 2	Title of the article/chapter the portion is from	Interfacial layers of stimuli-responsive poly-(N-isopropylacrylamide-co-methacrylic acid) (PNIPAM-co-MAA) microgels characterized by interfacial rheology and compression isotherms.
Editor of portion(s)	Brugger, Bastian; Vermant, Jan; Richtering, Walter	Author of portion(s)	Brugger, Bastian; Vermant, Jan; Richtering, Walter
Volume of serial or monograph	12	Issue, if republishing an article from a serial	43
Page or page range of portion	14573-14578	Publication date of portion	2010-11-21

## Appendix A: Permissions for reuse published articles

### Permission from for reprinting Figure 2-6c-d

HomeHelp ▾Email SupportLirong Cheng ▾



**Fundamental Study of Emulsions Stabilized by Soft and Rigid Particles**

Author: Zifu Li, David Harbottle, Erica Pensini, et al

Publication: Langmuir

Publisher: American Chemical Society

Date: Jun 1, 2015

Copyright © 2015, American Chemical Society

**PERMISSION/LICENSE IS GRANTED FOR YOUR ORDER AT NO CHARGE**

This type of permission/license, instead of the standard Terms and Conditions, is sent to you because no fee is being charged for your order. Please note the following:

- Permission is granted for your request in both print and electronic formats, and translations.
- If figures and/or tables were requested, they may be adapted or used in part.
- Please print this page for your records and send a copy of it to your publisher/graduate school.
- Appropriate credit for the requested material should be given as follows: "Reprinted (adapted) with permission from {COMPLETE REFERENCE CITATION}. Copyright {YEAR} American Chemical Society." Insert appropriate information in place of the capitalized words.
- One-time permission is granted only for the use specified in your RightsLink request. No additional uses are granted (such as derivative works or other editions). For any uses, please submit a new request.

If credit is given to another source for the material you requested from RightsLink, permission must be obtained from that source.

[BACK](#)

[CLOSE WINDOW](#)



## *Appendix A: Permissions for reuse published articles*

---

### Permission from for reprinting Figure 2-9

---

#### ELSEVIER LICENSE TERMS AND CONDITIONS

---

Jun 16, 2022

---

This Agreement between Riddet Institute, Massey University -- Lirong Cheng ("You") and Elsevier ("Elsevier") consists of your license details and the terms and conditions provided by Elsevier and Copyright Clearance Center.

---

License Number	5331010556351
License date	Jun 16, 2022
Licensed Content Publisher	Elsevier
Licensed Content Publication	Current Opinion in Colloid & Interface Science
Licensed Content Title	Small-angle X-Ray and neutron scattering in food colloids
Licensed Content Author	Elliot Paul Gilbert
Licensed Content Date	Aug 1, 2019
Licensed Content Volume	42
Licensed Content Issue	n/a
Licensed Content Pages	18
Start Page	55
End Page	72
Type of Use	reuse in a thesis/dissertation
Portion	figures/tables/illustrations
Number of figures/tables/illustrations	1
Format	both print and electronic
Are you the author of this Elsevier article?	No
Will you be translating?	No
Title	Physico-chemical properties and stability of droplet-stabilised emulsions
Institution name	Riddet Institute, Massey University
Expected presentation date	Jul 2022
Portions	Figure 1
Requestor Location	Riddet Institute, Massey University University Avenue, Fitzherbert Palmerston North, Manawatu-Wanganui 0632 New Zealand Attn: Riddet Institute, Massey University
Publisher Tax ID	GB 494 6272 12

---

## Appendix A: Permissions for reuse published articles

### Permission from for reprinting Figure 2-10



This is a License Agreement between Lirong Cheng ("User") and Copyright Clearance Center, Inc. ("CCC") on behalf of the Rightsholder identified in the order details below. The license consists of the order details, the CCC Terms and Conditions below, and any Rightsholder Terms and Conditions which are included below.

All payments must be made in full to CCC in accordance with the CCC Terms and Conditions below.

Order Date	17-Jun-2022	Type of Use	Republish in a thesis/dissertation
Order License ID	1237436-1	Publisher	ROYAL SOCIETY OF CHEMISTRY
ISSN	1744-6848	Portion	Chart/graph/table/figure

#### LICENSED CONTENT

Publication Title	Soft matter	Rightsholder	Royal Society of Chemistry
Article Title	Internal structure and colloidal behaviour of covalent whey protein microgels obtained by heat treatment	Publication Type	e-Journal
Author/Editor	Royal Society of Chemistry (Great Britain)	Start Page	4876
Date	06/01/2005	Issue	19
Language	English	Volume	6
Country	United Kingdom of Great Britain and Northern Ireland	URL	<a href="http://www.rsc.org/Publishing/Journals/sm/index.asp">http://www.rsc.org/Publishing/Journals/sm/index.asp</a>

#### REQUEST DETAILS

Portion Type	Chart/graph/table/figure	Distribution	Worldwide
Number of charts / graphs / tables / figures requested	2	Translation	Original language of publication
Format (select all that apply)	Print, Electronic	Copies for the disabled?	No
Who will republish the content?	Academic institution	Minor editing privileges?	Yes
Duration of Use	Life of current edition	Incidental promotional use?	No
Lifetime Unit Quantity	Up to 499	Currency	USD
Rights Requested	Main product		

#### NEW WORK DETAILS

Title	Physico-chemical properties and stability of droplet-stabilised emulsions	Institution name	Riddet Institute, Massey University
Instructor name	Lirong Cheng	Expected presentation date	2022-06-17

#### ADDITIONAL DETAILS

Order reference number	N/A	The requesting person / organization to appear on the license	Lirong Cheng
------------------------	-----	---	--------------

#### REUSE CONTENT DETAILS

Title, description or numeric reference of the portion(s)	Figure 5, Scheme 1	Title of the article/chapter the portion is from	Internal structure and colloidal behaviour of covalent whey protein microgels obtained by heat treatment
Editor of portion(s)	Bovay, Claudine; Bovetto, Lionel; Donato, Laurence; Leser, Martin E.; Moitzi, Christian; Rouvet, Martine; Schmitt, Christophe; Schurtenberger, Peter; Stradner, Anna	Author of portion(s)	Bovay, Claudine; Bovetto, Lionel; Donato, Laurence; Leser, Martin E.; Moitzi, Christian; Rouvet, Martine; Schmitt, Christophe; Schurtenberger, Peter; Stradner, Anna
Volume of serial or monograph	6	Issue, if republishing an article from a serial	19
Page or page range of portion	4876	Publication date of portion	2010-01-01

## Appendix A: Permissions for reuse published articles

---

### Permission from for reprinting Figure 2-11

---

#### ELSEVIER LICENSE TERMS AND CONDITIONS

---

Jun 16, 2022

---

This Agreement between Riddet Institute, Massey University -- Lirong Cheng ("You") and Elsevier ("Elsevier") consists of your license details and the terms and conditions provided by Elsevier and Copyright Clearance Center.

---

License Number	5331081455337
License date	Jun 16, 2022
Licensed Content Publisher	Elsevier
Licensed Content Publication	Journal of Colloid and Interface Science
Licensed Content Title	Ultrasound-based formation of nano-Pickering emulsions investigated via in-situ SAXS
Licensed Content Author	Yi-Ting Lee,David S. Li,Jan Ilavsky,Ivan Kuzmenko,Geng-Shi Jeng,Matthew O'Donnell,Lilo D. Pozzo
Licensed Content Date	Feb 15, 2019
Licensed Content Volume	536
Licensed Content Issue	n/a
Licensed Content Pages	10
Start Page	281
End Page	290
Type of Use	reuse in a thesis/dissertation
Portion	figures/tables/illustrations
Number of figures/tables/illustrations	2
Format	both print and electronic
Are you the author of this Elsevier article?	No
Will you be translating?	No
Title	Physico-chemical properties and stability of droplet-stabilised emulsions
Institution name	Riddet Institute, Massey University
Expected presentation date	Jul 2022
Portions	Figure 5, Figure 7
Requestor Location	Riddet Institute, Massey University University Avenue, Fitzherbert Palmerston North, Manawatu-Wanganui 0632 New Zealand Attn: Riddet Institute, Massey University
Publisher Tax ID	GB 494 6272 12

---

## Appendix A: Permissions for reuse published articles

### Permission from for reprinting Figure 2-12

---

#### ELSEVIER LICENSE TERMS AND CONDITIONS

---

Jun 16, 2022

---

This Agreement between Riddet Institute, Massey University -- Lirong Cheng ("You") and Elsevier ("Elsevier") consists of your license details and the terms and conditions provided by Elsevier and Copyright Clearance Center.

---

License Number	5331090436174
License date	Jun 16, 2022
Licensed Content Publisher	Elsevier
Licensed Content Publication	Journal of Colloid and Interface Science
Licensed Content Title	Interfacial structure of 70% fish oil-in-water emulsions stabilized with combinations of sodium caseinate and phosphatidylcholine
Licensed Content Author	Betül Yesiltas, Mika Torkkeli, László Almásy, Zoltán Dudás, András Ferenc Wacha, Robert Dalglish, Pedro J. García-Moreno, Ann-Dorit M. Sørensen, Charlotte Jacobsen, Matti Knaapila
Licensed Content Date	Oct 15, 2019
Licensed Content Volume	554
Licensed Content Issue	n/a
Licensed Content Pages	8
Start Page	183
End Page	190
Type of Use	reuse in a thesis/dissertation
Portion	figures/tables/illustrations
Number of figures/tables/illustrations	1
Format	both print and electronic
Are you the author of this Elsevier article?	No
Will you be translating?	No
Title	Physico-chemical properties and stability of droplet-stabilised emulsions
Institution name	Riddet Institute, Massey University
Expected presentation date	Jul 2022
Portions	Figure 4
Requestor Location	Riddet Institute, Massey University University Avenue, Fitzherbert Palmerston North, Manawatu-Wanganui 0632, New Zealand Attn: Riddet Institute, Massey University
Publisher Tax ID	GB 494 6272 12

---

## Appendix A: Permissions for reuse published articles

### Permission from for reprinting Figure 2-13



#### Contrast-Variation Time-Resolved Small-Angle Neutron Scattering Analysis of Oil-Exchange Kinetics Between Oil-in-Water Emulsions Stabilized by Anionic Surfactants

Author: Yi-Ting Lee, Lilo D. Pozzo

Publication: Langmuir

Publisher: American Chemical Society

Date: Nov 1, 2019

Copyright © 2019, American Chemical Society

#### PERMISSION/LICENSE IS GRANTED FOR YOUR ORDER AT NO CHARGE

This type of permission/license, instead of the standard Terms and Conditions, is sent to you because no fee is being charged for your order. Please note the following:

- Permission is granted for your request in both print and electronic formats, and translations.
- If figures and/or tables were requested, they may be adapted or used in part.
- Please print this page for your records and send a copy of it to your publisher/graduate school.
- Appropriate credit for the requested material should be given as follows: "Reprinted (adapted) with permission from {COMPLETE REFERENCE CITATION}. Copyright {YEAR} American Chemical Society." Insert appropriate information in place of the capitalized words.
- One-time permission is granted only for the use specified in your RightsLink request. No additional uses are granted (such as derivative works or other editions). For any uses, please submit a new request.


If credit is given to another source for the material you requested from RightsLink, permission must be obtained from that source.

[BACK](#)


[CLOSE WINDOW](#)

## Appendix A: Permissions for reuse published articles

### Permission from for reprinting full article in Chapter 3

Home Help Email Support Sign in Create Account

**Interfacial Structures of Droplet-Stabilized Emulsions Formed with Whey Protein Microgel Particles as Revealed by Small- and Ultra-Small-Angle Neutron Scattering**

 **Author:** Lirong Cheng, Aiqian Ye, Yacine Hemar, et al  
**Publication:** Langmuir  
**Publisher:** American Chemical Society  
**Date:** Sep 1, 2019

*Copyright © 2019, American Chemical Society*

**PERMISSION/LICENSE IS GRANTED FOR YOUR ORDER AT NO CHARGE**

This type of permission/license, instead of the standard Terms and Conditions, is sent to you because no fee is being charged for your order. Please note the following:

- Permission is granted for your request in both print and electronic formats, and translations.
- If figures and/or tables were requested, they may be adapted or used in part.
- Please print this page for your records and send a copy of it to your publisher/graduate school.
- Appropriate credit for the requested material should be given as follows: "Reprinted (adapted) with permission from {COMPLETE REFERENCE CITATION}. Copyright {YEAR} American Chemical Society." Insert appropriate information in place of the capitalized words.
- One-time permission is granted only for the use specified in your RightsLink request. No additional uses are granted (such as derivative works or other editions). For any uses, please submit a new request.


If credit is given to another source for the material you requested from RightsLink, permission must be obtained from that source.


[BACK](#) [CLOSE WINDOW](#)

© 2022 Copyright - All Rights Reserved | [Copyright Clearance Center, Inc.](#) | [Privacy statement](#) | [Terms and Conditions](#)  
Comments? We would like to hear from you. E-mail us at [customer-care@copyright.com](mailto:customer-care@copyright.com)

## Appendix A: Permissions for reuse published articles

### Permission from for reprinting full article in Chapter 4

HomeHelp ▾Email SupportSign inCreate Account



**Small-angle X-ray scattering (SAXS) and small-angle neutron scattering (SANS) study on the structure of sodium caseinate in dispersions and at the oil-water interface: Effect of calcium ions**

**Author:**  
Lirong Cheng, Aiqian Ye, Zhi Yang, Elliot Paul Gilbert, Robert Knott, Liliana de Campo, Ben Storer, Yacine Hemar, Harjinder Singh

**Publication:** Food Structure

**Publisher:** Elsevier

**Date:** April 2022

© 2022 Elsevier Ltd. All rights reserved.

#### Journal Author Rights

Please note that, as the author of this Elsevier article, you retain the right to include it in a thesis or dissertation, provided it is not published commercially. Permission is not required, but please ensure that you reference the journal as the original source. For more information on this and on your other retained rights, please visit: <https://www.elsevier.com/about/our-business/policies/copyright#Author-rights>

BACK

CLOSE WINDOW

© 2022 Copyright - All Rights Reserved | [Copyright Clearance Center, Inc.](#) | [Privacy statement](#) | [Terms and Conditions](#)  
Comments? We would like to hear from you. E-mail us at [customer-care@copyright.com](mailto:customer-care@copyright.com)

## Appendix A: Permissions for reuse published articles

### Permission from for reprinting full article in Chapter 6



#### Modification of the interfacial structure of droplet-stabilised emulsions during in vitro dynamic gastric digestion: Impact on in vitro intestinal lipid digestion

Author: Lirong Cheng, Aiqian Ye, Yacine Hemar, Harjinder Singh

Publication: Journal of Colloid and Interface Science

Publisher: Elsevier

Date: 15 February 2022

© 2021 Elsevier Inc. All rights reserved.

#### Journal Author Rights

Please note that, as the author of this Elsevier article, you retain the right to include it in a thesis or dissertation, provided it is not published commercially. Permission is not required, but please ensure that you reference the journal as the original source. For more information on this and on your other retained rights, please visit: <https://www.elsevier.com/about/our-business/policies/copyright#Author-rights>

BACK

CLOSE WINDOW



**Appendix B: DRC 16 Forms**

DRC 16



**STATEMENT OF CONTRIBUTION  
DOCTORATE WITH PUBLICATIONS/MANUSCRIPTS**

We, the candidate and the candidate's Primary Supervisor, certify that all co-authors have consented to their work being included in the thesis and they have accepted the candidate's contribution as indicated below in the *Statement of Originality*.

Name of candidate:	Lirong Cheng	
Name/title of Primary Supervisor:	Professor Aiqian Ye	
Name of Research Output and full reference:		
Published review article in journal		
In which Chapter is the Manuscript /Published work:	Chapter 2	
Please indicate:		
<ul style="list-style-type: none"> <li>The percentage of the manuscript/Published Work that was contributed by the candidate:</li> </ul>	90	
and		
<ul style="list-style-type: none"> <li>Describe the contribution that the candidate has made to the Manuscript/Published Work:</li> </ul>	Conceptualisation, Investigation, Visualisation, Writing – original draft.	
For manuscripts intended for publication please indicate target journal:		
Trends in Food Science and Technology		
Candidate's Signature:	Lirong Cheng	<small>Digitally signed by Lirong Cheng Date: 2022.06.15 16:31:17 +12'00'</small>
Date:	2022.06.15	
Primary Supervisor's Signature:	Aiqian Ye	<small>Digitally signed by Aiqian Ye DN: cn=Aiqian Ye, o=Massey University, ou=SF&amp;AT_email=a.m.ye@massey.ac.nz Date: 2022.06.15 20:52:08 +12'00'</small>
Date:	2022.06.15	

(This form should appear at the end of each thesis chapter/section/appendix submitted as a manuscript/ publication or collected as an appendix at the end of the thesis)



**STATEMENT OF CONTRIBUTION  
DOCTORATE WITH PUBLICATIONS/MANUSCRIPTS**

We, the candidate and the candidate's Primary Supervisor, certify that all co-authors have consented to their work being included in the thesis and they have accepted the candidate's contribution as indicated below in the *Statement of Originality*.

Name of candidate:	Lirong Cheng	
Name/title of Primary Supervisor:	Professor Aiqian Ye	
Name of Research Output and full reference:		
Published research article, Langmuir, 35(37), 12017–12027.		
In which Chapter is the Manuscript /Published work:	Chapter 3	
Please indicate:		
• The percentage of the manuscript/Published Work that was contributed by the candidate:	80	
and		
• Describe the contribution that the candidate has made to the Manuscript/Published Work:	Conceptualisation, Methodology, Validation, Formal analysis, Investigation, Data curation, Visualisation, Writing – original draft.	
For manuscripts intended for publication please indicate target journal:		
Candidate's Signature:	Lirong Cheng	Digitally signed by Lirong Cheng Date: 2022.06.15 16:31:17 +12'00'
Date:	2022.06.15	
Primary Supervisor's Signature:	Aiqian Ye	Digitally signed by Aiqian Ye DN: cn=Aiqian Ye, o=NZ, o=Massey University, ou=SF&AT, email=a.m.ye@massey.ac.nz Date: 2022.06.15 20:52:53 +12'00'
Date:	2022.06.15	

(This form should appear at the end of each thesis chapter/section/appendix submitted as a manuscript/ publication or collected as an appendix at the end of the thesis)



**STATEMENT OF CONTRIBUTION  
DOCTORATE WITH PUBLICATIONS/MANUSCRIPTS**

We, the candidate and the candidate's Primary Supervisor, certify that all co-authors have consented to their work being included in the thesis and they have accepted the candidate's contribution as indicated below in the *Statement of Originality*.

Name of candidate:	Lirong Cheng	
Name/title of Primary Supervisor:	Professor Aiqian Ye	
Name of Research Output and full reference:		
Published research article, Food Structure, 32(April), 100276.		
In which Chapter is the Manuscript /Published work:	Chapter 4	
Please indicate:		
• The percentage of the manuscript/Published Work that was contributed by the candidate:	75	
and		
• Describe the contribution that the candidate has made to the Manuscript/Published Work:	Conceptualisation, Methodology, Validation, Formal analysis, Investigation, Data curation, Visualisation, Writing – original draft.	
For manuscripts intended for publication please indicate target journal:		
Candidate's Signature:	Lirong Cheng	<small>Digitally signed by Lirong Cheng Date: 2022.06.15 16:31:17 +12'00'</small>
Date:	2022.06.15	
Primary Supervisor's Signature:	Aiqian Ye	<small>Digitally signed by Aiqian Ye DN: cn=Aiqian Ye, o=NZ, o=Massey University, ou=SF&amp;AT, email=a.m.ye@massey.ac.nz Date: 2022.06.15 20:53:33 +12'00'</small>
Date:	2022.06.15	

(This form should appear at the end of each thesis chapter/section/appendix submitted as a manuscript/ publication or collected as an appendix at the end of the thesis)



**STATEMENT OF CONTRIBUTION  
DOCTORATE WITH PUBLICATIONS/MANUSCRIPTS**

We, the candidate and the candidate's Primary Supervisor, certify that all co-authors have consented to their work being included in the thesis and they have accepted the candidate's contribution as indicated below in the *Statement of Originality*.

Name of candidate:	Lirong Cheng	
Name/title of Primary Supervisor:	Professor Aiqian Ye	
Name of Research Output and full reference:		
<b>Published research article in journal</b>		
In which Chapter is the Manuscript /Published work:	Chapter 5	
Please indicate:		
<ul style="list-style-type: none"> <li>The percentage of the manuscript/Published Work that was contributed by the candidate:</li> </ul>	85	
and		
<ul style="list-style-type: none"> <li>Describe the contribution that the candidate has made to the Manuscript/Published Work:</li> </ul>		
Conceptualisation, Methodology, Validation, Formal analysis, Investigation, Data curation, Visualisation, Writing – original draft.		
For manuscripts intended for publication please indicate target journal:		
Langmuir		
Candidate's Signature:	<b>Lirong Cheng</b>	<small>Digitally signed by Lirong Cheng Date: 2022.06.15 16:31:17 +12'00'</small>
Date:	2022.06.15	
Primary Supervisor's Signature:	<b>Aiqian Ye</b>	<small>Digitally signed by Aiqian Ye DN: cn=Aiqian Ye, o=Massey University, ou=GR&amp;AT, email=a.m.ye@massey.ac.nz Date: 2022.06.15 20:54:09 +12'00'</small>
Date:	2022.06.15	

(This form should appear at the end of each thesis chapter/section/appendix submitted as a manuscript/ publication or collected as an appendix at the end of the thesis)



**STATEMENT OF CONTRIBUTION  
DOCTORATE WITH PUBLICATIONS/MANUSCRIPTS**

We, the candidate and the candidate's Primary Supervisor, certify that all co-authors have consented to their work being included in the thesis and they have accepted the candidate's contribution as indicated below in the *Statement of Originality*.

Name of candidate:	Lirong Cheng	
Name/title of Primary Supervisor:	Professor Aiqian Ye	
Name of Research Output and full reference:		
Published research article, Journal of Colloid and Interface Science, 608, 1286–1296.		
In which Chapter is the Manuscript /Published work:	Chapter 6	
Please indicate:		
<ul style="list-style-type: none"> <li>The percentage of the manuscript/Published Work that was contributed by the candidate:</li> </ul>	85	
and		
<ul style="list-style-type: none"> <li>Describe the contribution that the candidate has made to the Manuscript/Published Work:</li> </ul>		
Conceptualisation, Methodology, Software, Validation, Formal analysis, Investigation, Data curation, Visualization, Writing – original draft.		
For manuscripts intended for publication please indicate target journal:		
Candidate's Signature:	Lirong Cheng	Digitally signed by Lirong Cheng Date: 2022.06.15 16:31:17 +12'00'
Date:	2022.06.15	
Primary Supervisor's Signature:	Aiqian Ye	Digitally signed by Aiqian Ye DN: cn=Aiqian Ye, o=NZ, o=Massey University, ou=SR&AT, email=a.m.ye@massey.ac.nz Date: 2022.06.15 20:54:44 +12'00'
Date:	2022.06.15	

(This form should appear at the end of each thesis chapter/section/appendix submitted as a manuscript/ publication or collected as an appendix at the end of the thesis)



**STATEMENT OF CONTRIBUTION  
DOCTORATE WITH PUBLICATIONS/MANUSCRIPTS**

We, the candidate and the candidate’s Primary Supervisor, certify that all co-authors have consented to their work being included in the thesis and they have accepted the candidate’s contribution as indicated below in the *Statement of Originality*.

Name of candidate:	Lirong Cheng	
Name/title of Primary Supervisor:	Professor Aiqian Ye	
Name of Research Output and full reference:		
Published research article in journal		
In which Chapter is the Manuscript /Published work:	Chapter 7	
Please indicate:		
• The percentage of the manuscript/Published Work that was contributed by the candidate:	85%	
and		
• Describe the contribution that the candidate has made to the Manuscript/Published Work:		
Conceptualisation, Methodology, Software, Validation, Formal analysis, Investigation, Data curation, Visualization, Writing – original draft.		
For manuscripts intended for publication please indicate target journal:		
Food hydrocolloids		
Candidate’s Signature:	Lirong Cheng	Digitally signed by Lirong Cheng Date: 2022.06.15 16:31:17 +12'00'
Date:	2022.06.15	
Primary Supervisor’s Signature:	Aiqian Ye	Digitally signed by Aiqian Ye DN: cn=Aiqian Ye, o=NZ, o=Massey University, ou=SF&AT, email=a.m.ye@massey.ac.nz Date: 2022.06.15 20:50:44 +12'00'
Date:	2022.06.15	

(This form should appear at the end of each thesis chapter/section/appendix submitted as a manuscript/ publication or collected as an appendix at the end of the thesis)